OPTICAL HOLEBURNING IN COLOUR CENTRES

By

NARLA RAJA SHEKHAR REDDY

A thesis submitted for the degree of

Doctor of Philosophy

at the Australian National University.

February 1989

DECLARATION

The studies described in this thesis were carried out by me while I was a full time graduate student at the Australian National University, Canberra.

Except where mentioned in the text the research described in this thesis is my own.

This thesis has never been submitted to another university or similar institution.

N.R.S. Reddy

NARLA RAJA SHEKHAR REDDY.

ACKNOWLEDGEMENTS

I wish to express my sincere thanks to my supervisor Dr.N.B.Manson for his help and encouragement during the course of this work. I also wish to thank Dr.Z.Hasan for his help with some experiments during the initial stages of this work.

I express my debt and appreciation of the help given to me by all the members of the Department of Solid State Physics (now part of the Laser Physics Centre) particularly Professor W.A.Runciman. I am thankful to Dr. E.Krausz for his help with the MCD experiments.

The assistance from technical staff particularly Mr. John Remmel and Mr. Gino Sampietro, is gratefully acknowledged. Thanks are also due to Mr Wolfgang Boehm for supplying liquid helium that was so essential for my experiments.

I am grateful to my parents for their encouragement and support during my long years of formal education. Finally, I would like to thank my wife Padma and children Vishnu and Deepti for allowing me to spend in the lab the time that was due to them. Thank you, everybody.

ABSTRACT

The thesis deals mainly with the spectroscopic investigation of colour centres in solids using high resolution of the optical holeburning technique. Though frequent use has been made of conventional spectroscopic techniques such as absorption, emission, laser excitation and the magnetic circular dichroism spectroscopy, such experiments were performed either as preliminary investigations before holeburning techniques or were needed to compliment the data obtained from the high resolution techniques. Therefore, only a brief and necessary account of such experiments is presented.

Chapter I is a basic introduction to holeburning spectroscopy. An account is also given of the two laser holeburning which has been utilized in the later part of the thesis to investigate N-V colour centre in diamond.

Chapter II deals with the experimental details of the techniques utilized in the studies but by no means is exhaustive, as some techniques have been described later on in the relevant chapters.

Chapter III deals with the holeburning in CaO:F centre. It has been shown that high resolution Zeeman measurements can be performed on the optical hole in the zero phonon line of the F centre with very low fields. The Zeeman measurements confirm the interpretation of the previous ODMR studies on this system. Results have also been presented for the stark effect on this centre and the phonon broadening of the holes. In both of these instances our results differ from the previous reports which concentrated mainly on low resolution techniques. Holeburning in this centre is proposed to be photochemical and the holeburning characteristics are discussed.

Chapter IV deals with the holeburning in the N-V centre in diamond where there is a short lived hole. A very detailed spectrum is obtained by using two lasers- one to burn and another to read. Two laser holeburning data has been crucial in revising the assignment of the zero-phonon line

of the N-V centre. Previous optical ODMR and single laser holeburning studies have not been able to correctly assign the multiplicity of the states involved. Revised assignment on the basis of two laser holeburning has been further checked by different techniques such as the optical- microwave double resonance, Zeeman studies on the antiholes and the temperature dependence of magnetic circular dichroism. All these measurements have been found to support the proposed assignment. The latter part of the chapter presents a model for holeburning in a $^3A \rightarrow ^3E$ transition and it is shown that by considering spin-orbit and strain a spectrum similar to that observed can be predicted.

Chapter V briefly deals with the other colour centre systems where some preliminary holeburning measurements suggested that a detailed investigation of such systems would require circumventing some technical problems, such as control on the production of the desired centre, with needed concentrations. Some suggestions are made to further advance in these directions.

Contents

Chapter 1

INTRODUCTION

A perfectly regular crystalline lattice devoid of any imperfections is rather an ideal case and in real crystals the periodicity of the lattice is broken by lattice imperfections like point defects and dislocations. This thesis concerns the investigations performed on particular type of point defects that are called colour centres. Most insulators are transparent to visible light because a large energy gap that exists between the valence and conduction bands. Lattice defects with energy levels in the band gap can cause selective absorption of visible light and such defects are called colour centres. Historically many of the spectroscopic studies on colour centres were concerned with alkali halides. The main reason for this is that it is fairly easy to obtain good quality crystals and it is straight forward to produce colour centres. In addition to additive colouration in metal vapour (discussed in chapter 3) commonly available ionising radiation sources like x-rays, γ-rays are quite effective in producing colour centres. Similar studies in other crystalline materials were not so extensive either because of the lack of good optical quality single crystals or due to difficulties in producing the colour centres. Optical holeburning studies in some colour centre systems where these problems have been overcome form the subject of this thesis.

The spectroscopy of zero-phonon lines has been the most important source of information about the symmetry and nature of colour centres in solids (Fitchen, 1968). The usefulness of these lines as probes of defect centres depends on their having a linewidth narrow enough to resolve shifts

and splittings due to external perturbations such as magnetic and electric fields and uniaxial stress. At liquid helium temperatures, the widths of the zero-phonon lines is substantially less than at higher temperatures, but they are still inhomogeneously broadened by static lattice strains inherent in all solids. At low temperatures each isolated defect centre has an intrinsic (homogeneous) linewidth Γ_h determined by the dephasing time T_2 ($\pi\Gamma_h = {T_2}^{-1}$). The dephasing time T_2 is related to the excited state lifetime T_1 and pure dephasing time T_2' (Macfarlane *et al*, 1983) by

$$\frac{1}{T_2} = \frac{1}{2T_1} + \frac{1}{T_2'}$$

T_2' is the average time interval during which the coherence of the excited states is destroyed by lattice phonons. At sufficiently low temperatures where the phonon scattering processes can be neglected ($T_2' =\approx 0$), the homogeneous linewidth Γ_h is determined by the excited state lifetime T_1. The inhomogeneous linewidth Γ_{inh} is associated with the envelope of a Gaussian distribution of homogeneously broadened transitions of Lorentzian line shape (of width Γ_h). The statistical distribution of resonance frequencies of the defect centres due to variation in local environment causes the Gaussian distribution. Impurities and other lattice defects contribute to the strains, this results in a residual width Γ_{inh} of 1-50 cm^{-1}. The phenomenon of inhomogeneous broadening is shown in figure 1.1(a).

Optical absorption lines associated with individual centres in solids can have very small homogeneous widths. For example in diamond at low temperatures the radiative lifetime (T_1) is expected to limit the width giving values of ~30 to 300 MHz for different centres. However, the linewidths observed in normal absorption measurements are typically ~300 GHz (which is about 3 to 4 orders of magnitude larger than the homogeneous width) as a result of random inhomogeneous strains which cause shifts of the absorption frequency of individual centres. Large residual linewidths can prevent resolution of splittings under external perturbations and necessitate the use of modulation techniques (Kaplyanskii *et al*, 1970) and moment analysis (Johannson *et al*, 1963) to extract any useful information. However, with the advent of tunable narrow band lasers the situation has changed dramatically and it is now possible to overcome the problem due to large residual inhomogeneous linewidths.

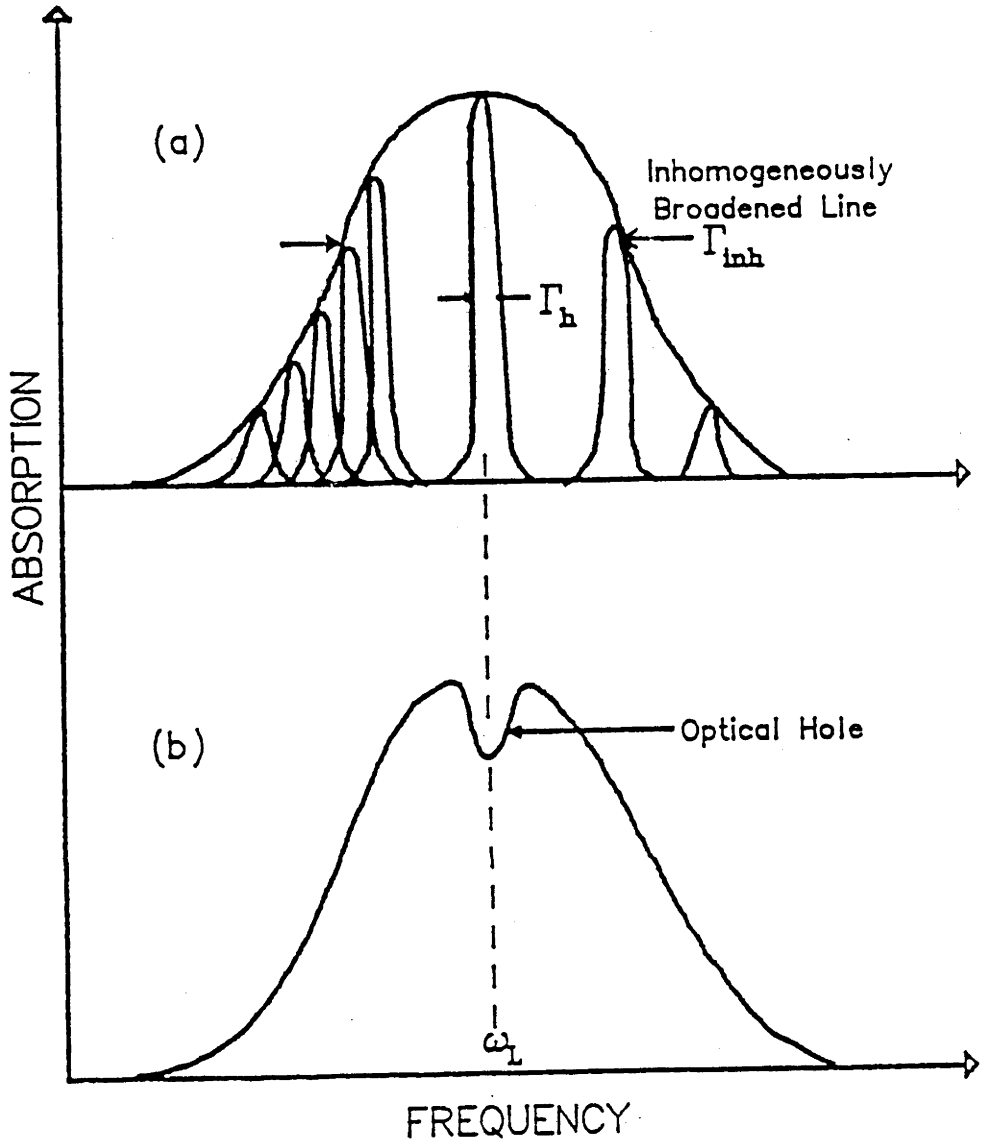

Figure 1.1 Illustration of inhomogeneous broadening of zero phonon lines (a) and optical holeburning (b) ω_L is the laser frequency.

Optical holeburning is a recent technique for the high resolution optical study of inhomogeneously broadened zero-phonon absorption lines using lasers of narrow linewidth. In optical holeburning an intense narrow bandwidth ($\sim$1 MHz) laser at fixed frequency (ω_L in figure 1.1) within an inhomogeneous line profile is used to excite only those centres which have a resonant frequency coincident with the laser. Most of the excited centres return within the radiative lifetime to the ground state but a small fraction (typically 10^{-3} to 10^{-8} per absorbed photon) may be held in a metastable state or undergo a photochemical change. The result is a long lived missing band of absorption frequencies or hole (figure 1.1(b)) in the inhomogeneously broadened absorption line. The hole may be detected by scanning the laser frequency at much lower intensity through the irradiation frequency and measuring the laser absorption or fluorescence level from the crystal under investigation. When the centre undergoes a phototransformation the lifetime of the hole can be as long as minutes to hours. In such cases, the hole can be burned and detected using the same laser. The fastest scanning speeds of the high resolution lasers available commercially are of the order of 2 Hz. Thus, if the lifetime of the hole is less than the shortest scan time (250 msecs) the situation is different. The holeburning spectrum can only be achieved with two high resolution lasers with one laser at fixed frequency used to burn the hole and the second scanned about the frequency of the first to detect the hole. An exception to this statement are the holeburning spectra (644 nm centre in NaF) reported in chapter 5 where the time evolution of the holeburning spectrum has been studied during the time scale of $<$250 msecs.. However in such cases the detail in the holeburning spectrum could partially be lost. In situations where the holeburning technique can be employed the hole width may approach the homogeneous optical linewidth for many of the systems reported in the literature and allow spectroscopic measurements with resolution of order 10^3 to 10^4 better than by conventional means.

REFERENCES

1) Fitchen D. B.
in *Physics of colour centres*, (Fowler W.B. ed), Academic press, New York (1968)

2) Johannson G. ,Von der Osten W. , Piehl R. and Waidelich W.
phys. stat. sol. , 34, 699 (1969)

3) Kaplyanskii A. A. , Medvedev V. N. and Skvortsov A. P.
Opt. Spectr. , 29, 481 (1970)

4) Macfarlane R.M. , Harley R.T. and Shelby R.M.
Radiation Effects, 72,1 (1983)

Chapter 2

EXPERIMENTAL DETAILS

2.1 HIGH RESOLUTION LASERS

Results of the holeburning experiments in the F centre in CaO and the N-V centre in diamond are described in this thesis. In the case of CaO the hole lifetime is of the order of hours and the holeburning mechanism is considered to be photochemical in nature. Hence these experiments involve only one high resolution laser. In the case of N-V centre in diamond, there is a weak photochemical component which can be detected with one laser (Harley *et al*, 1984). However, there is also a very short lived hole with a lifetime of few milliseconds. The presence of this hole and its associated structure is only accessible with the use of two separate lasers. This necessitated the use of two separate lasers: one as the burn laser and the other as the read laser. The two high resolution lasers used in the present study are Coherent CR 699-21 ring dye laser (so named because of the beam path inside the cavity) and Coherent CR 599-21 standing wave laser.

Both the lasers mentioned above are high resolution lasers and have a jitter induced bandwidth of $\sim$1 MHz. The ring dye laser was pumped with a Spectra-Physics argon ion laser (4w at 514 nm) while the standing wave laser was pumped with 3w at 514 nm from another Spectra-Physics argon ion laser. When a dye laser is made to lase in the single cavity mode with a standing wave inside the cavity, the problem of spatial holeburning is often

encountered. This is because the maxima and minima inside the cavity are stationary and hence there will be regions of unused gain in the amplifying medium (dye jet). Frequently the gain in these regions is high enough to sustain simultaneous lasing at a different frequency (mode). This causes the single mode operation of the laser to become unstable. This problem of spatial holeburning is overcome in the ring lasers with a unidirectional travelling wave. In this case most of the amplifying medium volume is used in amplifying the same mode and hence the laser is more stable. Thus, the ring dye laser is capable of delivering higher output powers than the standing wave laser. In the wavelength region of interest, for a input laser power of 4 watts the ring dye laser output is 150 mw while for the same amount of input power the standing wave laser gives about 50 mw. However the standing wave laser was normally pumped with 2W input power to avoid spatial holeburning.

As mentioned earlier the linewidth of the high resolution lasers used in the present study are ~1 MHz. Generally the linewidth of the laser depends on the number of cavity modes whose gain exceeds the lasing threshold and also on the stability of the cavity. Laser linewidth can hence, be minimised by limiting the number of lasing cavity modes to one and improving the stability of the cavity. The basic dye laser system (in the lasers used) without any intracavity elements has a line width of about 20 GHz. This is because the laser oscillation occurs at more than one longitudinal cavity mode. The number of transverse cavity modes in which lasing can occur is limited because the dimensions of the cavity end mirrors are very small compared to the cavity dimensions. In practice it is desirable to have the lasing limited to TEM_{00} mode (the Gaussian mode) because when higher order modes are involved the laser operation becomes unstable. This problem was encountered with the argon laser used to pump the ring dye laser. Even when the number of transverse modes is limited the laser oscillates in several longitudinal modes. Intracavity elements can be used to limit the laser oscillation to a single cavity mode. Mode selection in these lasers is achieved by using 3 intracavity elements viz. the birefringent filter, the thin etalon and the thick etalon. The free spectral ranges of these three elements are ~1000 A, 225 GHz and 10 GHz respectively. This results in laser oscillation in single cavity mode despite the fact that the smallest free spectral range (10 GHz) is much larger than the longitudinal cavity mode spacing (~300 MHz in the ring dye laser and ~500 MHz in the standing wave laser). This is possible because less than 1% discrimination in the form of cavity loss is needed to

be able to distinguish between adjacent cavity modes. The width of a single cavity mode has a lower limit (<1 Hz) determined by quantum noise as a result of spontaneous emission. In practice, the single mode width is determined by acoustical and mechanical disturbances causing fluctuations in cavity length and thus, fluctuations in the output frequency. By careful design of the cavity, these fluctuations are restricted to ~25 MHz.

The laser radiation frequency can be tuned across the dye gain curve by adjusting the birefringent filter which helps select a particular thin etalon mode, and the thin etalon offset which selects a particular thick etalon mode. Frequency stability (locking) in both these high resolution lasers is achieved in the following way. The components in the frequency locking setup are shown in figure 2.1 . A thick beam splitter gives two weak beams that provide information to the feedback system. These beams pass through a variable attenuator and a temperature and pressure stabilised Fabry-Perot interferometer (FPI) that constitute the laser reference channel. The laser intensity $I_t(\lambda)$ transmitted through the FPI is compared with the reference intensity I_R transmitted by the variable attenuator. The output signals S_1 and S_2 from the detectors D_1 and D_2 are fed into a difference amplifier which is adjusted so that its output voltage is zero for $\lambda_L = \lambda_R$ where λ_R is the desired frequency value (lock point). If the laser wavelength λ_L deviates from λ_R, S_2 becomes smaller or larger depending on the sign of λ_L - λ_R. The output of the difference amplifier is proportional to this deviation, provided I_t varies linearly with λ_L (figure 2.1 (b)) in the region where locking is desired. This is then amplified before being applied to the piezo mounted tweeter mirror and galvo driven brewster plate to provide the required frequency correction. In free run mode of the laser the frequency stability was $\pm$25 MHz and in lock mode it was about $\pm$1 MHz. It should be noted however that these values are relative to the lock frequency reference value provided by the Fabry Perot interferometer in the reference channel. It has been observed that this drifts with time at the rate of a few MHz per hour, which for the experiments described in this thesis was not a problem. Further details on frequency tuning and single frequency operation can be found in the Coherent CR699-21 model ring dye laser manual.

Most of the holeburning experiments described in this thesis were done by detecting the changes in the emission level in the phonon sideband. One laser holeburning in the case of the CaO:F centre was straight forward as all the manipulations of the laser frequency were available on the commercial

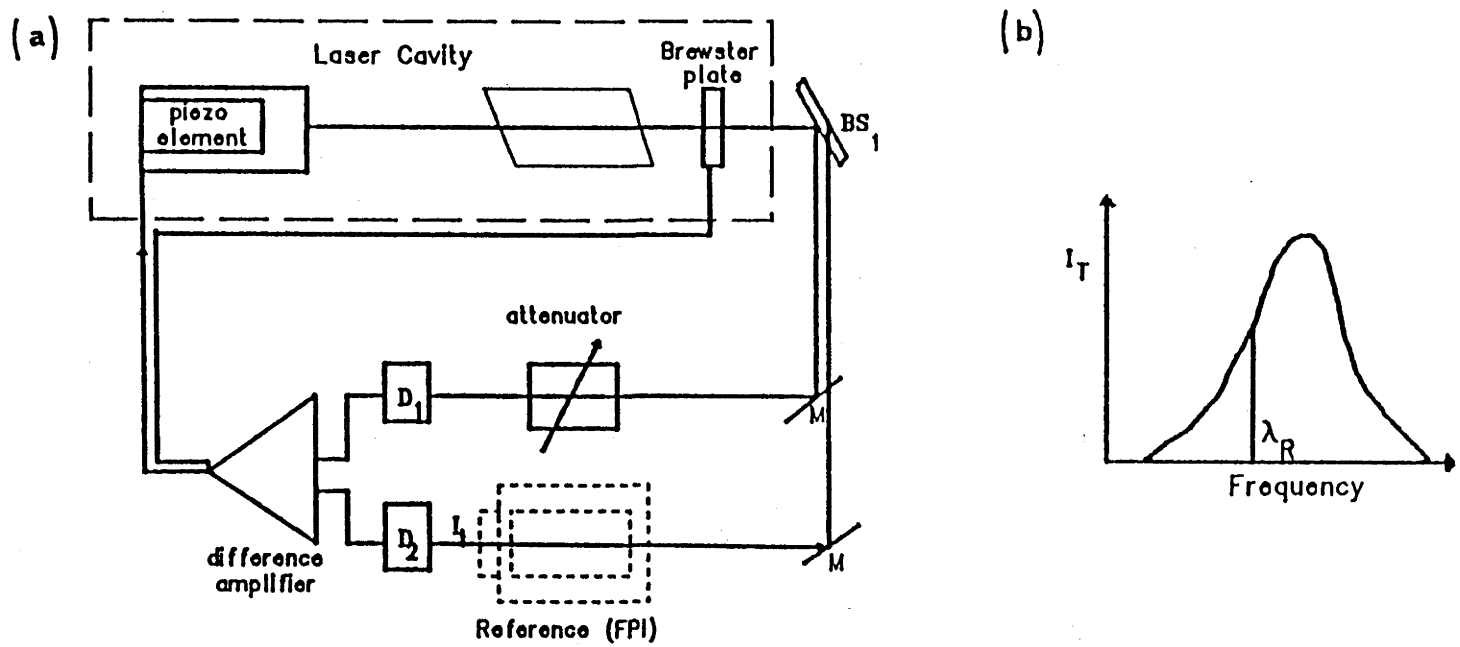

Figure 2.1 Schematic of the frequency stabilisation servo loop used in CR 699-21 and CR599-21 high resolution lasers (a) and proper choice of λ_R for the servo loop to be effective (b).

unit. The laser can be scanned by a preset amount between 0.01 and 30 GHz and can be stopped at any frequency within the range (to burn a hole). Since the absorption in the zero-phonon line is very weak it was advantageous to be as close to the peak of absorption as possible. The peak of the absorption line was located by tuning the birefringent filter to the absorption line and then using the thin etalon offset to fine tune at the peak of the absorption.

In the case of diamond where two separate lasers were used to burn and read the holeburning spectrum, it was necessary to tune both the lasers to the same frequency. Here and in the rest of the thesis, in a two laser experiment the laser whose frequency is fixed is referred to as the burn laser and the one whose frequency is scanned about the burn laser frequency is referred to as the read laser. The method employed to tune the two lasers used in the experiment to the same optical frequency is now described. An optical multichannel analyser has been used for this purpose. The burn laser is first tuned to within the zero-phonon line. A part of the burn laser light was focussed onto the input slit of a monochromator (3/4 metre Spex model 1732, resolution 12 A/mm). The monochromatic laser light gives one spectral line on the focal plane of the spectrometer. A vidicon (silicon diode array camera) tube is mounted at the exit slit of the monochromator such that the diode array is in the focal plane of the spectrometer. The video signal containing all the information about the spectrum ($\sim$180 A wide with silicon diode array width of 1.5 cms) projected onto the vidicon is processed and accumulated using an Optical Multi Channel Analyser (OMA). The output of the OMA is then used to obtain a electronic display of this laser line on an oscilloscope (X-position and Y-intensity). Since a broad spectrum ($\sim$180 A) can be recorded simultaneously the monochromator is used in a non scanning mode. After adjusting the monochromator to give an image due to burn laser at the centre of the OMA display, the frequency of the read laser was adjusted using the birefringent filter and the thin etalon offset to give an image due to the read laser as close as possible to the image due to the burn laser. More accurate frequency tuning involved the experiment itself. The read laser was then scanned in frequency while monitoring fluorescence (total light excited by both lasers) from the sample. The thin etalon offset on the read laser usually required further adjustment for the holeburning spectrum from the diamond to be detected. Apart from a coincidence in frequency, to get good signal to noise ratio it is also necessary that the read laser probes only the centres excited by the burn laser. This was most easily achieved by making the the burn laser beam diameter larger than the

read laser beam diameter. Typically the burn laser beam diameter at the diamond was 2 mm and that of the read laser was 1 mm.

2.2 CRYOSTATS

A split coil superconducting magnet cryostat (Oxford Instruments Ltd., England) was used for magnetic circular dichroism and Zeeman measurements at low temperatures. This is capable of providing magnetic fields of up to 5 Tesla. The sample sits at the centre of the bore of the superconducting coil and is cooled by helium exchange gas, which is in thermal contact with the liquid helium reservoir. The cryostat has two pairs of windows parallel and perpendicular to the bore of the coil so that both axial and transverse Zeeman measurements are possible. For experiments where a magnetic field was not necessary, a smaller home made glass metal hybrid cryostat was used. This was an immersion type cryostat where the sample is directly in contact with liquid helium. In this case however, to avoid noise in the spectrum due to boiling helium it was necessary to pump over the liquid helium surface which lowered the temperature to 1.6 K.

2.3 MAGNETIC CIRCULAR DICHROISM

Differential absorption of left and right circularly polarised light is known as circular dichroism. While circular dichroism is exhibited naturally by dissymetric molecules it can be induced in all matter by a longitudinal magnetic field. Since it is advantageous to have strong magnetic fields, these measurements are usually carried out in superconducting magnetic cryostats. The experimental set up for measuring the Magnetic Circular Dichroism (MCD) of a sample is described below. A monochromatic beam of light emerging from a monochromator is linearly polarised using a polariser. The linearly polarised light then passes through a photoelastic modulator (PEM). The PEM works on the principle of photoelastic effect (Kemp, 1969). An oscillating mechanical strain is sustained in a transparent optical element at a frequency of 50 kHz by applying an ac voltage, creating a periodic birefringence; the optical element acting as an oscillating wave plate. The relative

retardation between the two polarisation components can be varied by adjusting the voltage applied and it varies periodically between positive and negative values. In the MCD experiment the retardation is quarter wave. Thus, the PEM converts linearly polarised light alternately into left and right circularly polarised light. The modulated light beam passes through the sample placed in a cryostat and is focussed onto a detector (Photomultiplier tube). The signal from the detector consists of a dc- component and a small ac- component. The ratio of the ac- and dc- components is proportional to the difference in absorption of the left and right circularly polarised light (i.e. MCD). In practice, the magnitude of the dc- component is kept constant and the signal is rectified in a lock-in amplifier which gives a dc voltage proportional to the ac-component. The dc- voltage from the lock-in amplifier is proportional to the MCD. The MCD experiment consists of obtaining the MCD signal as a function of wavelength in the required wavelength region.

2.4 MICROWAVE EQUIPMENT

The microwave resonance experiments in diamond were done using a Hewlett Packard microwave oscillator (Model 572) with a power output of few milliwatts and tunable between 2 and 4 GHz. The scan width about any frequency could be set by specifying scan range of upto 10% of the central frequency. In our experiments this was the commonly used mode. The microwave power was then amplified using a Hewlett Packard (Model 491C) TWTA amplifier with a maximum output power of 1 watt. The microwave cavity consisted of two copper plates with the sample between them. No attempt was made to improve the Q factor of the cavity. This was not necessary as it was observed that increasing the microwave power does not increase the holefilling signal in the experiment. The microwave transmission line was terminated in a 50 ohm non-inductive load.

2.5 AUXILLARY EQUIPMENT

Apart from what has been described above some other equipment was also used viz. Acousto-optic modulators, pulse generators, photomultipliers and mechanical choppers. These are described at appropriate place later in the thesis.

REFERENCES

1) Harley R. T. , Henderson M. J. and Macfarlane R. M.
J. Phys. C: Solid state physics, 17, L233 (1984)

2) Kemp J.C.
J. Opt. Soc. Am. , 59, 950 (1969)

Chapter 3

HOLEBURNING IN CaO:F CENTRE

3.1 INTRODUCTION

Calcium oxide has the rocksalt crystal structure with two atoms per unit cell. This structure consists of two interpenetrating face centered cubic sublattices. The anions and cations are arranged alternately along the $< 100 >$ directions and the $\{111\}$ planes are alternately composed entirely of anions or cations. Thus each anion (cation) is surrounded by six cations (anions) in octahedral arrangement. The F centre in CaO comprises of two electrons localised by the net positive charge of the missing anion (oxygen). It can be produced by irradiating with high energy (> 1MeV) neutrons to a dose of 10^{16}-10^{18} nvt. Alternatively, these centres can also be produced by additive colouration (metal vapour treatment) techniques. The second method is used in the present study and is described later in this chapter.

The F centre in CaO is a charge neutral centre and has an obvious analogy to the helium atom. In the ground state both the electrons are in the 1s orbit forming the ^1S state which transforms as the irreducible representation $^1A_{1g}$ in O_h symmetry. Excited state configurations (1s)(2s) and (1s)(2p) will form singlet and triplet states ^1S, ^3S and ^1P, ^3P respectively. These atomic states transform as $^1A_{1g}$, $^3A_{2u}$, $^1T_{1u}$ and $^3T_{1u}$ in O_h symmetry. Transitions from the $^1A_{1g}$ to $^3A_{2u}$ and $^3T_{1u}$ are forbidden by spin selection rules. The $^1A_{1g} \rightarrow {}^1T_{1u}$ spin allowed transition occurs at 400 nm (Henderson *et al*,

1969, 1972, Modine, 1973). Emission following this excitation however, occurs from the $^3T_{1u}$ state, the $^3T_{1u} \rightarrow {}^1A_{1g}$ transition being made allowed by spin-orbit mixing between the $^1T_{1u}$ and the $^3T_{1u}$ states. This emission due to the $^3T_{1u} \rightarrow {}^1A_{1g}$ transition peaks at 600 nm and has a prominent zero-phonon line in the emission spectrum at 574.2 nm. The emission spectrum shown in figure 3.1 was obtained using the 514.5 nm line of argon ion laser as the excitation source. The energy level diagram of this centre is shown in figure 3.2 . The other sharp peak (at 571 nm) shown in figure 3.1 is the zero-phonon line of the F_2 centre and is discussed in chapter 5. The $^3T_{1u}$ state has a lifetime of 3 msecs at 4.2 K (Henderson *et al*, 1969) consistent with an oscillator strength of $5\text{x}10^{-7}$. This f value is in accordance with that expected for a spin forbidden transition. The line (~150 GHz halfwidth) is inhomogeneously broadened. In this chapter it is shown that narrow spectral holes can be burned in the absorption profile and used as high resolution probes of the $^1A_{1g} \rightarrow {}^3T_{1u}$ transition. Since the lifetime of the optical hole was of the order of hours, it was possible to use the same laser both to burn and probe the optical hole.

3.2 EXPERIMENTAL

3.2.1 EXPERIMENTAL EQUIPMENT

Zeeman experiments utilised the Oxford Instruments Ltd. superconducting magnet cryostat. The magnet was capable of providing magnetic fields of upto 5 Tesla. The voltage drop across a resistor in the magnet power supply is calibrated to give the strength of the magnetic field in the cryostat. Electric field experiments were performed using a conventional set up where the crystal is held between two copper plates that also serve as electrodes. In this arrangement light propagates in a direction perpendicular to the electric field. A thin layer of indium metal was placed between the crystal and the copper plates to ensure that the electric field was applied uniformly across the crystal surface.

For studying the effect of temperature on the optical hole the sample was placed in a hole in the copper block on the sample rod and packed with indium metal to ensure good thermal contact between the crystal and

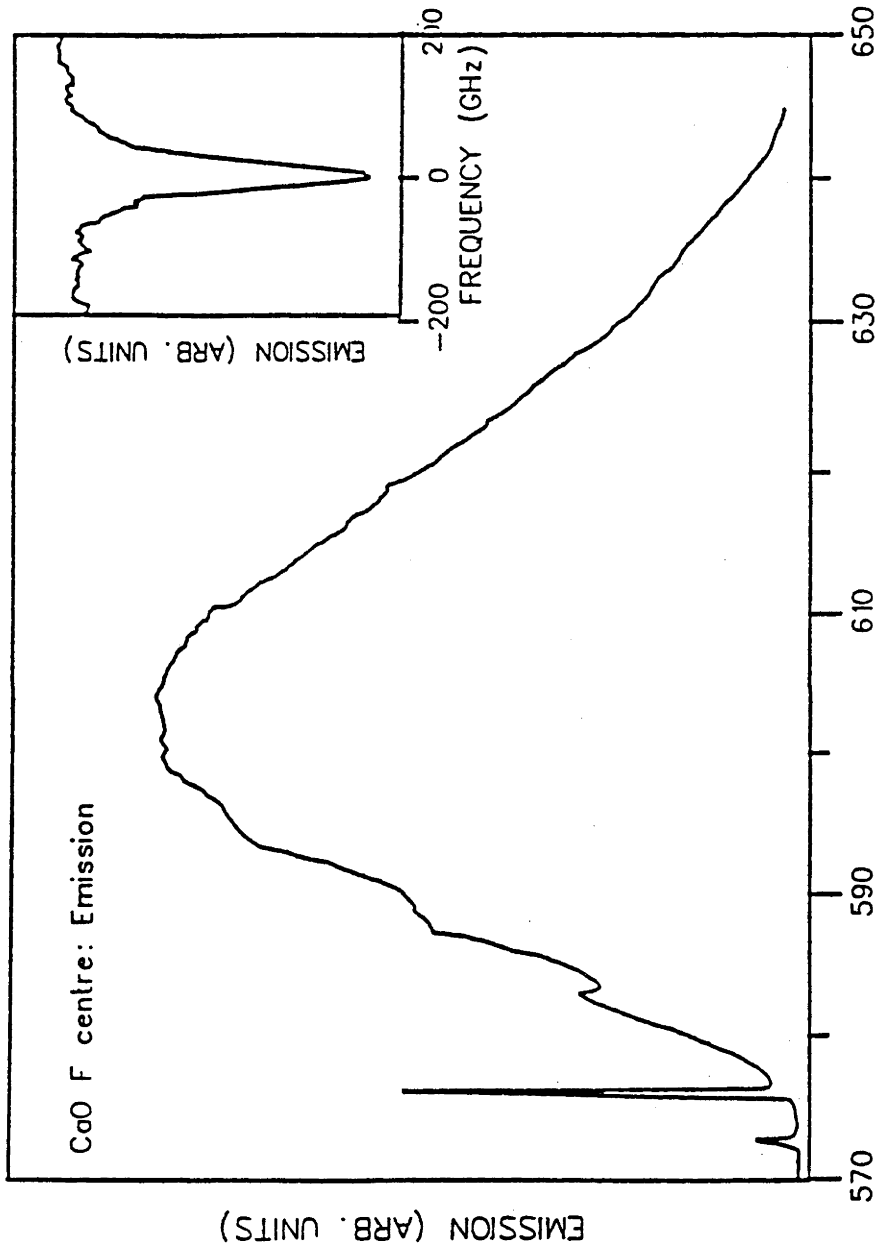

Figure 3.1 Luminescence spectrum of the F centre in CaO at 4.2 K. Luminescence was excited using a Ar^+-ion laser at 514.5 nm. Inset shows the optical hole burnt in the F centre zero phonon line.

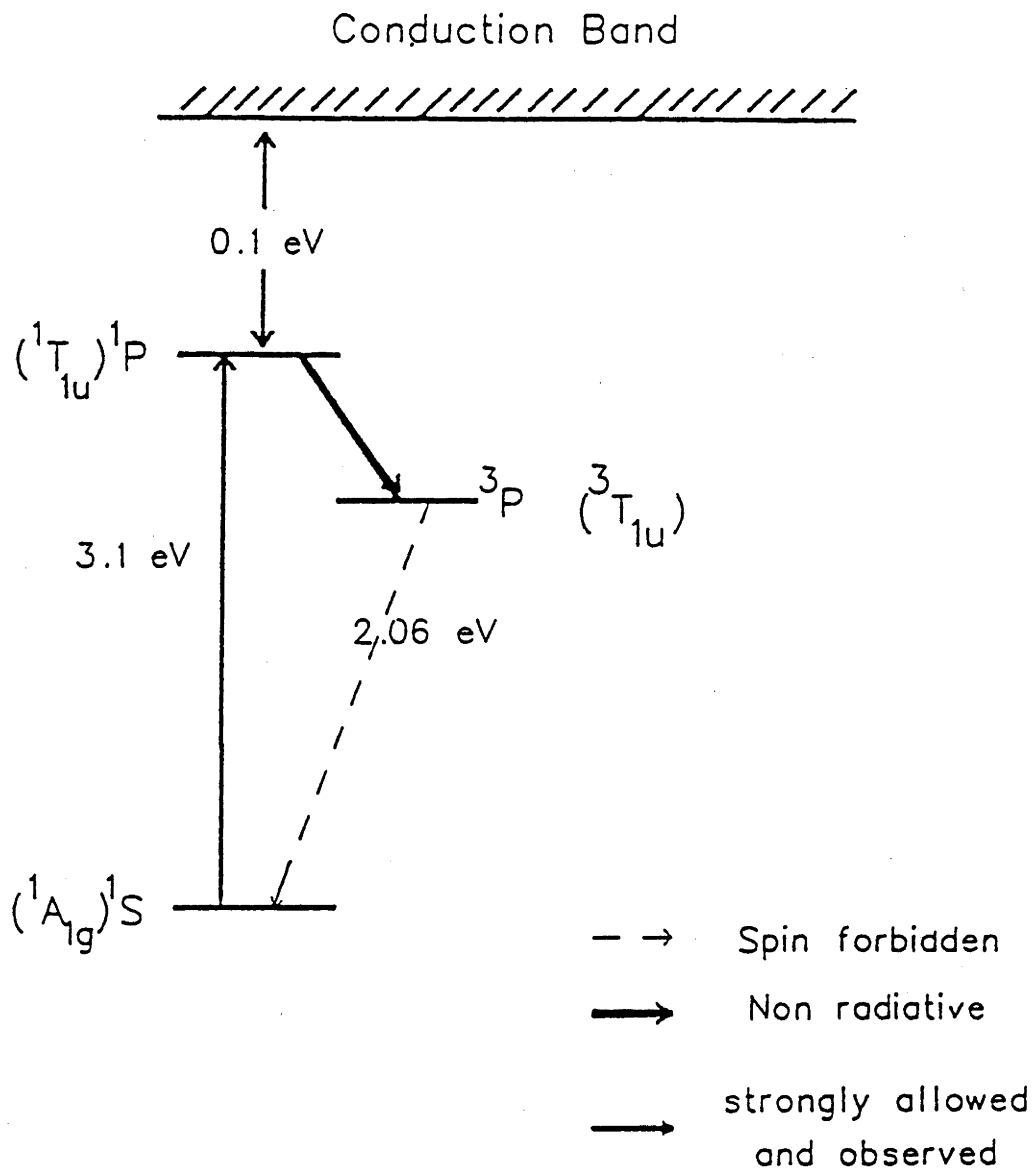

Figure 3.2 Energy level diagram of the CaO:F centre.

the copper block. In order to be able to vary the temperature, the sample space was evacuated before cooling the cryostat and filled with helium gas to a pressure of a few torr. It was then possible to vary the temperature between ~5K and 50K using a heater coil situated next to the sample. The sample temperature was measured using a Allen Bradley carbon resistor in the copper block 2 mm from the sample.

3.2.2 SAMPLE PREPARATION

Single crystals used in the present study grown by arc fusion method, were obtained from W.C.Spicer in boule form. Yellow coloured pieces were cleaved from the boules. As grown CaO crystals have in general a sufficient concentration of F centres to show a characteristic emission band with a peak at 600 nm when exciting with blue light. Weak emission could be detected when pumping in the zero-phonon line at 574.2 nm. No permanent holeburning effects could be observed in these crystals. The single crystals were irradiated to dose of 10^{18} nvt neutrons of energy greater than 1 MeV at the Australian Atomic Energy Commission neutron irradiation facility at Lucas Heights, Sydney. This did not result in any increase in the holeburning characteristic. As the heavily neutron irradiated crystals were radioactive for several weeks after irradiation no further experiments were attempted on them.

All the crystals used in the present study were additively coloured in calcium vapour following the method by Johnson *et al* (1969). The yellow coloured crystals were sealed at one end of a tantalum tube (3mm diameter) together with a small quantity of calcium metal at the opposite end. The tantalum tube was evacuated to a pressure of 10^{-4} torr and sealed. This was then heated in an r.f. furnace for 30 minutes. The temperature of the crystal end of the tube was 1900 K while that at the metal end was about 1500 K generating a calcium vapour pressure of ~100 torr inside the tube. The calcium atoms from the vapour attach themselves to the crystal surface (extend the crystal lattice) forming anion (oxygen) vacancies. These vacancies then diffuse into the bulk of the crystal. Since calcium atom enters the lattice as a divalent ion, each atom attaching itself to the crystal gives up two electrons on ionisation. In pure crystals the electrons are trapped at the anion vacancies forming the F centres. However, if the crystals are

impure (which is more often the case) the electrons could be trapped at some ionised impurities (e.g. Fe^{3+}, V^{3+} etc). This could then result in lesser number of F centres being formed. The calcium vapour treatment usually resulted in greenish yellow coloured crystals. The F centre emission was only marginally stronger but the crystals then did exhibit weak permanent holeburning effects.

3.2.3 X-IRRADIATION

Some enhancement in the holeburning characteristic was achieved with X-irradiation at room temperature. The crystals were irradiated for several hours using molybdenum radiation from an X-ray generator operated at 40 kV and 30 ma. While the hole depth in freshly prepared (but not X-irradiated) crystals was less than 10% of the zero phonon absorption line, hole depth in X-irradiated crystals was as high as 60%. The process of X-irradiation appears to ionise impurities and thus make more electron traps available for photochemical holeburning. The depth of the hole decreases with crystal usage as lesser number of electron traps are available for causing photochemical change in the F centre. However, this process of regenerating the holeburning characteristic using X-irradiation could not be repeated indefinitely and consequently each sample prepared could only be used to obtain about 10 experimental traces. This point is discussed in section 3.7 .

3.2.4 HOLEBURNING EXPERIMENT

For CaO:F centre, the holeburning measurements were performed using the high resolution tunable ring dye laser (CR699-21). The holeburning experiment was performed as follows. The laser frequency tuned to the zero-phonon line at 574.2 nm excited emission similar to that shown in figure 3.1. However, since the zero-phonon transition is spin forbidden, absorption at the zero-phonon wavelength is very weak. Correspondingly, the emission excited was weak. The emission level in the phonon sideband is directly proportional to the amount of absorption at the laser frequency. The weak absorption at the laser frequency (within the zero-phonon line) made it necessary to use most of the fluorescence that was excited in order to be able to

monitor the changes absorption at laser frequency. Since using a monochromator (to avoid laser frequency) implied a reduction of the already weak signal, this was avoided. Instead all the light from the sample was focussed onto a photomultiplier tube and a Corning glass filter (cutoff wavelength = 600 nm) was used to prevent the laser scatter (from the sample) being detected. Care was taken to ensure that no other light was detected by the photomultiplier tube. The resulting signal though weak was usable for experimental purposes.

In the majority of the studies the hole was burned with 50 mw of laser light tuned to the centre of the zero-phonon line for about 10 secs. The hole lifetime was several hours and it could be detected by scanning the laser about the burn frequency. To obtain a good signal to noise ratio the traces were averaged over several (typically 40) scans using a Princeton Applied Reseach signal averager (Model no. 4202). To minimise the holeburning effects during the reading process the laser power was attenuated by a factor 100. For a crystal temperature of < 5 K the halfwidth of the hole was of about 100 MHz (inset in figure 3.1). It was observed that the holewidth was dependent on the power of the burn laser and burning with lower powers resulted in shallower but narrow holes. For example, when burning with the laser attenuated by a factor 100 for 300 seconds the holewidth was 40 MHz. In this case however, since the signal to noise ratio was poor more averaging was required and this method was not satisfactory for perturbation measurements where the hole was split into several components. It should be noted that as in the case of many other colour centres, the holewidth is far greater than the homogeneous width of the transition.

3.3 JAHN TELLER STUDIES OF THE F CENTRE IN CaO

Optically detected EPR was observed in the excited $^3T_{1u}$ state of this centre by Edel *et al* (1972). The microwave frequency was set at 23 GHz and the angular variation of the EPR spectrum was studied by rotating the magnetic field in the {100} plane. The spectra showed the existence of three equivalent

tetragonal sites and the spectra could be fitted to the spin Hamiltonian

$$H = \beta.H.g.S + D\{S_z^2 - \frac{1}{3}S(S+1)\}$$

where S=1, $g_\perp = 1.998$, $g_{||} = 1.9991$ and $D = 603 \pm 2$ G. i.e. the orbital degeneracy of the T_{1u} state is partially lifted. This could happen due to the coupling of this state to lattice vibrations (Jahn-Teller effect) and/or due to static crystal field (of tetragonal symmetry) due to impurities at one of the nearest neighbour sites. The second possibility was ruled out since absorption and emission spectra are sample independent and Stark effect measurements showed that this centre is centrosymmetric (Gelineau *et al*, 1973). Hence, the observed tetragonal symmetry was interpreted as arising from a strong static Jahn-Teller effect in the $^3T_{1u}$ state. Only coupling to the E_g modes of vibration will reduce the symmetry from cubic to tetragonal.

The treatment of the vibronic problem given below closely follows that of Ham (1965). Neglecting the effects associated with spin, the vibronic Hamiltonian describing the interaction with a single pair of E_g vibrational modes, can be written as

$$H_{vib} = E_0 + H_{clus} + H_{int}$$

where E_0 is the energy of the $^3T_{1u}$ state before the Jahn-Teller effect is considered, H_{int} is the dynamic interaction between the centre and its surrounding ions and H_{clus} is the sum of the potential and kinetic energies of the centre and its surrounding ions. Assuming that the $^3T_{1u}$ state is linearly coupled to a single pair of vibrational modes (Q_θ,Q_ϵ) belonging to the irreducible representation E_g of the point group O_h, the total Hamiltonian describing the vibronic system can be written as

$$H_{vib} = E_0 I + \frac{1}{2\mu}\{P_\theta^2 + P_\epsilon^2 + \mu^2\omega^2(Q_\theta^2 + Q_\epsilon^2)\}I + V_E\{Q_\theta E_\theta + Q_\epsilon E_\epsilon\} \quad (1)$$

Here P_θ, P_ϵ are the momenta conjugate to Q_θ, Q_ϵ; μ is the effective mass associated with the E_g vibrational mode, ω is its angular frequency and V_E is the Jahn-Teller coupling coefficient. The energy of the $^3T_{1u}$ state before the Jahn-Teller interaction is considered is denoted by E_0. The values of E_θ

and E_ϵ in a X, Y and Z basis are

$$\begin{vmatrix} +1/2 & 0 & 0 \\ 0 & +1/2 & 0 \\ 0 & 0 & -1 \end{vmatrix} \quad \text{and} \quad \begin{vmatrix} -\sqrt{3}/2 & 0 & 0 \\ 0 & +\sqrt{3}/2 & 0 \\ 0 & 0 & 0 \end{vmatrix}$$

respectively and I is the unit matrix.

The vibronic eigenfunctions (solutions to the vibronic Hamiltonian) are products of one of the orbital states $|\ \beta >$, $|\ \beta >=$ X, Y or Z and a vibrational state $|\ \chi_\beta, n_\theta, n_\epsilon >$

$$i.e.\ \ |\ \beta, n_\theta, n_\epsilon >= |\ \beta > |\ \chi_\beta, n_\theta, n_\epsilon >$$

$|\ \chi_\beta, n_\theta, n_\epsilon >$ is an eigenstate of a displaced two dimensional harmonic (Q_θ, Q_ϵ) oscillator. The value of equilibrium displacement can be obtained by minimising the total energy (vibronic Hamiltonian) with respect to the displacement parameter Q. For example, applying the vibronic hamiltonian to the vibronic wavefunction $|\ Z >|\ \chi_Z, n_\theta, n_\epsilon >$ we obtain the values of Q_θ and Q_ϵ as $\left(\frac{V_E}{\mu\omega^2}\right)$ and 0 respectively. The equilibrium positions for the other two vibronic wavefunctions are

$$Q_{\theta\beta} = \frac{-V_E e_{\theta\beta}}{\mu\omega^2} \quad \text{and} \quad Q_{\epsilon\beta} = \frac{-V_E e_{\epsilon\beta}}{\mu\omega^2} \qquad (2)$$

where $e_{\theta\beta}$ and $e_{\epsilon\beta}$ are the appropriate diagonal components of the matrices E_θ and E_ϵ. The potential energy surfaces V(Q_θ, Q_ϵ) associated with the T_{1u} state are shown in figure 3.3 (a).

The explicit form of the vibrational eigenstate $|\ \chi_\beta, n_\theta, n_\epsilon >$ is

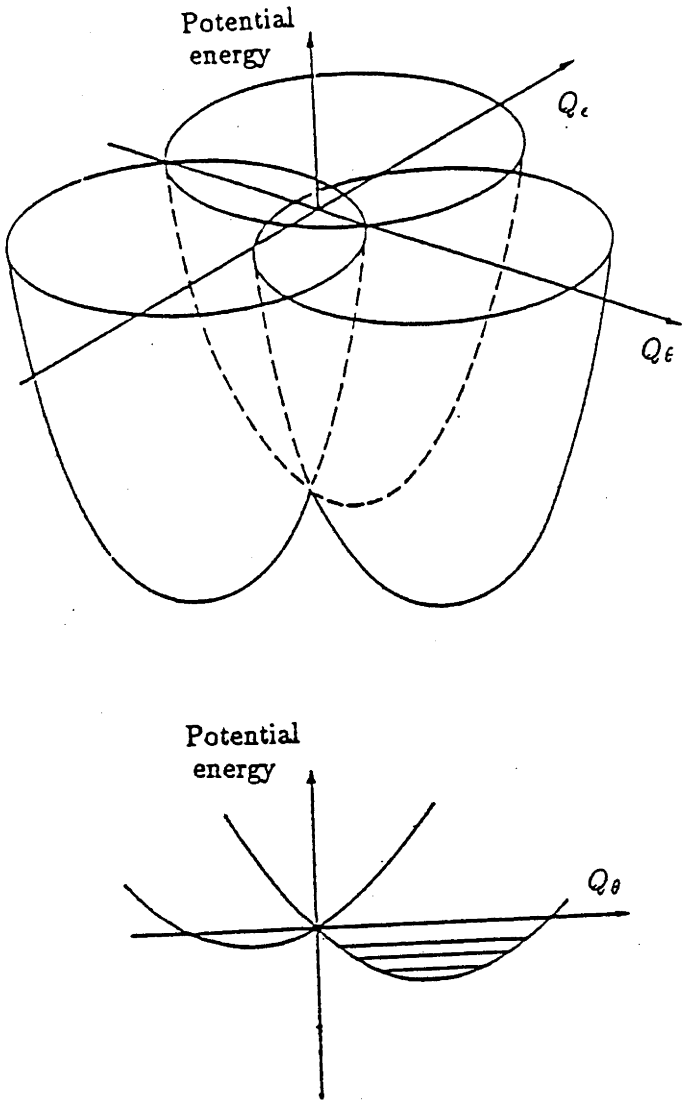

Figure 3.3 Potential energy surfaces $V(Q_\theta, Q_\epsilon)$ associated with the T_{1u} state that is coupled to an E_g mode of vibration (a) and a section of the potential energy surfaces along the Q_θ coordinate.

$$F_{n\theta}(Q_\theta - Q_{\theta\beta})F_{n\epsilon}(Q_\epsilon - Q_{\epsilon\beta})$$

where $F_{n\theta}$, $F_{n\epsilon}$ are the quantum states of one dimensional harmonic oscillators. F_n(y) is defined by the generating relation

$$exp(-S^2 + 2S\alpha y - \frac{1}{2}\alpha^2 y^2) = \pi^{\frac{1}{4}}\alpha^{-\frac{1}{2}} \sum_{n=0}^{\infty} \frac{F_n(y)}{(n!)^{1/2}}(S\sqrt{2})^n$$

with

$$\alpha = \left(\frac{\mu\omega}{\hbar}\right)^{1/2}.$$

The energy of a state in $\mid \beta, n_\theta, n_\epsilon >$ is

$$E_\beta, n_\theta, n_\epsilon = E_0 - E_{JT} + (n_\theta + n_\epsilon + 1)\hbar\omega$$

In the above expression E_{JT}, often known as the Jahn-Teller stabilisation energy, is the amount by which the energy of the electronic state is lowered as a result of the Jahn-Teller interaction. If the nuclear motion is neglected for the moment, the three coordinate pairs in the (Q_θ,Q_ϵ) space obtained from equation (2) above represent the stable equilibrium positions of the distorted complex with the electronic wavefunctions X, Y and Z. At each of these points the energy of the other two states is greater by an amount $3E_{JT}$. This situation is depicted in figure 3.3(b) for the Z vibronic wavefunction. It should be noted further that the vibronic wavefunction associated with the electronic functions X, Y and Z are orthogonal. i.e. the ground vibronic state (n_θ=n_ϵ=0) is still a T_{1u}.

The separation between the equilibrium positions of the three vibronic functions increases with increases in proportion to the strength of the Jahn-Teller interaction (V_E). With increasing separation (increasing V_E) the region of overlap between the *corresponding* oscillator states associated with

different electronic states is diminished. This effect is described by the overlap integral. The matrix element of any purely electronic operator between vibronic states is the product of the electronic matrix element and an overlap integral due to the vibrational part

$$< \beta, n_\theta, n_\epsilon \mid O \mid \beta, n'_\theta, n'_\epsilon >=< \beta \mid O \mid \beta >< \chi_\beta, n_\theta, n_\epsilon \mid \chi', n'_\theta, n'_\epsilon >$$

The oscillator overlap integral

$$< \chi_\beta, n_\theta, n_\epsilon \mid \chi'_\beta, n'_\theta, n'_\epsilon >= 1 \text{ for diagonal operators}$$

$$= exp(-3E_{JT}/(2\hbar\omega)) \quad \text{for off-diagonal operators}$$

The Jahn-Teller stabilisation energy (E_{JT}) can be estimated using the relation $E_{JT} = S.\hbar\omega_E$ where S is the Haung-Rhys factor and ω_E is the angular frequency of the phonon modes involved in the Jahn-Teller interaction. The value of S calculated from the fraction of intensity in the zero-phonon line (e^{-S}), is ~5.5 . From the temperature dependence of the first and second moments of the F centre emission band, the value of $\hbar\omega$ is estimated to be of the order of 200 cm^{-1} (Henderson *et al*, 1969, 1972). From this the value of E_{JT} and overlap integral $\exp(-3E_{JT}/(2\hbar\omega))$ can be calculated to be 1100 cm^{-1} and $\sim 2x10^{-4}$ respectively. Thus as a result of the Jahn-Teller interaction the orbital angular momentum is totally quenched.

Using symmetry considerations the effect of random internal strain on the F centre is considered now. Strain in a crystal lattice can be described using a second rank tensor requiring 9 components. From energy considerations it can be shown that this tensor is symmetric (i.e. $\sigma_{ij} = \sigma_{ji}$) where the suffixes run over the cube axes X,Y and Z and hence there are only six independent components (Bhagavantam, 1966). The transformation properties of these six independent tensor components are same as those of the quadratic functions X^2, Y^2, Z^2, XZ, YZ and ZX. For a centre of O_h symmetry in a cubic lattice these quadratic functions form the basis sets of the irreducible representations A_{1g}, E_g and T_{2g}. The effect of strain of different symmetries on a centre undergoing Jahn-Teller distortion is described now.

The effect of totally symmetric strain A_{1g} is not changed by the presence of Jahn-Teller interaction. The E type strain has only diagonal matrix elements in the X, Y, Z representation. i.e. it does not mix different vibronic states. The T_2 type strain however has only off-diagonal matrix elements and the magnitude of its effect depends on the amount of overlap between the vibronic wavefunctions involved. It follows, that the effect of T_2 type internal strain is reduced by exp $(\frac{-3E_{JT}}{2\hbar\omega})$ while that due to the E_g type strain is unaffected. The effect of the E_g type strain is similar to uniaxial stress along the < 100 > direction (Ham, 1965) and stabilises the F centre in one of the X, Y or Z distorted vibronic states. Since the orbital angular momentum operator has only off-diagonal matrix elements between the X, Y, Z states, the operator representing the spin-orbit interaction behaves the same way. Hence, the effect of spin-orbit interaction is quenched in first order but in second order it partially lifts the spin degeneracy of each of the three vibronic states. The major contribution to the zero field splitting of the spin states comes from the spin-spin dipolar interaction. The zero field spin splitting is 602 ± 3 G (Edel *et al*, 1972) which in frequency units is 1.8 GHz.

3.4 ZEEMAN SPECTRA

3.4.1 ZEEMAN INTERACTION

With the orbital angular momentum totally quenched the eigenstates can be approximated by the three spin projections M_S =X, Y and Z. The behaviour of these states on applying an external magnetic field can, in an X, Y, Z representation be described by the following matrix

$$\begin{vmatrix} 0 & -ig\beta H_Z & ig\beta H_Y \\ ig\beta H_Z & 0 & -ig\beta H_X \\ -ig\beta H_Y & ig\beta H_X & -D \end{vmatrix}$$

where g=2, β is the Bohr magneton, H_i denotes the magnetic field along

the direction i (i=X, Y or Z) and D is the zero field spin splitting. Since our experimental results are insensitive to the small differences in the values of $g_{||}(1.9991)$ and $g_{\perp}(1.998)$ an isotropic value of g (=2) is assumed. In the following sections it will be shown that only transitions to the spin doublet are allowed from the ground state. When a laser is tuned to resonance with this transition it burns a hole. In zero magnetic field holeburning gives one hole at the burn frequency. Subsequent application of a magnetic field splits the line as shown in figure 3.4 . The splitting of the hole represents a high resolution Zeeman spectra of the F centre transition. This is described in detail below.

3.4.2 INTENSITY MATRIX ELEMENTS

In the cubic group O_h the operator representing the electric dipole transitions has T_{1u} symmetry. Since the ground state of the F centre has A_{1g} symmetry, electric dipole transitions between the ground state and the excited $^1T_{1u}$ state are allowed both in absorption and in emission. The spin-orbit interaction (λl.s) between the $^1T_{1u}$ and the $^3T_{1u}$ states makes the spin forbidden $^1A_{1g} \rightarrow {}^3T_{1u}$ transition partially allowed. Hence, it is essentially the spin-orbit coupling between the $^3T_{1u}$ and $^3T_{1u}$ states that determines the intensities and polarisation of the transitions between the $^3T_{1u}$ and $^1A_{1g}$ states. In evaluating the matrix elements of spin-orbit interaction ($\lambda l.s$) the following points have to be remembered. a) When the F centre is in the excited state the two electrons are in the 2s and 2p orbitals and b) the operator representing the spin-orbit interaction ($\lambda l.s$) is a one electron operator. The wave functions for the $^3T_{1u}$ and $^1T_{1u}$ states are written in the form $| \, l_1 l_2 s_1 s_2 >$ where l and s represent the orbital and spin quantum states of the electrons 1 and 2 (denoted by the subscripts). When all the matrix elements are evaluated, the following are found to be non zero.

$$<^1 T_{1u}X \mid \lambda l.s \mid^3 T_{1u}Z >$$

$$<^1 T_{1u}Y \mid \lambda l.s \mid^3 T_{1u}Z >$$

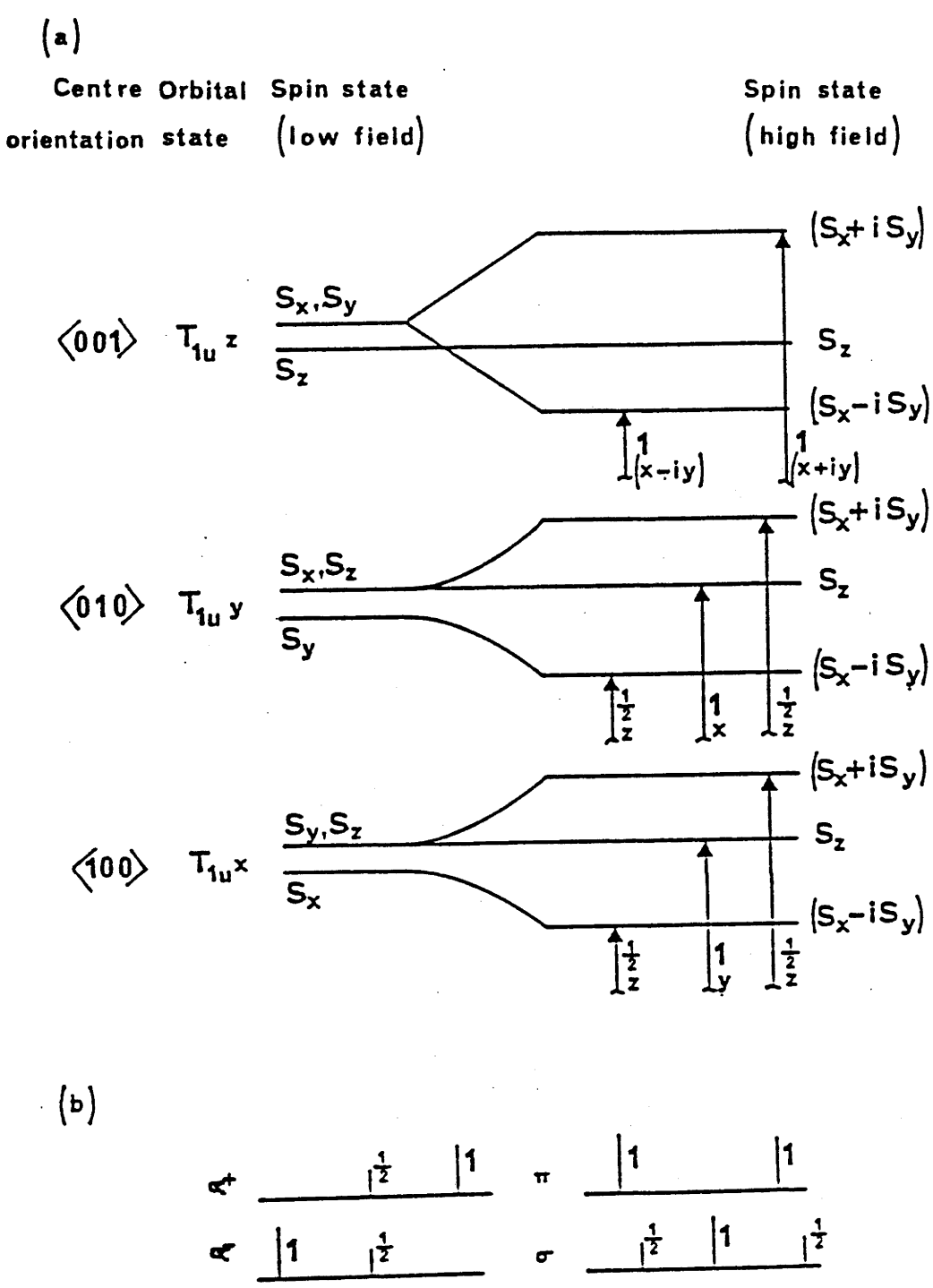

Figure 3.4 a) The splitting of the levels in a magnetic along the < 001 > direction and the predicted transitions; b)the resultant zeeman pattern in a high magnetic field.

$$<^1 T_{1u}Y \mid \lambda l.s \mid^3 T_{1u}X >$$

$$<^1 T_{1u}Z \mid \lambda l.s \mid^3 T_{1u}X >$$

$$<^1 T_{1u}Z \mid \lambda l.s \mid^3 T_{1u}Y >$$

$$<^1 T_{1u}X \mid \lambda l.s \mid^3 T_{1u}Y >$$

Internal strain stabilises the centres in one of the X, Y or Z distorted vibronic states. As mentioned previously, the spin degeneracy of this state is lifted by the second order spin-orbit interaction within the $^3T_{1u}$ manifold and the dipolar spin-spin interaction. This results in a spin doublet and a spin singlet. When the spin-orbit interaction matrix elements are evaluated it is seen that within each orbital state only transitions between the spin doublet and the ground state are allowed. In the rest of this chapter the labels X, Y, Z refer to the orbital state and x, y, z refer to the spin state.

3.4.2.1 < 001 > DISTORTED CENTRES

For centres where the distortion is along the < 001 > direction the orbital T_{1u}Z wavefunction is lowest in energy. This state is mixed via the spin-orbit interaction with the X and Y components of the $^1T_{1u}$. The components of the spin doublet can be chosen to transform in the same way as the functions $-\frac{1}{\sqrt{2}}$(x+iy) and $\frac{1}{\sqrt{2}}$(x - iy) in the cartesian coordinate system. The first function represents the M_S =1 state and the negative sign is the phase factor for wavefunctions representing positive odd values of M_S (Condon and Shortley, 1959, pp52). The operators representing the left and right circularly polarised transitions are also represented by $\frac{1}{\sqrt{2}}$(x+iy) and $\frac{1}{\sqrt{2}}$(x - iy). Since the spin-orbit interaction couples the $^3T_{1u}$Z state with X and Y

states of the ${}^1T_{1u}$ the non zero matrix elements for electric dipole transitions between the ${}^1A_{1g}$ ground state and the ${}^3T_{1u}$ excited state are of the form

$$< -\tfrac{1}{\sqrt{2}}(x+iy)|\ \tfrac{1}{\sqrt{2}}(x-iy)|\ O > \text{ and}$$

$$< \tfrac{1}{\sqrt{2}}(x-iy)|\ \tfrac{1}{\sqrt{2}}(x+iy)|\ O >$$

This predicts transitions allowed in the left and right circular polarisations respectively shown in top of figure 3.4 (a)

3.4.2.2 < 010 > AND < 100 > DISTORTED CENTRES FOR MAGNETIC FIELD ALONG < 001 >

For centres distorted along the < 010 > direction, the orbital ${}^1T_{1u}Y$ wavefunction is the lowest and the magnetic field is orthogonal to the axis of Jahn-Teller distortion. For these centres the field causes a mixing of one component of the degenerate spin state with the nondegenerate spin state while the other component of the degenerate spin state is unaffected. The wavefunctions representing the spin doublet are written as $-\frac{1}{\sqrt{2}}(x+iy)$ and 'z'. However for these centres the spin-orbit interaction couples the ${}^3T_{1u}Y$ with the X and Z states of the ${}^1T_{1u}$ state. Hence, the non zero matrix elements for electric dipole transitions are

$$< -\tfrac{1}{\sqrt{2}}(x+iz)|\tfrac{1}{\sqrt{2}}(x-iz)|\ O > \text{ and } < \tfrac{1}{\sqrt{2}}(x-iz)|\tfrac{1}{\sqrt{2}}(x+iz)\ |\ O >$$

This gives transitions only from the component of the spin doublet represented by Z. Similarly, for centres distorted along the < 100 > direction, the orbital ${}^1T_{1u}X$ wavefunction is the lowest and spin-orbit interaction couples the ${}^3T_{1u}$ X with Y and Z states of the ${}^1T_{1u}$ state. The non zero matrix elements of electric dipole transitions in this orientation are

$$< -\tfrac{1}{\sqrt{2}}(y+iz)|\tfrac{1}{\sqrt{2}}(y-iz)\ |\ O > \text{ and } < \tfrac{1}{\sqrt{2}}(y-iz)|\tfrac{1}{\sqrt{2}}(y+iz)\ |\ O >$$

This leads to selection rules in the lower part of figure 3.4 (a). The resulting intensity pattern for a Zeeman splitting are shown in figure 3.4 (b).

3.4.3 OBSERVED SPECTRA FOR < 001 > FIELD

The holes were burned with 50 mw linearly polarised laser light. Subsequently, the magnetic field is applied and the holeburning spectrum is scanned. For this a polariser is inserted in the read beam: circular in the case of axial geometry and linear in the case of transverse geometry. A Fresnel rhomb was used to convert laser light polarisation from linear to circular. When the sample is irradiated with laser light all allowed transitions resonant with laser frequency are excited. If a centre undergoes phototransformation when it is in the excited state then absorption at the laser frequency is decreased. This is the optical hole. If the holeburning is performed in the absence of any external perturbations only one hole at the laser frequency results. The other situation of holeburning in the presence of external perturbations is discussed in section 3.4.5 . In the present case only transitions between the spin doublet and the ground state are allowed. When holeburning is performed in zero magnetic field all centres that are resonant with the laser give rise to one hole at the laser frequency. As the magnetic field is turned on different centres behave differently depending on their orientation and properties. These aspects are discussed in the following sections.

3.4.3.1 AXIAL GEOMETRY

In this geometry light propagates in a direction parallel to the magnetic field. Assume that the magnetic field is along Z direction. Hence in the present case, the electric vector of light can only excite transitions that have transition moments perpendicular to the field. The dipole transition moment transforms as $\frac{1}{\sqrt{2}}(x \pm iy)$

Consider a centre distorted along < 001 > direction. As mentioned in previous subsection the only transitions that have non zero intensity are to the $M_S = \pm 1$ levels. In zero magnetic field these two levels are degenerate and it is possible to burn holes in transitions ending in these two levels. When a magnetic field is applied, these two levels split and give rise to transitions that are left and right circularly polarised. Transitions to the $M_S = 0$ level are forbidden in zero field and even in field, they can not be excited in this geometry. Hence, when the transitions are observed in circular polarisation,

the < 001 > distorted centres give only the left and right circularly polarised transitions that move symmetrically in field to low and high energies respectively (figures 3.5 and 3.6). Considering the centres distorted along < 010 >, in this geometry only transitions with dipole moments along the X direction can be excited. This level is orthogonal to the field and hence is unshifted in field giving rise to an unpolarised transition when observed in axial geometry. For the < 100 > distorted centres, only transitions with dipole moments along the Y direction can be excited. Again since this level is orthogonal to the field it is unshifted.

So, the total spectrum seen in axial geometry consists of two circularly polarised transitions due to the < 001 > distorted centres that are field dependent and two unpolarised transitions that arise from the < 010 > and < 100 > distorted centres and are field independent. The axial Zeeman spectrum is shown in figures 3.5 and 3.6 .

3.4.3.2 TRANSVERSE GEOMETRY

In this geometry light propagates in a direction perpendicular to the magnetic field direction and hence can excite and detect both σ (transitions with dipole moments perpendicular to the field) and π (transitions with dipole moments parallel to the field) transitions. Hence all the transitions mentioned in the previous subsection can be seen in σ polarisation. Further, the π transitions arising from the field dependent levels of the < 010 > and < 100 > distorted centres are seen as well. The transverse Zeeman spectrum is shown in figure 3.7 . Figure 3.7 shows the spectrum obtained in σ polarisation and figure 3.8 shows the spectrum in π polarisation.

The axial Zeeman spectrum shown in figure 3.5 and 3.6 can now be compared with the predicted behaviour from figure 3.4 (a). It can be seen that the splitting of the σ_+ and σ_- components is a linear function of the magnetic field. The observed splitting of the hole in magnetic field agrees well with that calculated using the Zeeman matrix assuming a value of g=2. The polarisation of the holes is total and the intensity ratios of the σ_+ (σ_-) and σ_x (σ_y) components is, within experimental error 2:1 as predicted.

The signal to noise ratio in the transverse Zeeman spectrum is significantly poorer than for the axial Zeeman spectra. In the experiments there

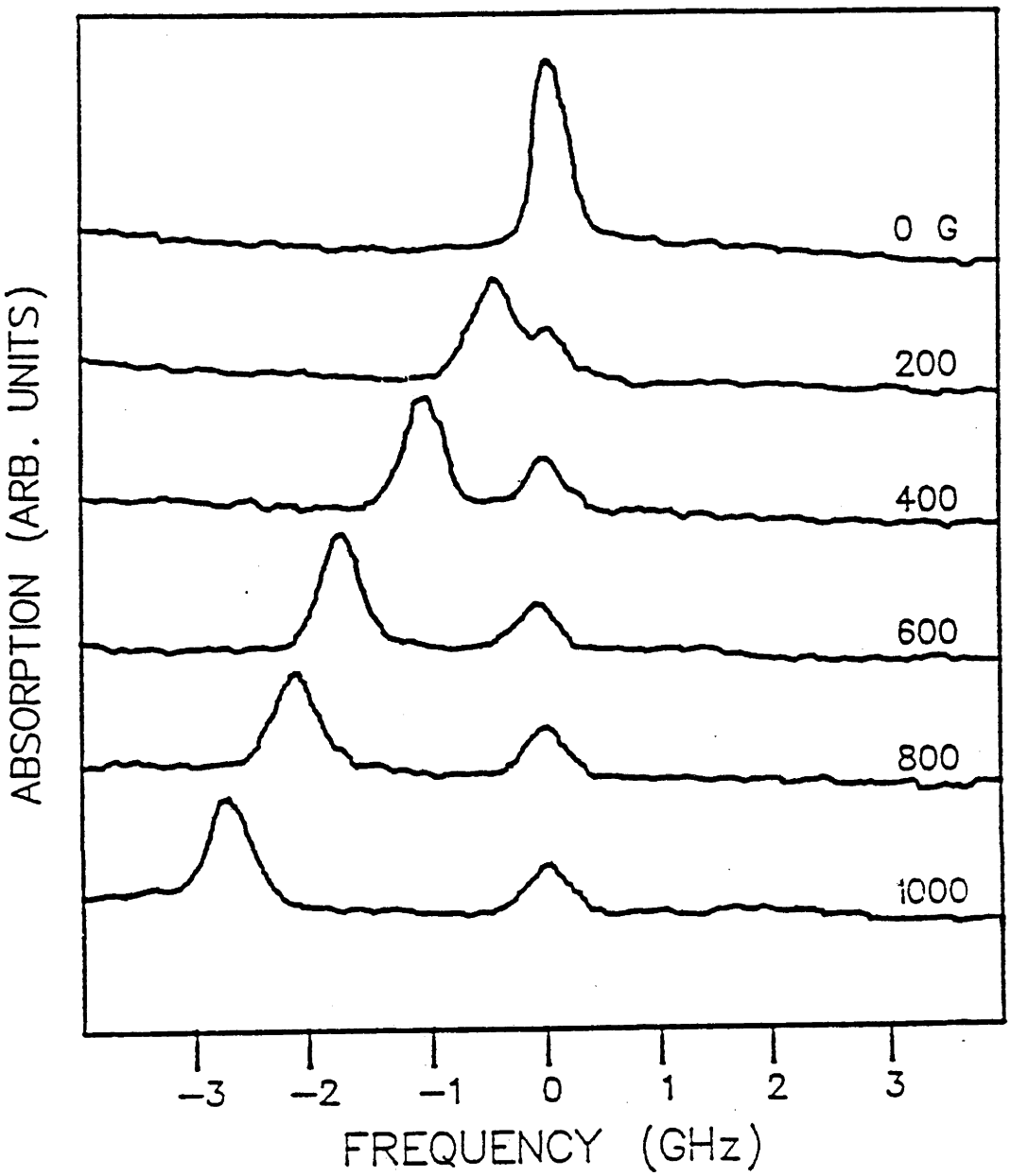

Figure 3.5 Zeeman splitting of the optical hole in the F centre zero phonon line at various magnetic field values. The laser beam is propagating along the direction of the magnetic field values. The hole was burnt with no polarisers in the laser beam. *Left* circular polariser was inserted in the laser beam while detecting the hole.

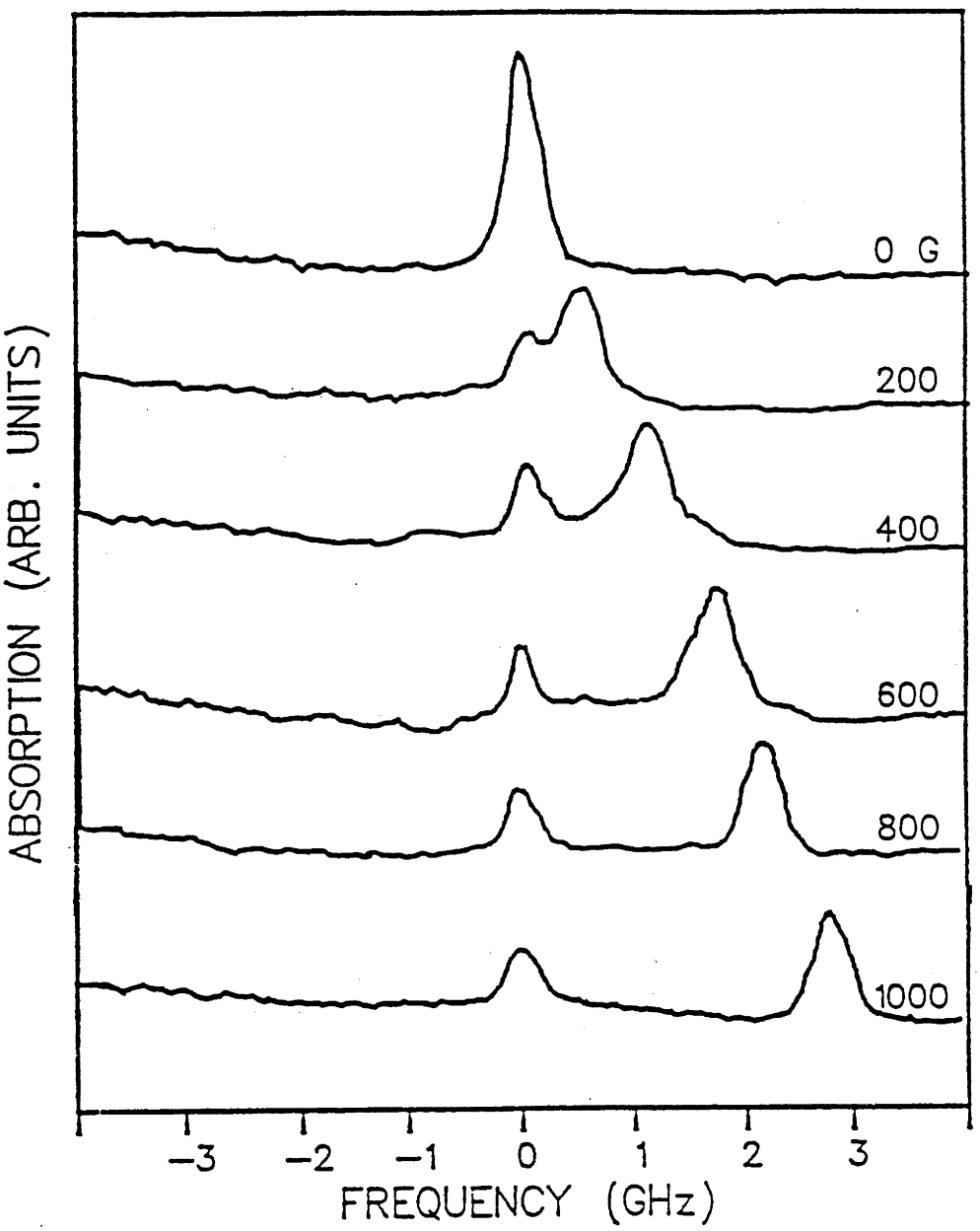

Figure 3.6 Zeeman splitting of the optical hole in the F centre zero phonon line at various magnetic field values. The laser beam is propagating along the direction of the magnetic field values. The hole was burnt with no polarisers in the laser beam. *Right* circular polariser was inserted in the laser beam while detecting the hole.

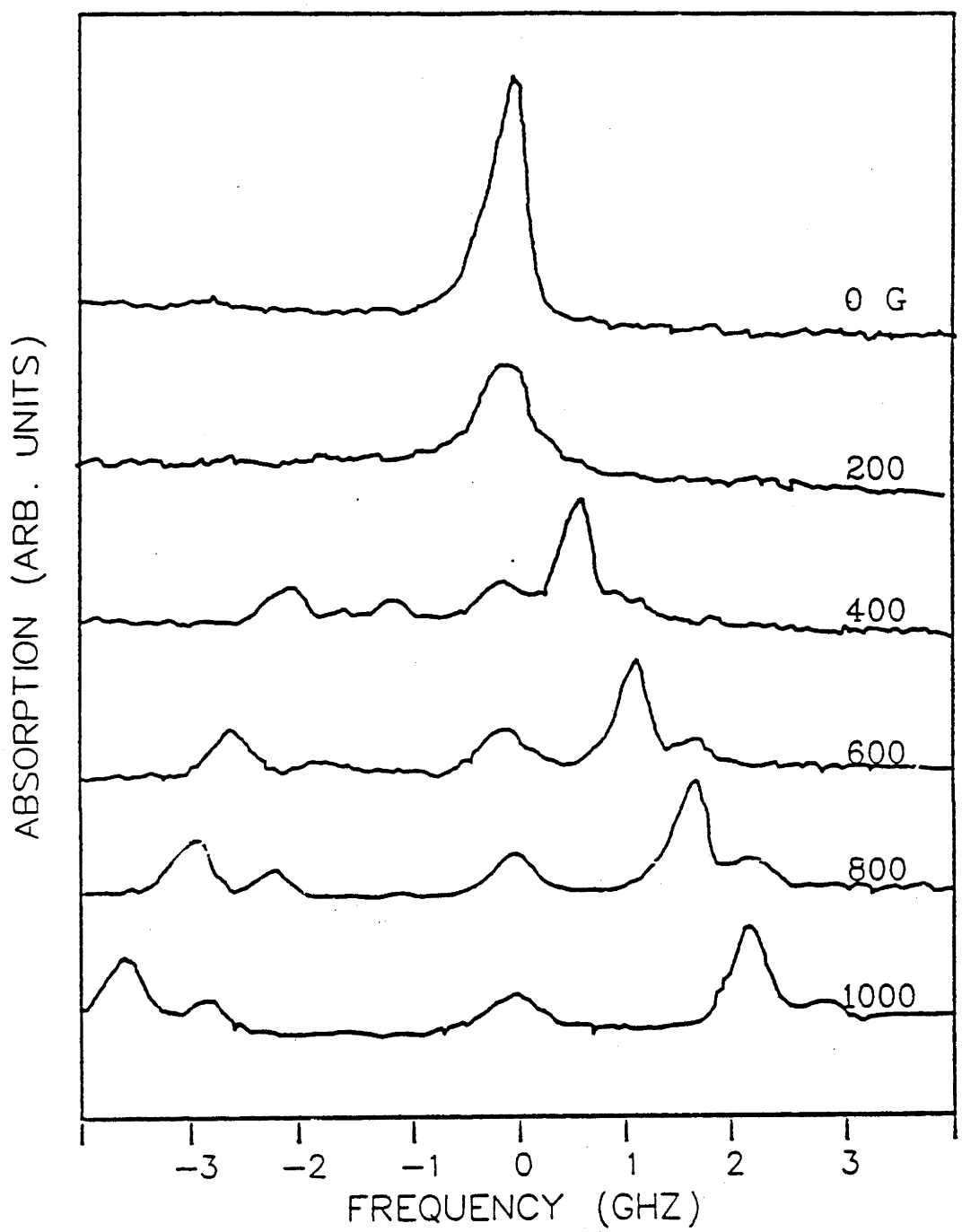

Figure 3.7 Zeeman splitting of the optical hole in the F centre zero phonon line at various magnetic field values. The laser beam is propagating perpendicular to the direction of the magnetic field values. The hole was burnt with no polarisers in the laser beam. π polariser was inserted in the laser beam while detecting the hole.

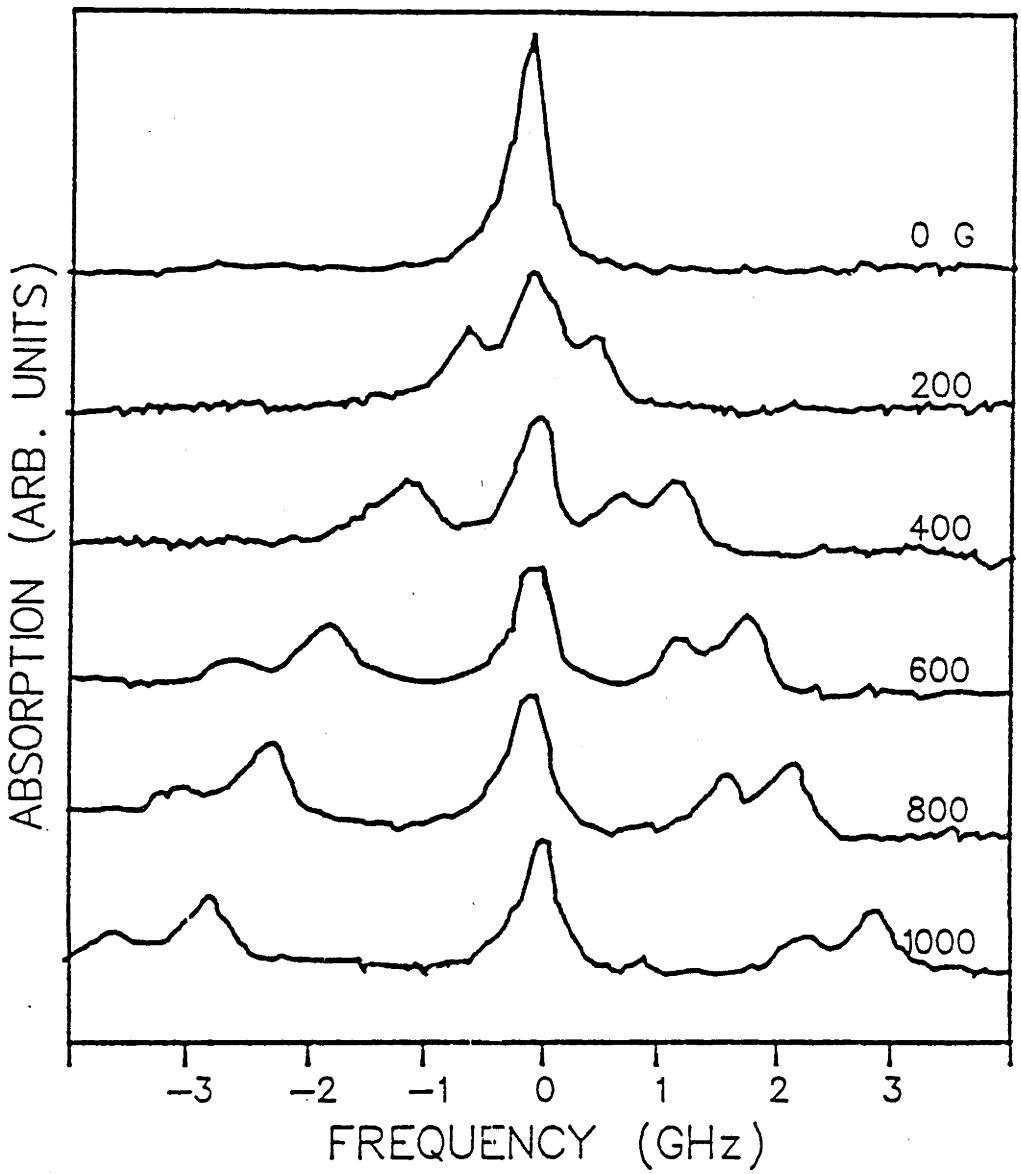

Figure 3.8 Zeeman splitting of the optical hole in the F centre zero phonon line at various magnetic field values. The laser beam is propagating perpendicular to the direction of the magnetic field values. The hole was burnt with no polarisers in the laser beam. σ polariser was inserted in the laser beam while detecting the hole.

were indications that the laser light is depolarised partially at the cryostat windows and partly at the crystal surface due to poor optical quality. Nevertheless, the selection rules given in figure 3.4 (a) give an adequate description of the strength and polarisation of the holeburning spectrum for < 001 > of the magnetic field. Although no new information is obtained in the present experiments the agreement of the experimental Zeeman spectra with those predicted by the Zeeman matrix (calculated using a g=2) confirms the observations made by Edel *et al* (1972) on these centres.

3.4.4 ZEEMAN SPLITTING FOR < 110 > FIELD

A second illustration of the Zeeman splitting of the spectral hole is shown for a magnetic field along < 110 > direction (figure 3.9(a)) although in this case no polarisation has been utilised. The hole is burned in zero magnetic field and subsequently probed at various magnetic field strengths. Any magnetic field in < 110 > direction can be resolved into two equal components along the < 100 > and the < 010 > directions. The expected splitting pattern can be calculated using the Zeeman matrix in section 3.4.2 . In this case there is only one orientation of the centre where the Jahn-Teller distortion axis is orthogonal to the magnetic field. Only one component of the spin doublet of centres in this orientation is unaffected by magnetic field and hence does not shift in field. The magnetic field variation of these centres is shown by lines marked with a * in figure 3.9(b). Since the components of the magnetic field along < 100 > and < 010 > are equal the centres distorted along these directions are equivalent and their magnetic field variation is shown by the remaining three lines in figure 3.9(b). The level marked by a + should be unaffected by field. However in our experiment it was observed that even this level shifts in field. This is due to the field being misoriented from the < 110 > direction. This error in the field direction has been calculated to be $\sim 9^{o}$ in the {110} plane. The expected splitting pattern after making allowance for this error is shown in figure 3.9(b). The high and low frequency holes are both closely spaced holes with a separation of ~200 MHz at 950 G. This 'splitting' is not resolved due to the width of the holes. According to electric dipole transition selection rules, the transition to the spin singlet level 1.8 GHz below the doublet level is forbidden at zero magnetic field. Magnetic field mixing with the doublet makes the transition to this level clearly visible for a field strength of ~500 G and for fields of ~1000 G it is

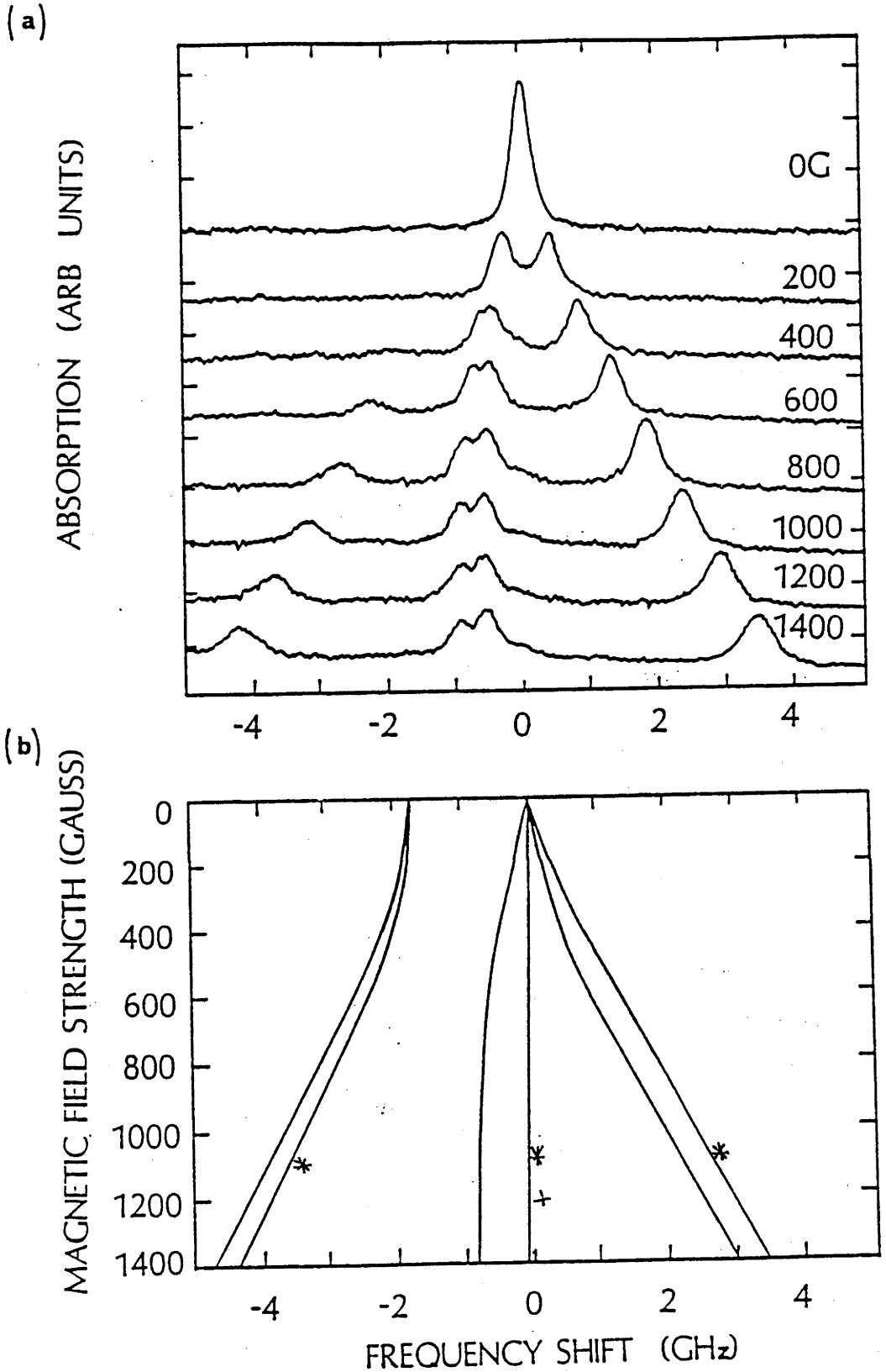

Figure 3.9 The zeeman splitting of the optical hole burned in the 574.2 nm zero phonon line for various field values (the field is aligned close to the $< 110 >$ direction) (a); predicted splitting for a field aligned 9^0 away from the $< 110 >$ direction (b).

of equivalent intensity to the other transition. This is clearly illustrated in our experiment as shown in figure 3.9(a).

3.4.5 HOLEBURNING IN THE PRESENCE OF MAGNETIC FIELD

When a hole is burned and probed in the presence of a magnetic field the observed spectra is complicated. The spectra obtained when the hole is burned in the presence of a magnetic field aligned along the $< 110 >$ direction is shown in figure 3.10 . In a magnetic field, the spin levels of any given centre are split and random strain causes each of these levels (from different centres) to come to resonance with the laser. When the field is changed these levels are shifted differently and the spectrum becomes more complex. However the spectrum can be understood with the aid of figure 3.11 where the effect of field on the energy levels pattern of any one centre (aligned along a particular Jahn-Teller axis) is shown. The traces shown are calculated using the Zeeman matrix of section 3.4.1 . When the magnetic field is along the $< 110 >$ direction the centres distorted along the $< 100 >$ and $< 010 >$ directions behave in same way. The splitting pattern due to these centres is shown in figure 3.11 (a). The splitting pattern due to the centres distorted along $< 001 >$ direction (which is orthogonal to the magnetic field direction) is shown in figure 3.11 (b). Figure 3.11 (c) shows the total splitting pattern due to the centres along $< 100 >$ and $< 010 >$, when a hole is burned in each of the spin levels labelled 1, 2 and 3 in figure 3.11 (a). Holes varying as a_1, a_2 and a_3 are due to centres in which a hole has been burned in the level labelled 1 in figure 3.11 (a). Holes varying as b_1, b_2, b_3 and c_1, c_2, c_3 are due to centres labelled in which a hole has been burned into the spin levels labelled 2 and 3 in figure 3.11 (a). Similarly, holes varying as a_4, a_5, a_6 and b_4, b_5, b_6 and c_4, c_5, c_6 are due to centres in which a hole has been burned into the spin levels labelled 4, 5 and 6 respectively in figure 3.11 (b). It should be remembered that in the presence of magnetic field, transitions to levels marked 1 and 4 in figure 3.11 (a) and (b) are made allowed due to magnetic field mixing. At lower values of magnetic field transitions to these levels become weak. The spectra shown in figure 3.10 is the sum of the splitting patterns shown in figures 3.11 (c) and (d).

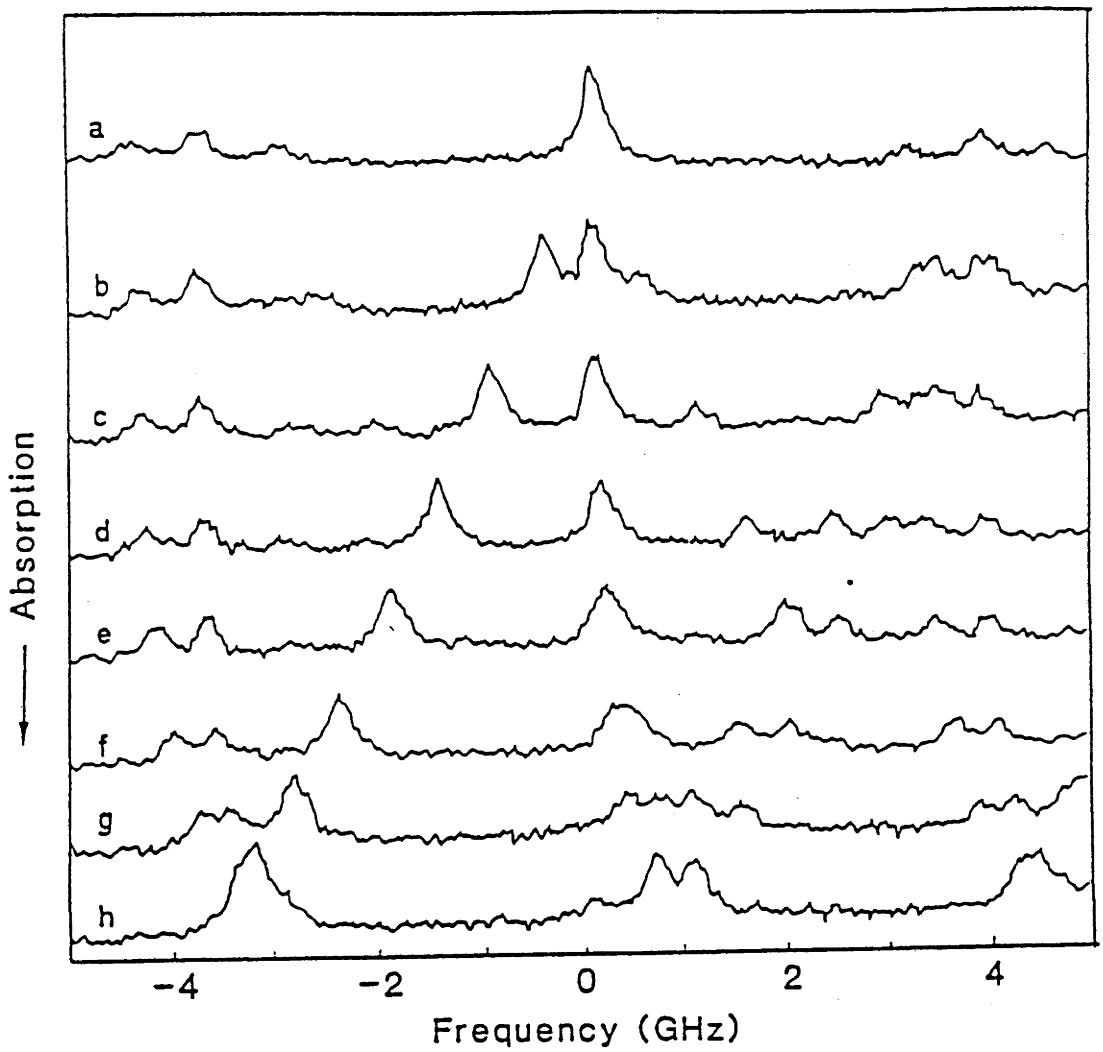

Figure 3.10 Observed zeeman spectra (unpolarised) when the optical hole is burnt in the presence of a magnetic field along the < 110 > direction. The magnetic field values are from 945 gauss (a) to 0 gauss (h) in regular steps of 135 gauss. The poor signal to noise ratio is because of the large number of components the hole is split into in the presence of a magnetic field.

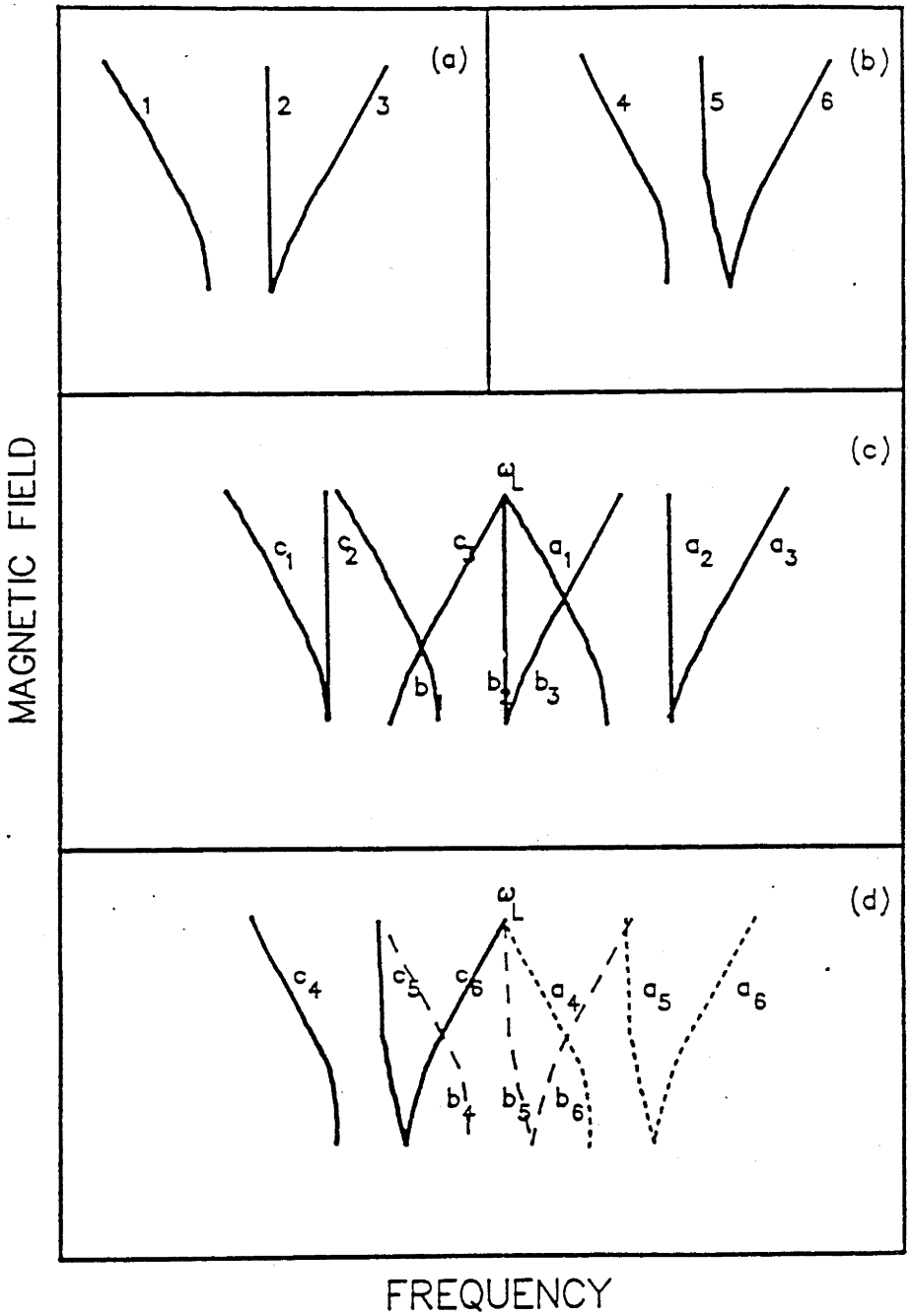

Figure 3.11 Zeeman splitting (qualitative) of the optical hole in the CaO:F centre (oriented along different directions) zero phonon line at various values of magnetic field along < 110 > direction. Centres distorted along either < 100 > or < 010 > directions (a); centres distorted along < 001 > direction (b). (c) refers to centres distorted along < 100 > (or < 010 >) directions. Holes varying as a_1, a_2 and a_3 in which a hole has been burnt in spin level labelled 1 in (a) and those varying as b_i and c_i (i=1, 2 and 3) are respectively due to centres in which a hole has been burnt in spin level labelled 2 and 3 in (a). (d) refers to centres distorted along the < 001 > direction. Holes varying as a_i, b_i and c_i (i=4,5 and 6) are respectively due to centres in which a hole has been burnt in spin level labelled 4, 5 and 6 in (b).

3.5 ELECTRIC FIELD

The effect of dc electric field on the holeburning spectra is now described. The spectra were taken with the electric field vector of the laser beam both parallel (π) and perpendicular (σ) to the dc electric field vector. In our experimental arrangement the laser beam propagated perpendicular to the dc electric field. Linear Stark effect is absent in centres with inversion symmetry but the high resolution of holeburning spectroscopy makes it possible to observe very weak higher order Stark effects. Electric fields upto 10 kV/cm were investigated and some broadening of the holes has been observed, larger in the π spectrum than in the σ spectrum as indicated in figure 3.12 . Holes were burned in zero electric field and later probed at various values of electric field. However, after removing the electric fields some broadening of the width of the hole in zero applied field was noted indicating that the electric field has caused some permanent changes to the environment of a significant proportion of the centres. This is not surprising as the holeburning effect itself causes changes in the valence of the active centre and a redistribution of charge in its neighbourhood. The electron released by the F centre is trapped at a neighbouring site but it could be moved to a more stable location upon the application of an external field. If this is the case, the electron will not return to its original trapping site when the electric field is removed and hence some change in the holeburning spectrum is expected.

A related effect has been observed by Gelineau *et al* (1973). They reported Stark measurements of the 574.2 nm zero-phonon line using ac electric fields (100 kV/cm) and observed that the signals diminished with the continual application of the fields. The values they subsequently quote are the largest values obtained for new crystals anticipating that this will minimise the effect of ageing. For a field along the $< 100 >$ direction quadratic shifts of 165±20 MHz for fields of 10 kV/cm were reported for measurements where the electric vector of the light is polarised parallel to the dc electric field. Only slightly smaller values of 123 MHz were reported for the perpendicular polarisation. Their values are not consistent with the present measurements for dc electric fields upto 10 kV/cm. At the maximum field the shift is much less than 50 MHz. Therefore, despite the use of much smaller electric field strengths an ageing effect presumably related to that observed by Gelineau *et al* (1973) has not been overcome. These effects have to be understood before further progress can be made in interpreting the small electric field effects.

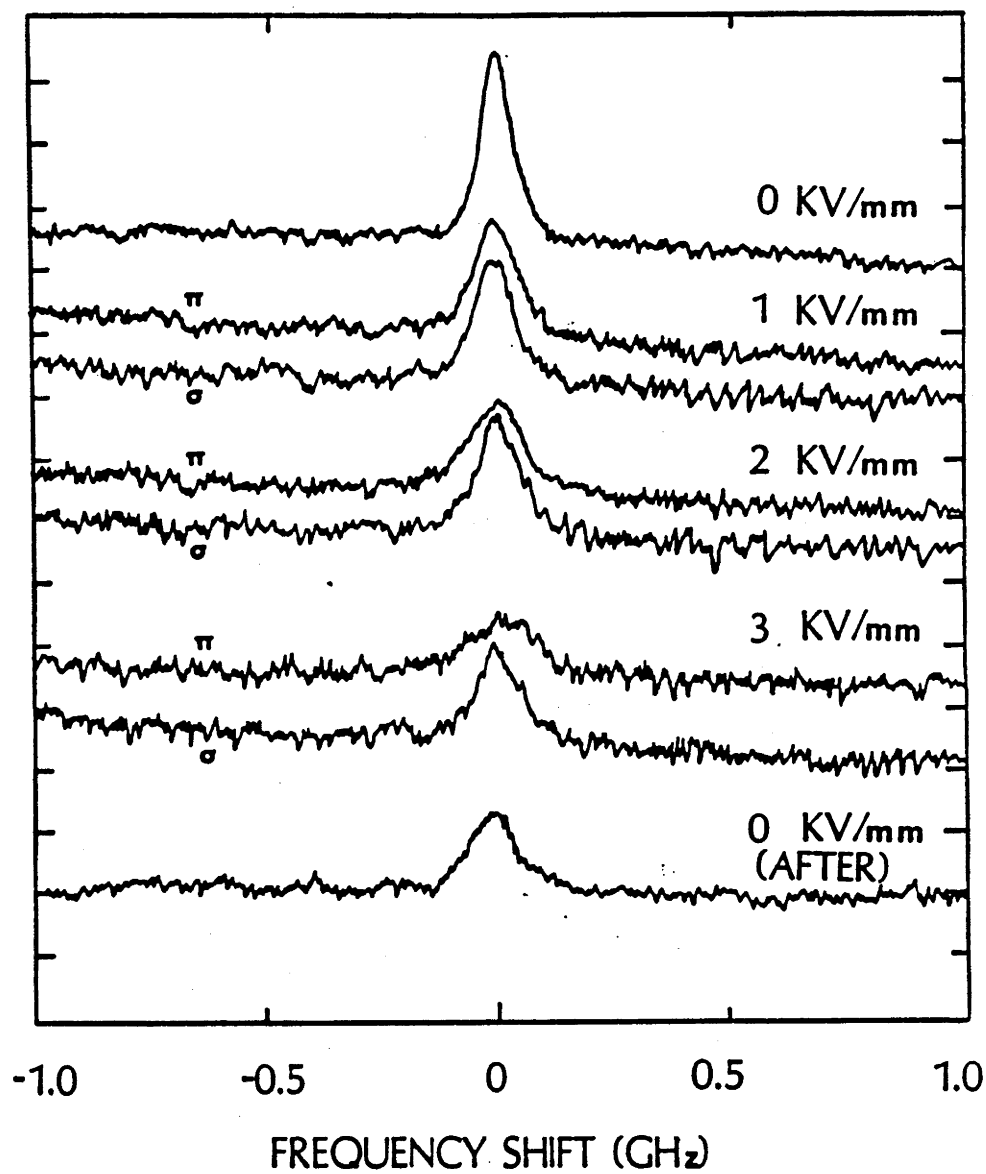

Figure 3.12 Stark splitting of hole burnt in the 574.2 nm line. The uppermost trace is the hole immediately after burning whereas that at the bottom is a remeasure of this hole at zero electric field but after fields upto 3kV/mm have been applied.

3.6 TEMPERATURE DEPENDENCE

Glasbeek *et al* (1983) using conventional spectroscopic techniques observed the broadening and shift of the zero-phonon line in the CaO: F centre (figure 3.14(a)). They obtained reliable data in the temperature range 30-50 K, the lower limit on temperature being set by the fact that only linewidth changes which are a significant fraction of the linewidth itself are easily detectable. At low temperatures (<30 K) the broadening is much smaller and cannot be reliably extracted from the total linewidth of the inhomogeneously broadened line. The zero-phonon line has a Voigt line profile (Lorentzian convoluted with a Gaussian) in the temperature range of study. The width of the Lorentzian component of the Voigt profile is taken as representative of homogeneous broadening. Its value is obtained using a deconvolution procedure due to Armstrong (1967). The lifetime (T_1) of the $^3T_{1u}$ excited state is, in this temperature range found to be of the order of msecs while the dephasing times (T_2) corresponding to the deconvoluted linewidths (Lorentzian component) are of the order of psecs. Hence pure dephasing (T_2') due to phonons is expected to be the process responsible for line broadening. Glasbeek *et al* (1983) explain their data assuming a sharply peaked phonon density of states with an effective mode frequency of 90 cm^{-1}.

We have used optical holeburning to obtain complementary data at lower temperatures. The results of our experiments are shown in figure 3.14(b) where the hole width and its shift are plotted as a function of temperature. We could obtain data only in the temperature region of 4.2 to 22 K (figure 3.13). It was not possible to obtain data above 22 K mainly because of the rapid broadening of the hole. A comparison of figures 3.14 (a) and (b) shows that the low temperature behaviour is very different. The reason for this could be that at very low temperatures the dominant (90 cm^{-1}) phonon states are not appreciably occupied and hence do not influence the zero-phonon line properties to the extent they do at higher temperatures. Our experimental results indicate a T^α variation where α is approximately equal to 1.4 for width and to 4 for shift. The limited temperature range of our study does not allow us to make a theoretical fit to the data.

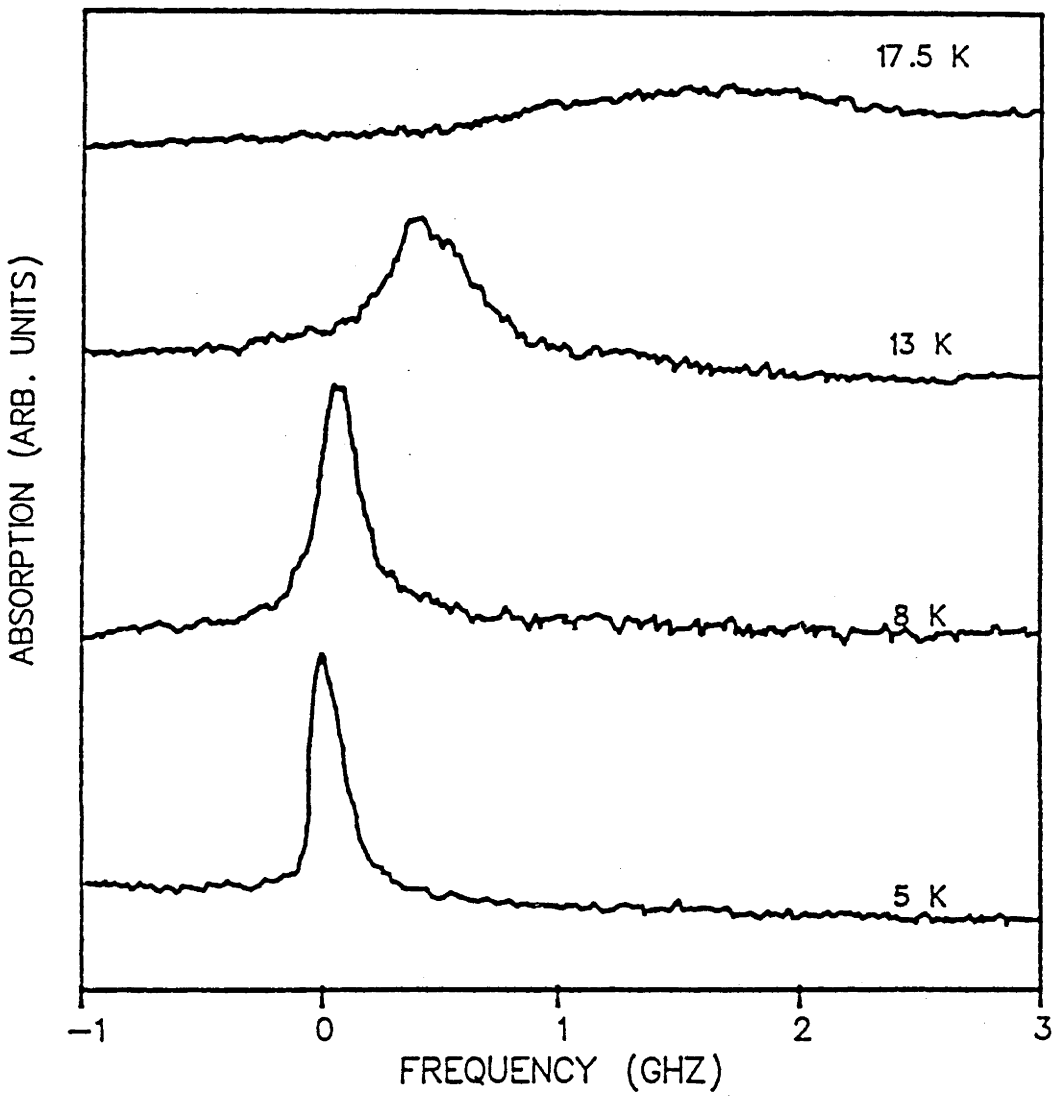

Figure 3.13 The temperature dependence of the optical hole burnt in the 574.2 nm zero phonon line of the CaO:F centre. The hole was burnt at 5 K with 50 mw of laser power. The horizontal axis gives the frequency detuning with respect to the original burn laser frequency.

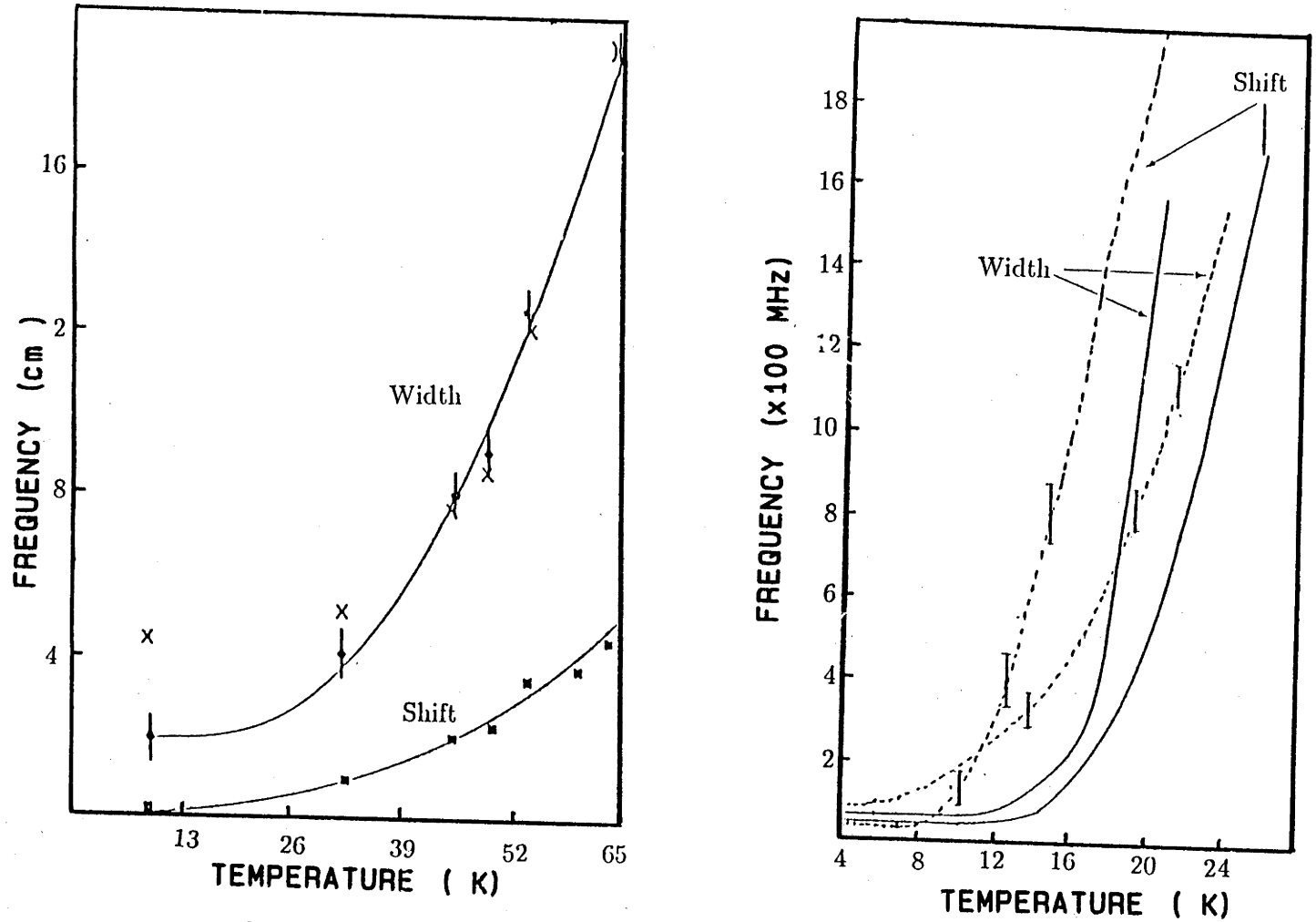

Figure 3.14 Broadening and shift of the zero phonon line as a function of temperature (Glasbeek *et al*, 1983) (a) and temperature dependence of the hole width and shift (present study) (b)

3.7 HOLEBURNING CHARACTERISTICS

As mentioned earlier holeburning in this transition is weak and dependent on sample preparation. Further the width of the hole that could be burned is dependent on the burn laser power and in any case is much broader than the homogeneous width of the transition suggested by radiative decay rate. These holeburning characteristics are discussed in this section.

Firstly, it should be noted that the $^1A_{1g} \rightarrow {}^3T_{1u}$ transition is spin-forbidden and holeburning in this transition is believed to be photochemical (discussed later in this section) where an electron tunnels to a nearby electron trap when the F centre is in its excited state. The efficiency of holeburning in these situations would directly depend both on the number of excited F centres (excited via the $^1A_{1g} \rightarrow {}^3T_{1u}$ absorption) and availability of electron traps. Weak absorption at the zero-phonon frequencies does not help in fulfilling the first condition efficiently. The availability of electron traps can however be improved using x-irradiation. In CaO crystals that contain ionised impurities (usually transition metal ions and especially Fe^{2+} and V^{2+}), the ionised impurities can act as electron traps and hence contribute partially to long lived holeburning. It is also observed that the excitation spectrum gave the zero-phonon line superimposed on a broad background. That is the F centre emission could be excited even when the laser frequency was shifted in frequency off the zero-phonon line. This is attributed to excitation from the traps into the conduction band followed by electron capture at the active centres (Summers *et al*, 1984). Such a process can not give rise to a narrow optical holes since it does not excite the $^1A_{1g} \rightarrow {}^3T_{1u}$ transition directly. For reasons mentioned above the holeburning (persistent) that occurs when the laser is tuned to the zero-phonon frequency is weak. The situation was improved by x-irradiating the sample prior to holeburning experiments. X-irradiation presumably helps converting the doubly ionised impurities in the sample to triply ionised state. The depth of the optical hole was only a small fraction of this direct $^1A_{1g} \rightarrow {}^3T_{1u}$ absorption. It is zero in the untreated crystals and in the best case had a depth of 60% in a freshly prepared and x-irradiated sample. The depth of the hole that could be burned in the zero-phonon line decreased with crystal usage with the number of electron traps decreasing (section 3.2.3).

3.7.1 PHOTOCHEMICAL PROCESS

When the lifetime of the hole is much longer than the lifetime of the excited state involved in the transition, it is obvious that a bottleneck that prevents the electron from reaching the ground state exists. This could be a metastable state (if one exists) or any electron trap external to the centre. Long lived optical holeburning in the CaO:F centre is considered to be photochemical in origin and this occurs because there is a small probability of an electron being lost from the centre in its excited electronic excited state through tunneling to a nearby electron trap. A similar process has been observed in other cases (Markham*et al*, 1953 and Macfarlane *et al*, 1979). In their studies in x-irradiated KBr, Markham *et al* (1953) observed that even at liquid helium temperatures optical irradiation in the F centre absorption band caused bleaching of the band. At low temperatures the electrons cannot be thermally excited from the excited state to the conduction band (energy gap=0.15 eV). From this data Markham *et al* (1953) infer that the electron tunnels to a nearby hole (electron trap) thus causing bleaching of the F centre. Long lived holeburning has been observed in another colour centre system (Macfarlane *et al*, 1979) where a similar mechanism of electron tunneling is proposed to be the cause for long lived optical holes.

In the present case the $F \rightarrow F^+$ photochemical conversion is known to occur during optical excitation (Kemp *et al*, 1967, Henderson *et al*, 1979, Welch *et al*, 1980). Furthermore, it has been established that this occurs by the electron tunneling from the excited F centre to adjacent F^+, F_A^+ or F_{AA}^+ centres to form F, F_A and F_{AA} centres respectively in their excited state (Ahlers *et al*, 1982). They detected the excited state tunneling between the F and F_A^+ centres by monitoring the magnetic circularly polarised emission (MCPE) from the excited triplet state of the F_A centre. The details of their experiment are as follows. The ground state of the F_A^+ centre is ^2S state with electron spin polarised "up" or "down". The F centre is excited by light at 404 nm. When the electron tunnels from the F centre to the F_A^+ centre, it forms an excited F_A centre in its triplet state. The relative populations of the $M_S = -1$ and $+1$ states are determined by the Boltzmann distribution in the ground state. MCPE was observed when no microwaves corresponding to the ^2S ground state splitting (F_{AA}^+) were applied. Application of microwaves before electron trapping equalises the ground state population distribution. Subsequently, when electron from the F centre is trapped forming the excited

F_A centre, the populations of the $M_S = \pm 1$ levels are equal and no MCPE is observed. This is taken by Ahlers *et al* (1982) as a direct evidence of the tunneling transfer of electrons in the excited state. The process is reversible so long as these latter centres remain in their excited states. However if the donor centres decay to the ground state the process cannot be reversed or not until the newly formed F, F_A or F_{AA} are again optically excited. In the absence of optical excitation the F, F_A and F_{AA} centres are stable and thus the process can account for the very long lived nature of the optical holes associated with the F centre.

3.7.2 HOLE WIDTH

The minimum width of a hole (Γ_{hole}) detected in a holeburning spectrum is equal to the twice the sum of the laser linewidth (Γ_{laser}) and the homogeneous linewidth (Γ_h) of the transition being probed. i.e.

$$\Gamma_{hole} = 2(\Gamma_{laser} + \Gamma_h)$$

The factor 2 in the above expression can physically be understood as follows. When the laser is tuned to the transition frequency it burns a hole of width Γ_h in the population distribution. When the same laser is used again to detect the hole (though often at a much lower intensity) it creates another hole of the same width (Γ_h) which is convoluted with the hole created during the burning process. As a result of this convolution, the width of the hole that is *detected* is twice the actual width of the hole that is burnt.

The lifetime of the $^3T_{1u}$ state is 3.2 msecs and the corresponding homogeneous width (Γ_h) is 50 Hz. The jitter induced laser linewidth (Γ_{laser}) is 1 MHz. So, in principle, the expected hole width (Γ_{hole}) is twice the laser linewidth (i.e. 2 MHz). However, as is obvious from the holeburning spectra presented thus far the observed holewidth is much larger. This observation is is not typical of holeburning in this transition only and has been observed in other colour centre systems. It has been observed in the N-V centre and the GR1 centre in diamond (Harley *et al*, 1984) and also in the 575.4 nm centre in NaF (Macfarlane *et al*, 1983). This could occur as a result of local heating (if the sample is highly absorbing at laser frequency) or power broadening. However in centres where absorption is not strong, spectral diffusion due to time varying fields is proposed to be a reason for the observed holewidths to

be greater than the lifetime limited width. When a colour centre undergoes photochemical holeburning electron transfer takes place between the centre and its surroundings. During the timescale of this electron transfer, the energy levels the nearby F centres are shifted by the presence of these electrons (Stark effect). The extent to which the energy levels are shifted depends on the distance between the electrons and the centres that are affected by them. This type of modulation of energy levels can induce holeburning in centres that are not otherwise resonant with laser frequency. Once the fields affecting the energy levels cease to exist, the absorption frequencies of the affected centres return to their original values thus causing a broadening of the hole. This phenomenon of spectral diffusion is also observed in amorphous systems (Brienl *et al*, 1984).

It is observed in this case that holewidth is dependent on the burn laser power. With 50 mw of laser power, the width of the holes that could be burned was about 100 MHz. The burning of the hole was very fast (about 10 secs). Burning for longer times at the same power level did not produce any increase in the holewidth or depth. When the laser power was reduced narrower holes could be burnt. This however, required longer burning times. Smallest holewidth (40 MHz) was obtained by burning for about 300 secs while the laser power was reduced by a factor of 100.

3.7.3 HOLE DEPTH AND ITS DETIORATION

It has been noted that not all the F centres will exhibit holeburning. This seems reasonable as the above process necessitates the availability of additional electron traps in the neighbourhood of the F centre. The Ca vapour reduction of CaO can produce a significant number of such individual vacancy centres or ionised impurities and a proportion of these must have other centres sufficiently close to the F centre for the electron tunneling mechanism to be operational. The active photochemical centres resulting in a stable and often more stable entity than the original weakly coupled pair and thus this is likely to arise as a consequence of other processes. It can certainly arise whenever the F centre is excited and this need not be through the direct $^1A_{1g} \rightarrow {}^3T_{1u}$ excitation. The final result can be a loss of the number of F centres for which holeburning can occur and it can be understood why there is a rapid detioration of the holeburning characteristic with time and optical excitation.

3.8 CONCLUSIONS

It has been shown that some of the colour centres in CaO undergo a photochemical change upon optical excitation and with selective excitation the effect can be used to produce narrow spectral holes in the 574.2 nm zero-phonon line. It is proposed that this only occurs for F centres with neighbouring trap sites such as F^+ or F_A^+ centres and the proportion of those centres is enhanced by heat treating the CaO sample in Ca vapour. The holeburning effect for samples prepared in this way is however still weak and deteriorates rapidly resulting in a less extensive study of the colour centre system than might have been desirable. However, electric fields have been shown to broaden the hole. The electric fields are also found to result in some broadening even when the field is removed. This effect of permanent broadening of the hole due to the electric field was not studied further.

Magnetic field studies were more satisfactory. The Zeeman splitting of the optical hole within the 574.2 nm zero-phonon line was well resolved at fields as low as 500 gauss. This represents as yet the best illustration of the use of the holeburning technique for measuring the electronic Zeeman effect of a colour centre system. The reason for the resolved splitting for this colour centre system stems from the Jahn-Teller quenching of the orbital angular momentum such that the magnetic field affects only the electronic spin. The splittings are then independent of strain and are the same for all the bleached centres. For a g$\sim$2 the splittings are 3 MHz per gauss and consequently for a hole with a width of 100 MHz it only requires a field of a few hundred gauss to give the resolved splitting. The g-values and zero field splitting determined in this way are found to be fully consistent with those determined previously from the ODMR measurements.

REFERENCES

1) Ahlers F. J. , Lohse F. and Spaeth J. M.
Solid State Commun. , 43, 321 (1982)

2) Armstrong B.H.
J. Quant. Spectrosc. Radiat. Transfer, 7, 61 (1967)

3) Bhagavantam S.
Crystal symmetry and physical properties, Academic press,
New York (1966)

4) Brienl W., Friedrich J. and Haarer D.
J. Chem. Phys., 81, 3915 (1984)

5) Condon E.U. and Shortley G.H.
The theory of atomic spectra, pp52 (1959)

6) Edel P. , Hennies C. , Merle d'Aubigne Y. , Romestain R. and
Twarowski Y.
Phys. Rev. Lett. , 28, 1268 (1972)

7) Gelineau A. , Buck T. , Geoffroy A. and Naud C.
J. Phys. C: Solid state physics, 6 , 774 (1973)

8) Glasbeek M. , Smith D. D. , Perry J.W. , Lamber Wm. R. and
Zewail A.H.
J. Phys. Chem. , 79, 2145 (1983)

9) Ham F.S.
Phys. Rev. , 138, A1727 (1965)

10) Harley R. T. , Henderson M. J. and Macfarlane R. M.
J. Phys. C: Solid state physics, 17, L233 (1984)

11) Henderson B.
J. Phys. C: Solid state physics, 13, 5811 (1980)

12) Henderson B. , Chen Y. and Sibley W.A.
Phys. Rev. , 6, 4060 (1972)

13) Henderson B. , Stokowski S.E. and Ensign T.C.
Phys. Rev. , 183, 826 (1969)

14) Johnson B.P. and Henseley E.B.
Phys. Rev. , 180, 931 (1969)

15) Kemp J. C. , Ziniker W. M. and Henseley E. B.
Phys. Letts. , 25A, 43 (1967)

16) Macfarlane R.M. , Harley R.T. and Shelby R.M.
Radiation Effects, 72, 1 (1983)

17) Macfarlane R.M. and Shelby R.M.
Phys. Rev. Letts. , 42, 788 (1979)

18) Markham J. J. , Platt R. T. Jr and Mador I.L.
Phys. Rev. , 92, 597 (1953)

19) Modine F.
Phys. Rev. , 7, 1574 (1973)

20) Summers G. P. , Chakrabarti K. and Chen Y.
Phys. Rev. B , 29, 5878 (1984)

21) Welch L. S. , Hughes A. E. and Summers G. P.
J. Phys. C: Solid state physics, 13, 1791, (1980)

Chapter 4

TWO LASER HOLEBURNING IN N-V CENTRE IN A DIAMOND

4.1 INTRODUCTION

Diamond crystallises in the face centred cubic lattice with each carbon atom tetrahedrally bonded to its four nearest neighbours. Based on the differences due to defect induced properties, diamonds are broadly classified into type I and type II diamonds. While type II diamonds absorb upto 255 nm in the ultra violet, type I absorb only upto 355 nm (Robertson *et al*, 1936). These two categories are further subdivided into groups a and b: type Ib being the one that contains isolated substitutional nitrogen atoms as impurities. This chapter details the studies performed on a defect centre in irradiated type Ib diamonds.

When electron or neutron irradiated type Ib diamonds (which contain isolated substitutional nitrogen atoms) are annealed at temperatures above 900 K in vacuum, they exhibit a strong optical zero-phonon absorption peak at 638 nm (1.945 eV) together with associated phonon assisted peaks spaced roughly 200 A apart (du Preez, 1965). A typical luminescence spectrum exciting at 630 nm of this centre is shown in figure 4.1. It was taken at 1.6 K with slits 100 μ wide where all features are fully resolved. The lifetime associated with the excited state is $\sim$13 nsecs. The inhomogeneously broadened zero-phonon linewidth is 1100 GHz (FWHM). When excited within

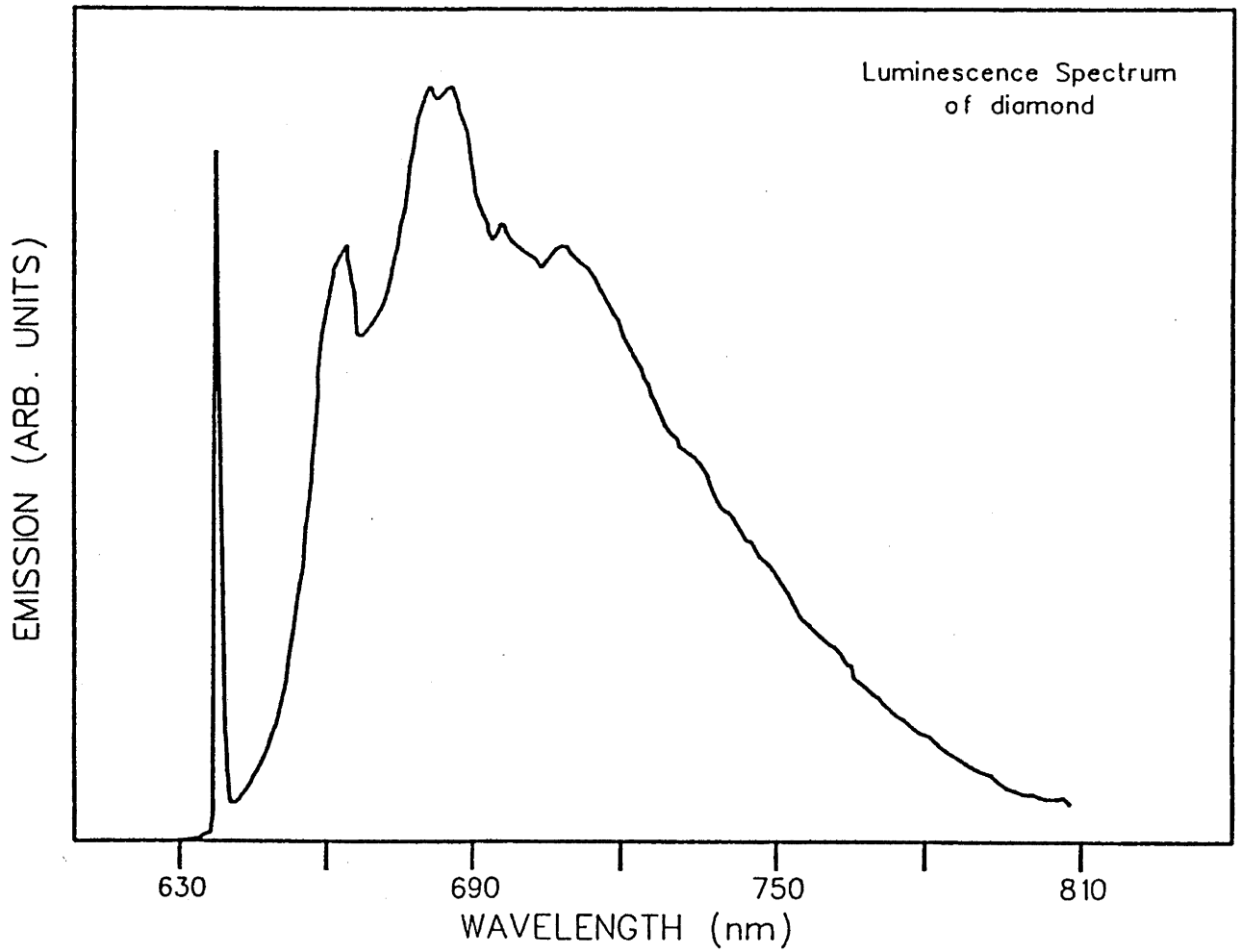

Figure 4.1 Luminescence spectrum of N-V centre in diamond at 4.2 K. Luminescence was excited using 630 nm radiation from ring dye laser.

the zero-phonon line with a narrow band laser, these centres exhibit optical holeburning. It was observed that holeburning in this centre consists of two components. One component that is weak and persists for several minutes can be studied using one laser. The other component has short lifetime ($\sim$1 msec) can only be studied using two lasers: one to burn the hole and the other to probe. Holeburning studies on this centre using the long lived component have already been performed by Harley *et al* (1984) using one laser. In this chapter the results of two laser holeburning studies on this centre are discussed.

4.2 STUDIES ON THE ZERO-PHONON LINE

Annealing studies on type Ib diamonds have been performed by Davies *et al* (1976) and are discussed in this paragraph. As mentioned earlier type Ib diamonds contain isolated nitrogen as substitutional impurities. The absorption spectra of unirradiated diamonds show a continous absorption with strength proportional to the concentration of nitrogen. Electron irradiation at room temperature produces a large number of centres and those with zero-phonon lines at 1.673, 2.535 and 3.15 eV are relatively strong. However, no line at 1.945 eV is observed. Annealing at 800 K destroys all but the 1.673 and 3.15 eV bands. The 1.673 eV line is associated (Mitchell, 1967) with vacancy centres (GR1) and the 3.15 eV line is associated (Davies *et al*, 1970) with interstitial nitrogen centre (ND1). Annealing at high temperatures (> 900 K) the concentration of both the GR1 and ND1 centres decreases with a simultaneous increase in the concentration of the 1.945 eV centre. Davies *et al* (1976) found that the zero-phonon line splits under stress into components whose position, polarisation and intensities are as predicted for a transition between an A ground and a E excited electronic state of a centre of trigonal symmetry. As trigonal symmetry is required it is unlikely that both the GR1 and ND1 centres are involved in the formation of the 1.945 eV centre.

The intensity and polarisation of the one phonon sideband were studied by Davies *et al* (1976) and it was shown that the E state coupled predominantly to A_1 modes of vibration. Their analysis is briefly summarised here. When uniaxial stress is applied along the <001> direction the lowest vibronic state from the E electronic state is that which transforms as $|E_Y>$ in

the unperturbed system (labelling of the states from the original paper). Luminescence from this state to the ground electronic state (A_1) would consist of either purely σ polarised component or equally strong σ and π components depending on whether the ground electronic state is coupled to A_1 or E modes of vibration respectively. Experimentally it was observed that the transition is ~90% σ polarised. Accounting for slight (10%) depolarisation induced by random internal stress in the crystal, Davies *et al* (1976) concluded that the E electronic state is predominantly coupled to the A_1 modes of vibrations. Hence, it is unlikely that there is any Jahn-Teller interaction involving the E excited state of this centre.

In condensed matter (and gases at high pressure) vibrational relaxation is usually much faster than excited state lifetime. Under these conditions if the optical centre is 'rigid', the emission band is expected to be a mirror image of the absorption band. But in the present case it has been observed that the emission spectrum is not a mirror image of the absorption spectrum. Since any Jahn-Teller interaction is unlikely, the lack of mirror symmetry is explained as being due to the tunneling of the nitrogen along the symmetry axis into the vacancy forming an equivalent V-N centre i.e. the centre is not rigid. The tunneling model is discussed later in this chapter. Earlier, polarised luminescence experiments performed by Clark *et al* (1971) on this centre also suggested that the transition, in emission, is $E \rightarrow A$ associated with isolated nitrogen and has either a trigonal or monoclinic I symmetry.

4.3 ELECTRONIC STRUCTURE OF THE N-V CENTRE

In diamond when a nitrogen atom substitutes for a carbon atom that is next to a vacancy, the nitrogen vacancy pair defines a C_3 axis. As the bonding in diamond lattice is tetrahedral, the point group symmetry of the N-V centre is C_{3v}. Loubser *et al* (1977), following the argument of Watkins (1967) for the aluminium-vacancy centre in silicon, derived LCAO molecular orbitals for the N-V centre. As shown in the figure 4.2, a, b, c and d are four sp^3 hybrid orbitals extending towards the vacancy from the four neighbouring atoms and c is the bonding orbital of nitrogen atom. The LCAO molecular orbitals are found by operating on any of the orbitals with the character projection

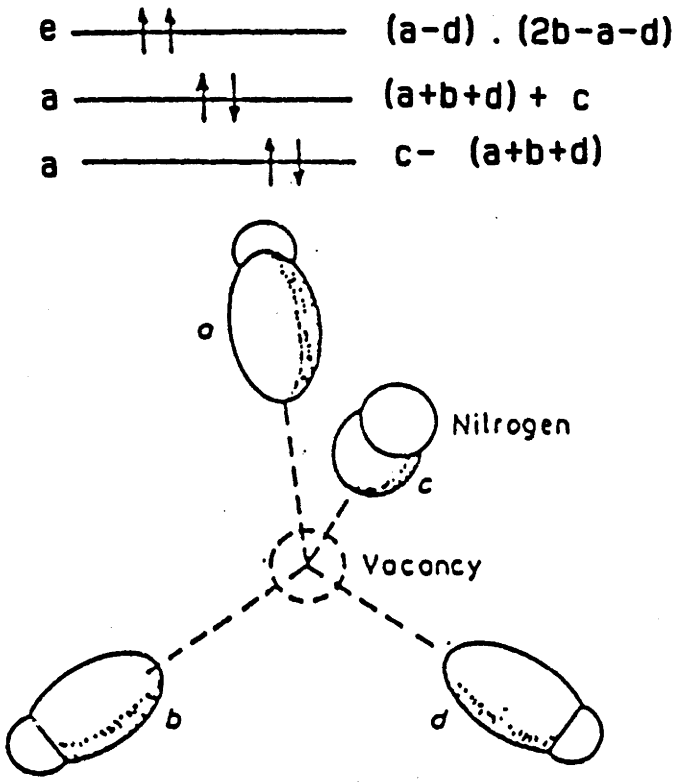

Figure 4.2 A possible energy level scheme and simple LCAO one electron molecular orbitals for the N-V pair (after Loubser *et al*, 1977)

operators of the C_{3v} group. One set of the resulting LCAO molecular orbitals is shown in figure 4.2 . Two of these molecular orbitals transform as A_1 and the third as E irreducible representations of the point group C_{3v}.

When nitrogen substitutes for a carbon in the diamond lattice it introduces into the lattice an extra nuclear charge and of course, an extra electron. The result then is that there are five electrons localised at the N-V centre. The presence of the triplet state (seen in EPR) suggests that there has to be an even number of electrons associated with the centre to obtain S=1. Hence, the centre either captures or loses an electron. Apart from the uncertainity in the number of electrons, the ordering of molecular orbitals as well is not clearly established. Since replacing a carbon with nitrogen is equivalent to adding an extra positive charge to the nucleus at that site, it is reasonable to assume that the molecular orbital a_1 involving that atom has the lowest energy. This is because the extra (fifth) electron tends to spend more time about the nitrogen nucleus that has the extra positive charge. Electron pairing takes place in that orbital and hence the energy associated with that orbital is lowered. Similar argument has been put forward by Watkins *et al* (1964) in a model for phosphorus-vacancy centre in silicon. Accepting also that the e orbital is the highest molecular orbital and considering the possibility of either four or six electrons being associated with the centre the following three cases exist.

CASE I

If there are six electrons and the possible molecular orbital ordering is as shown in figure 4.2, then one of the possible ways of filling the molecular orbitals is ${a_1}^2$, ${a_2}^2$ and e^2 where the superscripts denote the number of electrons in that molecular orbital. The e orbital can accommodate the two electrons with their spins parallel to form a triplet state S=1 or with their spins antiparallel to form a singlet S=0 state. The possible resultant orbital states with two electrons in the e orbital are A_1, A_2 and E. However, the application of Pauli's principle excludes three of the six possible states leaving only ${}^1A_1$, ${}^3A_2$ and ${}^1E$ states. Note that the ${}^3E$ state is not allowed when the electron configuration is ${a_1}^2{a_2}^2e^2$.

CASE II

Assuming the number (six) of electrons and ordering of the molecular

orbitals is the same as in case I, another way of filling the molecular orbitals is $a_1{}^2a_2{}^1e^3$. Since the e orbital can take up four electrons the configuration $a_1{}^2a_2{}^1e^3$ is the same as $a_1{}^2a_2{}^1e_h$ where e_h denotes a hole in the e orbital. In this case the resultant states are either ^1E or ^3E .

CASE III

If the number of electrons associated with the centre is four, then the possible molecular orbital configurations are $a_1{}^2a_2{}^2$, $a_1{}^2e^2$ and $a_1{}^2a_2{}^1e^1$. These three configurations together give $^1A_{1g}$, ^1E, $^3A_2$ and ^3E states.

The configurations described in II and III result in a ^3E state amongst other available states. Previous analysis (Loubser *et al*, 1977, Harley *et al* 1984) have considered the electron configuration to be as in case I. Loubser *et al* (1977) have proposed that the zero-phonon transition at 638 nm is between a $^1A_1$ ground state and a ^1E excited state. The EPR signal they detected was associated with a metastable ^3A state. Harley *et al* (1984) accepted their assignment in interpreting holeburning measurements. The inter configuration transitions that give rise to a ^3E state, therefore have not been considered. As there is no evidence against the configurations described in cases II and III, the possibility of a ^3E state existing in the centre is not ruled out. Irrespective of whether the N-V system has captured or lost an electron to form the even electron N-V centre, it is still possible to have a ^3E state.

4.4 EPR STUDIES

This centre does not show any EPR spectrum unless illuminated with light when a strong EPR spectrum is observed (Loubser *et al*, 1977). An unusual feature of the EPR spectrum was that the high field line of the EPR spectrum was seen in emission rather than in absorption. The experiment was done at liquid helium temperature where it is expected that both the $M_S = 0$ and the $M_S = \pm 1$ states would have only very small population differences and all the signals would be absorptive. Loubser *et al* (1977) interpret the presence emission lines as indicating preferential population of the $M_S = 0$ state. This characteristic persisted up to 550 K. Between 300 K and 550

K, the EPR signal is found to have a temperature dependence proportional to exp(900 cm^{-1}/kT) with a relaxation rate of ~40 msecs at 77 K. The variation of the intensity of EPR signal with the wavelength of the exciting light was measured. There is a strong correspondence between the phonon assisted lines in the absorption and excitation spectra. The strong zero-phonon line however, is not seen in the excitation spectrum and is attributed to poor resolution of the experiment. The centre was hence considered to be the same centre as that giving the zero-phonon line at 638 nm. Since the EPR signal is observed only when the N-V centre is optically excited, they suggest that the EPR spectrum is due to an *excited* triplet state of this centre. This triplet state has a zero field splitting of 2.88 GHz and the g value was determined to be 2.0028.

The zero field splitting in a triplet state is in general, due to the interaction between the spin momenta of the two electrons (spin-spin interaction) forming the triplet state or due to the spin-orbit interaction. In the F centre in CaO spin-spin interaction is the cause (~80%) for the zero field splitting (1.8 GHz) of the triplet state and the rest comes from the second order spin-orbit interaction. However, in the case of N-V centre there is no first order contribution from the spin-orbit interaction because the symmetry of the orbital state is A. The spin-spin interaction and second order spin-orbit interaction is expressed by

$$DS_Z^2 + E(S_X^2 - S_Y^2)$$

where D and E are the zero field splitting parameters and have the dimensions of energy. When the centre involved has a three fold or higher symmetry the parameter E is zero. In the N-V centre which has the three fold symmetry, the 2.88 GHz splitting is the value of the D parameter. The sign of D is however, unknown and hence the ordering of $M_S = 0$ and $M_S = \pm 1$ levels has not been established. Since no EPR was observed in the absence of light it was considered that the above triplet state was the metastable state and the ground state was not paramagnetic. The zero-phonon transition has consequently been assigned to be a $^1A_1 \rightarrow {}^1E$ transition.

4.5 ONE LASER HOLEBURNING EXPERIMENTS

The one laser holeburning experiments were done in two different ways. In one method, which is more conventional, the laser was tuned to a frequency within the zero-phonon line for few seconds and then multiple sweeps of the laser frequency about the original burn frequency were averaged. The other method is to average multiple cycles of one burn and one scan where the hole is reburned (refreshed) between subsequent scans. This method can also be used to obtain an idea about the lifetime of the spectral features when they are short lived. To achieve this, the frequency scan of the CR699-21 laser system was controlled externally. The waveform used is shown in figure 4.3 (c). It was obtained by triggering the triangular waveform ($\pm$5V) (figure 4.3 (a)) from the Datapulse signal generator using the square wave from another pulse generator (figure 4.3 (b)). The time required to scan the specified frequency range was equal to half the triangular wave width. By adjusting the square wave frequency relative to the triangular wave it was possible to hold the scan voltage fixed for required times, thereby holding the laser frequency fixed (i.e. burn a hole). In our experimental setup it was also possible to adjust the time between burning and subsequent detection of the hole. This was possible by adjusting the triangular wave. This is discussed in chapter 5. A similar burn-scan method was used by Cone *et al* (1984) in their experiments on $EuVO_4$. Using the second method it was seen that the holeburning in this centre has two components, one that had a lifetime comparable to the laser scan time ($\sim$300 msecs) while the other has a longer lifetime of about 30 minutes. This conclusion (about the short lived component) is possible because the signal to noise ratio is much better in the second case where the hole is refreshed between scans.

Harley *et al* (1984) were the first to report optical holeburning in the 638 nm zero-phonon line. They reported long lived photochemical holes and in addition to the hole at burning frequency they observed side holes at 0.63, 1.59 and 2.23 GHz on either side of the central hole. They consider the structure as due to the presence of small splittings in the E state perhaps associated with a dynamic Jahn-Teller effect but could not give a satisfactory interpretation. They observed that the holes broadened and shifted in an applied magnetic field at a tuning rate of $\sim$5 MHz/G. They did not observe

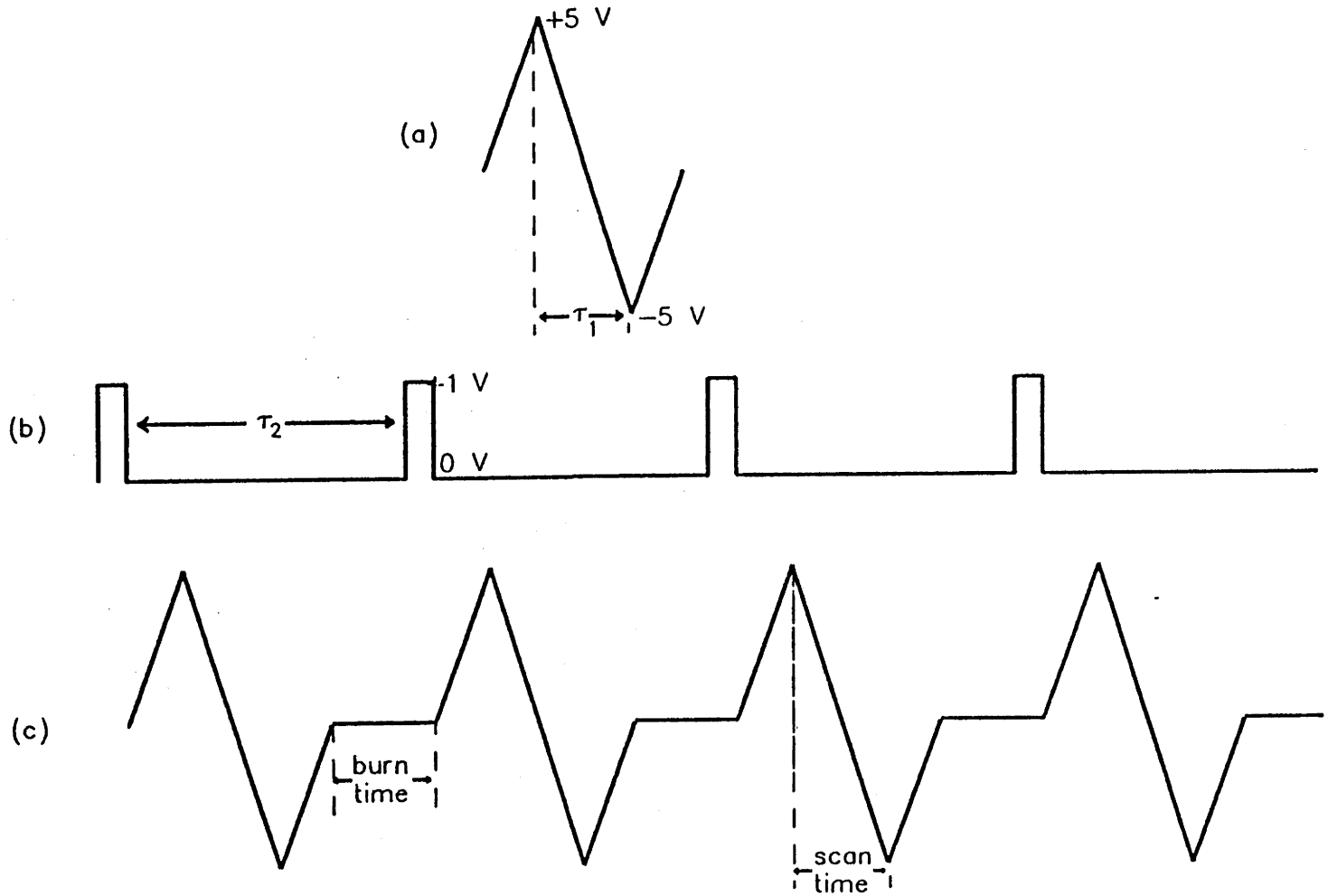

Figure 4.3 The waveform used to scan the ring laser frequency externally (c). The waveform in (a) is triggered by the pulse train (b) from another pulse generator to obtain the waveform in (c).

any splitting of the hole in a magnetic field and the hole was found to be insensitive to applied electric field.

Later, the effect of microwaves on holeburning was reported by Bloch *et al* (1985). It was observed that the depth of the hole decreased (holefilling) at a specific value of microwave frequency. They observed holefilling when the microwaves were resonant with the $^3A_2$ splitting of 2.88 GHz. In the presence of a magnetic field the holefilling resonance split into several components and occur at frequencies consistent with the splittings of the $^3A_2$ state as determined from the EPR data. The holeburning in the $^1A \rightarrow {}^1E$ transition was attributed to population storage in the long lived spin singlet component of the $^3A_2$ state. The application of the microwaves transfers the electrons from the singlet to the doublet component (of the $^3A_2$) from where the decay to the ground ^1A is much faster. The microwaves resonant with the splitting of the $^3A_2$ state would hence lead to reduction in the holeburning.

The optical holeburning spectrum in this centre is known to be sample dependent and figure 4.4 shows few spectra that give an indication of the extent of sample dependence. The one laser holeburning spectrum obtained by us is shown in figure 4.4 (a) together with the spectra obtained by others on the same centre. The spectra shown in figure 4.4 (b) and (c) were obtained by Harley *et al* (private communication). The interesting point to be noted in these spectra is the asymmetry. The side hole features always appear on the high energy side of the spectrum. In our case (figure 4.4 (a)) it appears on the low energy side. In our samples however, the side hole at 1.59 GHz (Harley *et al*, 1984) was not observed. Figure 4.4 (c) shows the spectra taken with a sample that had a high nitrogen concentration. Some samples gave a spectrum that has antihole features at close to 3 GHz (Harley *et al*, private communication). This feature is much clearer in the two laser holeburning experiments to be reported below. This gives a clue to the nature of the splittings occuring in the centre.

One other point to be mentioned here is that though the spectra show sample dependence, there are some common features but a feature present in the spectrum from a sample may or may not be present in the spectrum from another sample. The side hole at 2.2 GHz is common to both our spectra and those of Harley *et al* (1984). The side hole at 1.59 GHz seen in their spectra is missing in ours while they do not observe the side hole at 0.6 GHz on

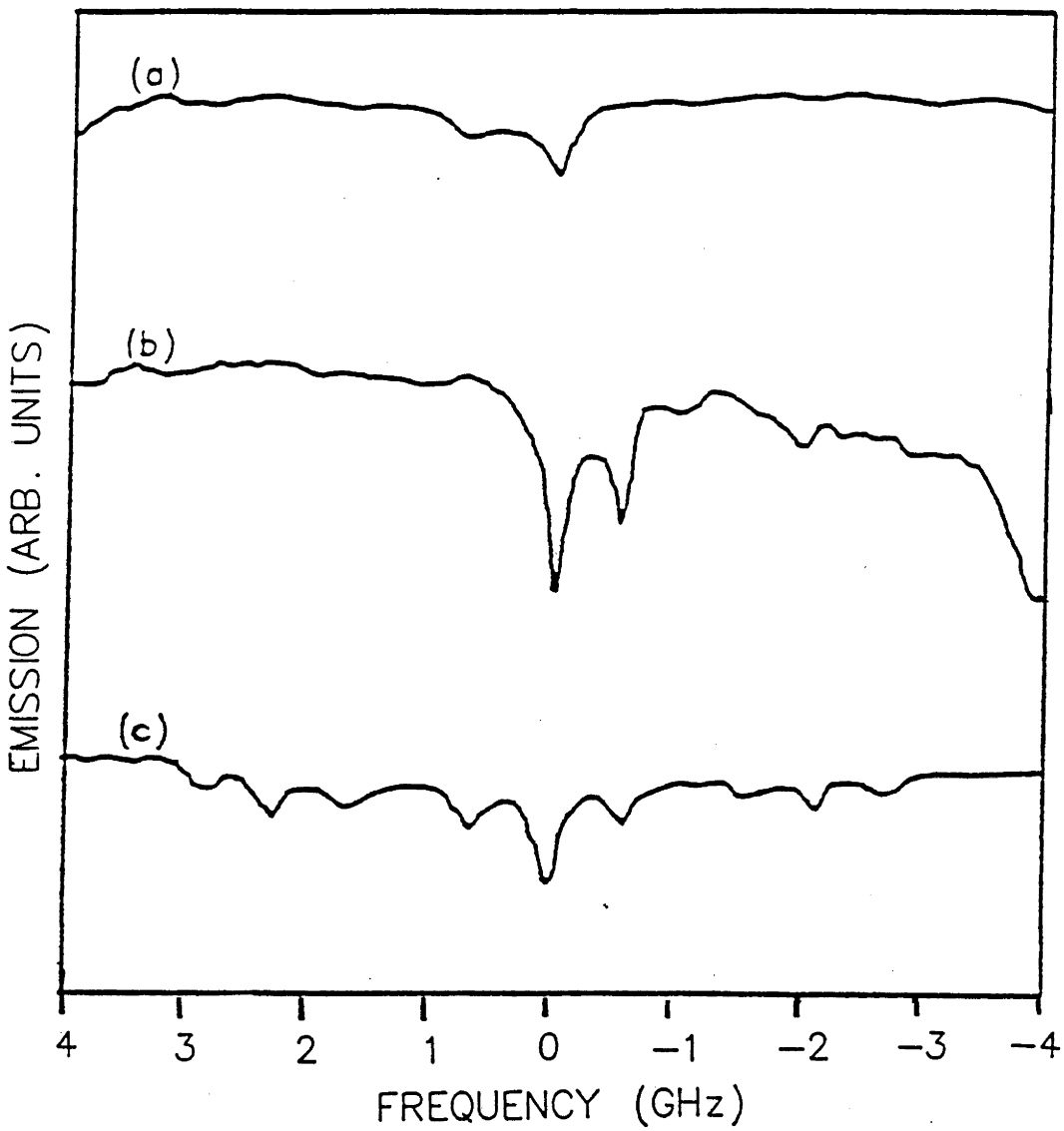

Figure 4.4 Comparison of the various one laser holeburning spectra. a) typical spectra obtained in the present study, b) and c) spectra obtained by Harley *et al* (private communication)

the high energy side which is seen in ours. The 0.6 GHz sidehole instead, is observed on the low energy side in their case. The degree of asymmetry in the holeburning spectra itself is found to be sample dependent. This indicates that there are several competing processes that cause the different features in the spectra and the variation in spectra is due to the dominance of some processes over others. Such variations could result from a variety of factors one of which is the different concentration of the single nitrogen centres present. The sample giving the four side hole pattern contained $\sim 10^{19} cm^{-3}$ whereas other samples had a much lower concentration $\sim 6x10^{17} cm^{-3}$.

4.6 QUANTUM TUNNELING OF NITROGEN

Figure 4.5 shows the typical spectrum obtained in a two laser holeburning experiment in the N-V centre. This spectrum, as is obvious, has many antihole features, one of them being at 2.88 GHz. As antiholes can occur *only* when there is ground state degeneracy, any model of the centre attempting to explain the holeburning spectrum should include ground state degeneracy. Following the historical development of the studies on this centre and accepting the $^1A \rightarrow {}^1E$ assignment for the zero-phonon transition, the only way ground state degeneracy is possible is through tunneling of the nitrogen along the N-V axis to form an equivalent V-N centre. This tunneling of nitrogen associates a splitting with each of the electronic states of the N-V centre. Tunneling of the nitrogen atom along the N-V axis to form an equivalent V-N centre has been proposed by Davies *et al* (1976). It was used to explain the 80 cm^{-1} splitting of the first vibronic state. The splitting due to tunneling depends on the overlap of wavefunctions which penetrate the potential barrier between the two wells. This overlap integral will be much smaller at the bottom of the potential well than for vibronic states lying close to the top of the potential barrier. Hence, it is not unreasonable to expect splittings of the order of GHz when the vibronic splitting is about 80 cm^{-1}.

Tunneling splitting could be the origin of the structure in the holeburning spectrum and a model as to how this can occur has been proposed by Manson *et al* (1985). This is summarised here with some modifications and corrections. If it is assumed that the zero-phonon transition is $^1A \rightarrow {}^1E$ then

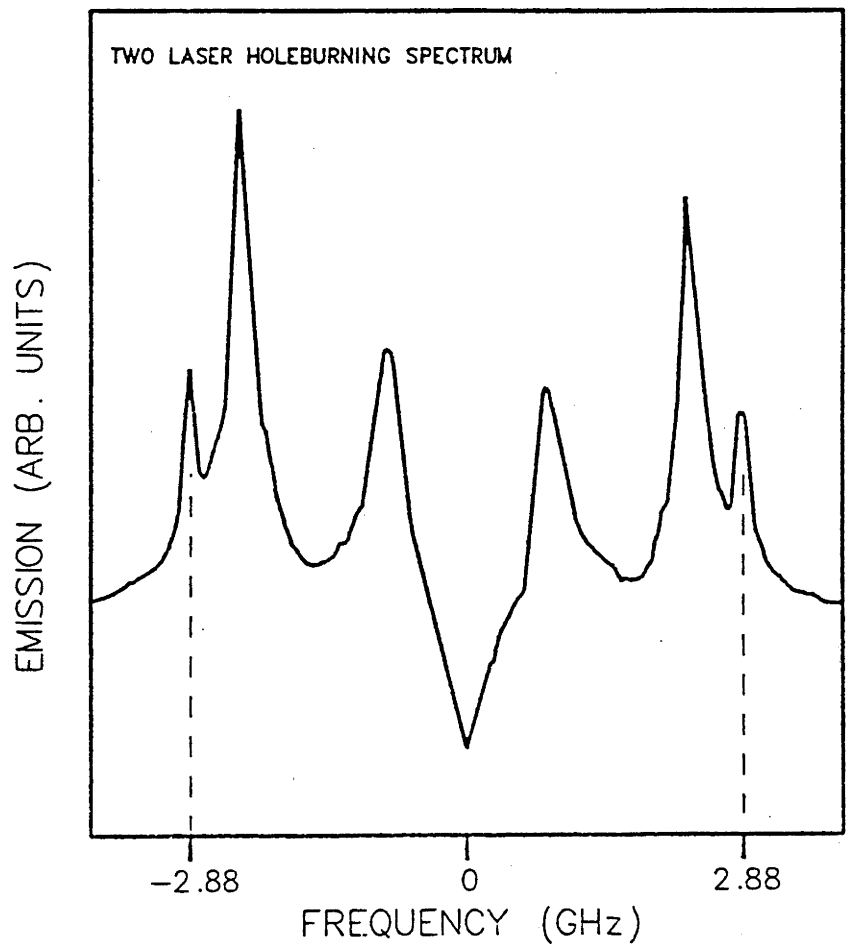

Figure 4.5 Typical two laser holeburning spectrum of the N-V centre obtained by monitoring total emission.

any of the ground state splittings will have to be an orientational effect. It is possible to imagine the N-V defect has more than one energetically equivalent configuration of different orientation separated by potential barriers. When the barrier height is infinite each vibrational state has a degeneracy equal to two. If the barrier is not infinitely high and there is small overlap of the states in different potential wells, the degeneracy is lifted and the vibrational states are split. This would then cause splittings of electronic states associated with quantum tunneling between configurations. It seems likely that the lowest potential barrier will be associated with motion of nitrogen atom along the N-V axis between two potential minima. Tunneling of the nitrogen atom along the N-V axis would increase the symmetry of the centre from C_{3v} to D_{3d} with a inversion point halfway between the nitrogen and vacancy sites (not a reflection plane as suggested by Manson *et al*, 1985). This effect in itself would cause the splitting of the ground and excited states. The wave functions describing the various tunneling states will be symmetric and antisymmetric with respect to the inversion operation. Since in D_{3d} symmetry the electric dipole operator has odd parity only cross transitions (symmetric→antisymmetric or vice versa) are allowed. The sample dependence of the spectra suggests that internal strain affects the holeburning spectrum. The effect of internal strain has been ignored in the above analysis and is being considered now. The orbitally degenerate E state would be split by strain by an amount which is a fraction of the inhomogeneous linewidth but much larger than the scan width of the holeburning spectrum (10 GHz). Thus in considering the holeburning process the excited as well as the ground state can be treated as non-degenerate electronic levels. Strain would have a further effect on the centre by making the two nitrogen sites inequivalent and thus removing the inversion symmetry. This distortion lowers the symmetry from D_{3d} and cause an admixture of the symmetric and antisymmetric wavefunctions. The transitions between symmetric (and antisymmetric) states will now be allowed which, as will be shown in the following, is sufficient to give a plausible explanation of the holeburning spectrum.

The tunneling of nitrogen along the symmetry axis of the N-V centre to form the equivalent V-N centre is similar to the tunneling of nitrogen in the ammonia molecule. It can be treated as a two state system. If the N-V and V-N configurations are denoted by ϕ_1 and ϕ_2 then any state of the system

can be written as a linear combination of the base states

$$\psi = C_1\phi_1 + C_2\phi_2$$

where C_1 and C_2 are the amplitudes for the system to be in the base states ϕ_1 and ϕ_2 respectively i.e. $C_1 =< \phi_1 \mid \psi >$ and $C_2 =< \phi_2 \mid \psi >$. The two amplitudes are time dependent. Since the two configurations N-V and V-N ϕ_1 and ϕ_2 are equivalent, in the absence of any interaction between the base states, the energy associated with ϕ_1 and ϕ_2 is the same and is denoted by E_0 . However, in the presence of any interaction connecting the two base states the time dependence of the two amplitudes C_1 and C_2 can be written as

$$i\hbar\frac{dC_1}{dt} = E_0C_1 + \Delta C_2$$

$$i\hbar\frac{dC_2}{dt} = E_0C_2 + \Delta C_1$$

where Δ is half the splitting caused by tunneling motion of nitrogen. The above equations can be solved to give the following expressions for the time dependence of the amplitudes C_1 and C_2.

$$C_1(t) = a\, exp[-\frac{i}{\hbar}(E_0 + \Delta)t] + b\, exp[-\frac{i}{\hbar}(E_0 - \Delta)t]$$

$$C_2(t) = a\, exp[-\frac{i}{\hbar}(E_0 + \Delta)t] - b\, exp[-\frac{i}{\hbar}(E_0 - \Delta)t]$$

The energy associated with ψ_1 when C_1=C_2 is $E_0 + \Delta$ and the energy associated with ψ_2 when C_1= $-C_2$ is $E_0 - \Delta$.

Thus tunneling of nitrogen causes the state ψ associated with energy E_0 to be split into states ψ_1 ($C_1 = C_2$) and ψ_2 ($C_1 = -C_2$). Since ψ does not denote any one state in particular, the splitting occurs in all the levels associated with the N-V centre. The magnitude of the splitting varies between electronic states and increases with increasing overlap between the base states ϕ_1 and ϕ_2. The tunneling splitting in the ground state is denoted by Δ_g and in the excited state by Δ_e.

The various transitions possible between symmetric (S) and antisymmetric (AS) states are $S \rightarrow AS$, $AS \rightarrow S$, $S \rightarrow S$ and $AS \rightarrow AS$. The first pair of

transitions are allowed even in the absence of strain and are strong whereas the second pair of transitions are allowed due to strain and are relatively weak. The transition strengths for the two types of transitions are denoted by A and F respectively.

Consider the first case where the optical pumping is negligible. Four groups of centres, corresponding to each of the four transitions being resonant with the laser, will undergo photochemical change. All of the absorptions associated with these centres will be missing and cause holes in the resultant spectrum. If the tunneling splittings in the ground and excited states are represented by Δ_g and Δ_e respectively, then four pairs of side holes are expected at $\pm\Delta_g$, $\pm\Delta_e$, $\pm(\Delta_e - \Delta_g)$ and $\pm(\Delta_e + \Delta_g)$. Refering to the figure 4.4 (c) it can be seen that the first two pairs should each have half the strength of the central hole. Similarly, the sum of the strengths of the second two pairs should be half that of the central hole, their ratio being A/F.

Many of the features seen in the one laser holeburning spectrum are due to photochemical holeburning. If the holeburning process is dependent on the nature of the centre and therefore not proportional to the transition strength at the laser frequencies, then centres with any of the four active transitions will have equal weighting. The holeburning process should give side holes at $\pm\Delta_g$, $\pm\Delta_e$ and $\pm(\Delta_e - \Delta_g)$ each with a strength that is half the intensity of the central hole. If due to strain the intensity of the forbidden transitions becomes significant then the side hole at $\pm(\Delta_e - \Delta_g)$ drops slightly and the intensity is gained by a new hole at $\pm(\Delta_e + \Delta_g)$. Only a small amount of strain is invoked, enough to induce the forbidden transition but not enough to cause any significant broadening of the holes. From the considerations of Davies *et al* (1976) involving the splitting of the vibronic sideband it is assumed that the splitting in the ground state is less than in the excited state. If $\Delta_g = 0.6$ GHz and $\Delta_e = 2.2$ GHz and a small amount of strain is invoked most of the spectral features in the one laser holeburning spectrum apart from the asymmetry can be reasonably explained.

The above model proposed by Manson *et al* (1985) does not allow for the fact that strain has even parity and although it will not affect, in first order, the selection rules (any change in the selection rules has to come from higher strain effects) it does affect the tunneling splitting. The overlap integral that

decides the tunneling splitting depends on the relative positions of the nitrogen and vacancy which vary with strain. Hence, strain in first order causes an inhomogeneous distribution of Δ_g's (the tunneling splittings). Thus, it is unlikely to result in sharp holes.

The validity or otherwise of the tunneling model can be checked however by studying the behaviour of the centre in the presence of external perturbations. Since the point group symmetry of the N-V centre is C_{3v} which lacks inversion symmetry, first order Stark effect is expected. However, tunneling of nitrogen along the defect axis introduces additional inversion symmetry and the point group symmetry will now be D_{3d}. Because of inversion symmetry there will be no first order Stark effect. However it can have off-diagonal matrix elements. The result is that when the effect of other perturbations (strain etc.) is small, electric field can produce discrete splittings of the zero-phonon line. Davies *et al* (1980) have studied the effect of electric fields of upto 10 kV/cm on this centre. They have observed a splitting which however, is not quantified. This implies that the Stark interaction they used must be greater than any tunneling splittings. This does not however, imply that the tunneling splittings do not exist. As mentioned earlier, one laser holeburning experiment does not detect any effect of electric fields. The result of the electric field experiment provides no evidence for the existence of tunnel states.

Harley *et al* (1984) have observed that the holes observed in a one laser holeburning spectrum broadened and shifted in applied magnetic field with a tuning rate of 5 MHz/G. However, it will be shown in two laser holeburning spectra that magnetic field splits the 2.88 GHz antihole and the splitting ($g\beta H$) is consistent with a g value of 2. This experiment suggests that the ground state splitting is associated with spin and is inconsistent with predictions of the tunneling model.

The discussion on the tunneling model is summarised below.

- Strain affects tunneling splittings but not selection rules. So, if any transitions between symmetric and antisymmetric states are to be observed it has to be due to higher order strain effects.
- With tunneling the symmetry of the centre changes to D_{3d} and since

the centre has inversion symmetry no first order Stark effect is expected. However this cannot rule out tunneling. It just implies that Stark splittings are much greater than tunneling splittings.

- It is possible that tunneling does exist and our observations concern transitions between symmetric and antisymmetric states only.

The weaknesses of the tunneling model are that it cannot explain Zeeman splittings and the asymmetry in the holeburning spectrum.

4.7 TWO LASER HOLEBURNING EXPERIMENTS

The two laser optical holeburning experiments on the 638 nm zero-phonon line in diamond gave the spectrum shown in figure 4.5 . The spectrum was obtained with both lasers delivering equal power (~50 mw).

A very significant feature in this spectrum is the presence of prominent antiholes in the spectrum. The presence of antiholes implies the existence of ground state splittings. According to the previous work (Davies *et al*, 1976), the transition being investigated is assigned to a $^1A \rightarrow {}^1E$ of a centre with C_{3v} symmetry. Furthermore it can be seen that one of the antiholes is at 2.88 GHz which, according to previous work, corresponds to the zero field splitting of the $^3A_2$ metastable state. The main reasons for assigning the ground state to be a ^1A is the observation of EPR *only* under optical excitation. Here we assign this transition to be a $^3A_2 \rightarrow {}^3E$ as it is only then can we account for the antihole at 2.88 GHz. There are however several other experimental observations which support this assignment and these will be discussed in later sections. The prominent features at 0.85 GHz and 2.2 GHz will be discussed later.

4.7.1 ANTIHOLE LIFETIME

Since one of the antiholes in the two laser holeburning spectrum is at 2.88 GHz, it suggests that the $^3A_2$ state (whose zero field splitting is also 2.88

GHz) is somehow involved in the holeburning process. Loubser *et al* (1977) report that the EPR signal (at liquid nitrogen temperature) decays with a lifetime of 40 msecs after the exciting light is blocked. If the antihole is indeed due to the *metastable* $^3A_2$ state, its lifetime would be expected to be the same as that of the EPR signal (40 msecs). Hence, the following experiment was performed with an idea of determining the lifetime of the antihole features in the two laser holeburning spectrum.

The lifetime of the holeburning spectrum was determined using the experimental set up shown in figure 4.6 . The experiment is in principle a burn-delay-read experiment. By performing the experiment at various time delays, the lifetime of various features in the holeburning spectrum can be estimated. The experiment makes use of two high resolution lasers. The time evolution of the holeburning spectrum created by one laser (the burn laser) is probed by the other (the read laser) after a time delay. Since the time evolution of the spectrum due to the burn laser is being investigated, it is necessary that the burn laser be pulsed in time. The pulsing of the burn laser is achieved by using an extracavity acousto-optic modulator which is described in the following. An acoustic standing wave is set up in a $PbMoO_4$ crystal by applying a high frequency (85 MHz) electrical waveform to a piezoelectric transducer attached to one end of the crystal. The acoustic wave generated by the transducer causes a sinusoidal perturbation of the density of the crystal and consequently its index of refraction. The $PbMoO_4$ crystal then behaves as a diffraction grating. When light passes through the crystal under such conditions (i.e. when the acoustic wave is present) it is diffracted. The burn beam used in the experiment was the first order diffracted beam from an acousto-optic modulator operated at 85 MHz and the 85 MHz electrical waveform was gated on and off (time τ_b) to give a square wave of desired characteristics - the presence or absence of the diffracted beam is controlled by the external waveform. The read laser is continously on and the signal from the photomultiplier is passed through a box-car integrator. The box-car integrator is triggered simultaneously with the end of burn pulse. The box-car is then adjusted so that only the signal at a delay (τ) after the burn pulse is collected. This cycle of burn-delay-read at an interval T was repeated as the frequency of the read laser was swept very slowly. The output of the box car was recorded as a function of the read laser frequency to give the holeburning spectrum at a time τ after the burn beam had been switched off. This could then be repeated for different delays τ. In order to be sure about the actual delay between the burn pulse

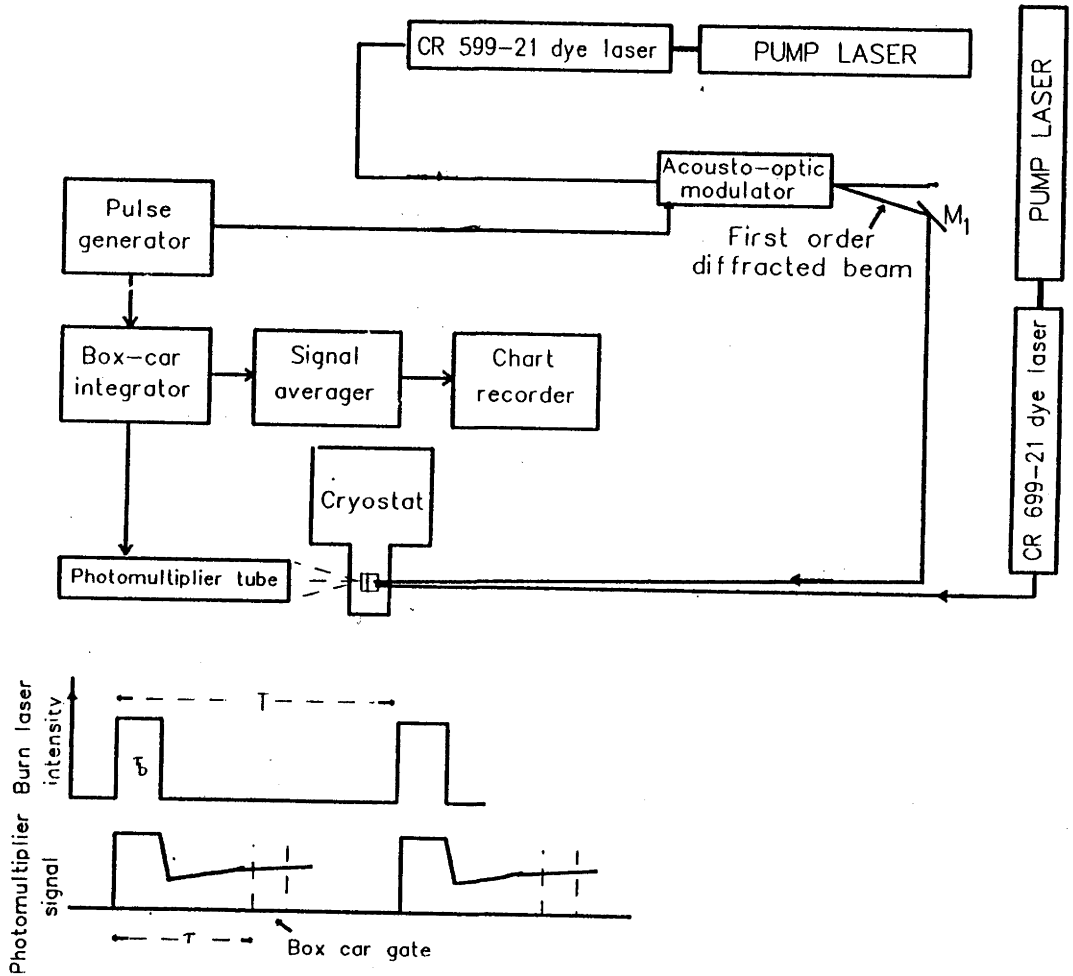

Figure 4.6 Schematic of the experimental setup used for the study of the decay of the holeburning spectrum

and opening of the box car gate, the time delay between the application of waveform and its effect on the diffracted beam was checked in the following manner. The burn laser beam was directed onto a photodetector whose output was displayed on a oscilloscope together with the waveform driving the acousto-optic modulator. The time delay between the two was found to be 8 nsecs. This delay did not present a problem in the present experiment since it is much shorter than the time delay used in the experiment. The repetetion time T was not constant and was adjusted in such a way that there is no appreciable time delay between the detection and the next burn pulse. i.e. the burn pulse frequency was dependent on the delay between the burn pulse and the detection time. This was desirable to reduce the duty cycle of the box car integrator and thus increase the signal to noise ratio of the spectrum.

The data obtained in this experiment is shown in figure 4.7 .

When both the lasers are on at zero delay (uppermost trace in figure 4.7) the signal corresponds to the emission stimulated by both lasers. As soon as there is a delay, the signal arises from the read laser only. Consequently there is an immediate change in the spectrum as soon as a delay is introduced and this seen by comparing the the traces at zero delay and at 50 μsecs (figure 4.7 (a) and (b)). The change seen between the two traces does not correspond to any type of relaxation and the asymmetry in the spectrum will be discussed later.

To obtain the relaxation times one should neglect the trace at zero delay. The antihole features in the spectrum as seen in other traces decay with a lifetime of 500 μsecs $\pm$ 200 μsecs (figure 4.8) with no clear difference detected in the decay rate of the various side hole and antihole features. The lack of accuracy comes from the inability to establish the base line corresponding to very long delays. This is due to the fact that the detection cycle (burning and reading) continually modifies the spectrum through photochemical holeburning. Clearly the lifetime of the antiholes is not the same as that of the EPR signal. But this does not prove that the antihole feature is not due to the $^3A_2$ state. This point is further discussed later in the chapter.

The holeburning spectrum produced by a single laser at fixed frequency is that obtained with a minimum delay (figure 4.7(b)) and attempts will be

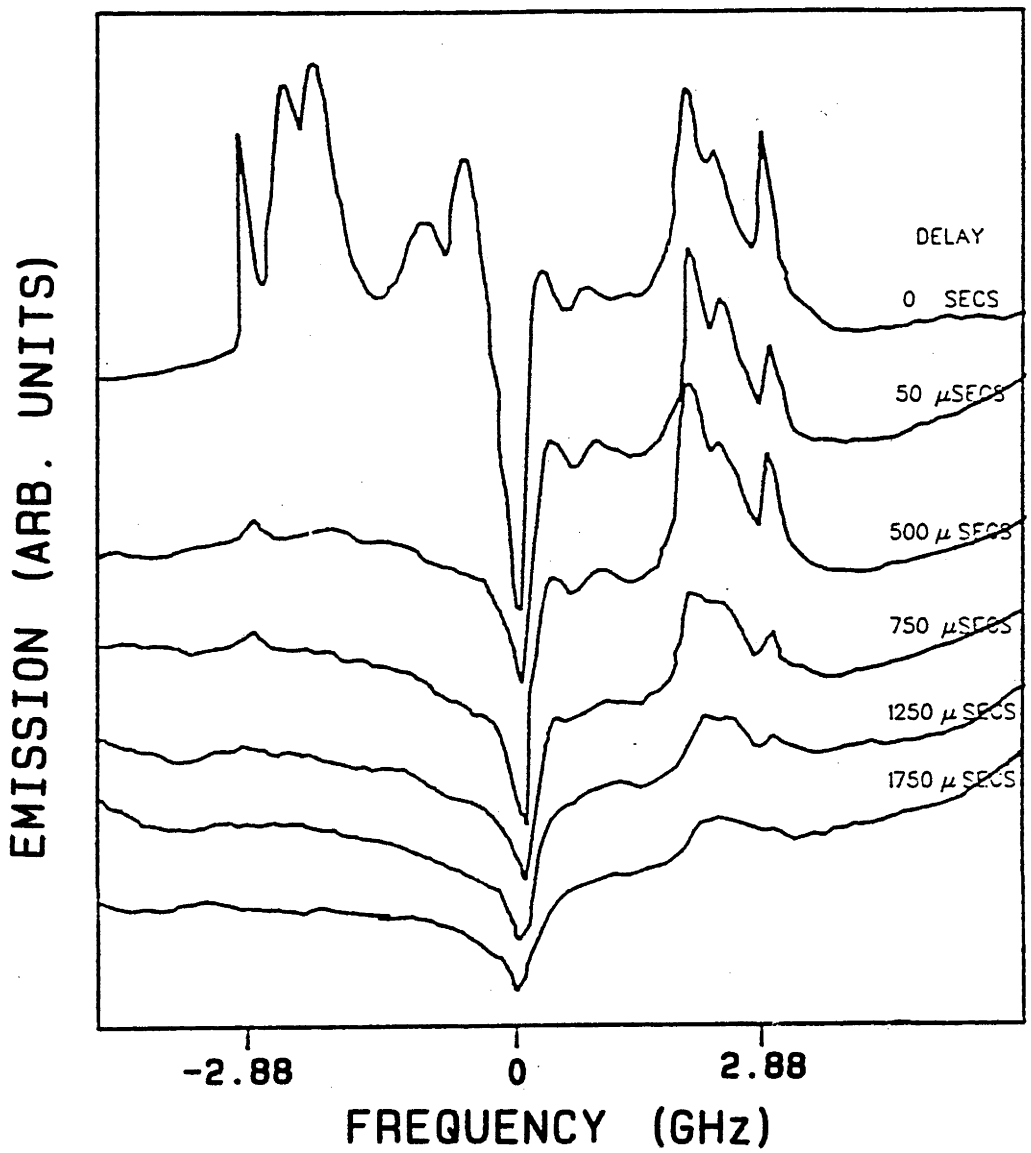

Figure 4.7 Lifetime studies of the antihole features in the two laser hole-burning spectrum.

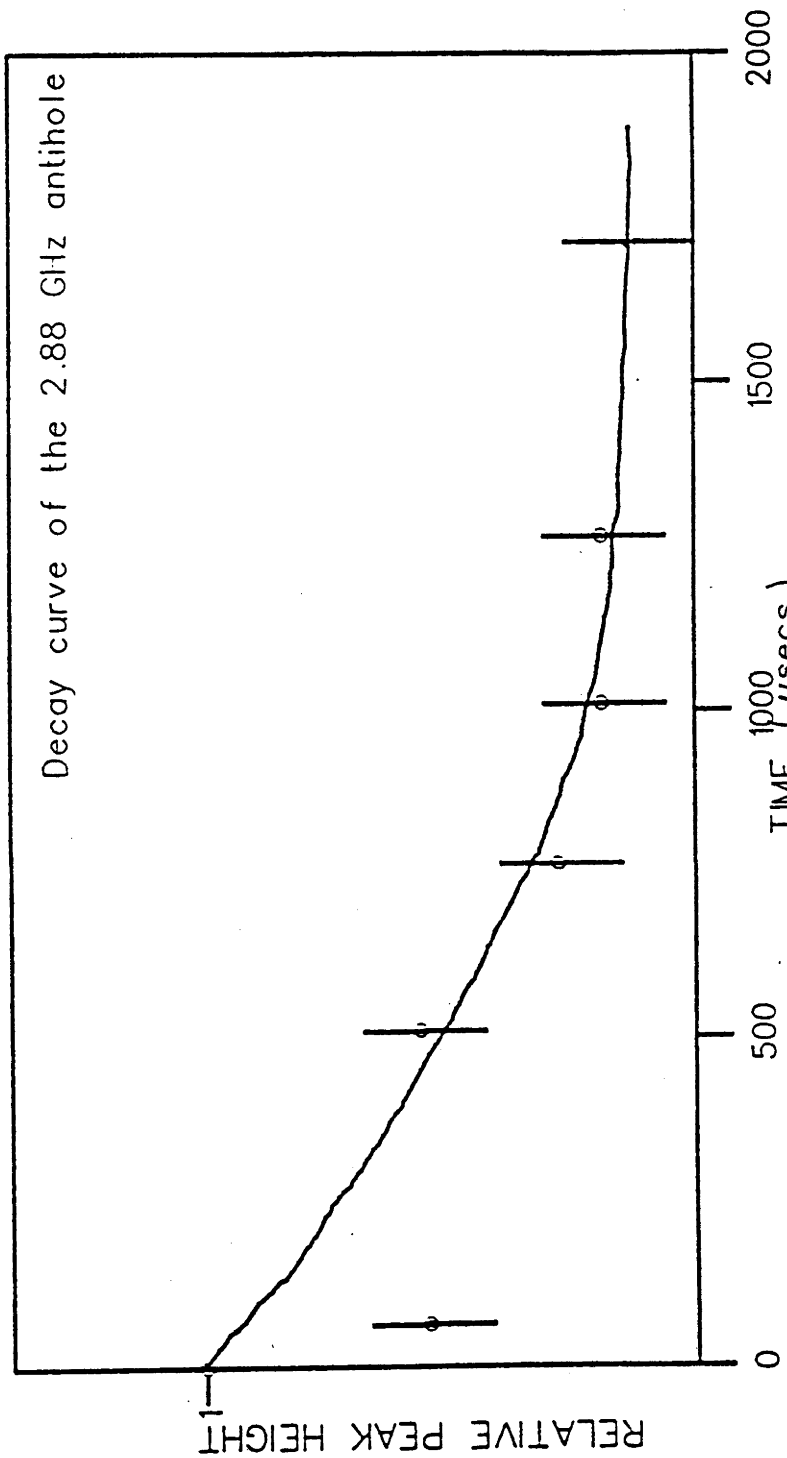

Figure 4.8 Decay of the two laser holeburning spectrum. The read laser was delayed between 0 and 1.75 msecs after the burning.

made to account for the features and asymmetry of this spectrum in a later section (Section 22). The asymmetry itself has been checked by transmission measurements described in the next section.

4.7.2 HOLEBURNING TRANSMISSION MEASUREMENTS

When measuring in transmission and looking for interference effects between the two lasers the most sensitive technique is to detect the transmission of one beam while modulating the other beam. The laser beam was modulated at 680 Hz using a mechanical chopper. The intensity of the laser beam was detected using a photomultiplier tube. A suitable combination of neutral density filters was placed in the beam path to enable the photomultiplier tube to operate in a linear region. Doing this and using beams of equivalent powers (~50 mw) gave the spectra shown in figure 4.9 . The spectrum in figure 4.9 (a) is obtained by monitoring the read laser beam transmission while modulating the burn laser. It is perhaps slightly misleading to call the lasers 'burning' and 'reading' but the convention is maintained (see chapter 2). As is obvious the holeburning spectrum is highly asymmetric. It is very similar to that seen in the lifetime measurements (figure 4.7 (b)) as expected since modulating the burn laser will cause a modulation of the holeburning spectrum. The holeburning spectrum obtained by monitoring the burn beam while modulating the read laser is shown in figure 4.9 (b). It gives the same spectrum (as figure 4.9 (a)) except for a reversal of intensities on high and low energy sides. This can be understood if the 'read' laser also causes burning and hence modifies the depth of the hole burned by the burn laser. When the read laser frequency is 2.88 GHz below the burn laser frequency its (read laser) antihole coincides with burn laser frequency. In this situation more centres are available in the sample to absorb the burn laser. This will cause a decrease in the transmission (antihole) of the burn laser and this antihole will be on the low frequency side. Similarly other antiholes appear on the low frequency side of the spectrum. In this experiment it is necessary that the decay of the instantaneous holeburning spectrum caused by the 'read' beam is fast compared with the sweep speed. The decay rate is ~500 μsecs whereas sweeping through the sharpest feature requires ~10 msecs and so the condition is satisfied.

The spectrum obtained when monitoring the emission is the sum of the

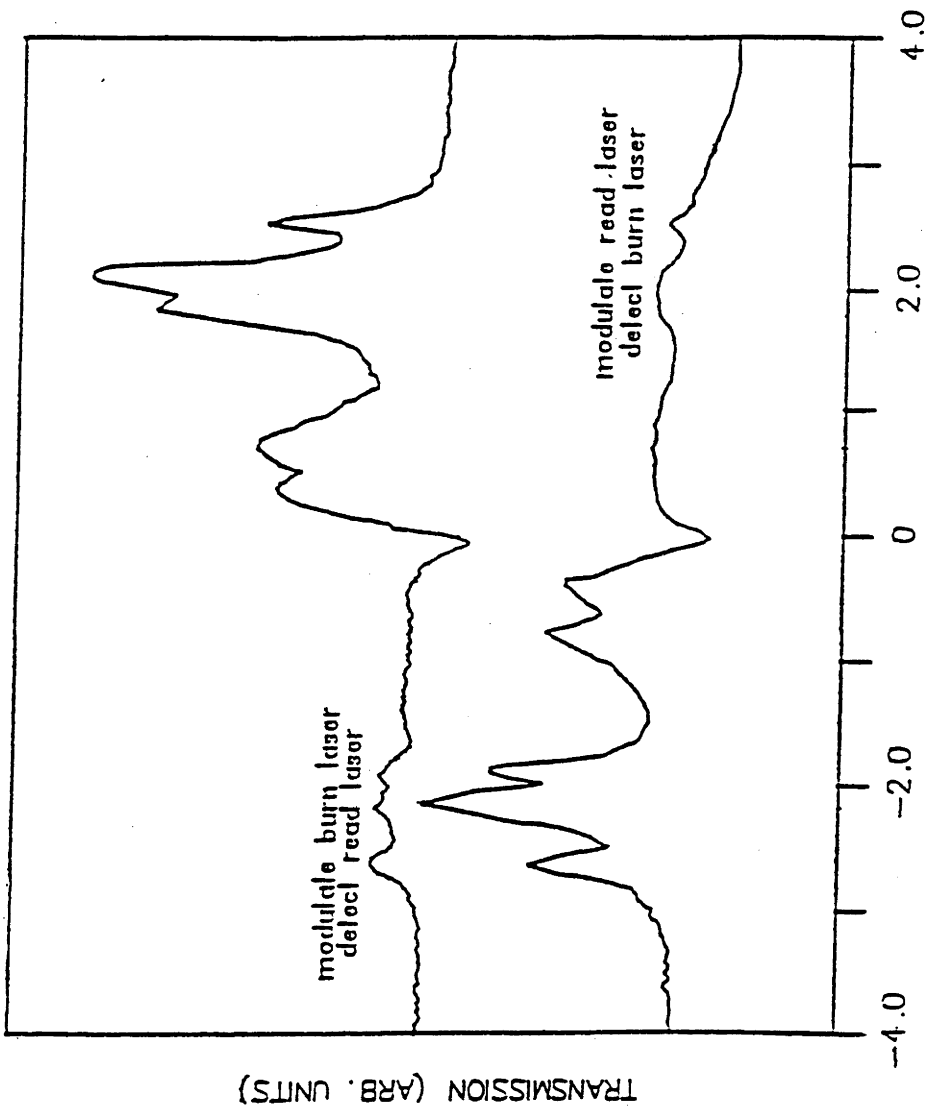

Figure 4.9 Two laser holeburning spectrum detected by monitoring the laser beam transmission

two spectra shown in figure 4.9 (a) and (b). i.e. In the two laser experiment both lasers are burning and both the lasers are reading. This is possible because of the extremely easy burning nature of this centre. When the read laser is on the low frequency side of the burn laser the antihole due to it affects (decreases) the burn depth of the burn laser and hence increasing the total emission level. When it is on the high energy side of the burn laser the antihole structure due to the burn laser affects (decreases) the burning due to the read laser and hence the increase in the emission level. In a normal two laser experiment both the lasers are present at all times and hence the 'symmetric' spectrum is detected.

4.7.3 POWER DEPENDENCE OF THE HOLEBURNING SPECTRUM

The symmetry of the two laser holeburning spectrum when measuring all the spectrum is destroyed once the powers of the two lasers are different and this is illustrated in figure 4.10 . The spectrum obtained when the powers of the two lasers are same (50 mw) is shown in figure 4.10 (a). When the power of the read laser is reduced to 5 mw, the result is that the gain of the reading process is reduced. Correspondingly, the features on the high energy side created by the burn laser are detected with lesser gain and the spectrum on that side of the central hole appears weaker. When the read laser power is reduced further (to 0.5 mw) the features on the high energy side become much weaker. In figure 4.10 (c) the gain of the detection system has been increased by a factor of 3.

The read beam at 50 mw power appears to have reached saturation as far as the holeburning spectrum it produces is concerned and hence reducing the power does not reduce its holeburning effect. The features detected by the intense burn beam are then not affected appreciably by decreasing the power of the read beam.

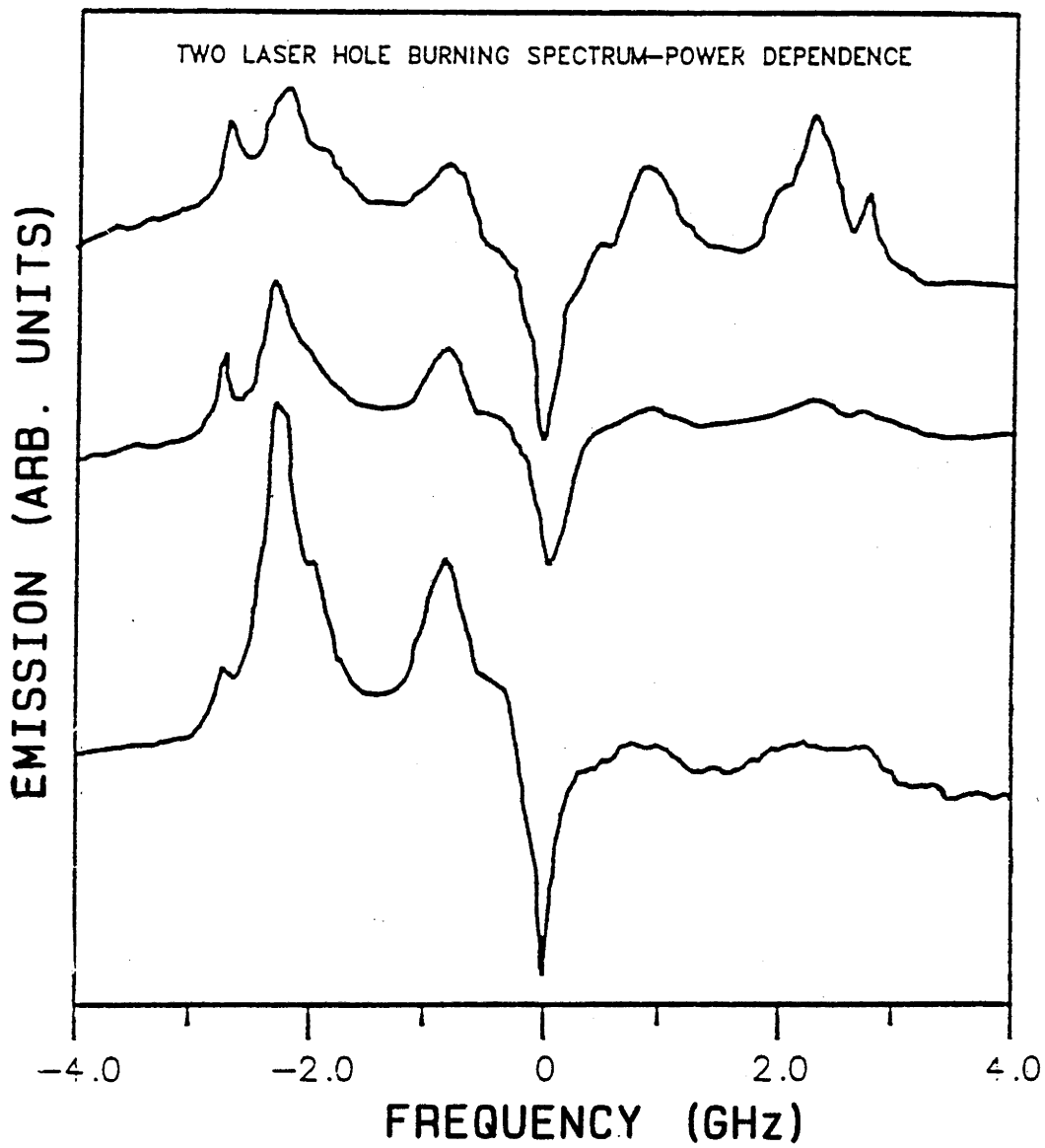

Figure 4.10 Power dependence of the two laser holeburning spectrum a) the burn and the read laser have approximately the same power (50 mwatts) b) the read laser is weaker by a factor 10 c) read laser weaker by a factor 100 and the gain of the detection system is increased by a factor of 3.

4.7.4 HOLEBURNING SPECTRUM AT VARIOUS POSITIONS ACROSS THE CRYSTAL

This experiment was done to see if the macroscopic properties of the crystal (eg. strain) had any effect on the spectrum. The spectra were taken by exciting centres at various positions across the crystal face. The crystal was irregularly shaped. The {111} faces had the largest area of about 4 mm^2 (2mmx2mm). The crystal thickness between the {111} faces was 1mm. In order to be able to correlate the spectra to changes in crystal strain, it is necessary that the spectra be taken at nearby points across the crystal surfaces. It should be remembered that the centre holeburns very easily. In the experiment the read laser was weakly focussed using a 30 cms focal length lens (to reduce the read beam diameter). The data was obtained at 8 positions across the crystal surface by a systematic movement of the read laser in steps of about 0.5 mm. The spectra obtained are shown in figure 4.11 . For systematic variation across the crystal no systematic variation is observed in the spectrum. The observed variation is attributed to strain in the crystal.

4.7.5 HOLEBURNING SPECTRUM AT VARIOUS WAVELENGTHS WITHIN THE ZERO-PHONON LINE

As mentioned earlier in this chapter the zero-phonon line of this centre has width of about 1100 GHz. In the ring dye laser system, the thin etalon modes are spaced 200 GHz apart. Hence by adjusting the thin etalon, it was possible to obtain the spectra at five values of wavelengths spaced 200 GHz apart. All the spectra were taken from the same region in the crystal. The spectra obtained are shown in figure 4.12 . The central hole at the burn laser frequency becomes broader as the wavelength is decreased and in figure 4.12(d) the side hole at 0.6 GHz on the high energy side of the burn laser frequency is obvious. This is in accordance with the 0.6 GHz side hole seen in the one laser holeburning experiments (Figure 4.4(a)). This behaviour was not reproducible in all samples. Hence, it is concluded that the spectra observed are dependent on the strain experienced by the centres.

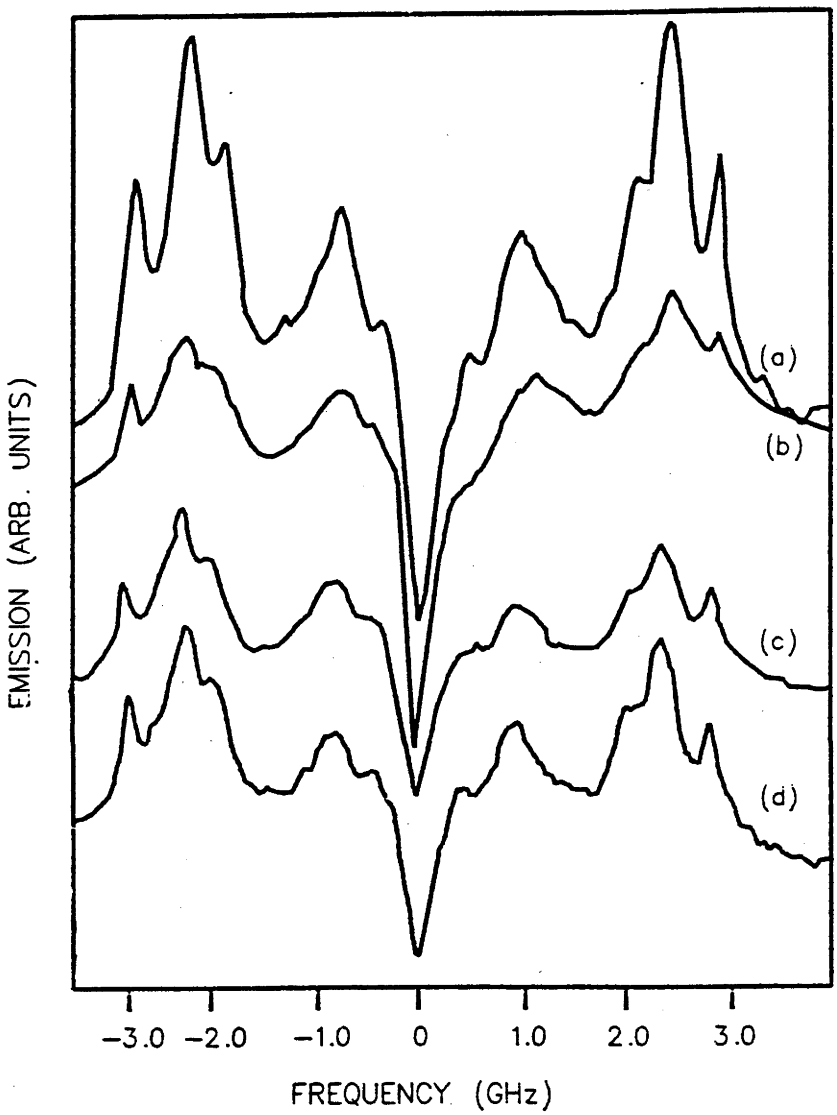

Figure 4.11 Two laser holeburning spectrum at various positions across the crystal

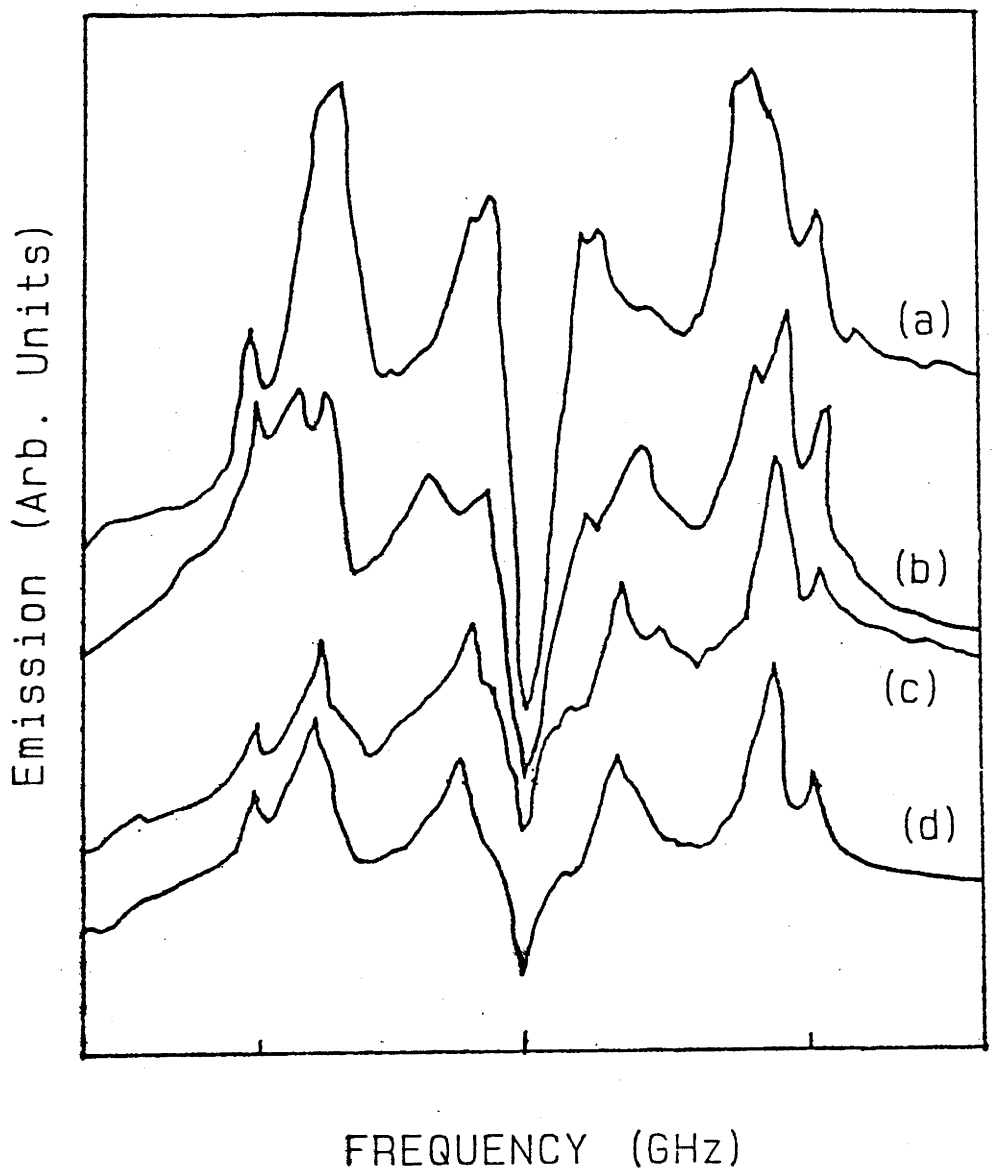

Figure 4.12 Two laser holeburning spectrum at various wavelengths within the zero phonon line.

4.8 MAGNETIC CIRCULAR DICHROISM OF INHOMOGENEOUSLY BROADENED ZERO-PHONON LINE

Information about electronic states involved in a transition can, in general, be obtained by applying perturbations such as magnetic field, electric field and uniaxial stress to the system. If a degenerate electronic state is involved, the degeneracy is usually lifted by the application of magnetic field. From the resulting spectra one can then obtain information about the symmetry and degeneracy of the electronic state. This is conventional Zeeman effect. An essential requirement for the usefulness of this method is that the splitting due to the perturbation should be resolvable. However, MCD (Magnetic Circular Dichroism), which measures the difference in the absorption of left and right circularly polarised light in the presence of magnetic field is more useful than the Zeeman effect when the Zeeman splittings are not resolved. Hence, it can be applied to the study of broad bands where the splittings are much smaller than the width of the band.

The MCD experiments were performed to obtain information about the spin state of the $A \rightarrow E$ transition of the N-V centre. Let E_X and E_Y represent the two degenerate levels of the excited E state before the application of external magnetic field. Then the magnetic field along the Z direction will lift the degeneracy and the levels can then be represented by $E_{-(X+iY)}$ and $E_{(X-iY)}$. Transitions to these levels are left and right circularly polarised as shown in figure 4.13 (a). The absorption line shape in the absence of magnetic field is shown in figure 4.13 (b). When the absorption in left and right circular polarisations is measured, one line for each polarisation separated by the Zeeman splitting would be observed as in figure 4.13 (c). Since MCD is the difference in the absorption of left and right circularly polarised light, it will have the line shape shown in figure 4.13 (d).

If the transition is $E \rightarrow A$ the splitting and selection rules would be same as before but because the splitting is in the ground state, the population of the Zeeman components would be determined by the appropriate Boltzmann distribution. The relative intensities of the left and right circularly polarised components depends on temperature. At high temperatures, the MCD signal has a symmetrical derivative line shape, similar to that discussed before. At

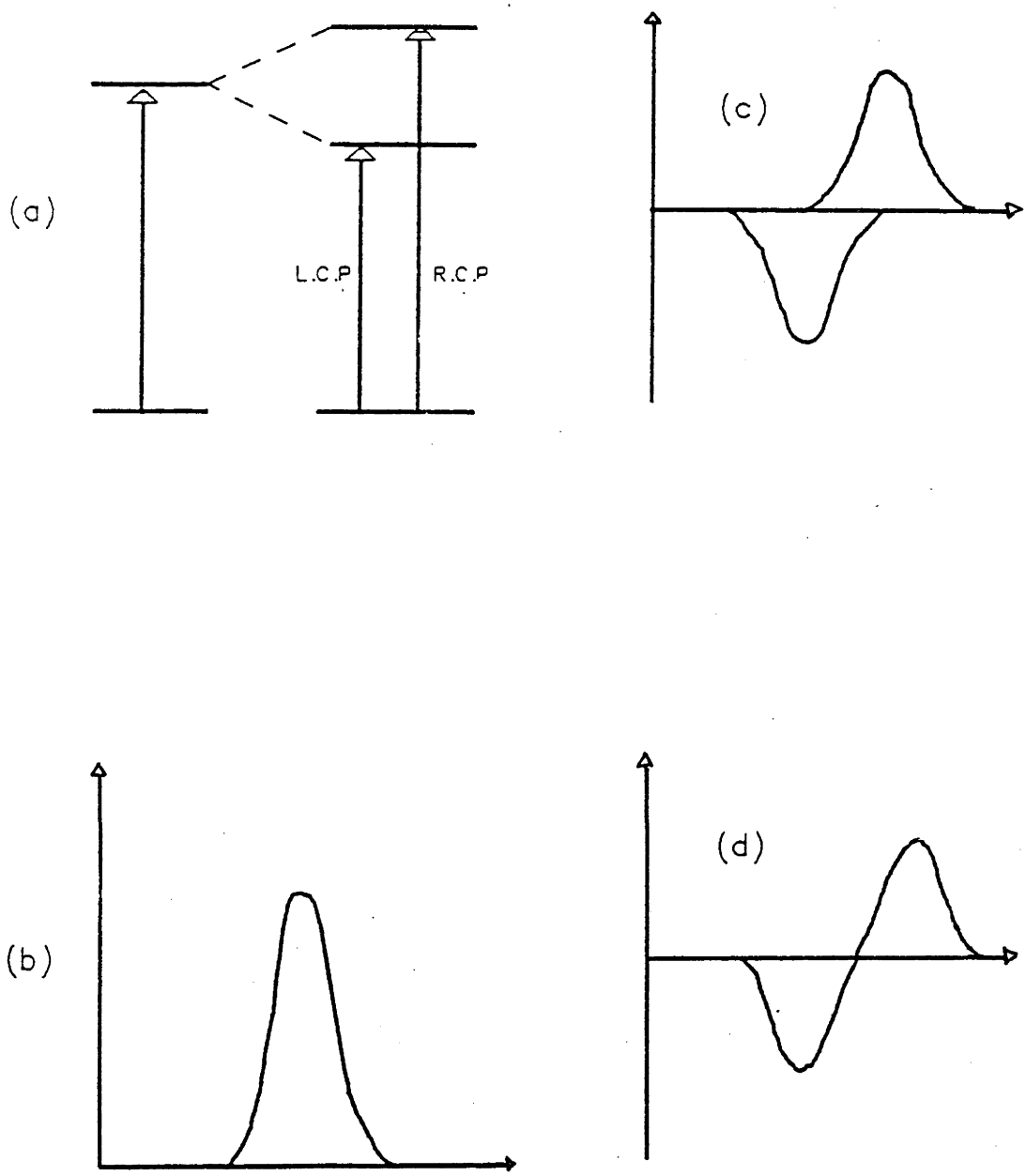

Figure 4.13 a) Effect of magnetic field on ^1A and ^1E states and the selection rules for absorption of lcp and rcp. b) Absoption of circularly polarised light in zero magnetic field. c) Absorption of lcp and rcp presence of magnetic field as a function of wavelength. d) MCD induced by the magnetic field $\Delta\epsilon = \epsilon_{lcp} - \epsilon_{rcp}$.

low temperatures, however the transition from the upper split level will lose intensity (due to decrease in population) and the resulting patterns are shown in figure 4.14 (c) and (d). The MCD line shape becomes absorptive as in figure 4.14 (d). The important point to note is that the MCD is temperature dependent whenever there is a ground state degeneracy.

Apart from those mentioned above there is another situation where a temperature dependent MCD signal can be expected. The MCD in the 638 nm transition is temperature dependent. This transition is known to be $A \rightarrow E$ but clearly this cannot be ${}^1A \rightarrow {}^1E$ or else the MCD to be reported below would be temperature independent. A ${}^2A \rightarrow {}^2E$ is not considered as the centre is established to be an even electron system. The situation for a ${}^3A \rightarrow {}^3E$ is illustrated in figure 4.15 . When there is spin degeneracy, in a magnetic field levels with different M_S values are split. These levels are further split due to the orbital g factor and each level with a particular M_S value is split into E_+ and E_-. But more significantly, as will be detailed later in this section, this splitting differs with the M_S value. Since the size of the MCD signal depends on the splitting, it will be different for transitions ending in different spin states. Now if the relative population between various spin states can be varied with temperature then a temperature dependent MCD signal is to be expected although shape of the MCD signal should not change.

The method of moments was first introduced by Henry *et al* (1965) while discussing the effect of external perturbations on optical spectra of colour centres. The theory was generalised by Stephens (1970) to absorption bands. The technique is very useful in extracting information about electronic states by integrating absorption and MCD data. From the theory of MCD it follows that g is proportional to the ratio of the first moment of MCD to the zeroth moment of absorption. This point is explained in the following. Consider an $A \rightarrow E$ transition which in zero magnetic field has an intensity I. In the presence of a magnetic field the E state splits into two components. Transitions to these components are left and right circularly polarised as

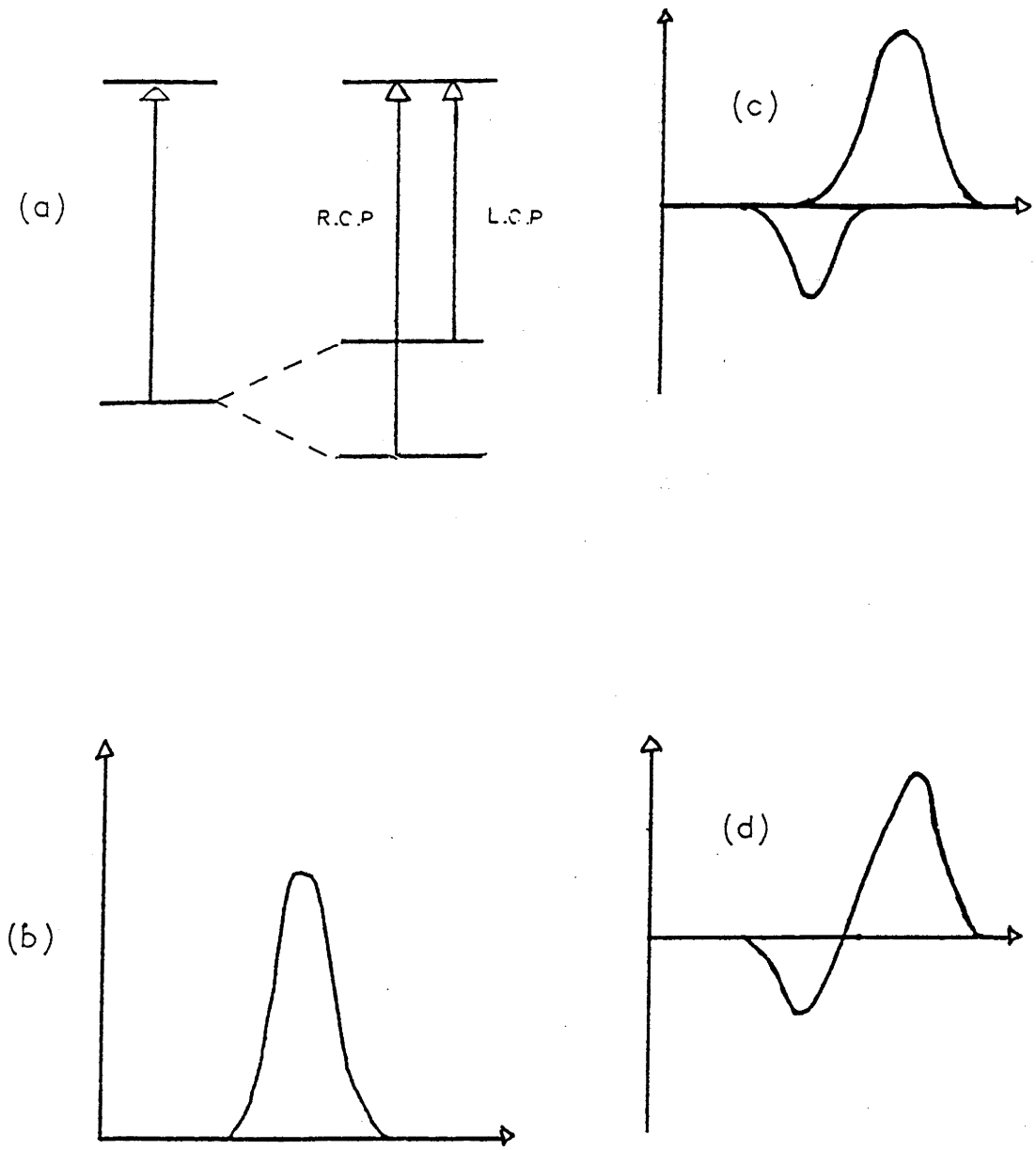

Figure 4.14 a) Effect of magnetic field on ^1A and ^1E states and the selection rules for absorption of lcp and rcp. b) Absoption of circularly polarised light in zero magnetic field. c) Absorption of lcp and rcp presence of magnetic field as a function of wavelength (at low temperature). d) MCD induced by the magnetic field $\Delta\epsilon = \epsilon_{lcp} - \epsilon_{rcp}$ (*at low temperature*).

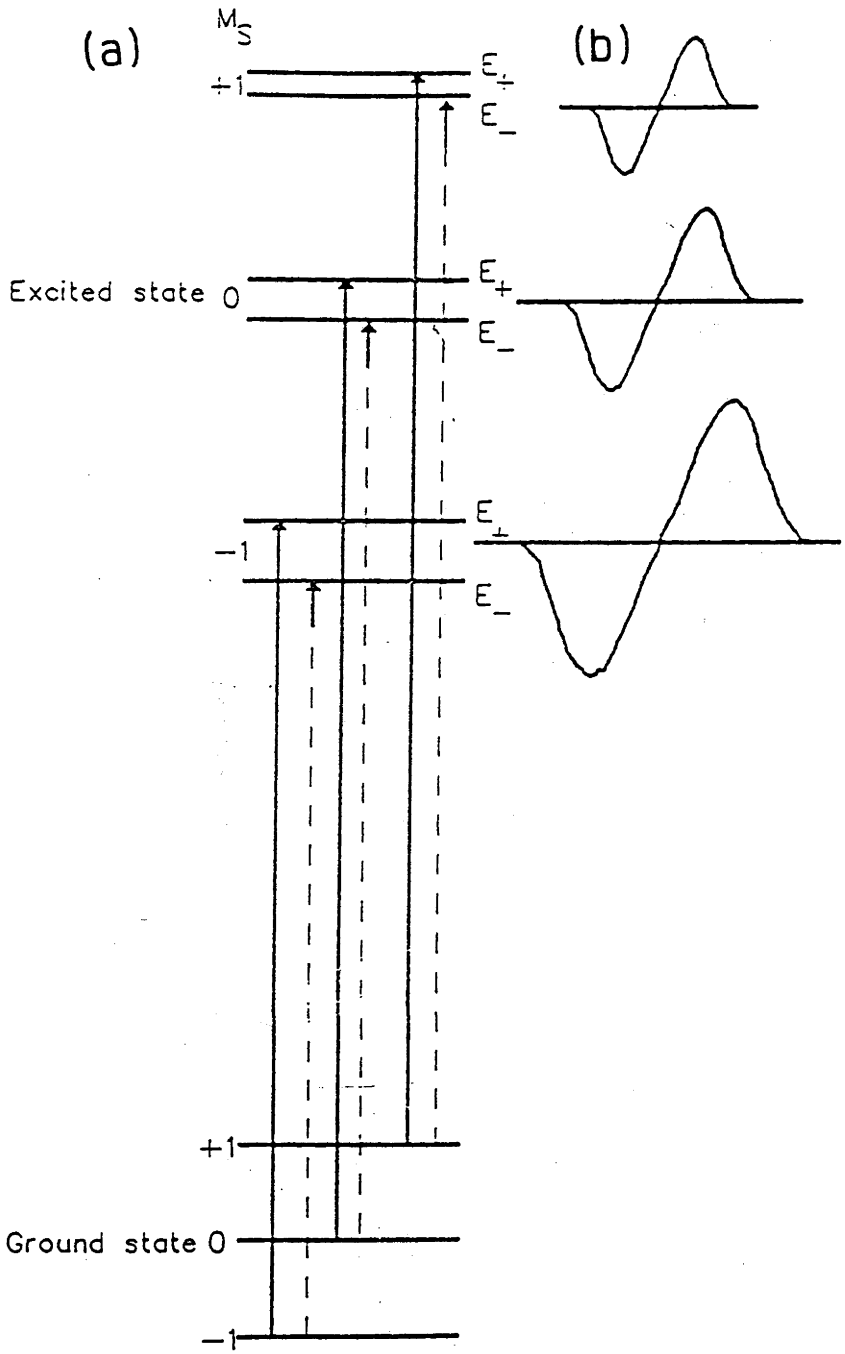

Figure 4.15 a) Effect of magnetic field on ^3A and ^3E states and selection rules for the absorption of lcp and rcp in the presence of a magnetic field. b) MCD associated with each of the spin states.

shown in the figure below.

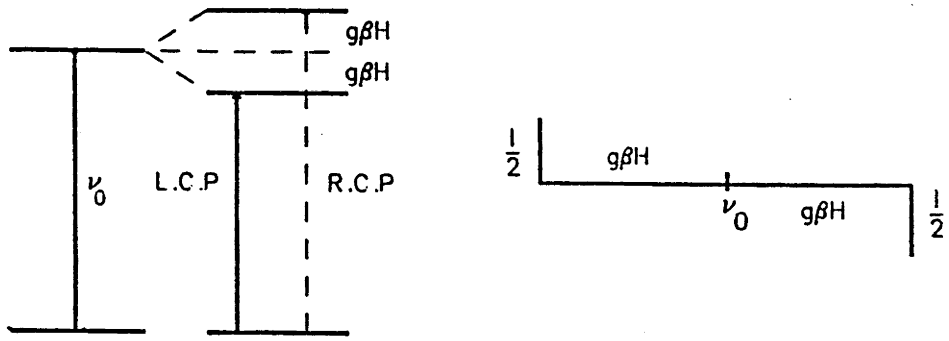

The intensity of each of these transitions is half that at zero magnetic field. Assuming delta line shape for these transitions, the first moment of MCD is defined as the sum of the product of the intensity and splitting. i.e. First moment of MCD=$\frac{I}{2}$.gβH + $\frac{I}{2}$.gβH = I.gβH. The zeroth moment of absorption is just the intensity of the transition i.e. I. From the expressions it follows that the ratio of of the first moment of MCD to the zeroth moment of of absorption is equal to gβH. The procedure for analysing the data when the transitions have a finite line shape is discussed in the above mentioned references (Henry *et al*, 1965 and Stephens, 1970).

To get the equivalent expression for a $^3A \rightarrow {}^3E$ we have to consider spin-orbit interaction in ^3E. It was noted earlier that the MCD signal is temperature dependent and that this was due to different orbital splitting associated with different spin states. This arises because of spin-orbit interaction and is treated here. The spin-orbit interaction Hamiltonian H_{so} and the Hamiltonian describing the effect of the magnetic field H_H can be written as

$$H_{so} = \lambda l.S \quad and \quad H_H = \beta H.(L + 2S).$$

Consider a ^3E state and X, Y, Z basis. Assume the magnetic field to be along the Z direction, then the Hamiltonian $H_{so} + H_H$ can be written as

$$\lambda(L_X S_X + L_Y S_Y + L_Z S_Z) + \beta H_Z.(L_Z + 2S_Z).$$

When the spin-orbit interaction is anisotropic, the above expression can be written as

$$\lambda'(L_X S_X + L_Y S_Y) + \lambda(L_Z S_Z) + \beta H_Z.(L_Z + 2S_Z)$$

where λ' is different from λ.

In large magnetic fields where the spin splittings are large, only the diagonal terms need be considered. These matrix elements in a $|LM_S>$ basis where L=E_+ or E_- and M_S =0 or ± 1 are given below.

	$E_+ +$	$E_- +$	$E_+ 0$	$E_- 0$	$E_+ -$	$E_- -$
$E_+ +$	$(2S+L).\beta H+\lambda$					
$E_- +$		$(2S-L).\beta H-\lambda$				
$E_+ 0$			$+L\beta H$			
$E_- 0$				$-L\beta H$		
$E_+ -$					$(-2S+L).\beta H-\lambda$	
$E_- -$						$(-2S-L).\beta H-\lambda$

The splitting represented by this matrix is illustrated in figure 4.15 .

The electric dipole transition operator does not contain spin. Hence the $^3A \rightarrow {}^3E$ transition can be considered as three separate transitions between the spin +1 states, spin 0 states and spin -1 states (figure 4.15). Each of these is an $A \rightarrow E$ transition and will give left and right circularly polarised absorption when the E state is split by $g_{orb}\beta H$. For S=0 level the splitting between the components of the E state is just $g_{orb}\beta H$ while for the M_S=± 1 levels it is given by

$$g_{orb}\beta H + \lambda < S_Z > .$$

The first term in the above expression is the orbital zeeman interaction term and is temperature independent while the second term is the tem-

perature dependent spin polarisation term. The expression for $< S_Z >$ is obtained below.

Consider an orbitally non degenerate ground state of spin S. In a magnetic field it splits into 2S+1 levels with M_S values - S, - S+1..... , S. Since an orbitally non degenerate state is being considered, the spin states can be chosen to represent various levels. The time averaged value of S_Z in any one level is equal to the M_Z value of that level. Then the time averaged value of S_Z for the complete system can be obtained by summation over all levels. Assuming a Boltzmann population distribution

$$< S_Z >= \frac{\sum_i < S_Z >_i exp(-E_i/kT)}{\sum_i exp(-E_i/kT)}$$

$$< S_Z >= \frac{\sum_{M_S} M_S exp(-g\beta H M_S/kT)}{\sum_{M_S} exp(-g\beta H M_S/kT)} \quad (1)$$

Since the MCD is directly proportional to $< S_Z >$, from the above expression it is clear that MCD will have a temperature (T) dependence and will vary as as above.

4.9 MCD-EXPERIMENTAL RESULTS

The trace shown in figure 4.16 is the zero-phonon absorption line of the N-V centre taken at 100 K and figure 4.17 is the MCD signal of the same at magnetic field value of 4 Tesla along < 111 > direction. The splitting due to the magnetic field ($g\beta H$) calculated from the expression had all the centres been oriented along the < 111 > direction gives a value of 0.63 cm^{-1} for the splitting. Hence, the value of g is 0.36 cm^{-1}. However, there is a correction factor to be included for various orientations of the defect centre. For a trigonal centres there is an equal probability of centres along all four of the possible axes. When a field is along a symmetry direction of the cube these centres make different angles with the field, and overall Zeeman pattern will

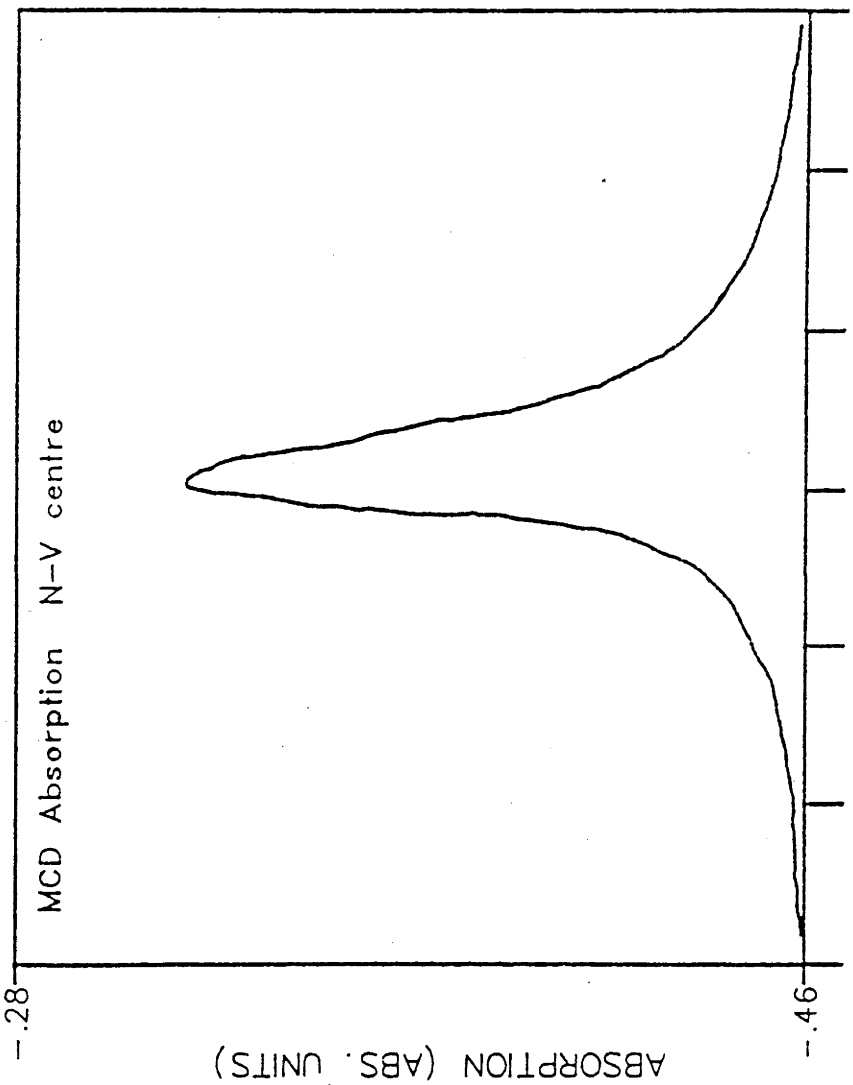

Figure 4.16 Zero phonon absorption line of the N-V centre in diamond

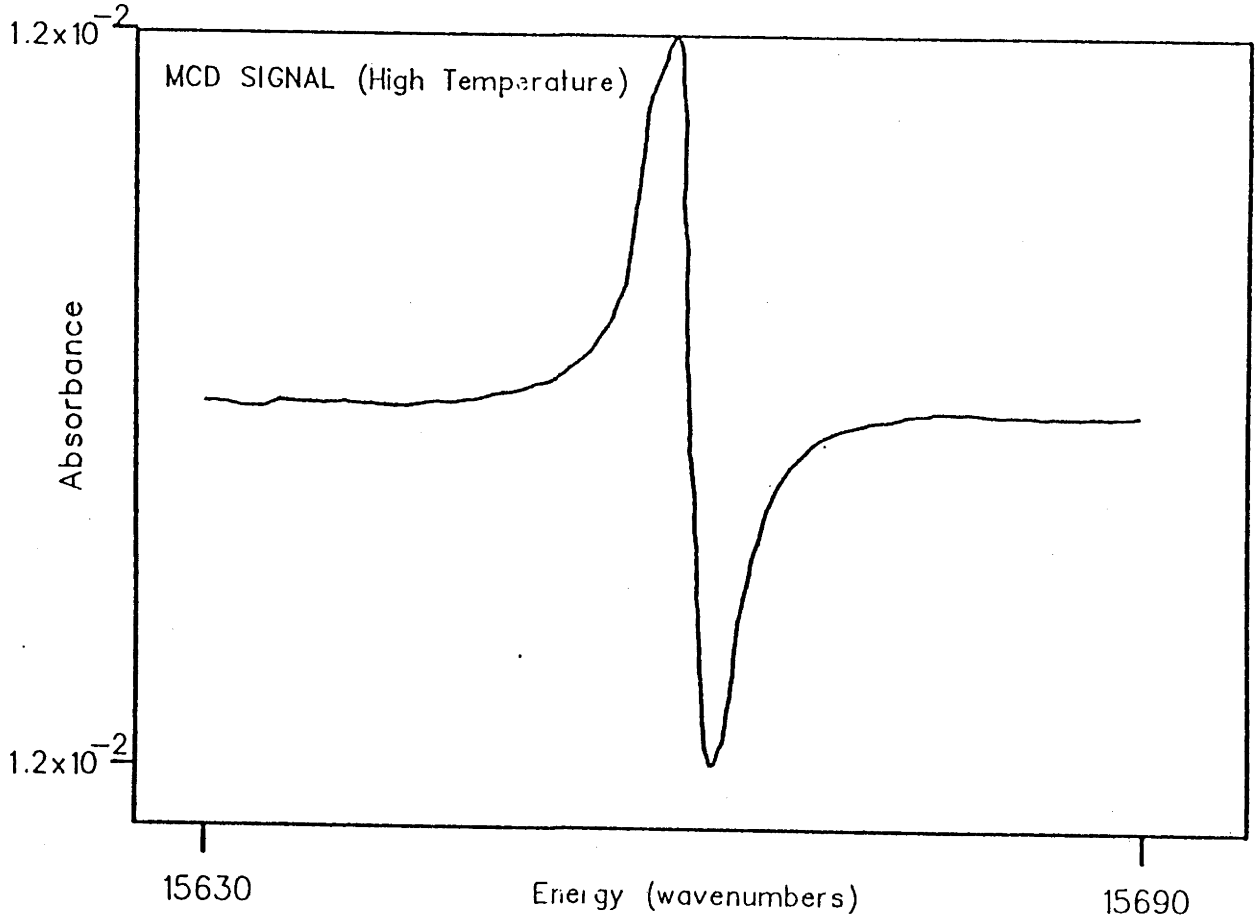

Figure 4.17 Magnetic circular dichroism signal of the zero phonon line of the N-V centre at high temperature.
H=3 tesla and T=100 K

be the statistical average of the contributions from each group of sites. When the magnetic field makes angle θ with trigonal axis, the splitting is reduced by cosθ and the lines are no longer totally polarised. A transition which is completely polarised and has intensity I for θ =0 is reduced in intensity to $(1/2 - \cos^2\theta)I$ and a transition which is completely forbidden for θ =0 gains an intensity $(1/2 + \cos^2\theta)I$. For a field along a < 111 > direction this results in an axial Zeeman pattern as given by Shah (1976). It is noted that the moment of MCD for such a pattern is increased to 3/2 of its value when all the centres are aligned along the < 111 > axis. It has been pointed out by Shah (1976) that the MCD is isotropic, so any misorientation about the < 111 > direction would not change its value. Thus the corrected value of g_{orb} is 1.5 times that given above. This gives the corrected g value as 0.54 .

The results of experiments on temperature dependence of MCD in this N-V centre are shown in figure 4.18 . The experiment was done at two values of magnetic field, 4 Tesla and 3 Tesla. The MCD signal has a derivative line shape and its magnitude increases with decreasing temperature. The shape of the MCD signal however, does *not* change. In a magnetic field levels with different M_S values will be split. The relative populations of the levels with M_S values -1, 0 and +1 would, as described previously, be dependent on temperature. At very low temperature (1.6 K) the time averaged value of spin is -0.96 while at 100 K it is -0.03. Since MCD varies as $< S_Z >$, the percentage change in MCD seen in figure 4.19 is as can be expected from expression for $< S_Z >$ (equation (1) in previous section). Further since the effective spin value decreases with temperature it can be inferred that the spin-orbit coupling constant (λ) is negative (or the orbital g value is negative). When the spin-orbit coupling constant is negative the splitting between E_+ and E_- levels for $M_S = -1$ is greater than that for $M_S = +1$. Since at low temperatures the total MCD signal is predominantly due to the levels associated with $M_S = -1$, it is greater (because of larger splitting) than at higher temperatures. At high temperatures, all the three spin levels are equally populated ($< S_Z >$ at 100 K is -0.03). The total MCD, which is the average of the signal from the three spin states will be less because of smaller contributions from the $M_S = 0$ and +1 states. Hence the results of the MCD experiments show that the ground state of this centre is degenerate and because it is an orbital singlet the degeneracy has to come from spin. The conclusion that this temperature dependent MCD does not arise from orbital degeneracy is supported by the fact that the shape170

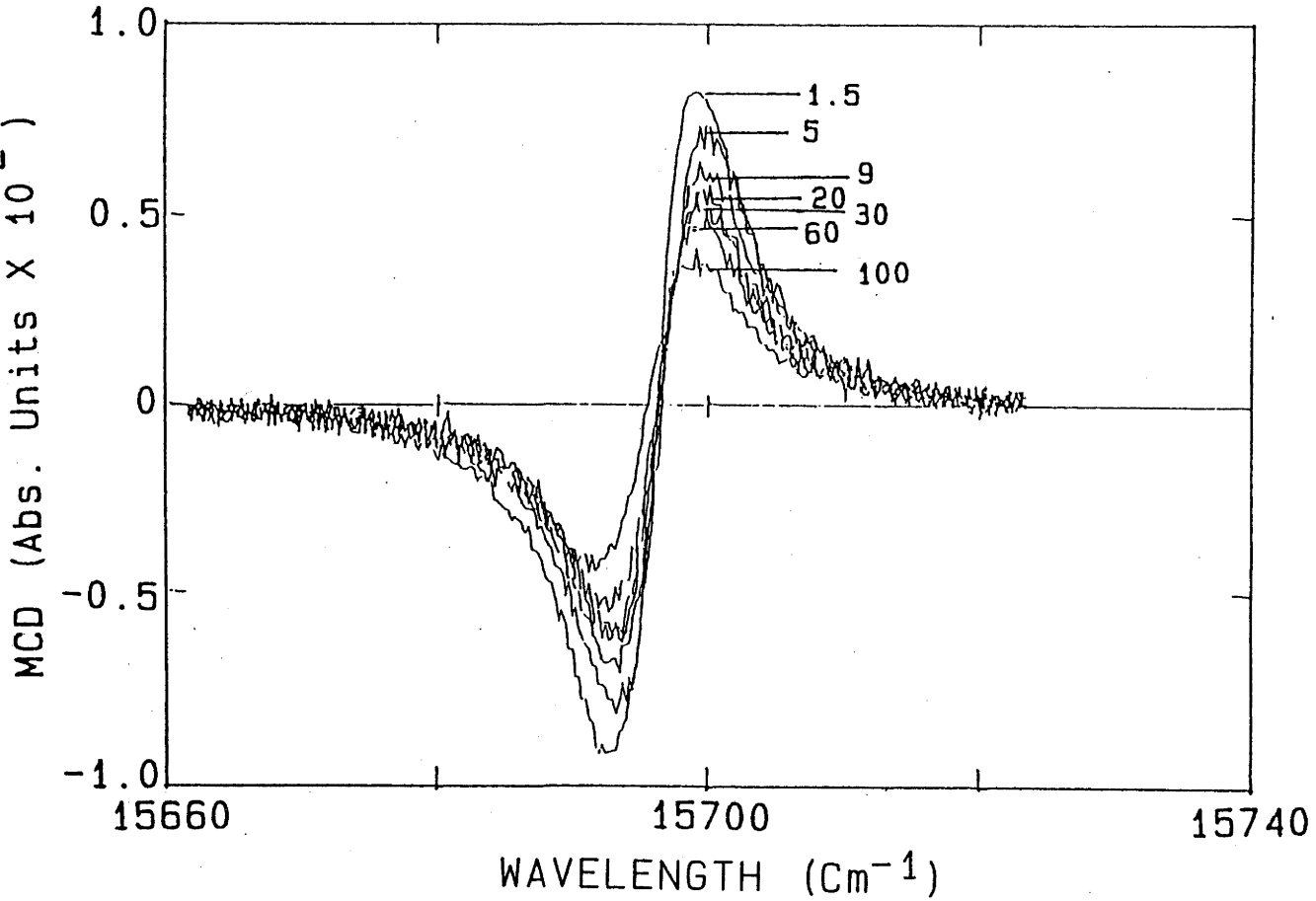

Figure 4.18 Magnetic Circular Dichroism experimental results as a function of temperature (values as shown). The experiments was performed at 4 Tesla. Note that the shape of the signal does not change with temperature.

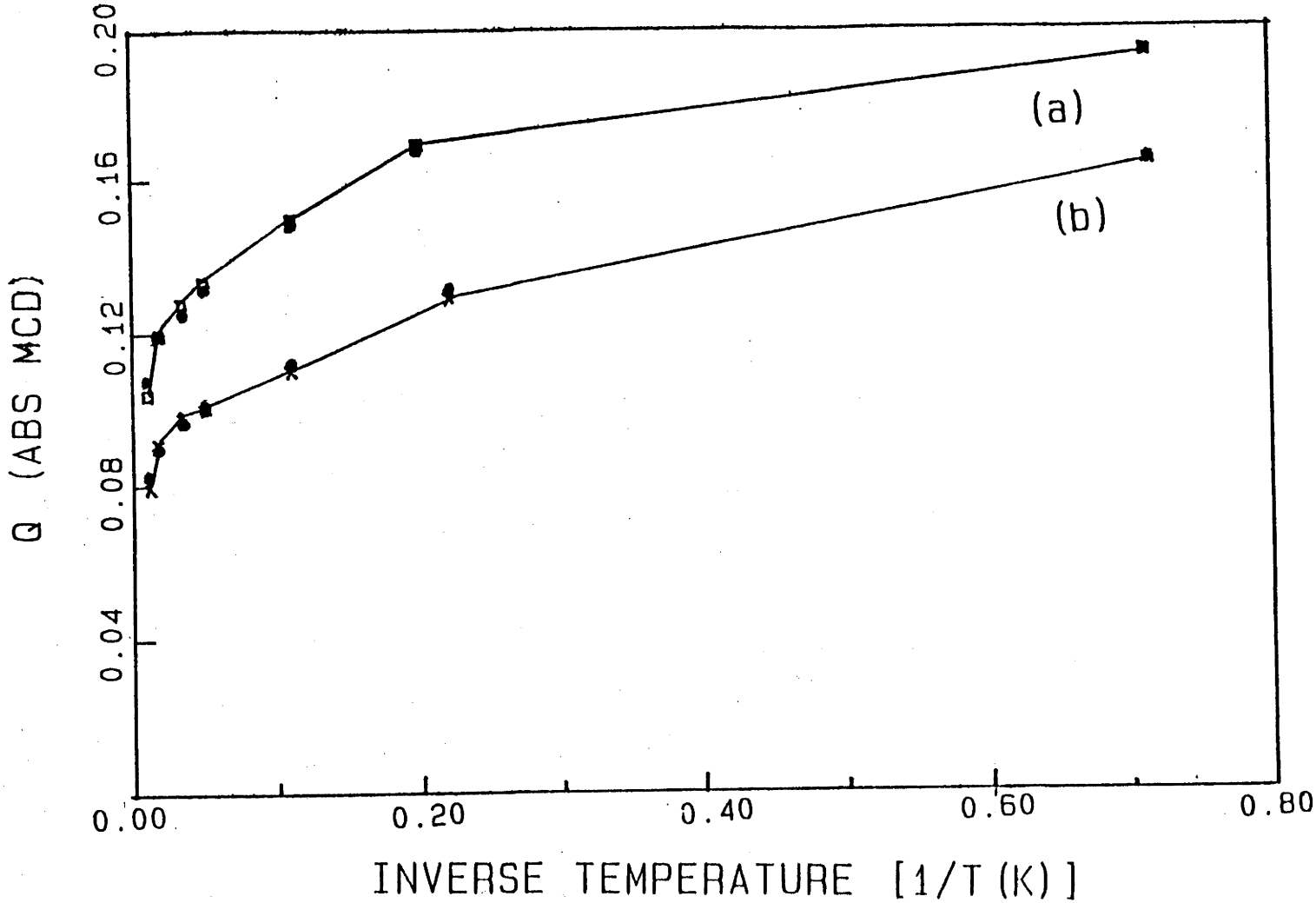

Figure 4.19 Variation of Magnetic Circular Dichroism signal with temperature (experimental traces shown in figure 4.18) at 4 Tesla (a) and 3 Tesla (b). '■' represent the variation calculated using equation for $< S_Z >$ (refer text).

of orbital degeneracy the shape of the MCD changes from absorptive (low temperature) to derivative (high temperature) line shape as the temperature is increased. From the relative contributions of the temperature independent MCD ($g_{orb}\beta$H) and the temperature dependent MCD ($g_{orb}\lambda < S_Z >$) at high (100 K) and low (1.5 K) temperatures the value of λ is estimated. The values of the spin-orbit parameter and and g_{orb} calculated from the temperature dependence of MCD are λ = -1.0 $\pm$0.1 cm^{-1} and g_{orb} = 0.54 $\pm$0.05 respectively.

4.10 EFFECT OF ELECTRIC FIELD ON THE TWO LASER SPECTRUM

The experimental arrangement for observing electric field effects was already described in chapter 3. Electric fields upto 10Kv/cm were applied along the < 111 > direction in diamond after obtaining the spectrum at zero field and storing it in one memory channel of Princeton Applied Research model 4142 signal averager. The spectrum in the presence of electric field was then detected and compared with the spectrum at zero field. The two spectra were found to be same. Difference trace of the two spectra obtained on the signal averager was in fact a straight line.

4.11 EFFECT OF MAGNETIC FIELD ON THE TWO LASER SPECTRUM

Zeeman studies on this centre using the two laser spectrum were quite informative. When a field of about 100 G was applied to the sample using hand held bar magnets the 2.88 GHz antihole was observed to split. Since microwave holefilling signal at 2.88 GHz is associated with this centre, it was logical to compare the two experiments in detail.

The ODMR (Optically Detected Magnetic Resonance) technique was used to observe the 2.88 GHz microwave resonance. This experiment was very similar to the ODMR experiment performed by Bloch ***et al*** (1985) on the

same centre. However the explanation of the observed holefilling is different. A description of the microwave equipment used in the present experiment has already been given in chapter 2. The microwave resonance was detected by monitoring the emission level from the centre while the microwaves are scanned. When the high resolution laser is tuned to the zero-phonon line at 638 nm, some of the optically excited centres exhibit holeburning (i.e. they do not return directly to the original ground level). When the microwave frequency is at 2.88 GHz the hole depth becomes less and thus there is an increase in the emission level.

For a field along < 111 > direction the microwave resonance (detected by holefilling) is shown in figure 4.20 . The two outer most resonances corresponding to $M_S = 0 \rightarrow M_S = \pm 1$ are due to the centres with their defect axis along the magnetic field and hence have the maximum splitting ($g\beta$H). The other two resonances are due to the centres oriented perpendicular to the < 111 > axis. The entire spectrum can be explained using the spin hamiltonian

$$H = g\beta.H.S + D[S_Z^2 + \frac{1}{3}S(S+1)]$$

The above explanation for the holefilling resonances is valid irrespective of the $^3A_2$ state being a metastable state or the ground state.

The diamond was mounted in the microwave sample holder and placed in a glass cryostat. Magnetic field along < 100 > was applied externally using a pair of Helmholtz coils. The two laser holeburning spectrum was obtained using the normal procedure and then the magnetic field was applied. When the magnetic field is along the < 100 >direction all the centres aligned along the four trigonal directions are equivalent. Thus, in a microwave holefilling experiment only two resonances are observed. Experimentally, the 2.88 GHz antihole is observed to split into two components. To obtain a better measure of the splitting the following procedure was observed. The read laser frequency was shifted with respect to the burn laser by 2.88 GHz so that the antihole is now at the centre of the scan and then the scan width of the read laser was reduced suitably (to about 5 GHz) to give a spectrum shown in figure 4.21 . Then without changing the magnetic field the read laser beam was blocked and microwave resonances were measured as described above.

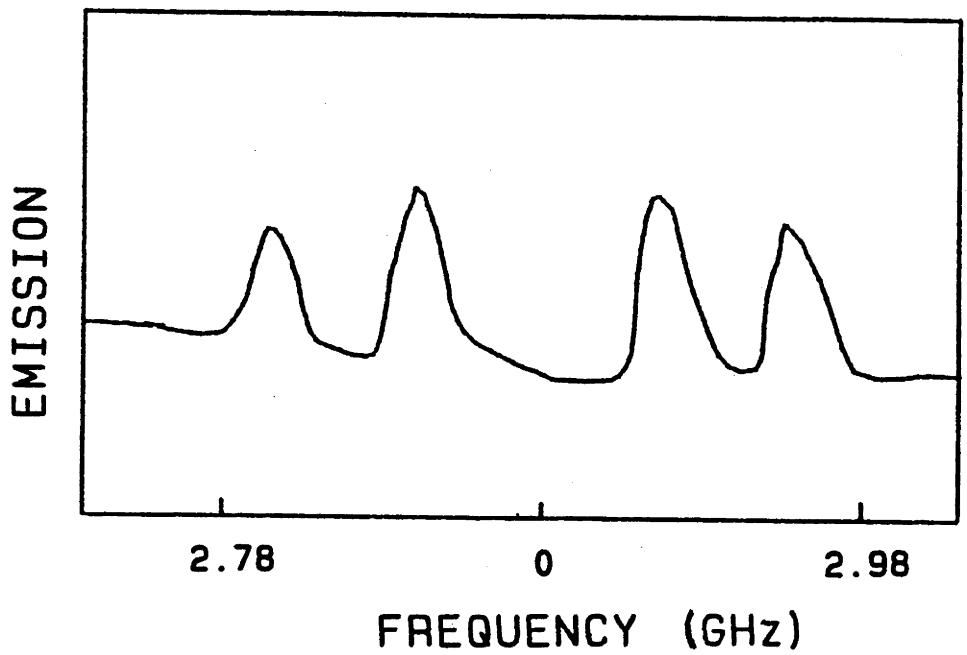

Figure 4.20 Microwave holefilling resonances observed at a magnetic field value of 100 Gauss along the < 111 > direction.

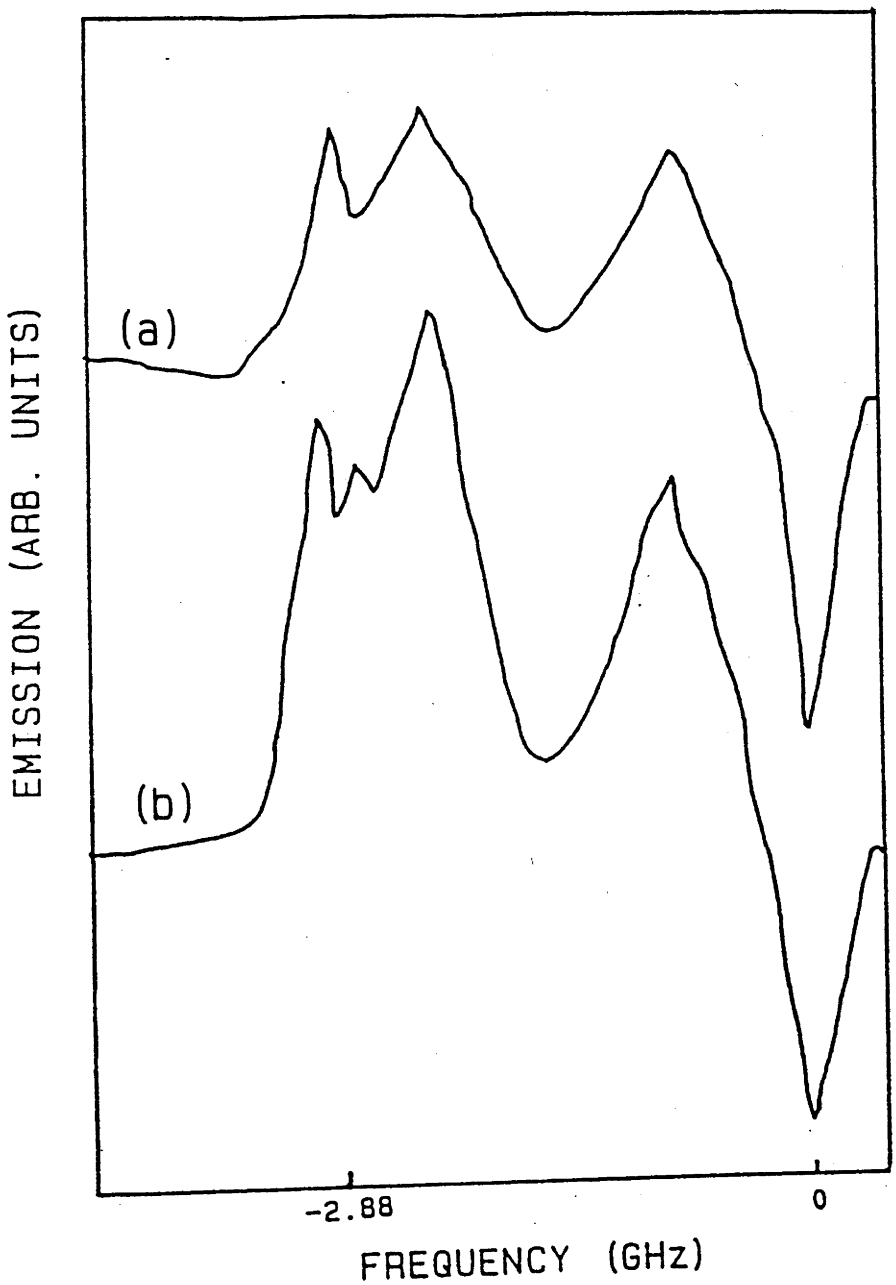

Figure 4.21 Zeeman splitting of the 2.88 GHz antihole (b). The magnetic field (100 gauss) is along the < 100 > direction where all the centres are crystallographically equivalent. (a) represents the trace at zero magnetic field.

This procedure was repeated at various values of magnetic field and the results obtained are plotted in figure 4.22 . It is concluded that the magnetic field splitting of the 2.88 GHz antihole in the two laser holeburning spectrum is the same splitting as the microwave resonance signal. This confirms that the separation of 2.88 GHz obtained from the holeburning spectrum is the same splitting as seen in ODMR and the ground state splitting of the $^3A_2$ state deduced from EPR data.

4.12 EFFECT OF MICROWAVES ON POPULATION HOLEBURNING

The lifetime of the excited state in this centre, measured by luminescence experiments (Collins *et al*, 1983) is 13 nsecs. This suggests that the transition is spin allowed and that the predominant decay path after optical excitation, is directly to the ground state. This however does not preclude the possibility of decay into a different level of the ground state when the ground state consists of more than one level. A small fraction of the excited state population may also decay indirectly via a metastable state. In either case the original population of centres with transitions resonant with the laser is redistributed. The result is that the population of centres resonant with the laser is decreased and hence an optical hole results. The characteristics of such a hole depends directly on the relaxation rates that cause the centre to decay to its original state. If the relaxation rates can be affected using the microwaves then the hole characteristics are changed. The effect of microwaves on holeburning were detected by monitoring the emission level (as described in the previous section) and the results are shown in figure 4.19 . Two schemes are proposed for explaining the ODMR signals observed for the present diamond system.

i) If the energy level scheme of Loubser *et al* (1977) is accepted with a metastable triplet state ($^3A_2$) is accepted then the effect of microwaves on hole depth are as discussed by Bloch *et al* (1985). They assume that the relaxation paths to the ground state from the $M_S = \pm 1$ and $M_S = 0$ levels of the metastable $^3A_2$ state are different and holeburning occurs due to lower relaxation from the $M_S = 0$ level to the ground state. The relaxation rate to the ground state from the $M_S = \pm 1$ level is three orders of magnitude faster

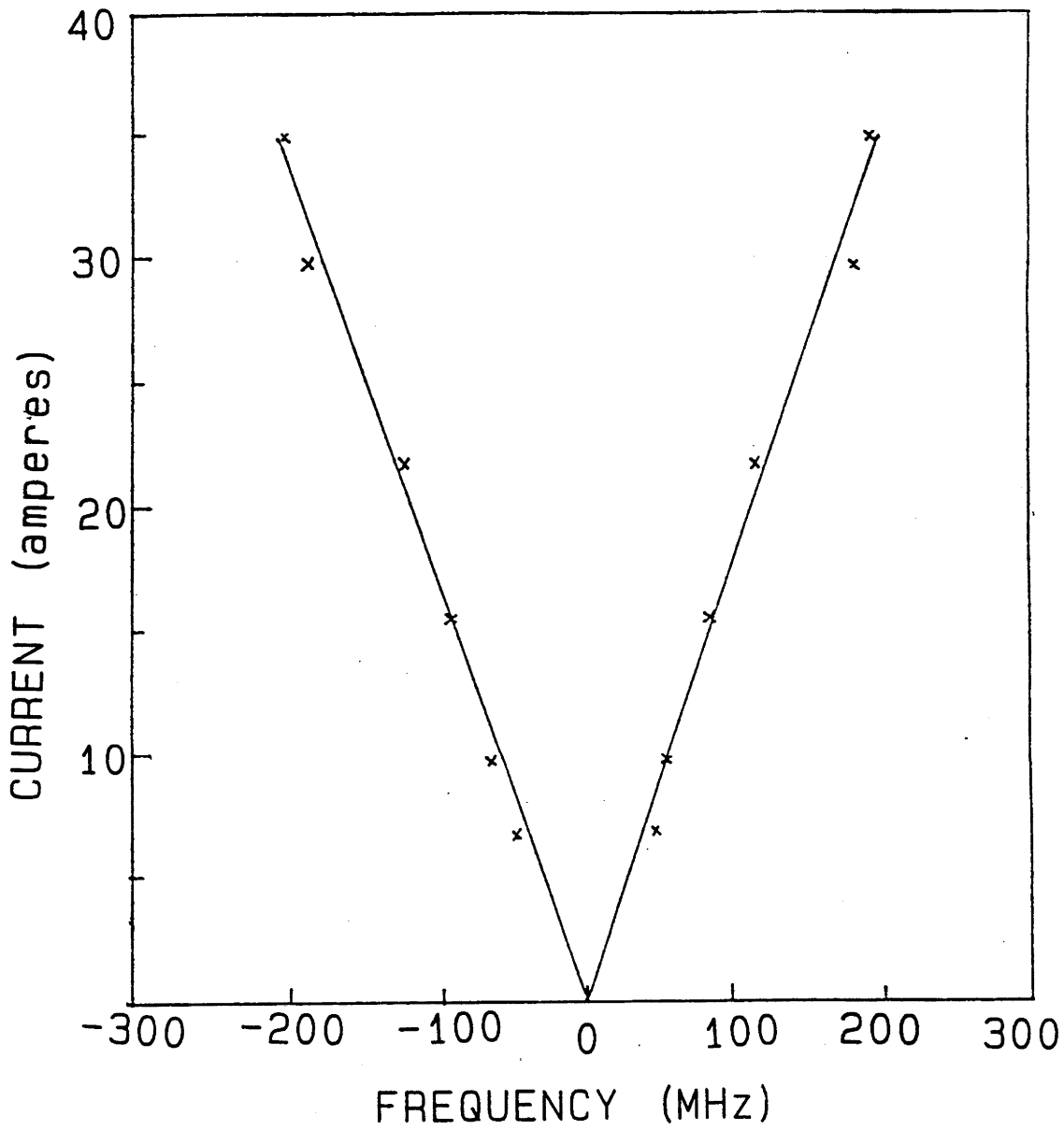

Figure 4.22 Zeeman splitting of the 2.88 GHz antihole versus magnetic field. Solid lines indicate represent expected variation assuming a triplet state with zero field splitting of 2.88 GHz.

than from the M_S= 0 level. When the microwaves applied to the diamond are resonant with this splitting (2.88 GHz) centres decay to the ground state much faster and thus the hole depth is reduced.

ii) Similar holefilling effect can be seen when the $^3A_2$ state is assumed to be the ground state. This requires selective feeding of the electrons into one of the levels of the $^3A_2$ due to either selection rules or due to the presence of another metastable state. When this happens effect of microwaves is to equalise the population between the two spin levels (M_S= 0 and M_S= $\pm$1) and hence affect the depth of the hole.

The above two schemes explain the ODMR signals in a magnetic field equally well. Hence, these results by themselves cannot distinguish between the situations (^3A being metastable state or the ground state) but it is emphasised that the ODMR signals are fully consistent with a ^3A ground state.

4.13 EFFECT OF MICROWAVES ON PHOTOCHEMICAL HOLEBURNING

Photochemical holeburning normally occurs through the centre losing an electron when it is in an optically excited state. Such a process would qualitatively depend on the time the centre remains excited. Since microwaves affect the relaxation rate to the ground state the effect of microwaves on photochemical holeburning was studied. The lifetime of the photochemical hole was more than 30 minutes. The depth of the hole without any external perturbations was studied and the hole depth is plotted against time in figure 4.23 . Microwaves were applied to the diamond when the hole was being burned and it was observed to have no effect on the depth of the hole that could be burnt. Next part of the experiment microwaves were applied to the crystal after the hole was burnt. In all the cases the decay curve of the hole was found to be the same within experimental error. This indicates that the 2.88 GHz microwave resonance is not involved in anyway with photochemical holeburning process. If the 2.88 GHz microwave resonance is connected with a metastable state (or the excited state) from where the centre loses an electron in the process of photochemical holeburning, then in the presence of

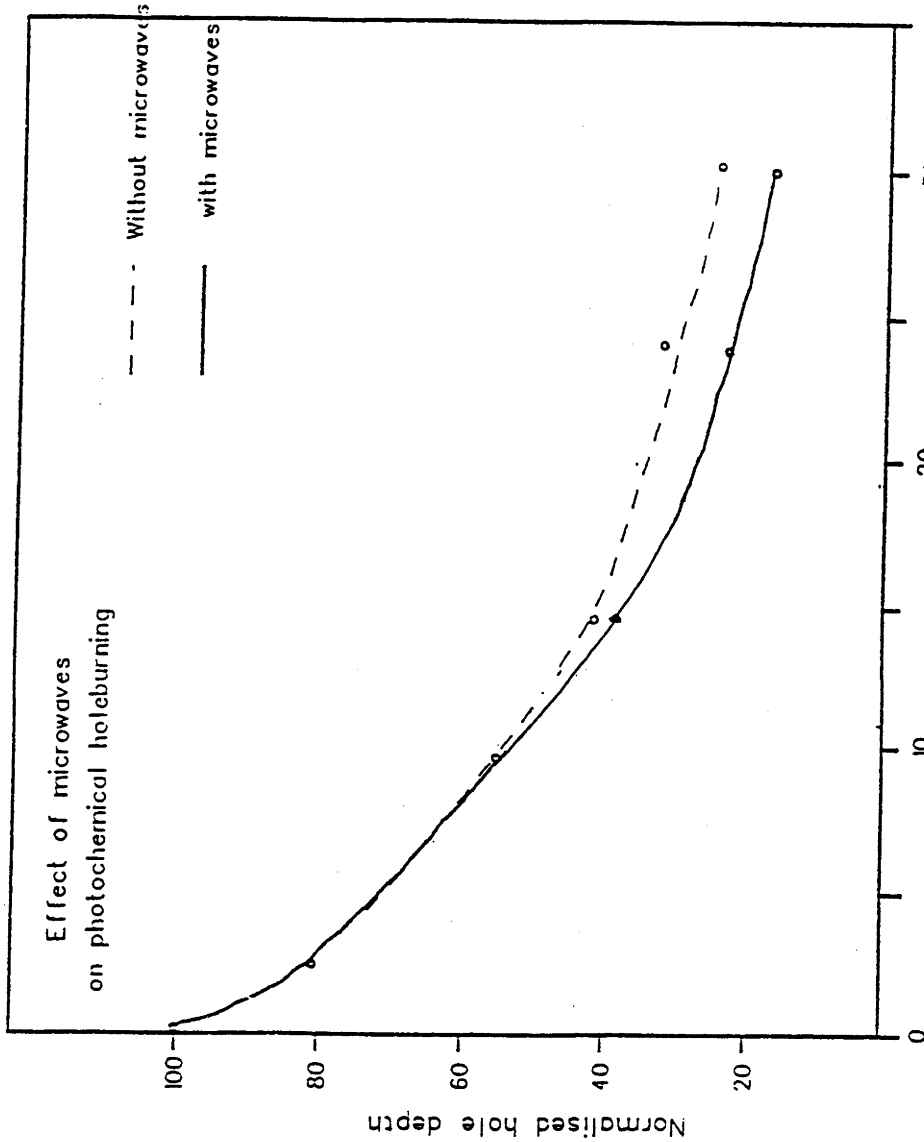

Figure 4.23 The effect of microwaves on photochemical component of the hole . The hole was burnt in the presence of the 2.88 GHz microwaves.

microwaves which increase the relaxation to the ground state, the depth of the photochemical hole should decrease. But this is contrary to observation. Hence, these results are thus suggestive (but not conclusive) of a ^3A ground state.

4.14 MICROWAVE RESONANCE WHEN PUMPING IN THE ABSORPTION BAND

ODMR resonances are also observed when the exciting laser is tuned to within the vibronic band rather than in the zero-phonon line at 638 nm. However, the emission was found to decrease rather than increase when microwaves were resonant at 2.88 GHz (figure 4.24).

It is noted that if the metastable ^3A state scheme is accepted then there would be holeburning effect even when pumping in the band as a percentage of the centres would be held in the metastable state. Microwaves would therefore again give an increase (similar in magnitude) in the emission level. However, this is contrary to observation.

If the ^3A is the ground state then there will be no holeburning effect when pumping in the band and no microwave resonance is expected. The signals are certainly very much smaller and the effect is attributed to very small difference in absorption strength out of the two ground state levels. Optical pumping and microwaves can both affect the population of these levels and hence some resonance at 2.88 GHz is expected. Thus, this observation although not clearly understood gives further support for the ^3A ground state.

4.15 CALCULATION OF HOLEBURNING SPECTRUM

In previous sections of this chapter all the results obtained by us on the N-V centre in diamond were discussed. These are briefly summarised here

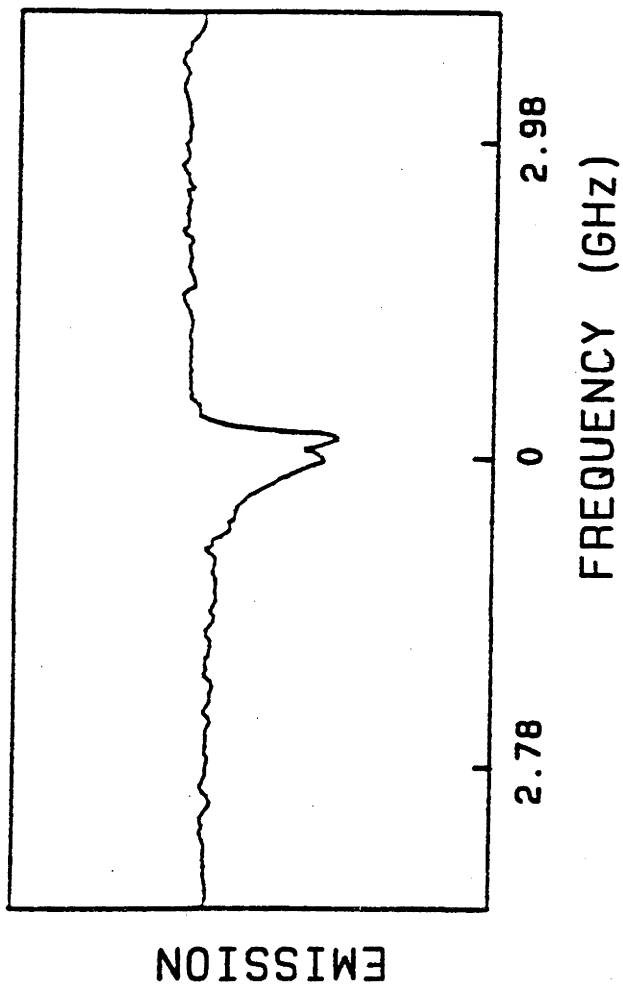

Figure 4.24 Microwave resonance observed when pumping in the vibronic band.

and in the rest of the chapter a theoretical model attempting to explain the experimental results is presented. The important studies performed by others on this centre are listed below.

- Luminescence experiments (Clark *et al*, 1971)
- Uniaxial Stress experiments (Davies *et al*, 1976)
- One laser holeburning experiments (Harley *et al*, 1984)
- EPR experiments (Loubser *et al*, 1977)
- Microwave holefilling experiments (Bloch *et al*, 1985)

First three of the experiments listed above are insensitive to the spin multiplicity of the transition being studied and EPR experiments suggest that this is a singlet→singlet transition with a metastable triplet state. Although Bloch *et al* (1985) explain their microwave holefilling experimental results assuming a triplet metastable state (following Loubser *et al*, 1977) their results are not inconsistent with the model of a triplet ground state. However, the 2.88 GHz antihole in our two laser holeburning spectrum, the temperature dependence of MCD and the Zeeman splitting of the 2.88 GHz antihole strongly suggest that this transition is a $^3A \rightarrow ^3E$ instead of a $^1A \rightarrow ^1E$. All the experimental results of previous workers (except EPR) are consistent with $^3A \rightarrow ^3E$ model. Apart from suggesting that the absence of EPR without optical excitation was due to poor sensitivity, we do not have any other explanation.

In this section the effect of strain and spin-orbit coupling on the holeburning pattern for a $^3A \rightarrow ^3E$ transition is calculated and with some assumptions it is shown that it is possible to obtain a theoretical spectrum similar to that observed experimentally. It has been concluded earlier that variation in strain causes the variations in the holeburning spectrum and hence, strain is considered in modelling the holeburning spectrum. Strain will principally affect the orbital doublet E state and therefore the effect of spin-orbit interaction ($\lambda \mathbf{l}.\mathbf{S}$) and strain on the ^3E state is discussed in the following. A Gaussian distribution of strain is assumed and the spin-orbit interaction parameter deduced from MCD measurements is used in the calculation.

4.15.1 STRAIN

The perturbation due to strain experienced by electronic states (H_{ST}) can be written as

$$H_{ST} = \sum_{i,j} L_{ij}\sigma_{ij}$$

i,j=X,Y or Z where σ_{ij} is the stress tensor and L_{ij} are electronic operators. The stress tensor is symmetric and there are six independent components. For a trigonal centre this can be expressed in symmetry adapted form as

$$H_{ST} = L_{A_1}\sigma_{Z^2} + L_{A_2}\sigma_{X^2+Y^2} + L_{E_X}\sigma_{X^2-Y^2} + L_{E_Y}\sigma_{XY} + L_{E'_X}\sigma_{YZ} + L_{E'_Y}\sigma_{XZ}$$

where as implied by the notation the components in the first two terms transform as A irreducible representation and the latter terms contain components transforming as E irreducible representation (E_X and E_Y).

So in effect the types of strain experienced by a trigonal centre in a cubic lattice is restricted to A type or E type. Each type has however more than one origin and in the general case one should consider a distribution of each of these strains. This would require at least six adjustable parameters and for a simple model is unlikely to lead to any physical insight into the real origin of the problem. To proceed with the calculation only one term of each symmetry is retained.

$$V = L_A\sigma_A + L_{E_X}\sigma_{E_X} + L_{E_Y}\sigma_{E_Y}$$

Since strain operates on orbital states only leaving spin unaffected, the effect of the above three components of strain in an E_X, E_Y basis can be written as

	E_X	E_Y
E_X	$L_A + L_{E_X}$	L_{E_Y}
E_Y	$-L_{E_Y}$	$L_A - L_{E_X}$

where L_A, L_{E_X}, L_{E_Y} are the matrix elements of the strain operator.

The full effect of the strain on the ^3E state in the chosen ($| E_i S_k >$ i = X, Y and k = X, Y or Z) basis is given by the matrix

MATRIX I

	$E_X S_X$	$E_Y S_X$	$E_X S_Y$	$E_Y S_Y$	$E_X S_Z$	$E_Y S_Z$
$E_X S_X$	$L_A + L_{E_X}$	L_{E_Y}				
$E_Y S_X$	$-L_{E_Y}$	$L_A - L_{E_X}$				
$E_X S_Y$			$L_A + L_{E_X}$	L_{E_Y}		
$E_Y S_Y$			$-L_{E_Y}$	$L_A - L_{E_X}$		
$E_X S_Z$					$L_A + L_{E_X}$	L_{E_Y}
$E_Y S_Z$					$-L_{E_Y}$	$L_A - L_{E_X}$

4.15.2 SPIN-ORBIT INTERACTION

The effect of spin-orbit interaction is considered next. In a cubic system the spin-orbit interaction (λL.S) is isotropic and hence can be written in the form

$$\lambda(L_X S_X + L_Y S_Y + L_Z S_Z)$$

where λ is the spin-orbit coupling constant. But when considering a trigonal centre in a cubic lattice the interaction can be split into components transforming as E and A representations of the C_{3v} group. The spin-orbit coupling constants of these two components need not be equal (anisotropic spin-orbit interaction) and the interaction Hamiltonian can be written as

$$\lambda'(L_X S_X + L_Y S_Y) + \lambda(L_Z S_Z).$$

where λ and λ' are the spin-orbit coupling constants. The effect of L_Z and L_X using an E_X, E_Y basis are

$$\begin{vmatrix} 0 & \lambda \\ -\lambda & 0 \end{vmatrix} \quad \text{and} \quad \begin{vmatrix} \lambda' & 0 \\ 0 & -\lambda' \end{vmatrix}$$

respectively. The effect of L_Y is the same as that of L_Z replacing λ by λ'.

Since the ^3E state is an S=1 system (S is the total spin angular momentum), the effect of spin operators S_X, S_Y and S_Z using a X, Y, Z basis is

$$\begin{vmatrix} 0 & -S_Z & S_Y \\ -S_Z & 0 & -S_X \\ S_Y & -S_X & 0 \end{vmatrix}$$

The effect of spin-orbit interaction on the ^3E state is represented by the following matrix.

MATRIX II

	$E_X S_X$	$E_Y S_X$	$E_X S_Y$	$E_Y S_Y$	$E_X S_Z$	$E_Y S_Z$
$E_X S_X$				λ		$-\lambda'$
$E_Y S_X$			$-\lambda$		λ'	
$E_X S_Y$		$-\lambda$			λ'	
$E_Y S_Y$	λ					$-\lambda'$
$E_X S_Z$		λ'	$-\lambda'$			
$E_Y S_Z$	$-\lambda'$			$-\lambda'$		

4.15.3 SPLITTING OF THE ^3E STATE

Hence the full matrix representing the effect of strain and spin-orbit interaction on the ^3E state is obtained by combining matrix I and matrix II

	$E_X S_X$	$E_Y S_X$	$E_X S_Y$	$E_Y S_Y$	$E_X S_Z$	$E_Y S_Z$
$E_X S_X$	$L_A + L_{E_X}$	L_{E_Y}		λ		$-\lambda'$
$E_Y S_X$	$-L_{E_Y}$	$L_A - L_{E_X}$	$-\lambda$		λ'	
$E_X S_Y$		$-\lambda$	$L_A + L_{E_X}$	L_{E_Y}	λ'	
$E_Y S_Y$	λ		$-L_{E_Y}$	$L_A - L_{E_X}$		$-\lambda'$
$E_X S_Z$		λ'	$-\lambda'$		$L_A + L_{E_X}$	L_{E_Y}
$E_Y S_Z$	$-\lambda'$			$-\lambda'$	$-L_{E_Y}$	$L_A - L_{E_X}$

From the temperature dependence of the MCD, the value of the spin-orbit interaction constant λ, is calculated to be -1 cm^{-1} (30 GHz). The value of λ' is considered to be smaller than λ. When a centre does not experience any internal strain, the ^3E state is split due to spin-orbit interaction into three levels separated by λ. However when the centre experiences strain the situation is different. The ^3E state would then be split into six levels in accordance with the matrix above.

It can be seen from the matrix above that the effect of A type strain is to shift all the levels of the ^3E state by the same amount (the matrix elements L_A of A type strain are diagonal and have the same magnitude and sign). In a holeburning experiment, the effect of A type strain is to bring various levels of the ^3E into resonance with the laser. In the present calculation this is accounted for by considering all transitions between the different levels of the ground and excited states. So, by using this approach, the effect of A type strain is being considered but in what follows it is not necessary to include it in evaluating the matrix. The splitting of the ^3E state for various values of strain is shown in figure 4.25 .

Further, as can be seen from figure 4.25 for any reasonable value of strain (of the the order of 5 to 10 cm^{-1}) the levels arising from the ^3E branch out into two groups, those with orbital component E_X and those with orbital component E_Y. Each of these two groups is a spin triplet. The splitting between the components of the triplet is detailed in figures 4.26, 4.27 and 4.28 . It can be seen from these figures that the splittings saturate for strain values greater than about 400 GHz. The saturation values of these splittings are dependent on the chosen values of λ and λ' The diagrams for the L_{E_Y} strain are identical to that for L_{E_X}. This is because of symmetry and indeed the strain splitting will be isotropic for any given magnitude of E strain $L_E = \sqrt{L_{E_{X^2}} + L_{E_{Y^2}}}$.

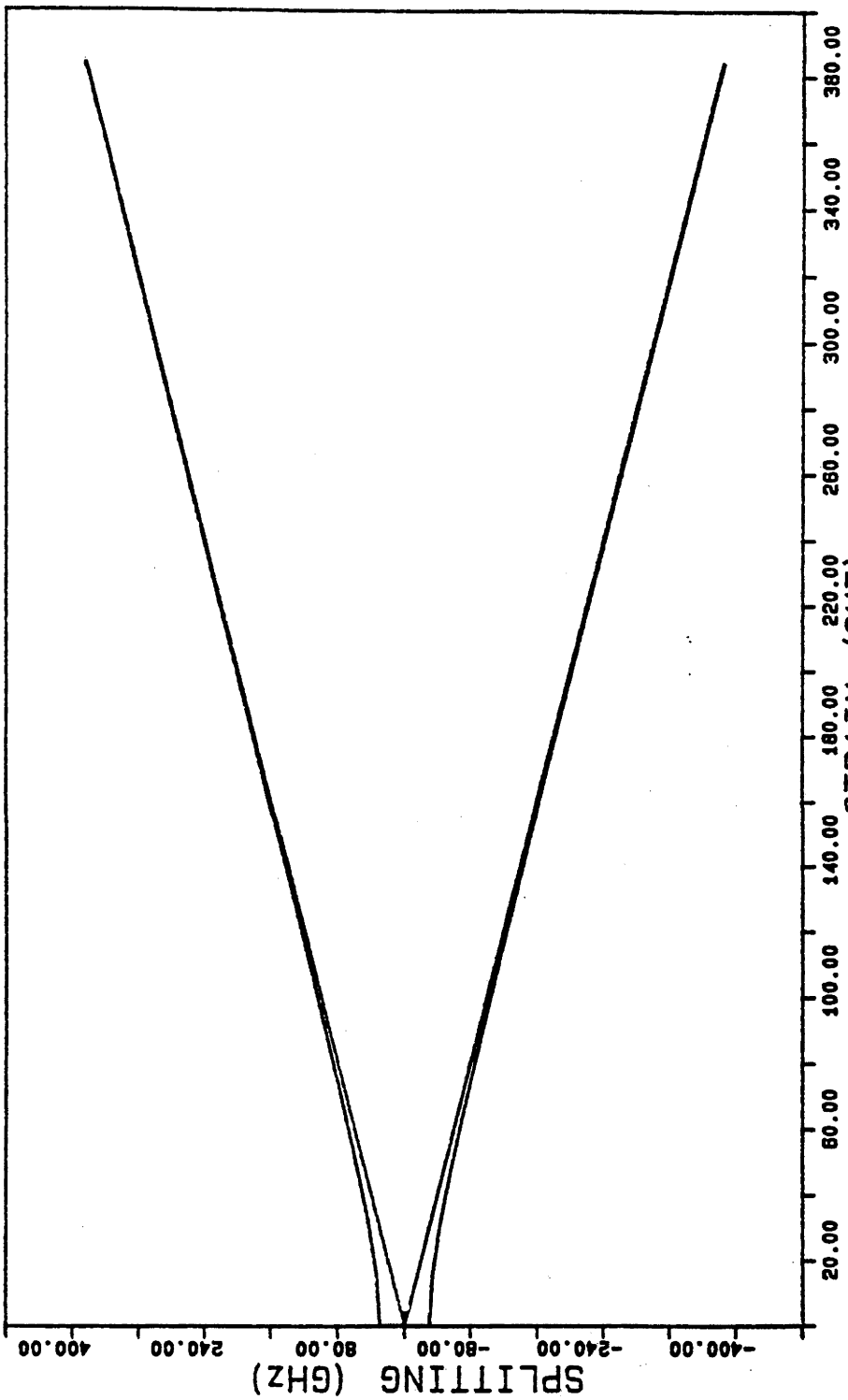

Figure 4.25 Splitting of the ${}^3E$ state as a function of strain experienced by the centre.

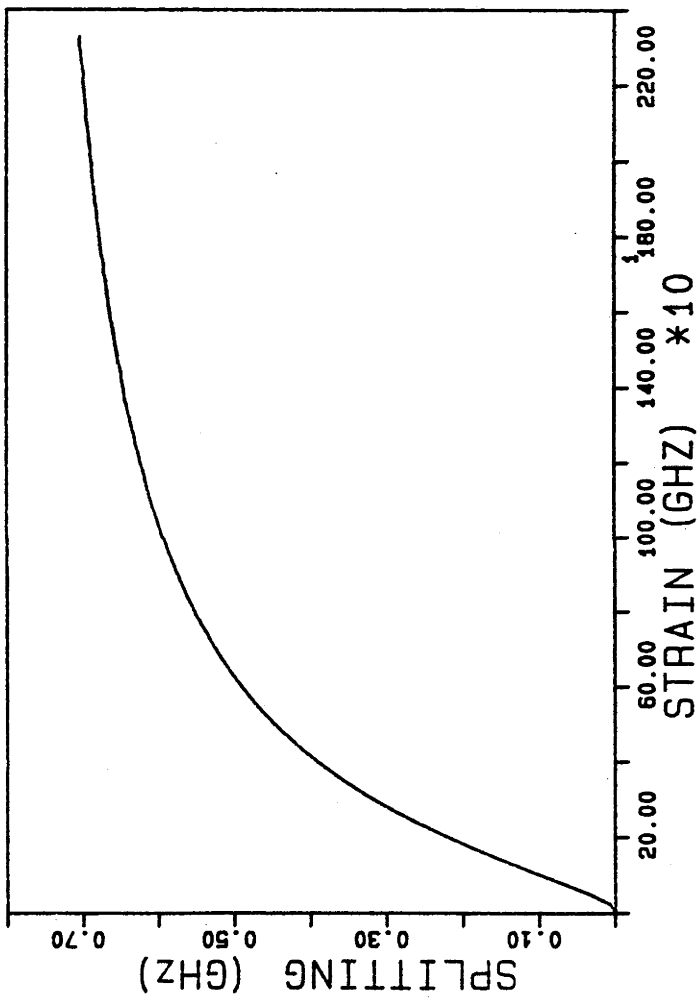

Figure 4.26 Splitting between the spin levels X and Y as a function of strain. $\lambda = 30$ GHz and $\lambda' = 1$ GHz.

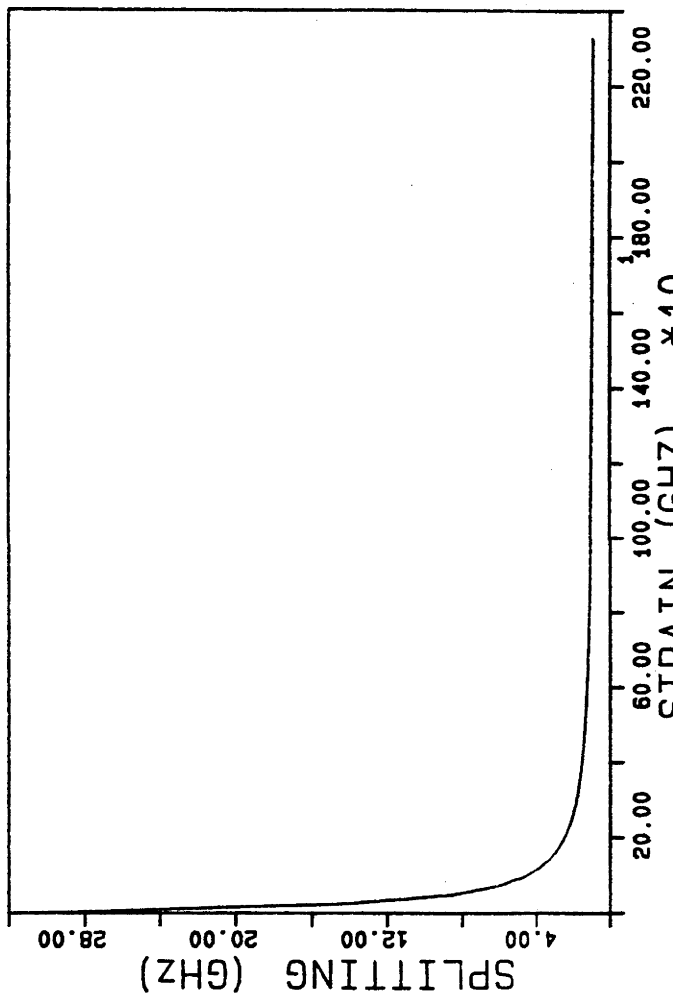

Figure 4.27 Splitting between the spin levels X and Z as a function of strain. $\lambda = 30$ GHz and $\lambda' = 1$ GHz.

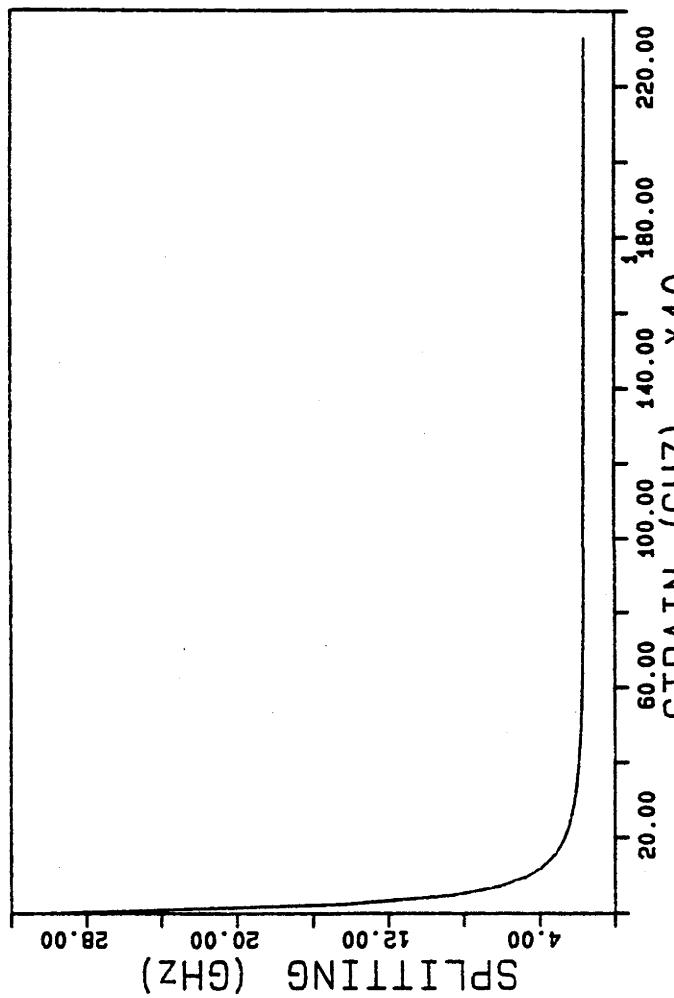

Figure 4.28 Splitting between the spin levels Y and Z a function of strain. $\lambda = 30$ GHz and $\lambda' = 1$ GHz.

As mentioned in chapter II, the scan range of a high resolution laser is from .01 GHz to 29.99 GHz. Hence, in a holeburning spectrum only the spectral features associated with transitions between one branch of the ^3E and the ground state need be considered. In our model fairly large strain splittings ($\sim$12 cm^{-1}) are considered to dominate and in this case the upper component will exhibit fast relaxation to the lower component. This will lead to line broadening. Therefore, the holeburning into the lower component of the ^3E only need be considered.

4.15.4 HOLEBURNING FOR A $^3A \rightarrow ^3E$ TRANSITION

In the absence of any optical excitation, the population distribution of centres in the ground state follows the thermal Boltzmann distribution. However, when the centres are optically excited continously, the population distribution becomes non-thermal. It is then determined by the selection rules and relaxation rates between the ground and excited states.

If in this situation, the absorption spectrum around the original laser frequency is detected, it contains information about the relative populations of the various levels. If the population in any one particular level increases due to optical excitation, there will be increased absorption from that level. This increased absorption from a level seen in the holeburning spectrum is known as antihole. Likewise, decreased absorption from a level due to optical excitation results in a hole. Holes occuring at frequencies different from the original laser frequency are known as sideholes. At this point it is worth repeating that antiholes can occur *only* when the centre after optical excitation relaxes to *different* level in the *ground* state.

The splitting of the ^3E has been considered in the previous subsection-where it has been shown that for modest strain it splits into two spin triplets (orbital singlets) and holeburning need only be considered for the lower orbital state. The splitting in the ground spin triplet (^3A) is taken as 'a' and 'b' and that in the excited state (^3E) as 'c' and 'd'. The eigenstates are assumed to be X, Y and Z in the ground state and X', Y' and Z' in the excited state. This in effect assumes that the axis of quantisation due to strain is the same in the ground and excited state. This is fair for the Z states as it is defined by the axis of the centre. It could also be true for the

X and Y states but will certainly be valid when the ground X, Y states are eventually taken as degenerate. For the moment all the separations are considered to be non zero as shown below.

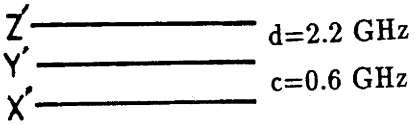

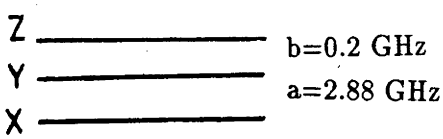

The figure shown above is not to scale and in the actual calculation the X and Y states in the ground state are considered to be degenerate. i.e. the value of splitting 'b' is set equal to zero.

4.15.5 ANTIHOLES

For threefold degenerate ground and excited states, antiholes would be found at 42 frequencies, 21 on either side of the original laser frequency. A total of 27 frequencies are listed in Table 1 , with three frequencies having contributions from three different transitions. The formation and detection of antiholes is a three step process. In step one, the laser excites the centre from a ground state level to an excited state level. The centre then relaxes to a different ground state level (step 2). When the centre is subsequently probed, it is excited from the ground state level to a level in the excited state (step 3).

Refering to the Table 1, in column 1 the frequency of the antihole relative

TABLE I

$c - a*$	$y \to x' \to z \to y'$	www		$z \to y' \to y \to x'$	wsw
$d - b*$	$x \to y' \to y \to z'$	wsw		$y \to z' \to x \to y'$	www
$(c + d) - (a + b)$	$x \to x' \to z \to z'$	sws		$z \to z' \to x \to x'$	sws
a	$z \to z' \to y \to z'$	sww		$y \to y' \to z \to y'$	sww
a	$z \to x' \to y \to x'$	www		$y \to x' \to z \to x'$	www
a	$z \to y' \to y \to y'$	wss		$y \to z' \to z \to z'$	wss
b	$y \to x' \to x \to x'$	wss		$x \to x' \to y \to x'$	sww
b	$y \to y' \to x \to y'$	sww		$x \to y' \to y \to y'$	wss
b	$y \to z' \to x \to z'$	www		$x \to z' \to y \to z'$	www
$a + b$	$z \to z' \to x \to z'$	sww		$x \to x' \to z \to x'$	sww
$a + b$	$z \to x' \to x \to x'$	wss		$x \to y' \to z \to y'$	www
$a + b$	$z \to y' \to x \to y'$	www		$x \to z' \to z \to z'$	wss
$(c + d) - a$	$y \to x' \to z \to z'$	wws		$z \to z' \to y \to x'$	sww
$c - (a + b)$	$x \to x' \to z \to y'$	sww		$z \to y' \to x \to x'$	wws
$d + a$	$z \to y' \to y \to z'$	wsw		$y \to z' \to z \to y'$	wsw
$(c + d) + (a + b)$	$z \to x' \to x \to z'$	wsw		$x \to z' \to z \to x'$	wsw
$d + (a + b)*$	$z \to y' \to x \to z'$	www		$x \to z' \to z \to y'$	wsw
$c + a$	$z \to x' \to y \to y'$	wws		$y \to y' \to z \to x'$	sww
$d - a$	$y \to y' \to z \to z'$	sws		$z \to z' \to y \to y'$	sws
$d - (a + b)$	$x \to y' \to z \to z'$	wws		$z \to z' \to x \to y'$	sww
$(c + d) + a*$	$z \to x' \to y \to z'$	www		$y \to z' \to z \to x'$	wsw
$(c + d) - b$	$x \to x' \to y \to z'$	sww		$y \to z' \to x \to x'$	wws
$c + b$	$y \to x' \to x \to y'$	wsw		$x \to y' \to y \to x'$	wsw
$(c + d) + b*$	$y \to x' \to x \to z'$	wsw		$x \to z' \to y \to x'$	www
$d + b$	$y \to y' \to x \to z'$	sww		$x \to z' \to y \to y'$	wws
$c + (a + b)*$	$z \to x' \to x \to y'$	wsw		$x \to y' \to z \to x'$	www
$c - b$	$x \to x' \to y \to y'$	sws		$y \to y' \to x \to x'$	sws

to the original laser frequency is given. In column 2 the three step process described above is shown. The notation used to describe the process is as follows. The first two letters give the initial and final levels involved in step 1, the second and third letters refer to step 2 while the third and fourth letters refer to step 3. With the spin is quantised in the same way in both ground and excited states, transitions involving no spin flip are labelled strong (s) and those involving a spin flip are labelled weak (w). In column 3, the intensity of antihole is given as the product of the transition strengths of the three steps involved in the formation and detection of the antihole. While columns 2 and 3 refer to antiholes occuring on the high energy side of the laser frequency, columns 5 describe transitions occuring on the low energy side. The intensity of the transition shown in column 5 is given in column 6.

4.15.6 HOLES AND SIDEHOLES

The positions and intensities of the side holes are shown in table 2 using the same notation as in table 1 with the difference that step 3 is now separated from step 2 by a colon mark because step 3 does not originate where step 2 ends. Since holeburning is essentially redistribution of population, the integrated area under the antiholes should equal that under the holes (i.e. the vector sum of intensities of holes and antiholes should be zero). It should be noted here, that the spectrum though symmetric in frequency is not so in the intensities of the antiholes. Corresponding antiholes that have unequal intensities are marked by an asterisk in table 1. These transitions do not give rise to significant intensities in our spectrum calculated later and are not thought to be the source of experimental asymmetry. Their significance is not explored further here.

4.15.7 HOLEBURNING SPECTRUM FOR ONE CENTRE

The holeburning spectrum due to one centre is calculated (figure 4.29) in this section for the following values of ground and excited state splittings. The ground state ^3A splittings 'a' and 'b' are given the values 2.88 GHz and 0.2 GHz respectively. Since a side hole at 0.6 GHz is observed in most

TABLE II

0	$x \to x' \to y : x \to x'$	sws		$x \to x' \to z : x \to x'$	sws
0	$x \to y' \to y : x \to y'$	wsw		$x \to y' \to z : x \to y'$	www
0	$x \to z' \to y : x \to z'$	www		$x \to z' \to z : x \to z'$	wsw
0	$y \to x' \to x : y \to x'$	wsw		$y \to x' \to z : y \to x'$	www
0	$y \to y' \to x : y \to y'$	sws		$y \to y' \to z : y \to y'$	sws
0	$y \to z' \to x : y \to z'$	www		$y \to z' \to z : y \to z'$	wsw
0	$z \to x' \to x : z \to x'$	wsw		$z \to x' \to y : z \to x'$	www
0	$z \to y' \to x : z \to y'$	www		$z \to y' \to y : z \to y'$	wsw
0	$z \to z' \to x : z \to y'$	sws		$z \to z' \to y : z \to z'$	sws
c	$x \to x' \to y : x \to y'$	sww		$x \to y' \to y : x \to x'$	wss
c	$x \to x' \to z : x \to y'$	sww		$x \to y' \to z : x \to x'$	wws
c	$y \to x' \to x : y \to y'$	wss		$y \to y' \to x : y \to x'$	sww
c	$y \to x' \to z : y \to y'$	wws		$y \to y' \to z : y \to x'$	sww
c	$z \to x' \to x : z \to y'$	wsw		$z \to y' \to x : z \to x'$	www
c	$z \to x' \to y : z \to y'$	www		$z \to y' \to y : z \to x'$	wsw
d	$z \to y' \to x : z \to z'$	wws		$z \to z' \to x : z \to y'$	sww
d	$z \to y' \to y : z \to z'$	wss		$z \to z' \to y : z \to y'$	sww
d	$x \to y' \to y : x \to z'$	wsw		$x \to z' \to y : x \to y'$	www
d	$x \to y' \to z : x \to z'$	www		$x \to z' \to z : x \to y'$	wsw
d	$y \to y' \to x : y \to z'$	sww		$y \to z' \to x : y \to y'$	wws
d	$y \to y' \to z : y \to z'$	sww		$y \to z' \to z : y \to y'$	wss
$c+d$	$x \to x' \to y : x \to z'$	sww		$x \to z' \to y : x \to x'$	wws
$c+d$	$x \to x' \to z : x \to z'$	sww		$x \to z' \to z : x \to x'$	wss
$c+d$	$y \to x' \to x : y \to z'$	wsw		$y \to z' \to z : y \to x'$	wsw
$c+d$	$y \to x' \to z : y \to z'$	www		$y \to z' \to x : y \to x'$	www
$c+d$	$z \to x' \to x : z \to z'$	wss		$z \to z' \to x : z \to x'$	sww
$c+d$	$z \to x' \to y : z \to z'$	wws		$z \to z' \to y : z \to x'$	sww

Figure 4.30: table II

of the one laser holeburning spectra, the excited state splittings 'c' and 'd' are assigned the values 0.6 GHz and 2.3 GHz respectively. In the actual calculation of the spectrum (subsequent sections) the value of 'b' is set to zero (i.e. X and Y levels in the ground state are taken to be degenerate). When all the transitions have equal intensity, the expected spectrum for this one centre would be as shown in figure 4.29 (a). If it is assumed that the ratio of transition strengths s/w (allowed/forbidden) is 100, then the expected spectrum changes to that shown in figure 4.29 (b). Although the antihole at 2.88 GHz is prominent there is little else about the spectrum that resembles the experimental trace.

4.15.8 HOLEBURNING SPECTRUM FOR A DISTRIBUTION OF CENTRES

In the present model, it is assumed that the distribution of each of the strain components (L_{E_X} and L_{E_Y}) can be described by a Gaussian statistic.

$$g_i(L_{E_i}) = \frac{2\sqrt{ln2}}{\Delta L_{E_G}\sqrt{\pi}} exp(-(\frac{2\sqrt{ln2}L_{E_i}}{\Delta L_{E_G}})^2)\Delta L_{E_i}(i = X or Y)$$

where ΔL_{E_G} is the full width at half maximum of the strain distribution.

This function describes the fraction of centres experiencing strain whose value is between L_{E_X} and $L_{E_X} + \Delta L_{E_X}$ (or L_{E_Y} and $L_{E_Y} + \Delta L_{E_Y}$). Both these distributions are centred around zero strain. Further, since neither strain component is prefered over the other, the halfwidths of both the distributions of L_{E_X} and of L_{E_Y} are assumed to be equal.

It should be noted that the splitting in the ^3E state (and hence the holeburning spectrum) in a centre is dependent on the resultant strain (L_R) experienced by the centre. The resultant strain in this case is equal to $\sqrt{L_{E_X}^2 + L_{E_Y}^2}$. Though for the distribution described by the Gaussian statistic stated above the prefered (most probable) value of strain is zero, when resultant strain (L_R) is considered the most probable value of strain is not zero. i.e. the function describing the strain distribution of centres peaks at a value different from zero. This point is discussed further below.

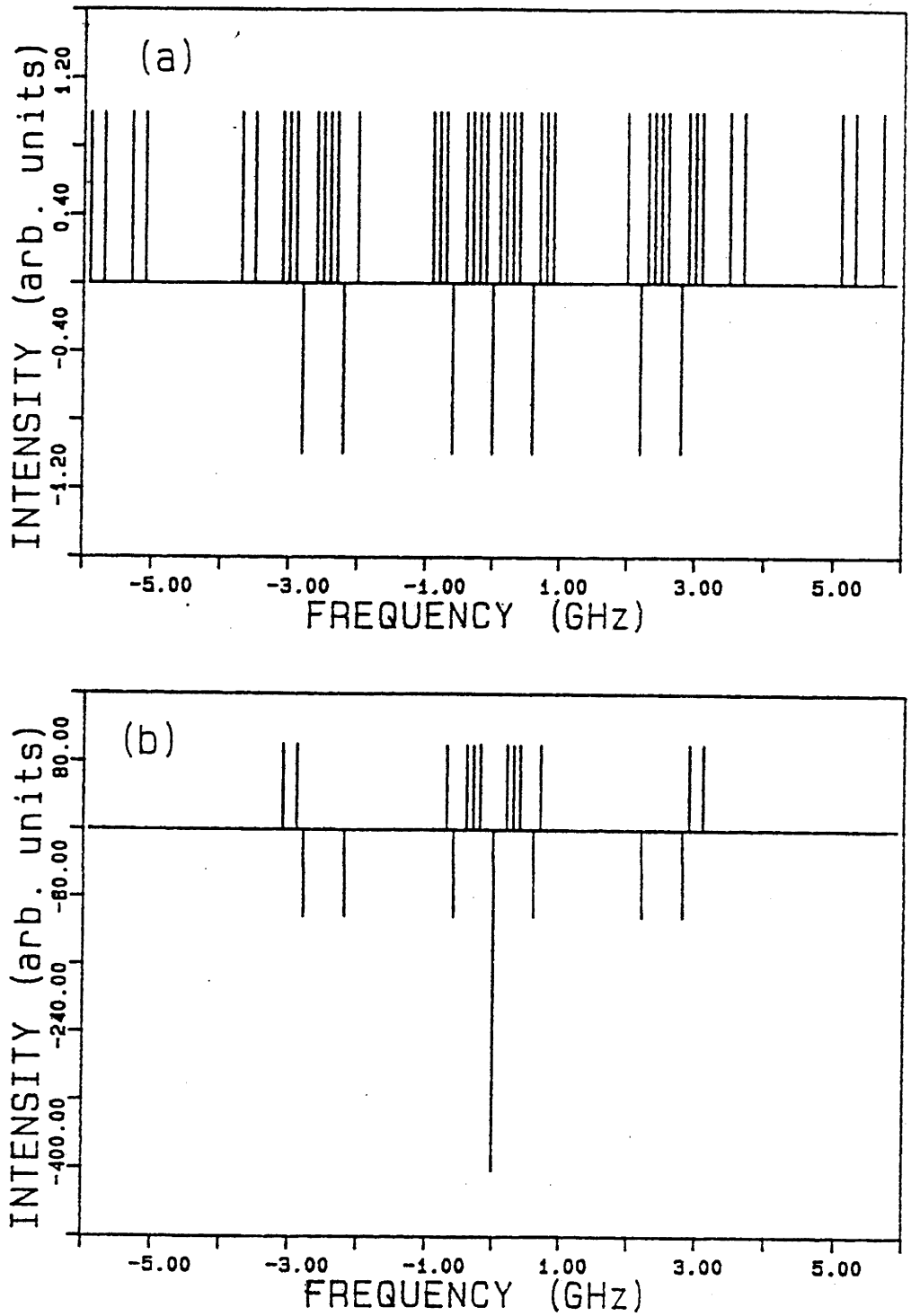

Figure 4.29 Holeburning spectrum due to one centre assuming a $^3A \rightarrow ^3E$ transition. The splittings are 0.2 GHz and 2.88 GHz in the ground state and 0.6 GHz and 2.2 GHz in the excited state. (a) shows the pattern when all the transitions (allowed and forbidden) are of equal intensity while (b) shows the spectrum when the allowed transitions are 100 times stronger than the forbidden. It is to be noted that intensities of antiholes (and holes) occuring at the same frequency are *not* added up.

Since the strain distributions L_{E_X} and L_{E_Y} are independent, the probability that a centre experiencing a strain of value between L_{E_X} and $L_{E_X} + \Delta L_{E_X}$ also has a strain of value between L_{E_Y} and $L_{E_Y} + \Delta L_{E_Y}$ is equal to the product of the strain distributions along the two directions. This is equal to

$$g(L_{E_{XY}}) = \frac{4ln2}{\Delta {L_{E_G}}^2 \pi} exp(-4ln2(\frac{L_{E_X}}{\Delta L_{E_G}})^2) exp(-4ln2(\frac{L_{E_Y}}{\Delta L_{E_G}})^2) \Delta L_{E_X} \Delta L_{E_Y}$$

$$g(L_{E_{XY}}) = \frac{4ln2}{\Delta {L_{E_G}}^2 \pi} exp(-4ln2(\frac{{L_{E_X}}^2 + {L_{E_Y}}^2}{\Delta {L_{E_G}}^2})) \Delta L_{E_X} \Delta L_{E_Y}$$

If, instead of the individual strain components, L_{E_X} and L_{E_Y}, the resultant strain L_R $(=\sqrt{L_{E_X}^2 + L_{E_Y}^2})$ is considered, it is evident that the most probable value of strain is not zero (it is less probable that both L_{E_X} and L_{E_Y} strains experienced by a centre are *simultaneously* zero). The distribution of L_R can be obtained by integrating over the annular area between L_R and $L_R + \Delta L_R$. This is equal to $2\pi L_R \Delta L_R$. Doing this the fraction of centres having a strain between L_R and $L_R + \Delta L_R$ is obtained as

$$\frac{2L_R.4ln2}{\Delta {L_{E_G}}^2} exp(-4ln2(\frac{{L_R}^2}{\Delta L_{E_G}^2})) \Delta L_R \qquad (1)$$

In fact this strain distribution is similar to the velocity distribution of molecules confined to two dimensions. This function is plotted in figure 4.30 (a), (b), (c), (d), (e) and (f) for various values of half width (Δ_{E_G}). This function has been normalised to unity to enable comparison of intensities in spectra due to different strain distributions (Δ_{E_G}'s).

For a given value of strain, the eigenstates and eigenvalues can be calculated from matrix III. The eigenfunctions can be used to calculate the intensities of various transitions between the ground and excited states. The variation of intensities of transitions as a function of strain is described in figure 4.31 (a) through (i). The above procedure used in obtaining the

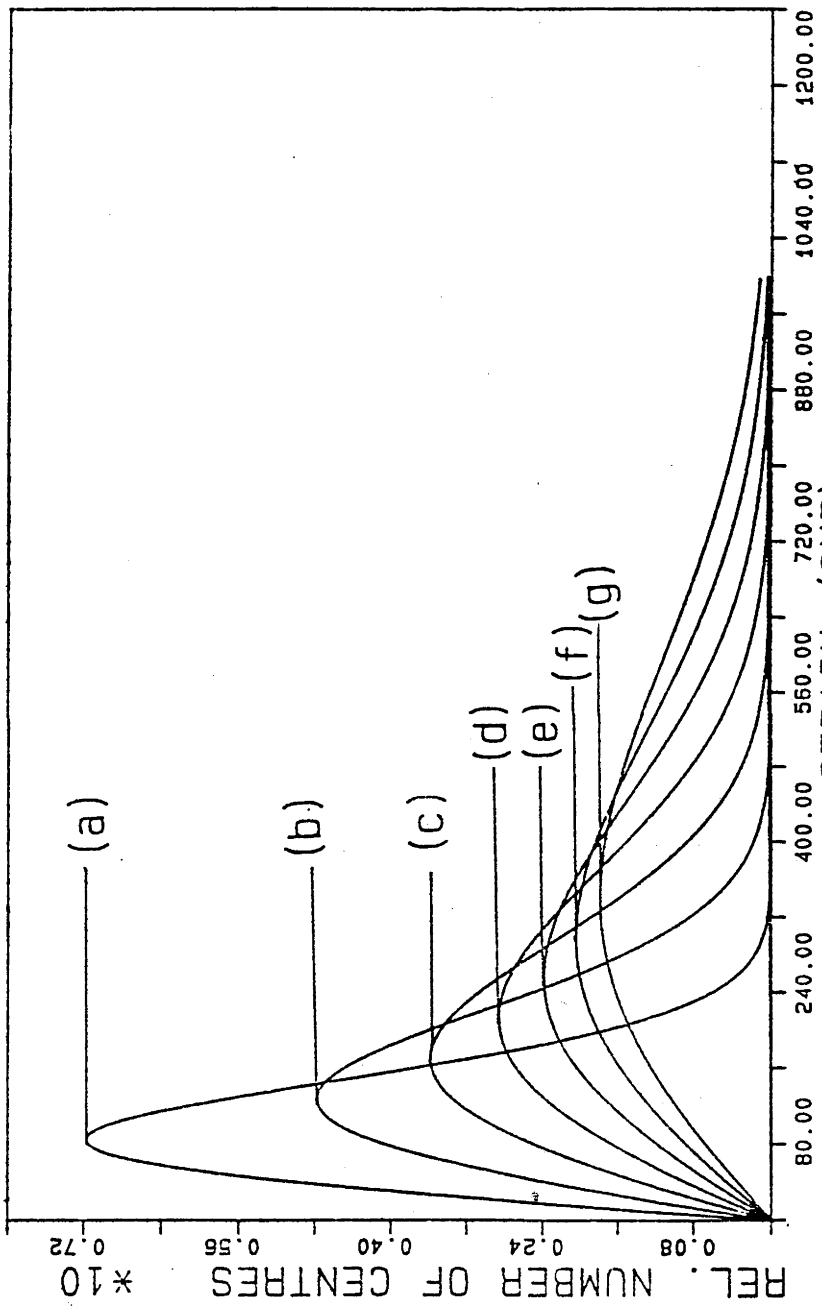

Figure 4.30 Strain distribution of centres for various halfwidth values. The halfwidths are (a) 200 GHz, (b) 300 GHz, (c) 400 GHz, (d) 500 GHz, (e) 600 GHz, (f) 700 GHz and (g)800 GHz. The distribution function (equation (1)) is normalised to unity.

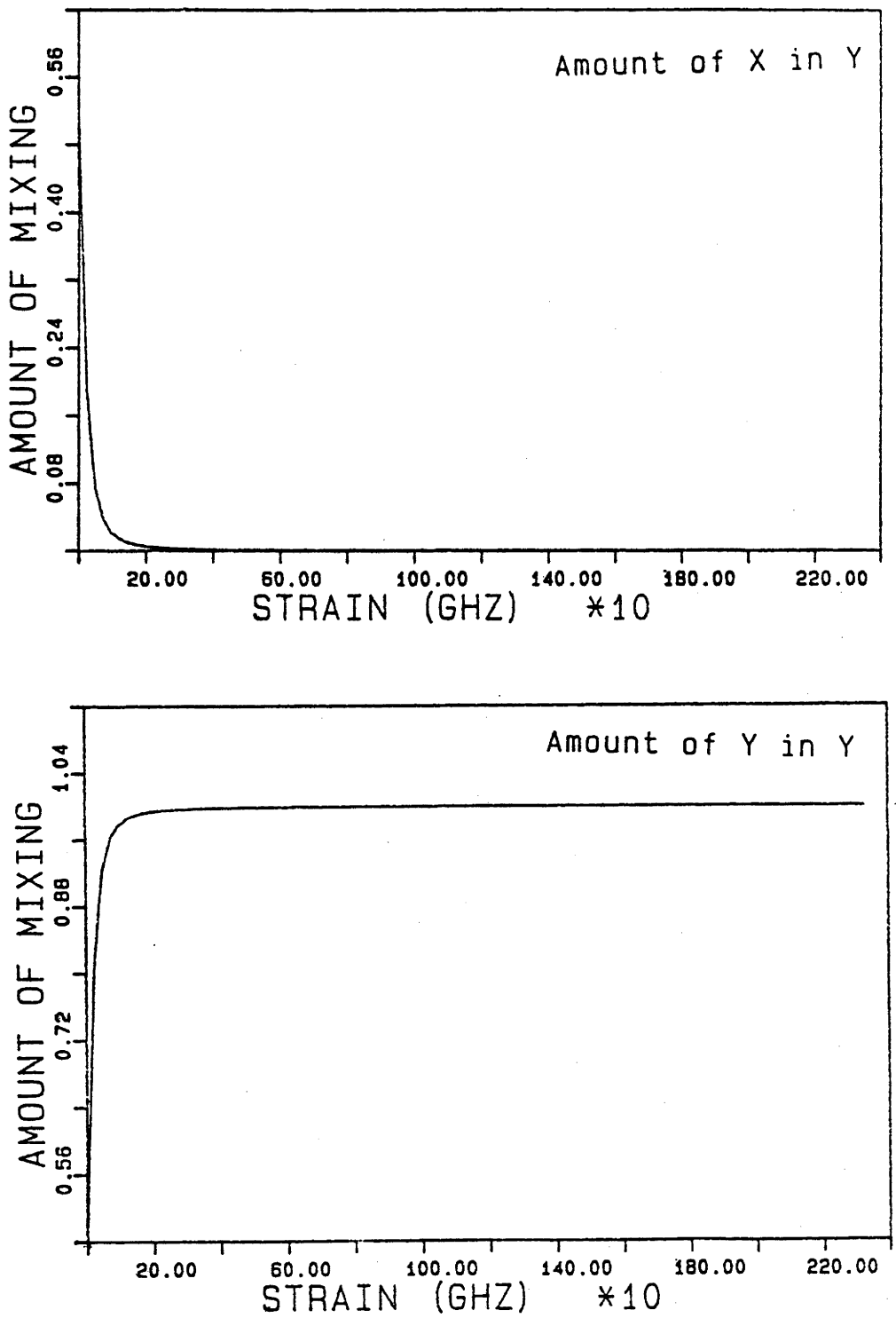

Figure 4.31 Strain variation of transition intensities when $\lambda = 30$ GHz and $\lambda' = 1$ GHz; necessary for intensity calculations.

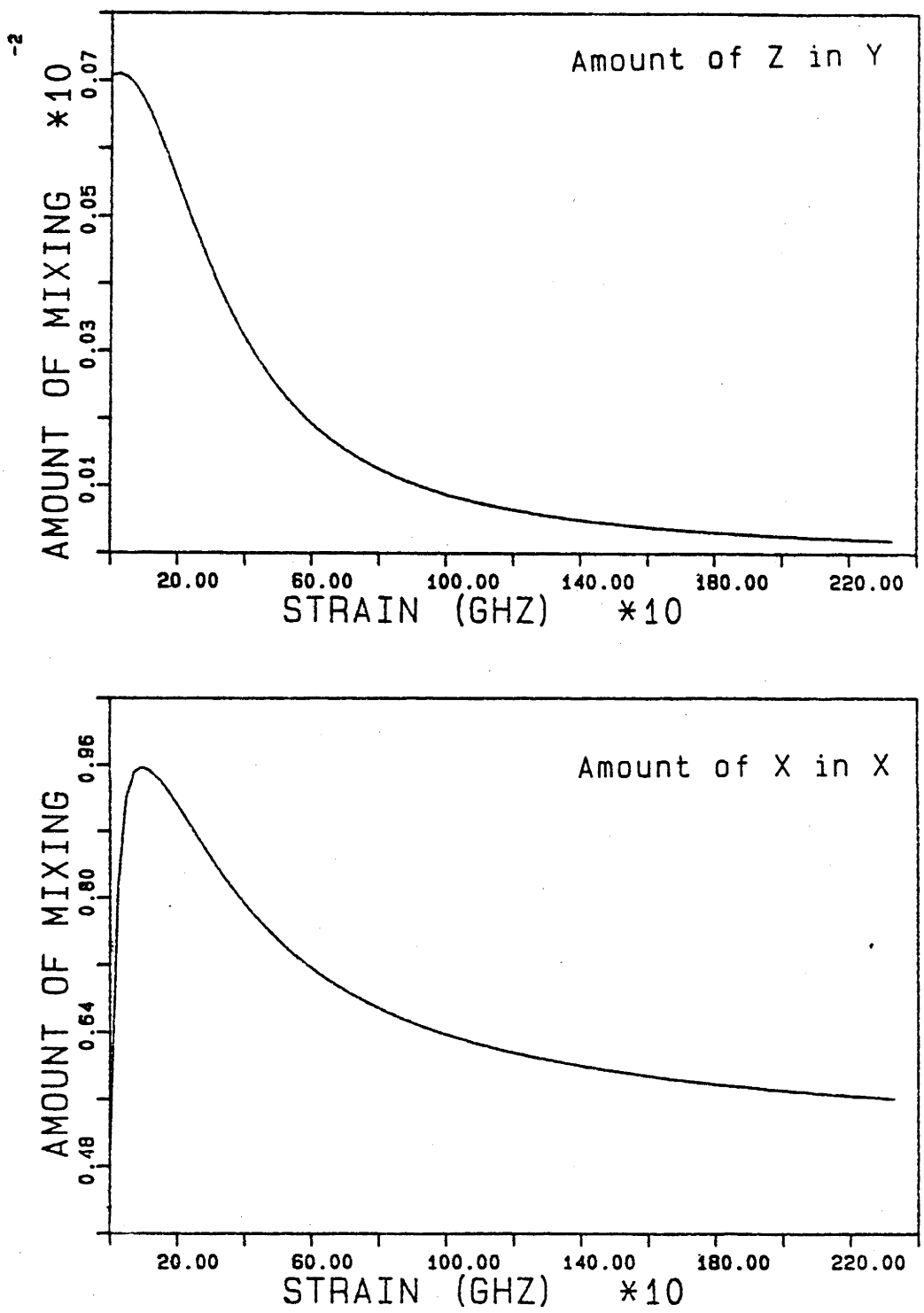

Figure 4.31 Strain variation of transition intensities when $\lambda = 30$ GHz and $\lambda' = 1$ GHz. (continued)

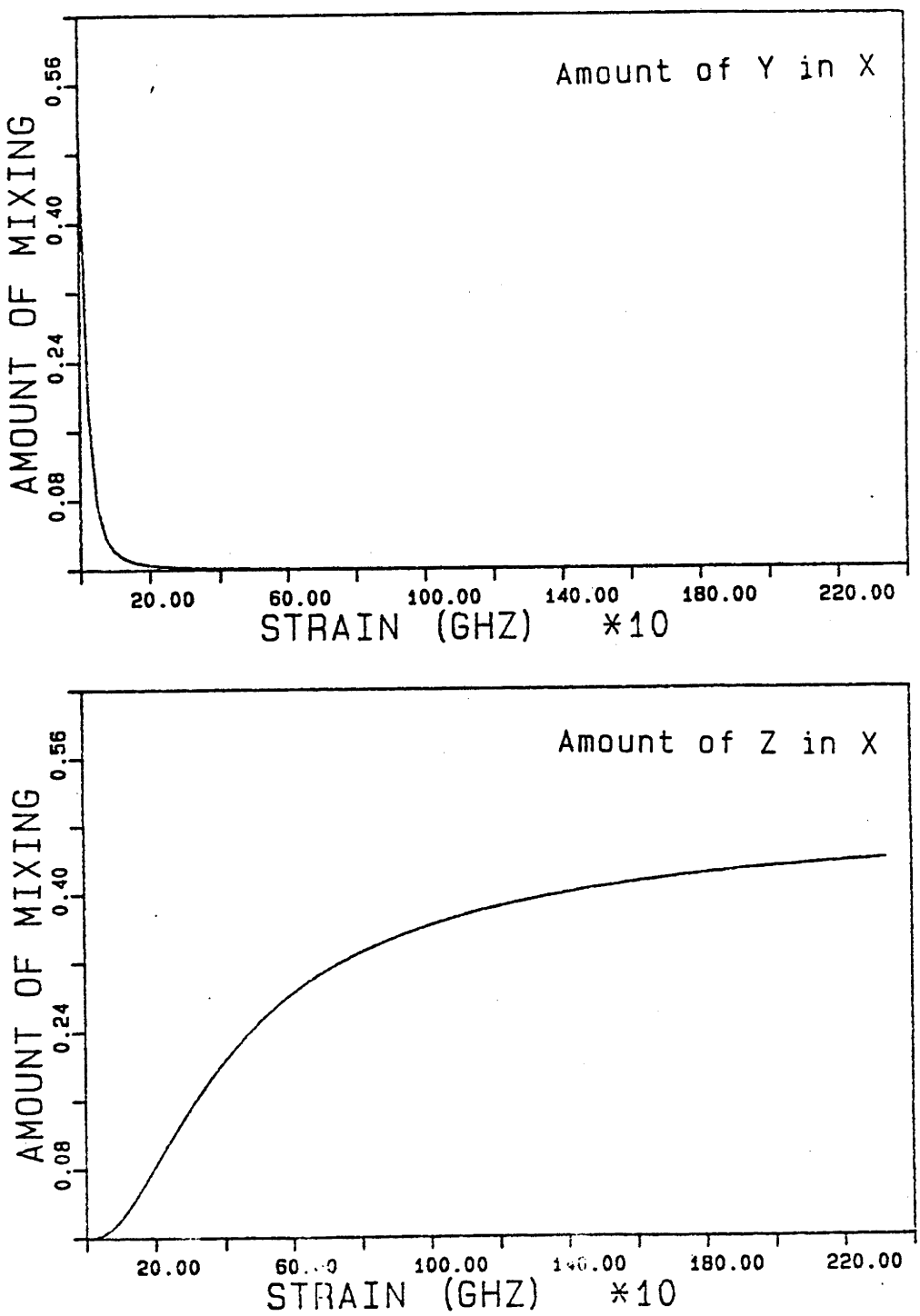

Figure 4.31 Strain variation of transition intensities when $\lambda = 30$ GHz and $\lambda' = 1$ GHz. (continued)

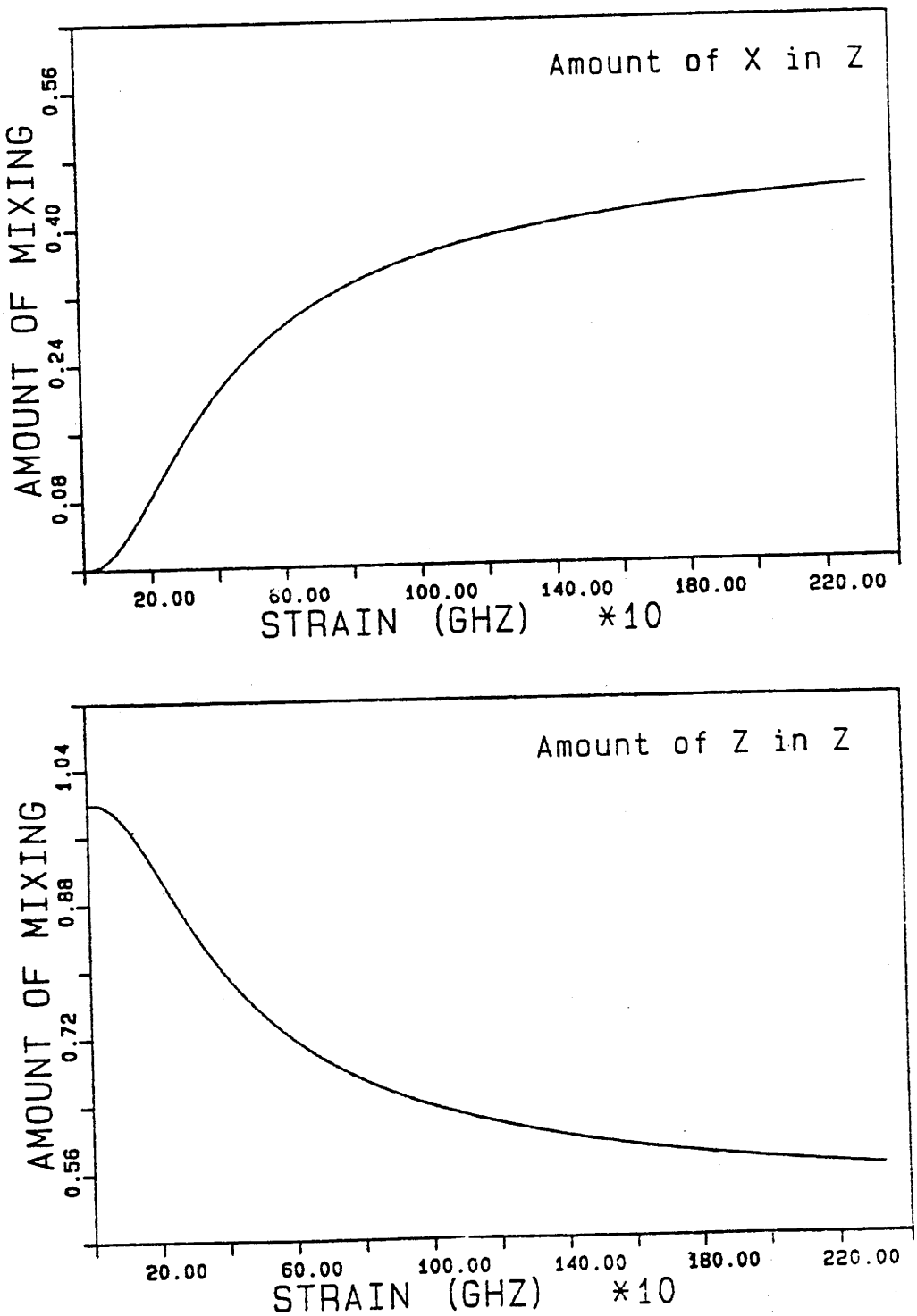

Figure 4.31 Strain variation of transition intensities when $\lambda = 30$ GHz and $\lambda' = 1$ GHz. (continued)

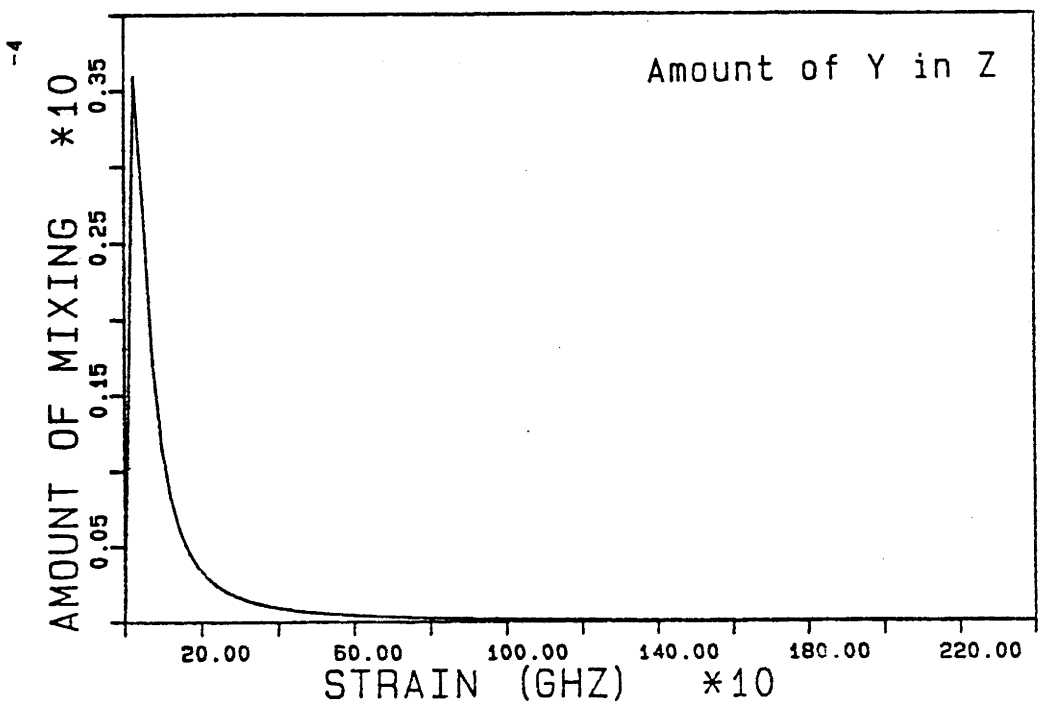

Figure 4.31 Strain variation of transition intensities when $\lambda = 30$ GHz and $\lambda' = 1$ GHz.

holeburning spectrum from one centre can now be extended to a distribution of centres. However, before proceding to that various steps in calculation of the holeburning spectrum are recapitulated. The following data is required for the calculation of the holeburning spectrum.

- Excited state splittings. These are functions of strain and their variation is similar to that shown in figures 4.25 through 4.28. It should be remembered these splittings also depend on the values of the spin-orbit interaction constants (λ and λ').
- Ground state splittings. These splittings are independent of strain and spin-orbit interaction. The splitting between the M_S=0 and $M_S = \pm 1$ levels is taken to be 2.88 GHz.
- Transition intensities. These are functions of strain and also spin-orbit interaction and were described in figure 4.31 (a) through (i).
- Strain distribution of centres. This is described by equation (1) above and is represented graphically in figure 4.30 . This function depends on the assumed value of the half width (ΔE_G) of the E_X (or E_Y) strain distribution.

It can be seen from figure 4.30 that the *total* width of strain distribution described by equation (1) above is less than twice the halfwidth of the corresponding Gaussian distribution (ΔE_G). The spectra are calculated at 100 equidistant points in the strain distribution described by equation (1) above between the strain limits 0 and $2\Delta E_G$. To obtain the final spectrum, the spectrum due to centres experiencing a particular strain is weighted proportional to the number of centres with that strain and this procedure is repeated for all the values of strain. The resultant spectrum is shown in figure 4.32 . The position of the lines represents frequency of the antiholes and side holes while the height of the line represents their intensity. Strain has the effect of varying the frequencies of antiholes and side holes. When more than one feature (antiholes or side holes) occur at a frequency then the intensities are added up vectorially. To smooth the discrete line spectrum obtained by the above procedure each line is given a Lorentzian intensity distribution with a half width of 25 MHz (corresponding to the excited state lifetime) and peak height of the Lorentzian is equal to the intensity of the

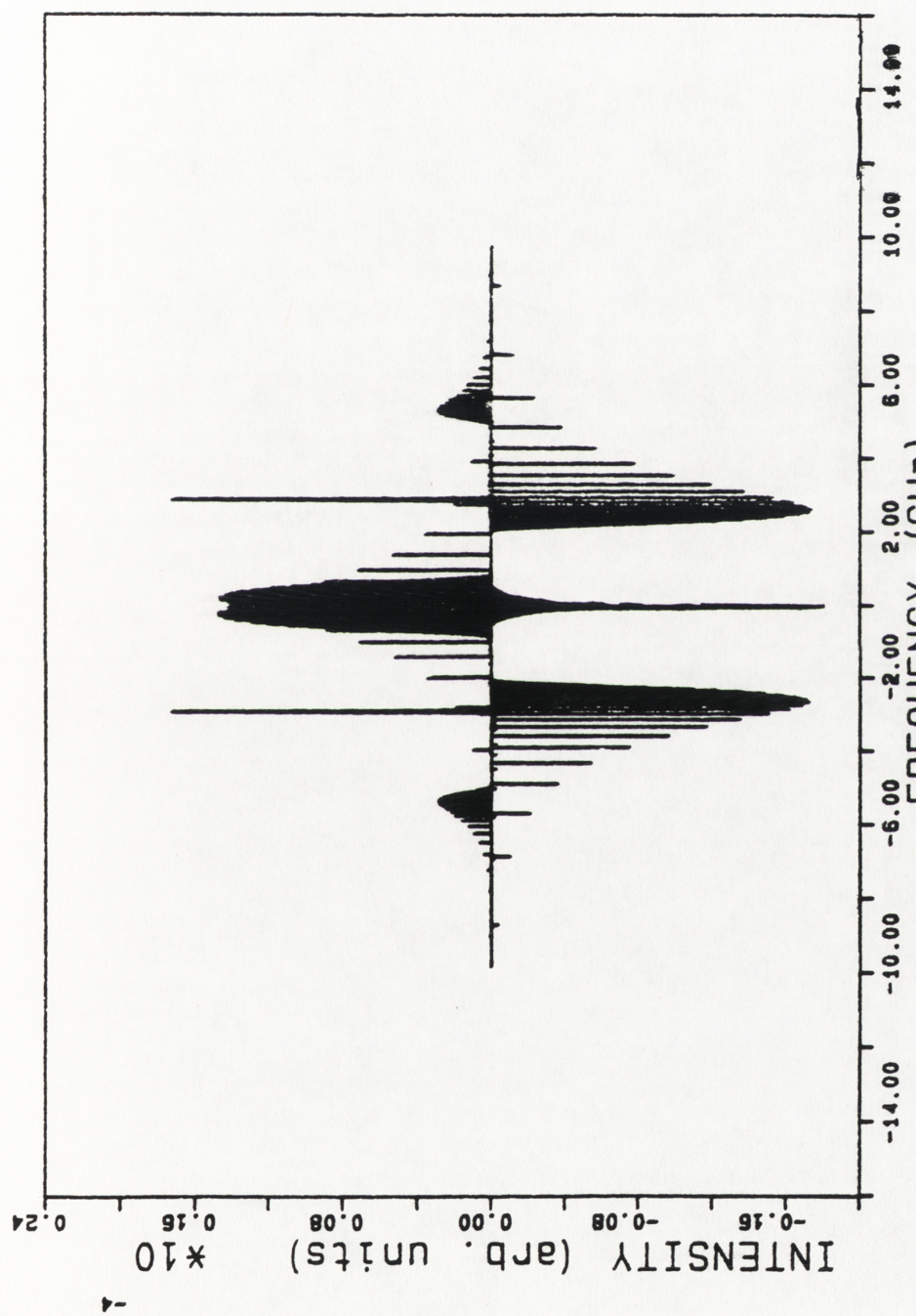

Figure 4.32 Calculated holeburning spectrum for a distribution of centres (strain halfwidth = 600 GHz) when λ = 30 GHz and λ' = 1 GHz.
It is to be noted that intensities of antiholes (and holes) occuring at the same frequency are *not* added up.

antihole or side hole (i.e. the height of the line). The spectrum is recalculated at each point (40/GHz) along the frequency axis by summing the intensities of all the Lorentzians contributing to intensity at that point. The resultant spectrum is shown in figure 4.33 (a). The values of λ and λ' used in obtaining the spectrum in figure 4.33 (a) are 30 GHz and 1 GHz respectively while the halfwidth of the Gaussian strain distribution is taken to be 600 GHz. The width of the spectrum has been set to ± 10 GHz about the burn laser frequency as the intensities of features outside this frequency range are 4 orders of magnitude weaker relative to the intensity of 2.88 GHz antihole. The apparent difference in the content of figures 4.32 and 4.33 (a) is due to the fact that the features occuring at 2.88 GHz are relatively less affected (shifted) by strain and hence vectorially add up, whereas other features (except the hole at laser frequency) do not. It can be seen from the figure 4.33 (a) that the spectrum is symmetric and the antihole features at 2.88 GHz are the dominant feature. There are other features common to the experiment and further comments on that are made later in this chapter.

4.15.9 ASYMMETRICAL HOLEBURNING

The EPR data (Loubser and van Wyk, 1977) has suggested that the centres relax preferentially into one of the spin components (either $M_S = 0$ or $M_S = \pm 1$) of the ^3A state now considered to be the ground state and this has earlier been suggested to be the origin of asymmetric holeburning pattern (Bloch *et al*, 1985). In our model, the $M_S = \pm 1$ level of the $^3A_2$ ground state is assumed to be lower in energy (figure in section 4.15.4) than the $M_S = 0$ level. To give antihole features on the high energy side of the burn laser, the centres have to relax preferentially into the $M_S = \pm 1$ level. The degree of asymmetry in the holeburning spectrum depends on the degree of preferential relaxation in to the $M_S = \pm 1$ level. Selective feeding has been incorporated in the present model by introducing a multiplicative factor (feeding factor) to all the intensities of all the transitions (step 2 of the holeburning process described in section 4.15.5) ending in X or Y levels of the ground state. Assuming $\lambda = 30$ GHz, $\lambda' = 1$ GHz and $\Delta E_G = 600$ GHz the holeburning spectra for various values of the feeding factor are shown in figure 4.33 (b) through (f). The holeburning spectra with no preferential relaxation for the above values of the parameters has already been shown in figure 4.33 (a). From these figures it is noted that a feeding factor of

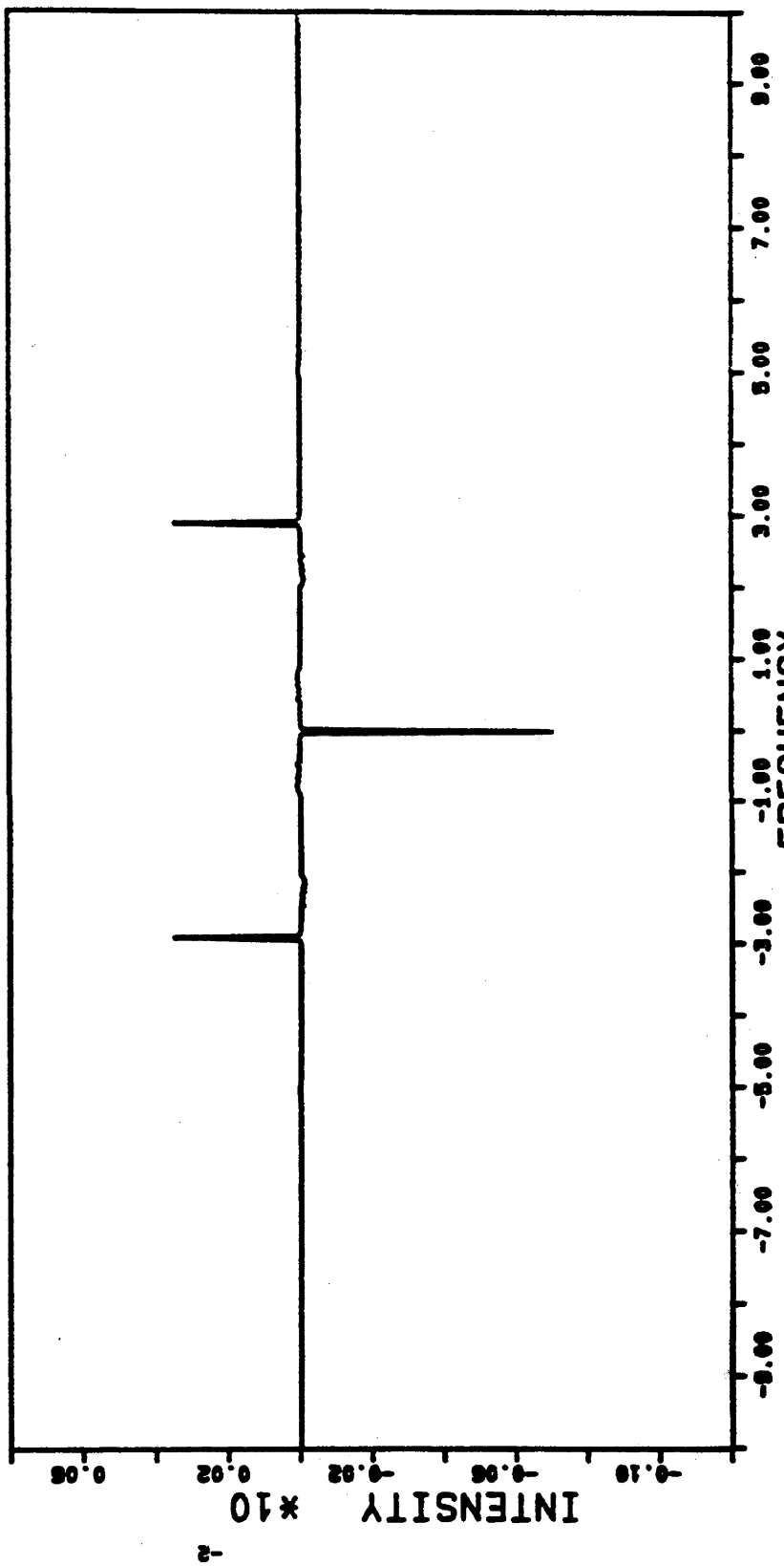

Figure 4.33 (a) Same as figure 4.32 except that the intensities of various features are added up vectorially where ever necessary. Each feature is replaced by a lorentian of corresponding intensity and a halfwidth of 25 MHz. The value of the feeding factor (to include preferential relaxation) is equal to 1.

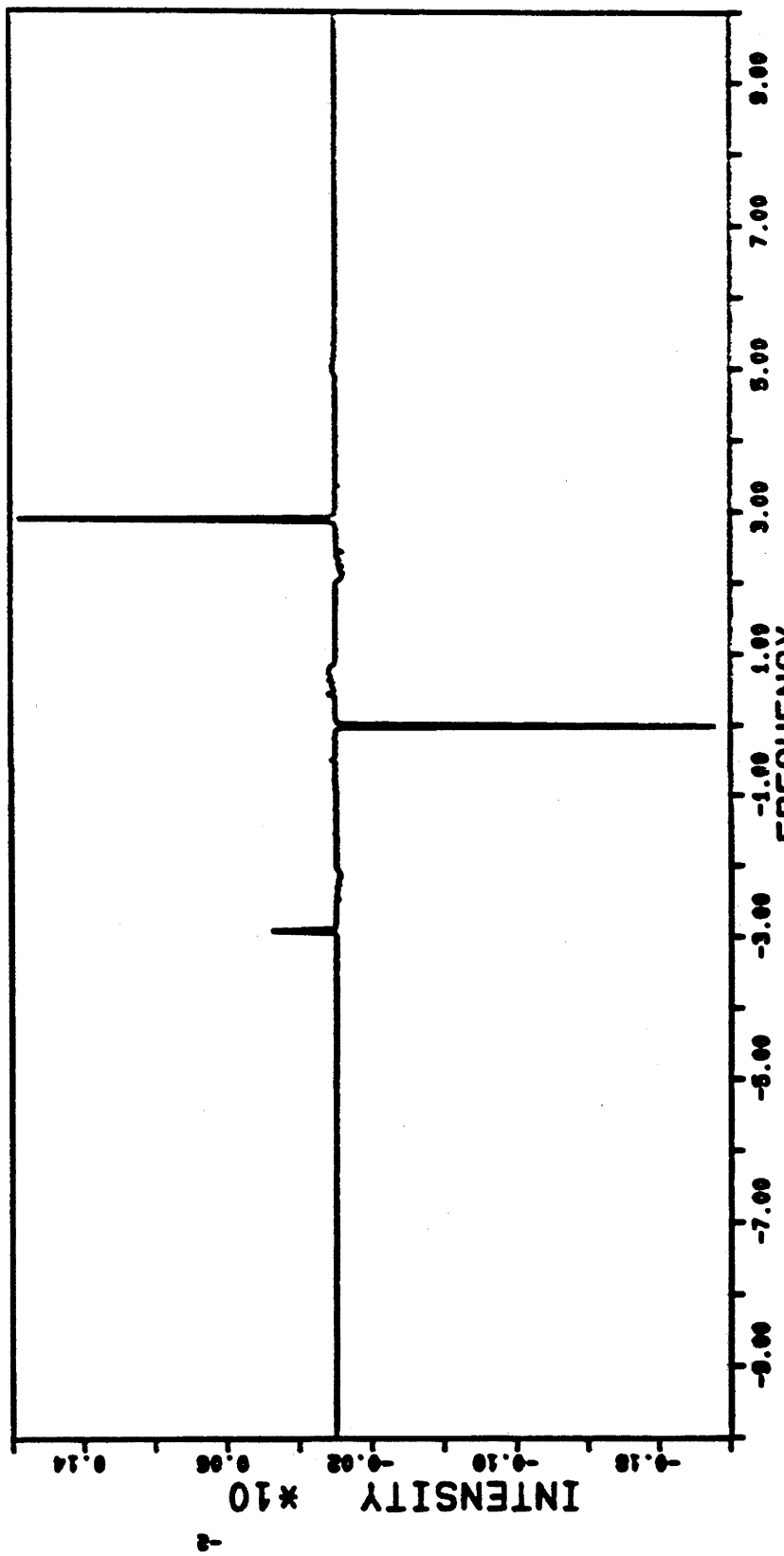

Figure 4.33 (b) Effect of variation of feeding factor on the calculated hole-burning spectrum. The values of the parameters are strain halfwidth = 600 GHz, λ = 30 GHz, λ' = 1 GHz and feeding factor = 5.

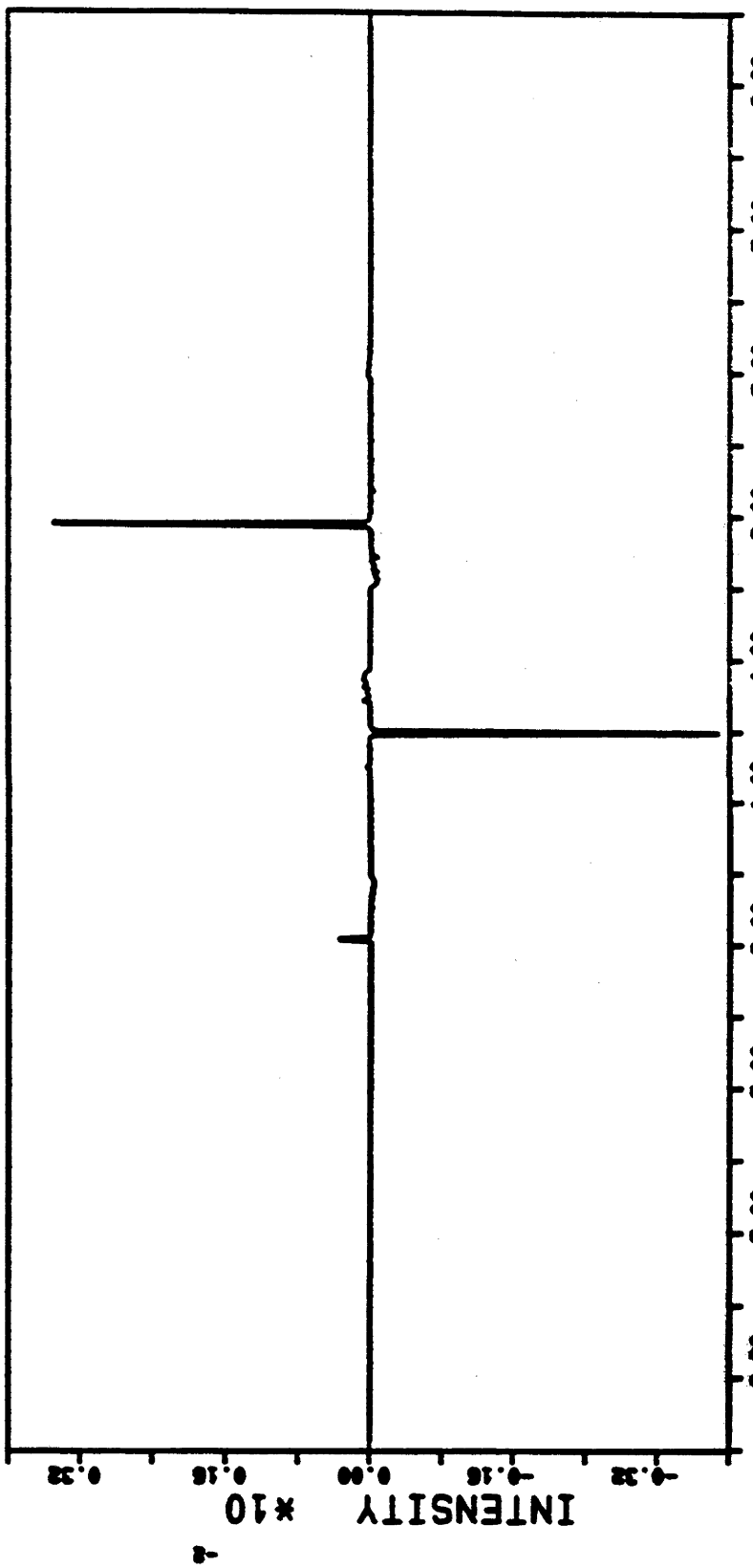

Figure 4.33 (c) Effect of variation of feeding factor on the calculated hole-burning spectrum. The values of the parameters are strain halfwidth = 600 GHz, λ = 30 GHz, λ' = 1 GHz and feeding factor = 10.

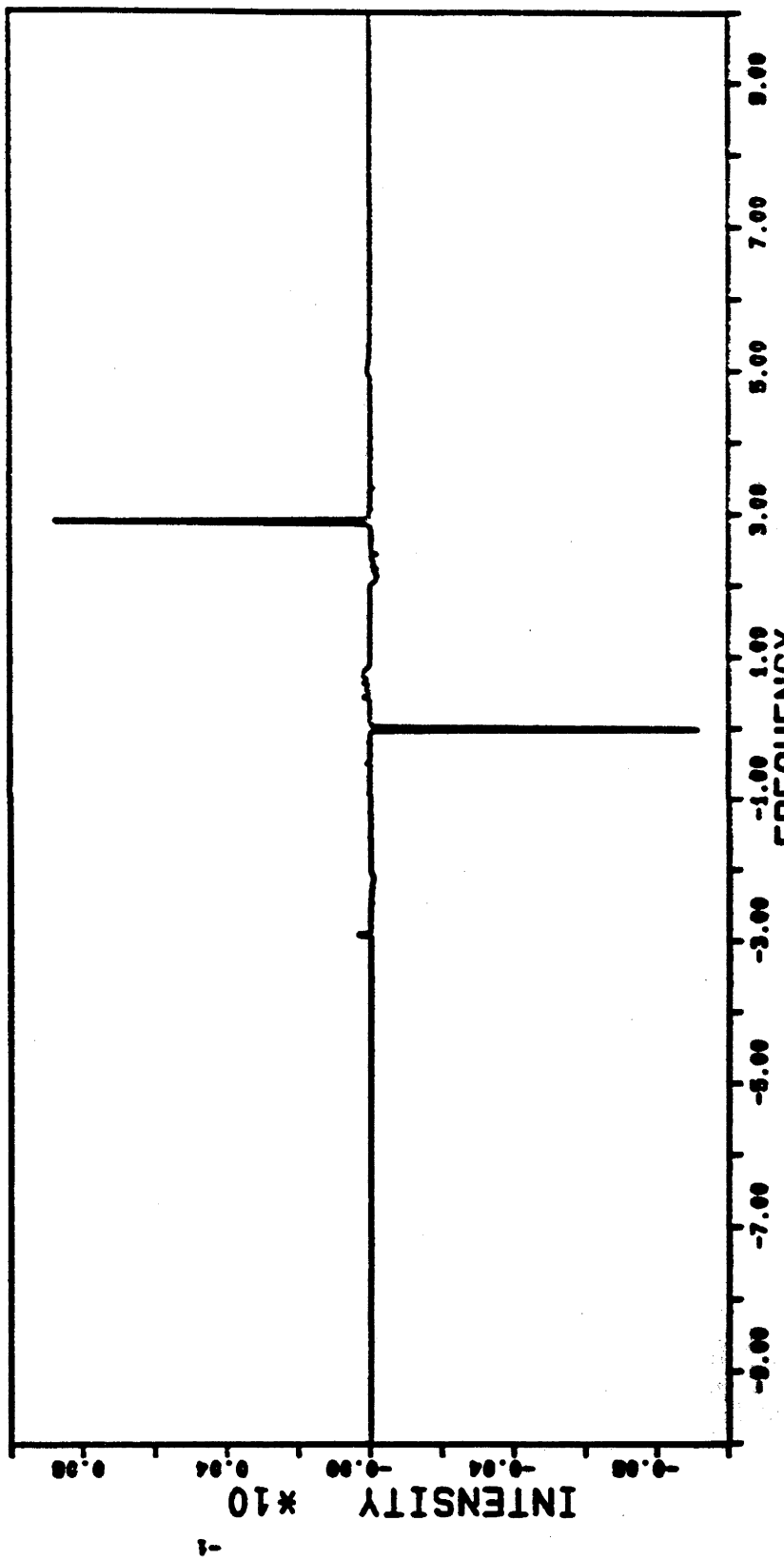

Figure 4.33 (d) Effect of variation of feeding factor on the calculated hole-burning spectrum. The values of the parameters are strain halfwidth = 600 GHz, $\lambda = 30$ GHz, $\lambda' = 1$ GHz and feeding factor = 25.

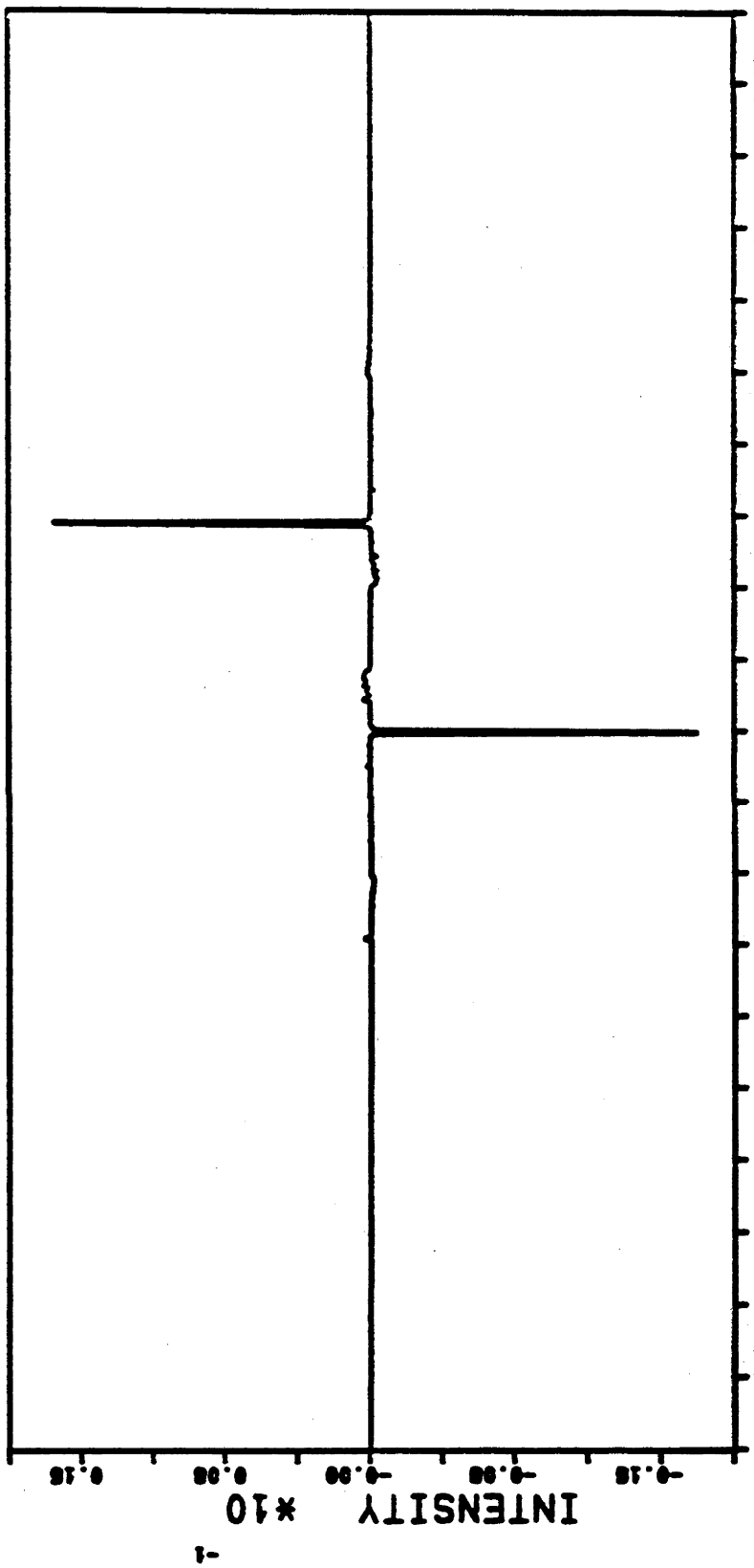

Figure 4.33 (e) Effect of variation of feeding factor on the calculated hole-burning spectrum. The values of the parameters are strain halfwidth = 600 GHz, λ = 30 GHz, λ' = 1 GHz and feeding factor = 50.

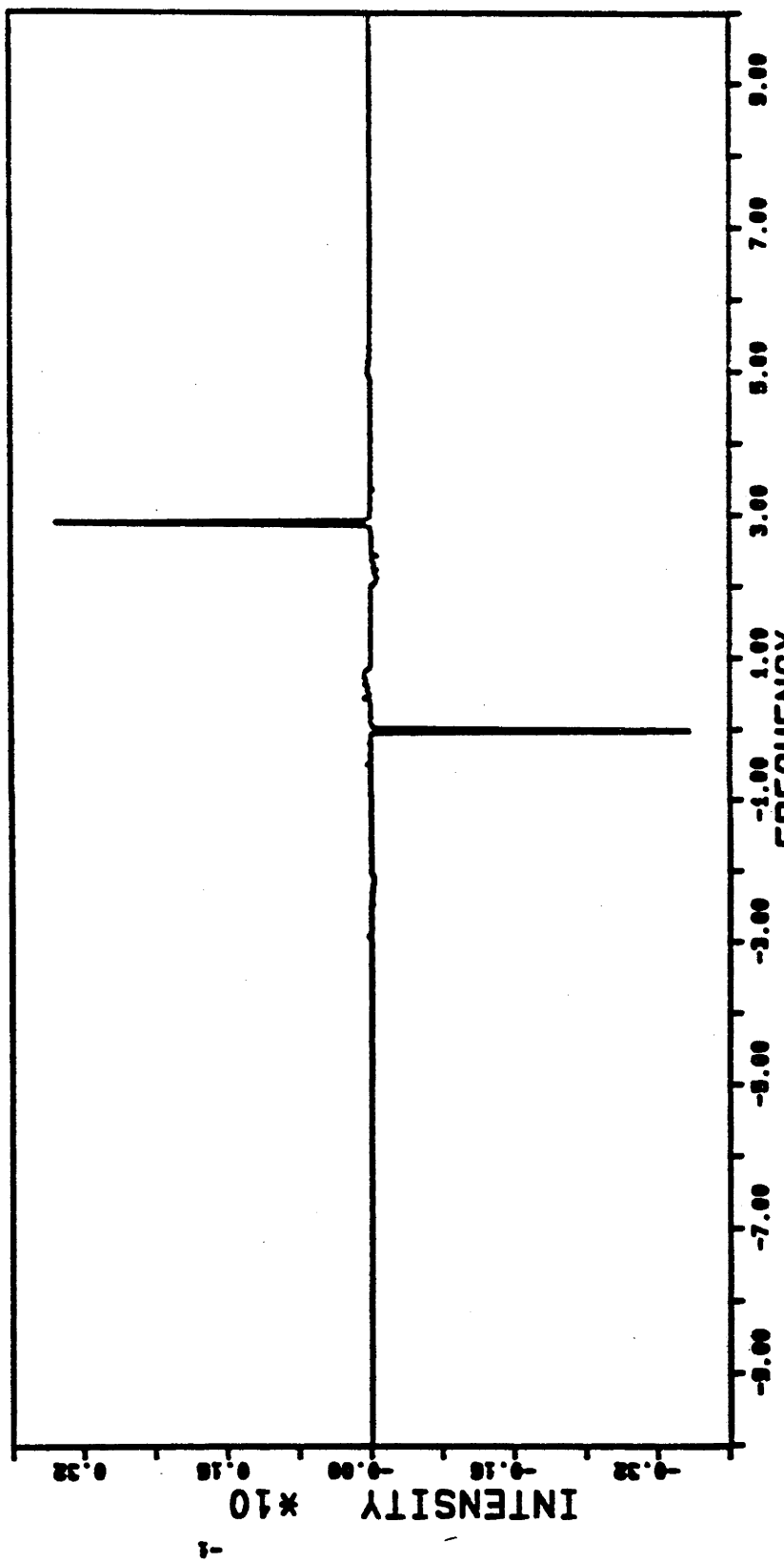

Figure 4.33 (f) Effect of variation of feeding factor on the calculated hole-burning spectrum. The values of the parameters are strain halfwidth = 600 GHz, λ = 30 GHz, λ' = 1 GHz and feeding factor = 100.

50 approximately reproduces the degree of asymmetry in the experimental hole burning spectrum. We do not at present understand the cause for preferential relaxation into the $M_S = \pm 1$ level.

From the holeburning spectra that are already presented (figure 4.32 and 4.33 (a) through (f)), it can be seen that there are other features other than the dominant antihole at 2.88 GHz and the hole at burn laser frequency. The intensities of these features are very low. Following the arguments in previous sections, it can be seen the position and intensity of these features are dependent on the chosen values of the parameters in the calculation. It has been observed that strain and spin-orbit interaction parameter directly affect these low intensity features.

4.15.10 EFFECT OF STRAIN ON THE HOLEBURNING SPECTRUM

The effect of strain on the calculated holeburning spectra is now discussed. The value of the halfwidth of Gaussian strain distribution (ΔE_G) affects the relative weighting of the centres experiencing different values of strain (equation (1) in section 4.15.8). The peak of the strain distribution shifts to higher values of strain with increasing values of ΔE_G (figure 4.30). It can be seen also from figure 4.30 that the total width of the strain distribution is approximately equal to $2\Delta E_G$. When the peak of the strain distribution shifts to lower values, its effect is to increase to increase the weighting of low strain centres in the holeburning spectrum. Further, in this regime the excited state splittings are more sensitive to strain (figures 4.26 through 4.28). This has the effect of broadening the strain sensitive features in the holeburning spectrum. The strain sensitivity of the excited state splittings together with large variation of transition intensities (figure 4.31) in the low strain regime results in 'noisy' holeburning spectra. As the value of ΔE_G is increased centres whose excited state splittings and transition intensities have much less strain dependence contribute more to the holeburning spectrum. The resulting spectrum then consists of relatively narrow and smooth strain sensitive features. The effect of variation of the holeburning spectra with ΔE_G is calculated for values of ΔE_G from 200 GHz to 800 GHz in steps of 100 GHz. The results are shown in figure 4.34 (a) through (g).
As mentioned earlier apart from the 2.88 GHz antihole and the central hole,

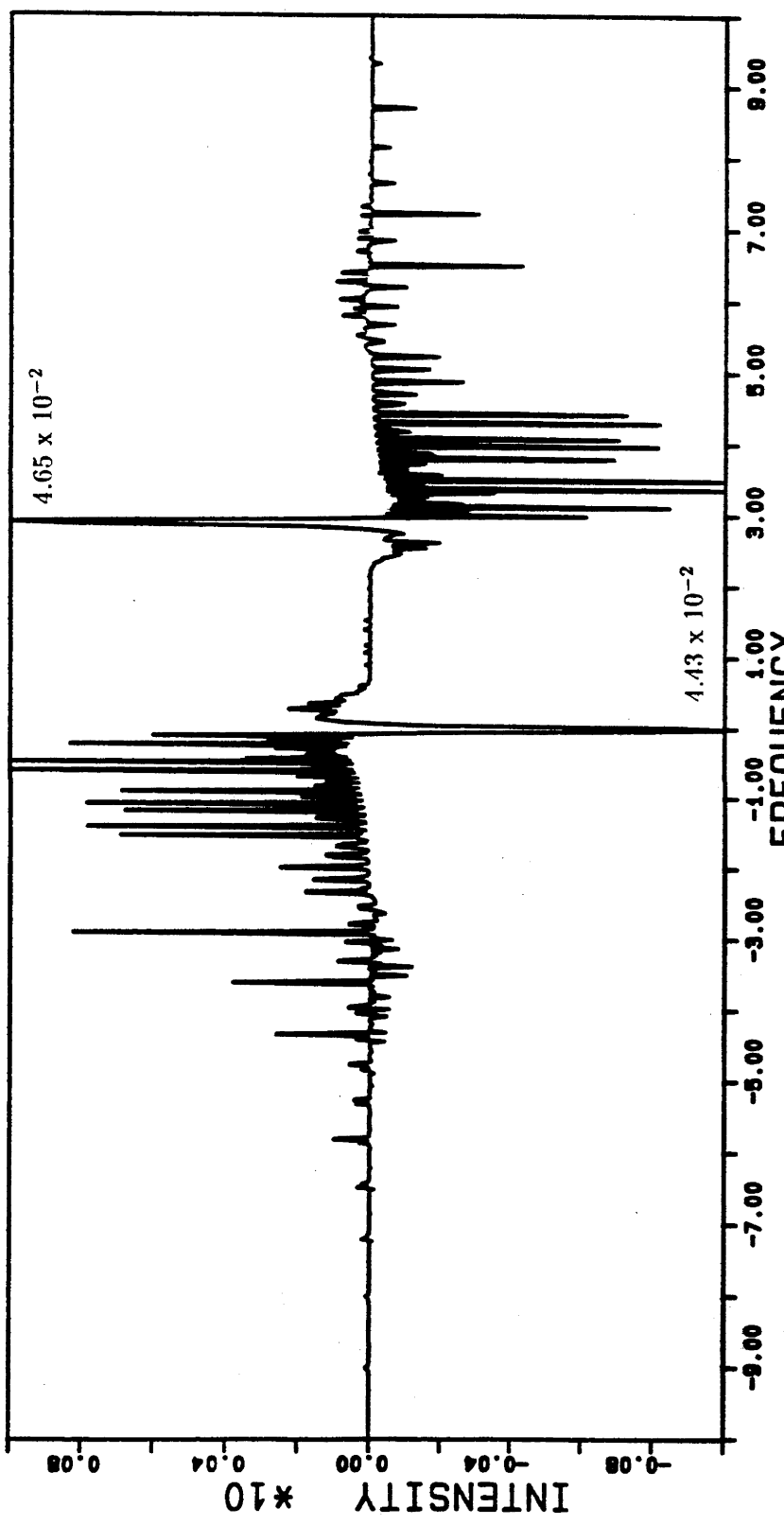

Figure 4.34 (a) Effect of variation of the halfwidth of strain distribution (ΔE_G) on the calculated holeburning spectrum. The values of the parameters are $\lambda = 30$ GHz, $\lambda' = 1$ GHz, feeding factor = 50 and strain halfwidth (ΔE_G) = 200 GHz.

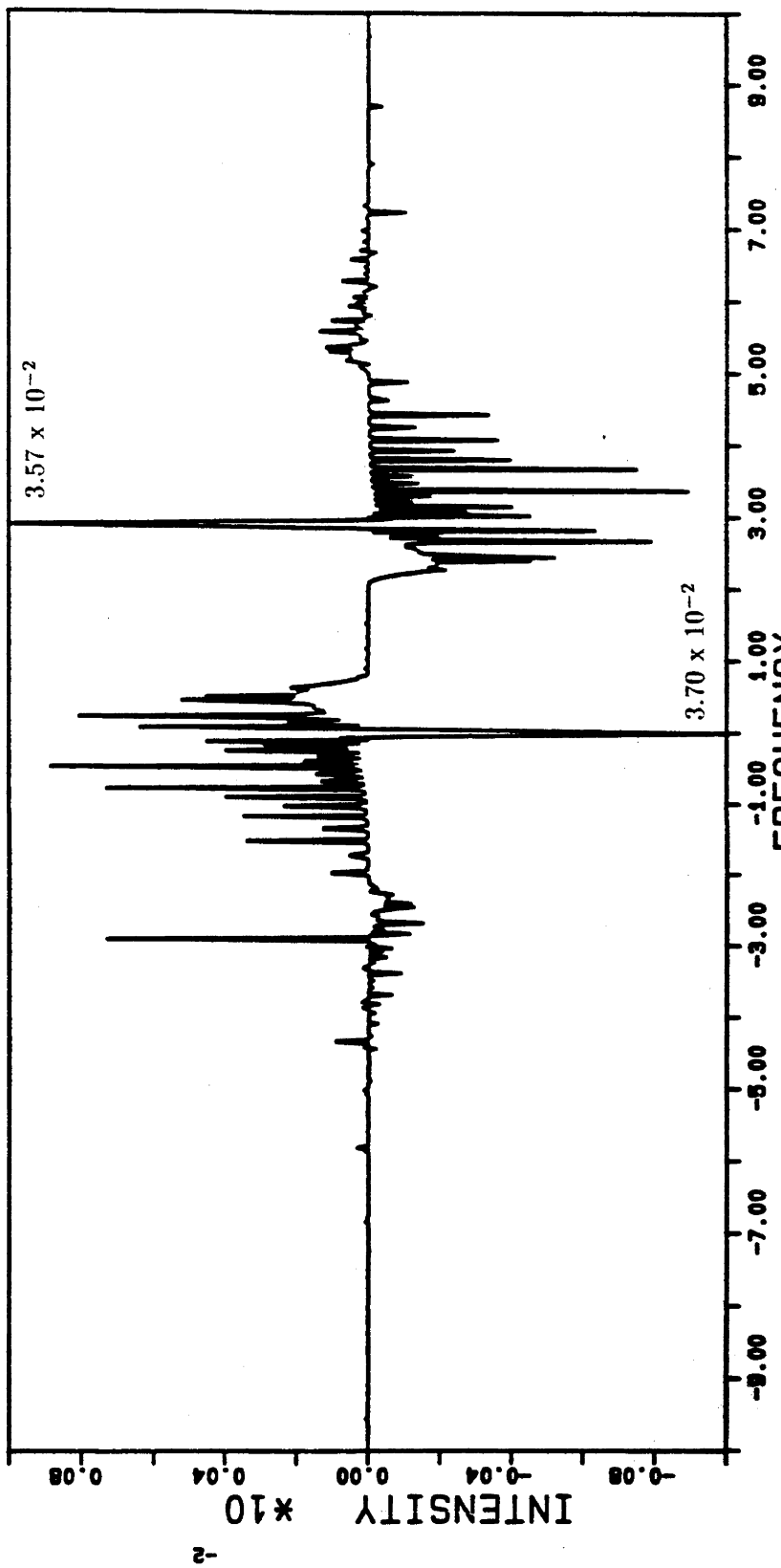

Figure 4.34 (b) Effect of variation of the halfwidth of strain distribution (ΔE_G) on the calculated holeburning spectrum. The values of the parameters are $\lambda = 30$ GHz, $\lambda' = 1$ GHz, feeding factor = 50 and strain halfwidth (ΔE_G) = 300 GHz.

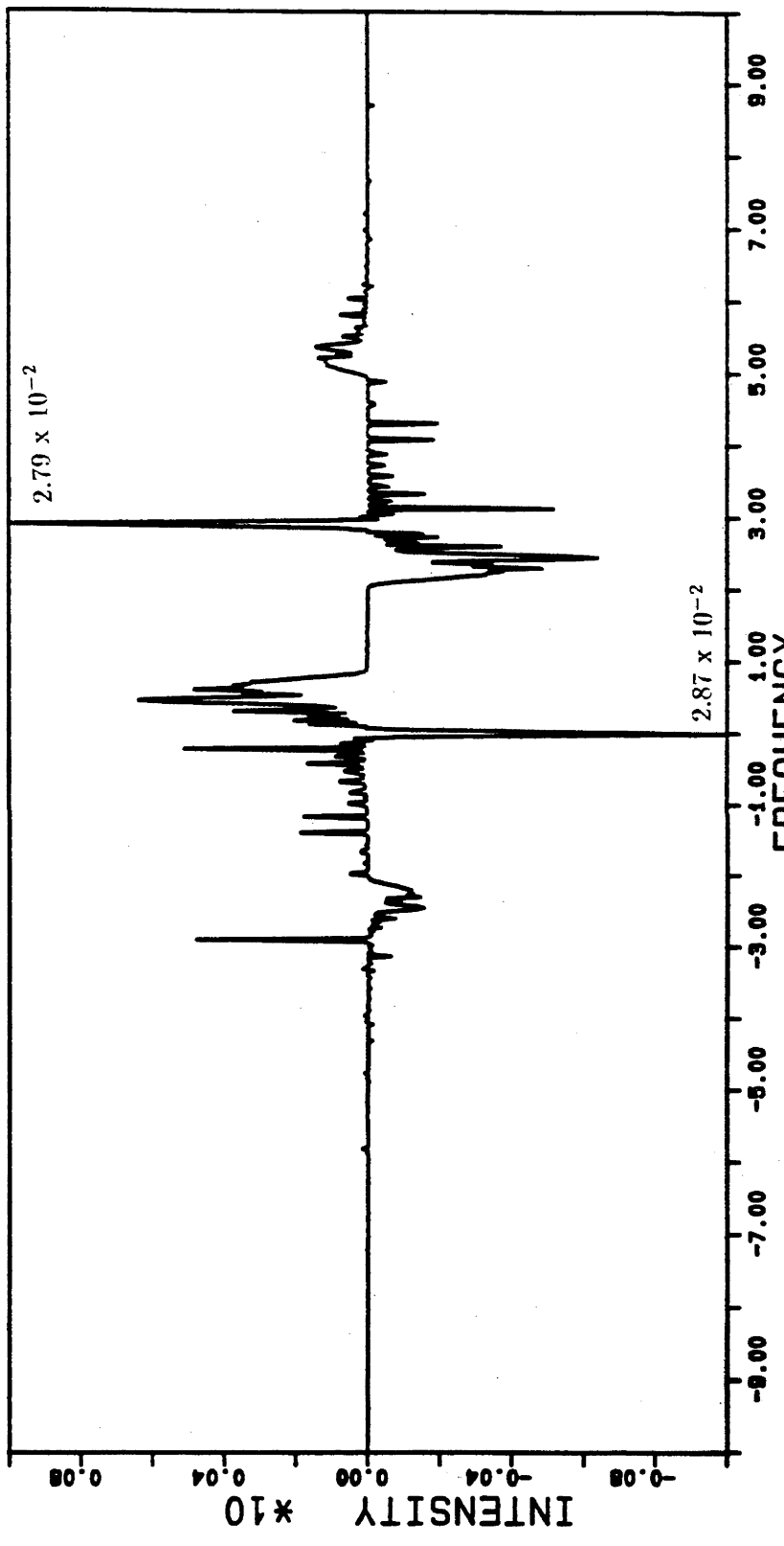

Figure 4.34 (c) Effect of variation of the halfwidth of strain distribution (ΔE_G) on the calculated holeburning spectrum. The values of the parameters are $\lambda = 30$ GHz, $\lambda' = 1$ GHz, feeding factor = 50 and strain halfwidth (ΔE_G) = 400 GHz.

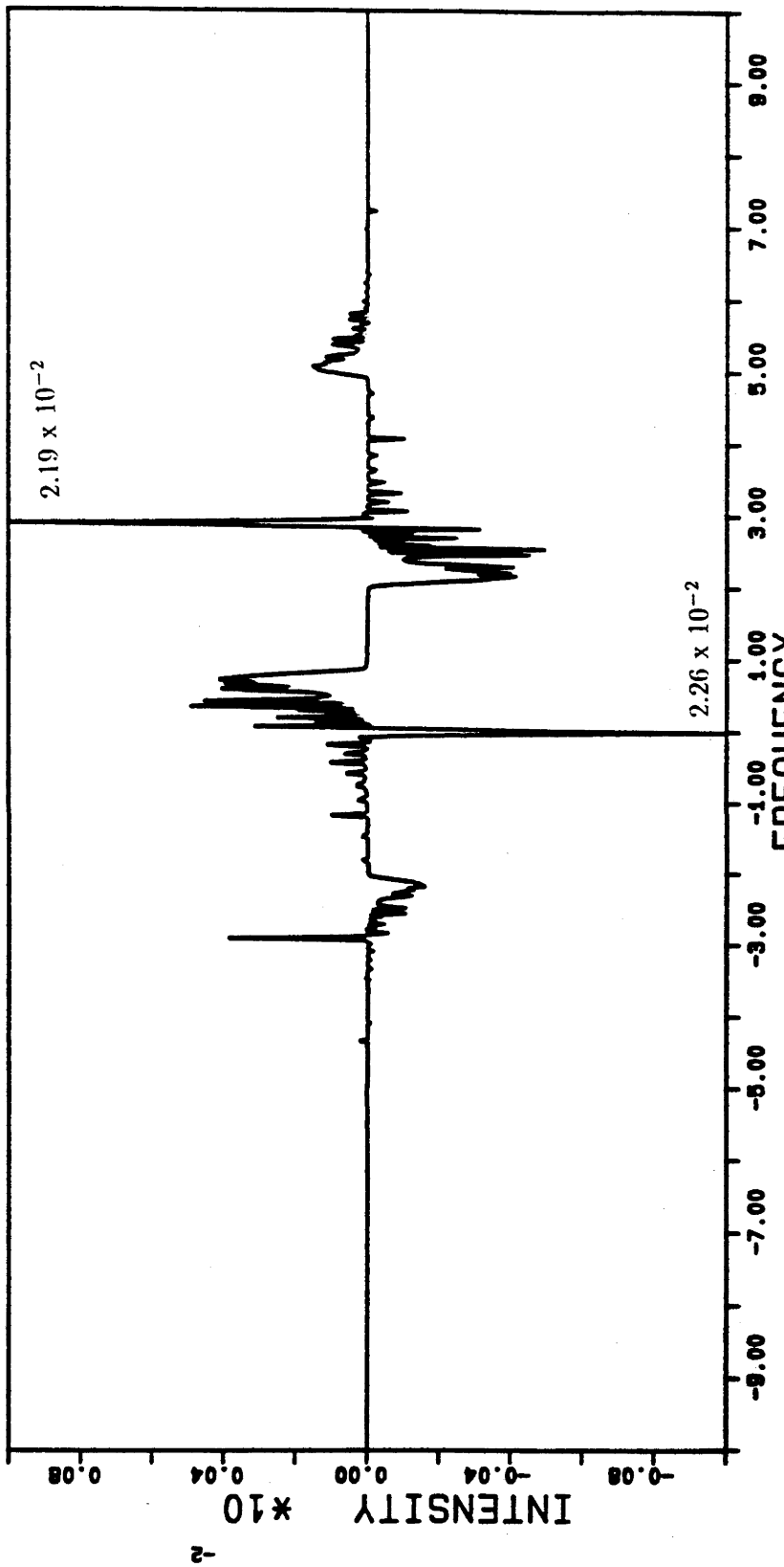

Figure 4.34 (d) Effect of variation of the halfwidth of strain distribution (ΔE_G) on the calculated holeburning spectrum. The values of the parameters are λ = 30 GHz, λ' = 1 GHz, feeding factor = 50 and strain halfwidth (ΔE_G) = 500 GHz.

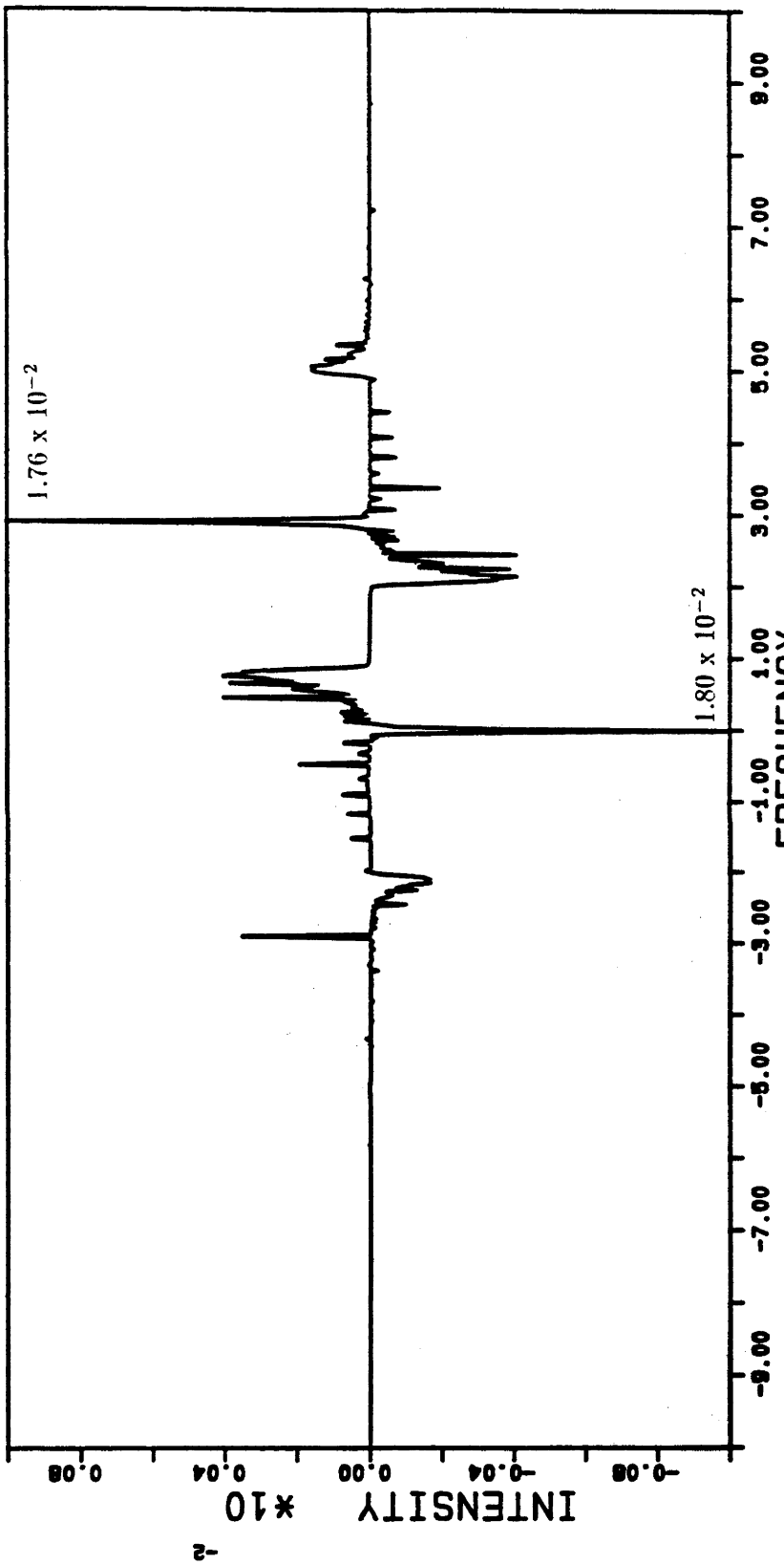

Figure 4.34 (e) Effect of variation of the halfwidth of strain distribution (ΔE_G) on the calculated holeburning spectrum. The values of the parameters are $\lambda = 30$ GHz, $\lambda' = 1$ GHz, feeding factor = 50 and strain halfwidth (ΔE_G) = 600 GHz.

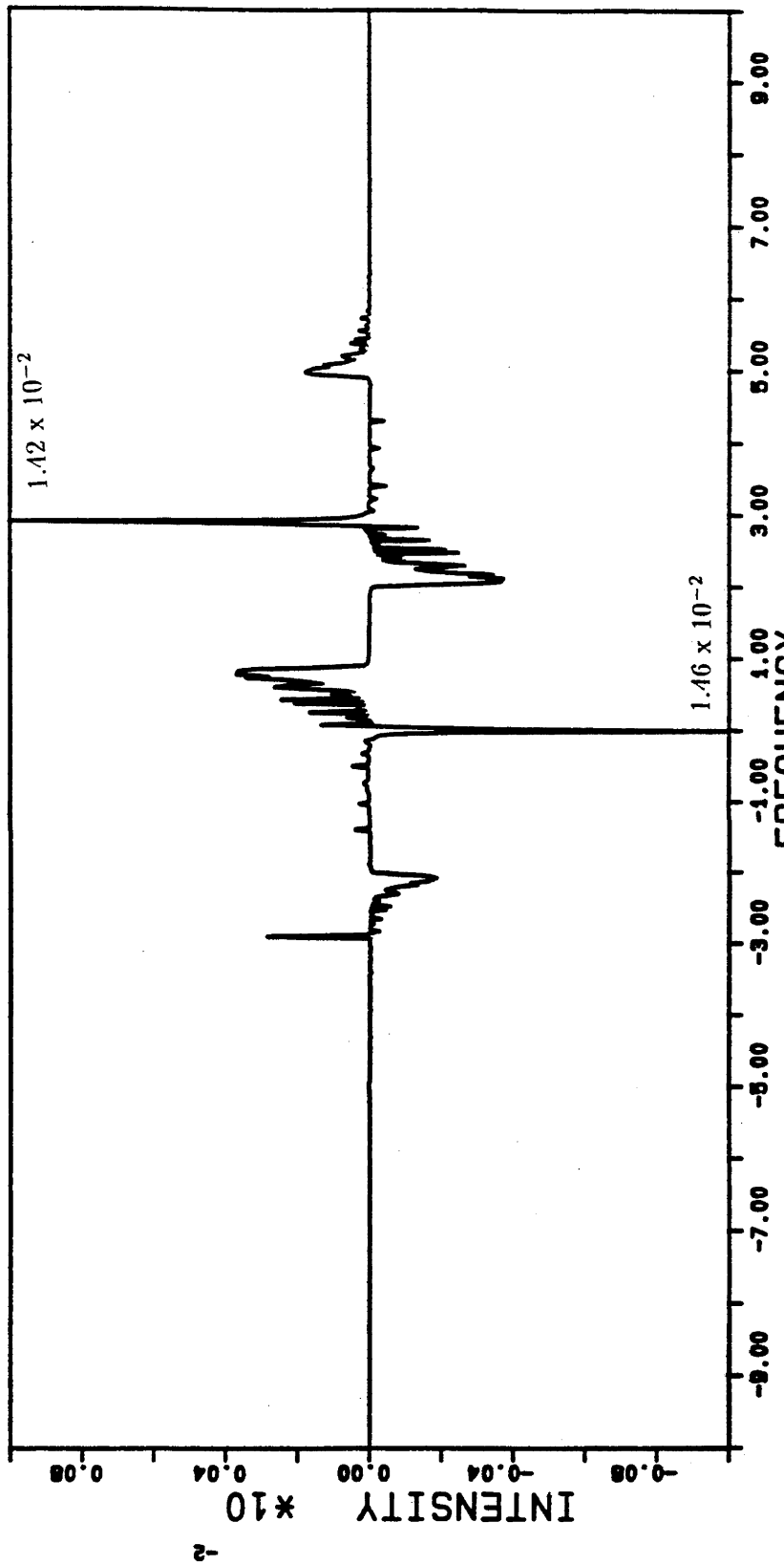

Figure 4.34 (f) Effect of variation of the halfwidth of strain distribution (ΔE_G) on the calculated holeburning spectrum. The values of the parameters are $\lambda = 30$ GHz, $\lambda' = 1$ GHz, feeding factor = 50 and strain halfwidth (ΔE_G) = 700 GHz.

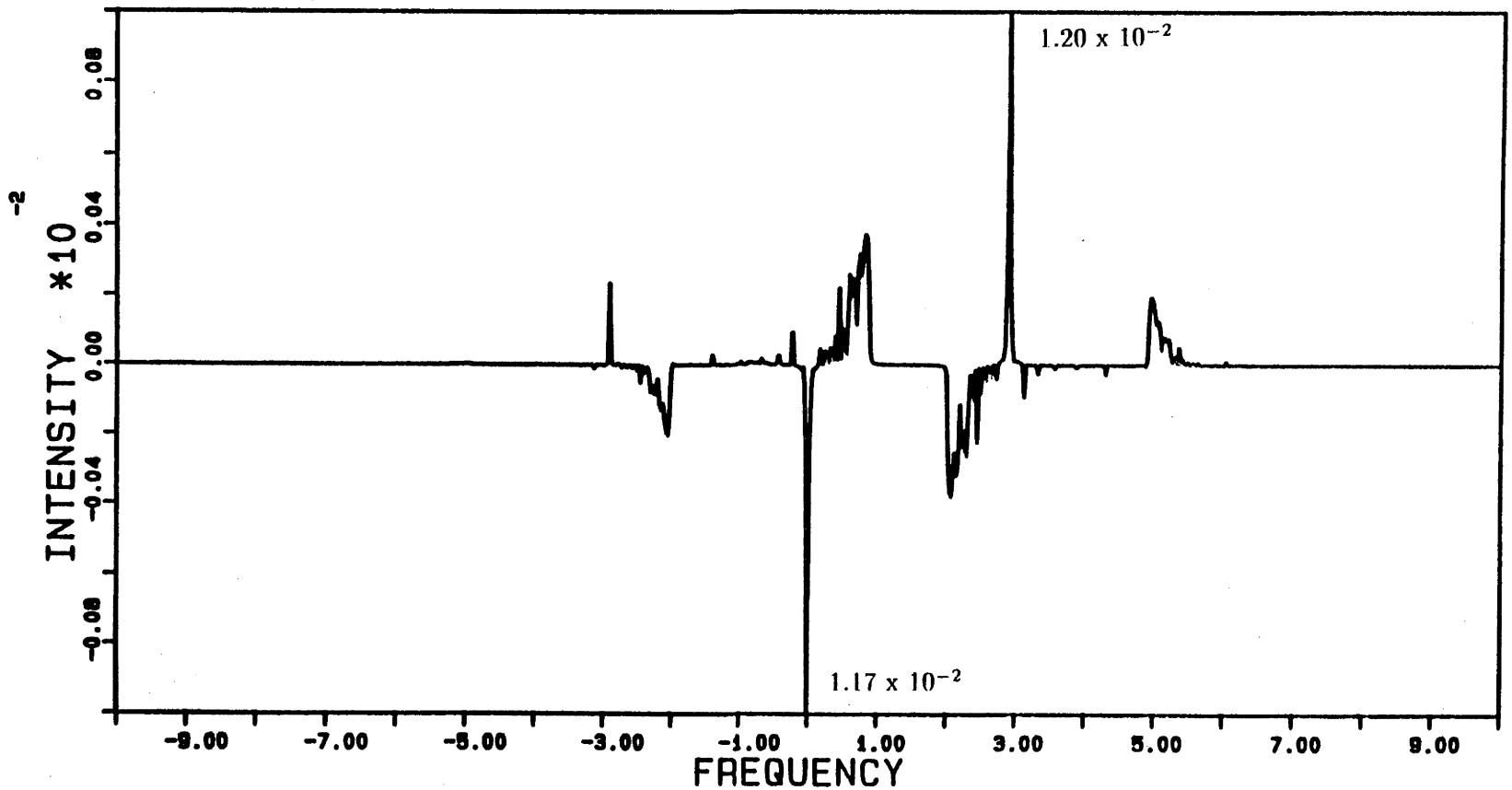

Figure 4.34 (g) Effect of variation of the halfwidth of strain distribution (ΔE_G) on the calculated holeburning spectrum. The values of the parameters are λ = 30 GHz, λ' = 1 GHz, feeding factor = 50 and strain halfwidth (ΔE_G) = 800 GHz.

many features in the holeburning spectra (calculated) are of low intensity.

These calculations were done on a VAX 8600 computer. The program required for performing the calculations was written in FORTRAN language and makes use of matrix diagonalisation subroutines of the NAG library (on the computer). The data was then transferred on to another VAX 11/750 computer that contained plotting programs (PLOTLIB). The holeburning spectra were plotted out on a HP 7550A graphics plotter. The subroutines used from the PLOTLIB had automatic scaling features. i.e. the range of the X and Y axis of the plot was determined by the plotting subroutines using the data to be plotted. In the presence of strong features like the 2.88 GHz antihole and the central hole, the nature of the low intensity features can not be made clear on a normal plot (figure 4.33). Hence, the intensity of the strong features was artificially reduced. The data was preprocessed using a program that sets a limit (1x10$^-$3) on the maximum value of the intensity(the Y coordinate) to be plotted. The true value in those cases is shown next to the peak.

4.15.11 EFFECT OF SPIN-ORBIT INTERACTION ON THE HOLEBURNING SPECTRUM

After discussing the effect of strain on the holeburning spectrum, the effect of spin-orbit interaction is now considered. The value of λ has been obtained from the MCD data (section 4.9) and is determined to be 1 cm^{-1} (30 GHz). But the value of λ' depends on the degree of anisotropy in the spin-orbit interaction (section 4.15.2). Hence, in calculating the holeburning spectra λ' is treated as a parameter. The degree of anisotropy is expected to be small and in the calculation λ' is assigned values between .25 and 3 GHz. The resulting holeburning spectra are shown in figure 4.35 (a) through (f). The ^3E excited state of a centre experiencing zero strain is split into 3 doubly degenerate levels spaced λ apart. At increasing strain values the orbital degeneracy of the ^3E state is lifted and each of the orbital 'singlets' is a spin triplet. The separation of levels in this spin triplet is essentially determined by the values of λ' and λ. It should be remembered that the value of λ' not only determines the excited state splittings but also affects the transitions intensities. In our calculation only λ' is treated as a parameter and its effect on the holeburning spectrum is calculated for various values of λ'. The

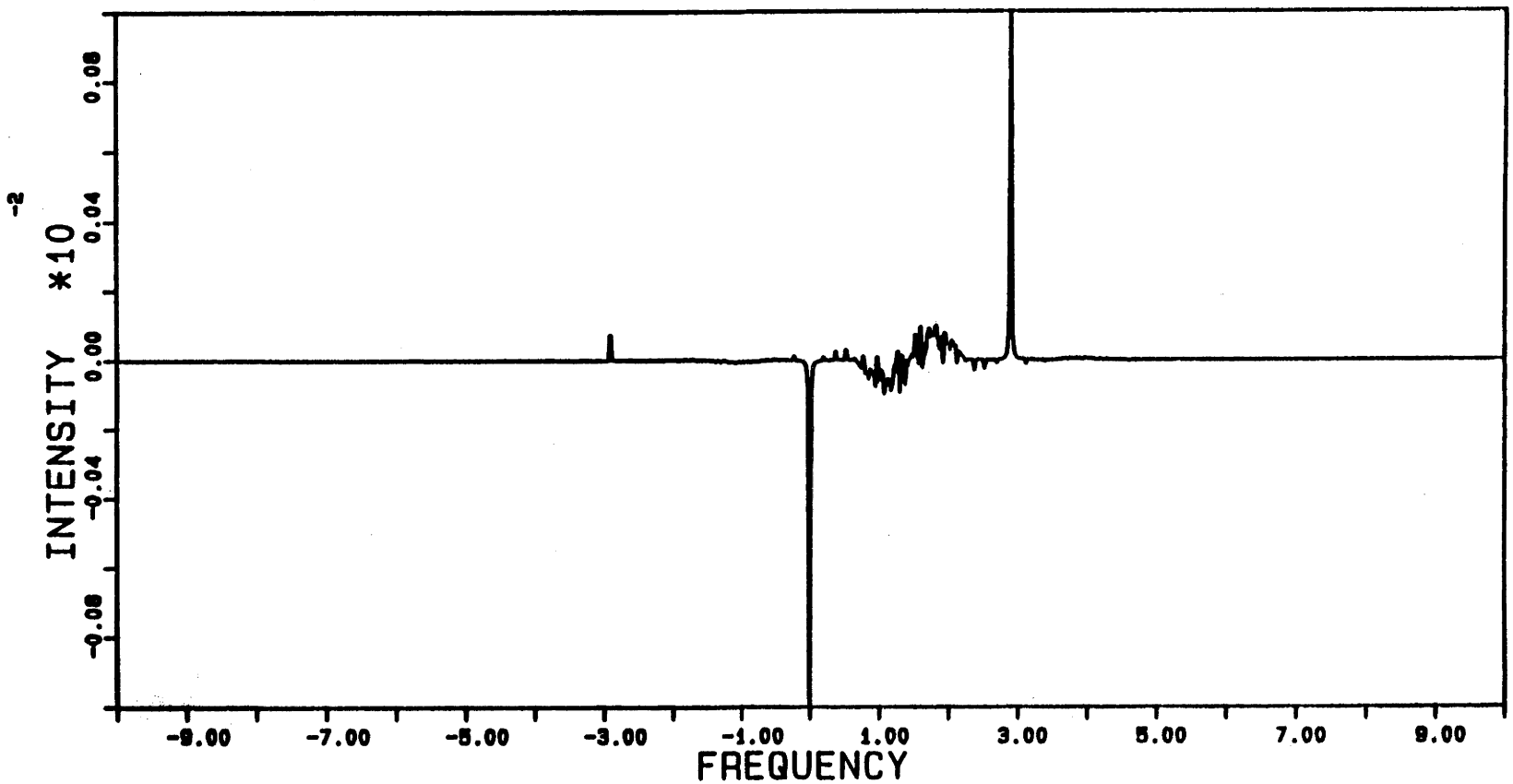

Figure 4.35 (á) Effect of variation of λ' on the calculated holeburning spectrum. The values of the parameters are λ = 30 GHz, feeding factor = 50, strain halfwidth (ΔE_G) = 600 GHz and λ'= 0.25 GHz

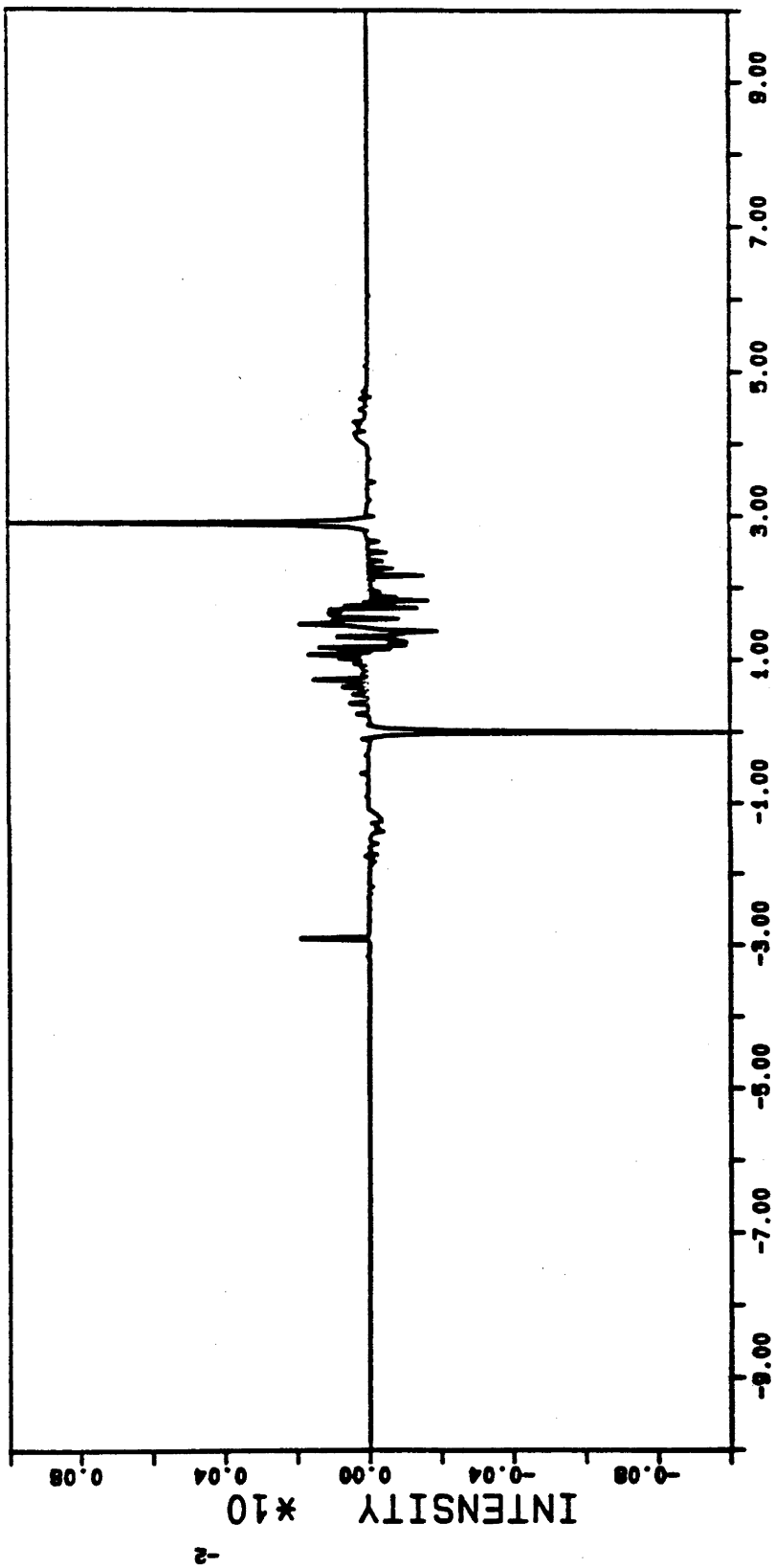

Figure 4.35 (b) Effect of variation of λ' on the calculated holeburning spectrum. The values of the parameters are $\lambda = 30$ GHz, feeding factor = 50, strain halfwidth (ΔE_G) = 600 GHz and $\lambda' = 0.50$ GHz

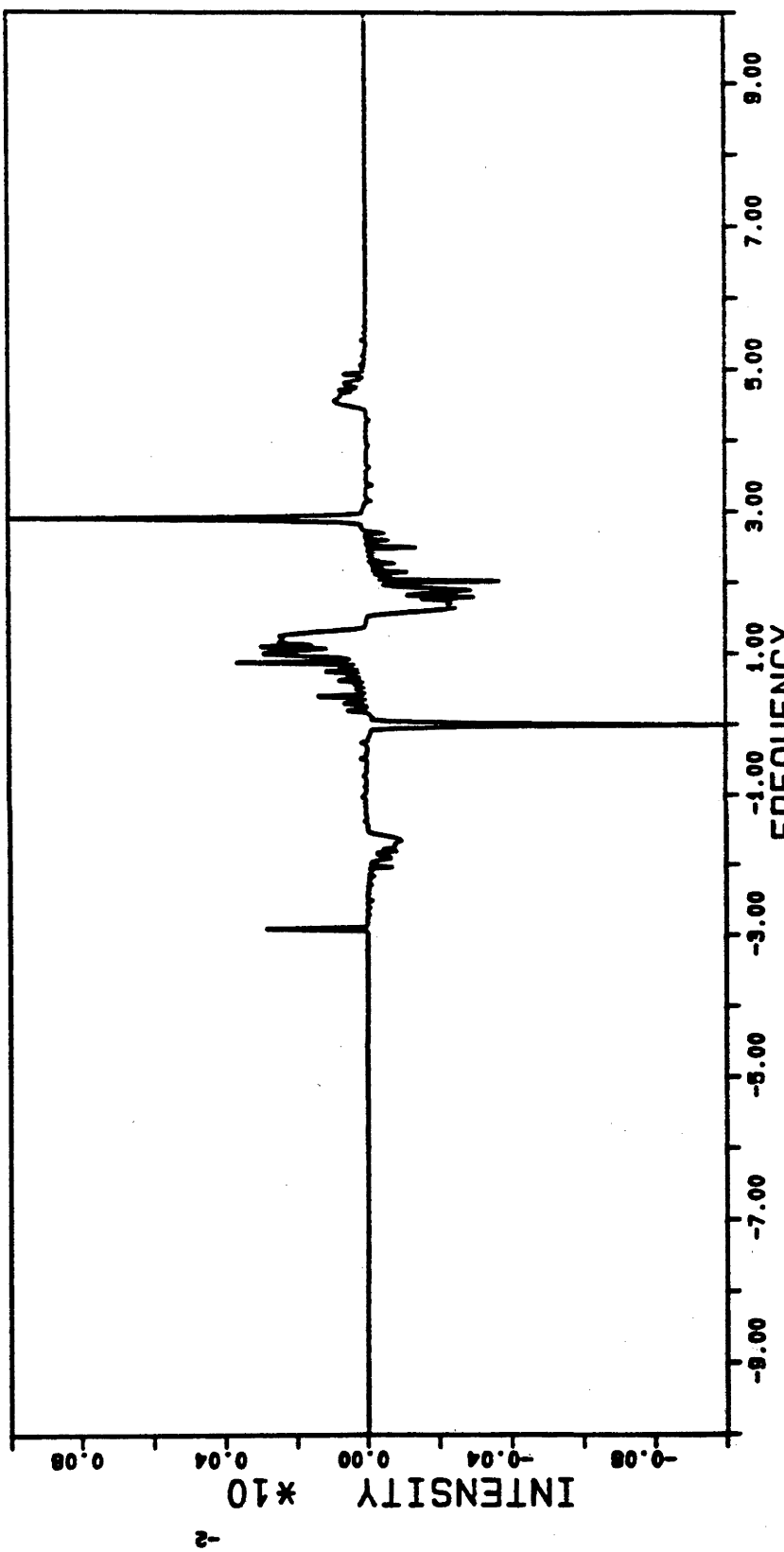

Figure 4.35 (c) Effect of variation of λ' on the calculated holeburning spectrum. The values of the parameters are λ = 30 GHz, feeding factor = 50, strain halfwidth (ΔE_G) = 600 GHz and λ'= 0.75 GHz

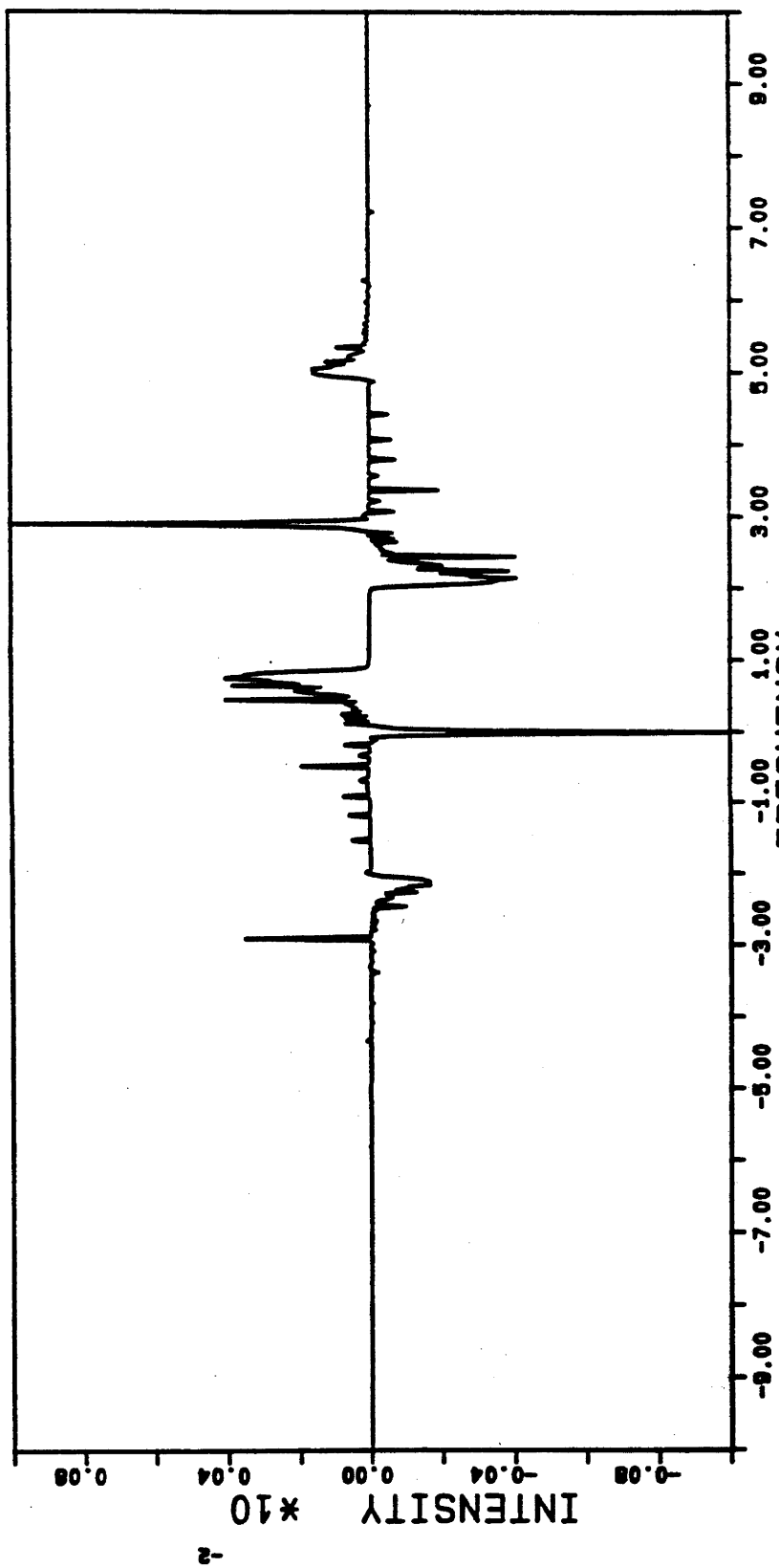

Figure 4.35 (d) Effect of variation of λ' on the calculated holeburning spectrum. The values of the parameters are $\lambda = 30$ GHz, feeding factor = 50, strain halfwidth (ΔE_G) = 600 GHz and $\lambda' = 1$ GHz

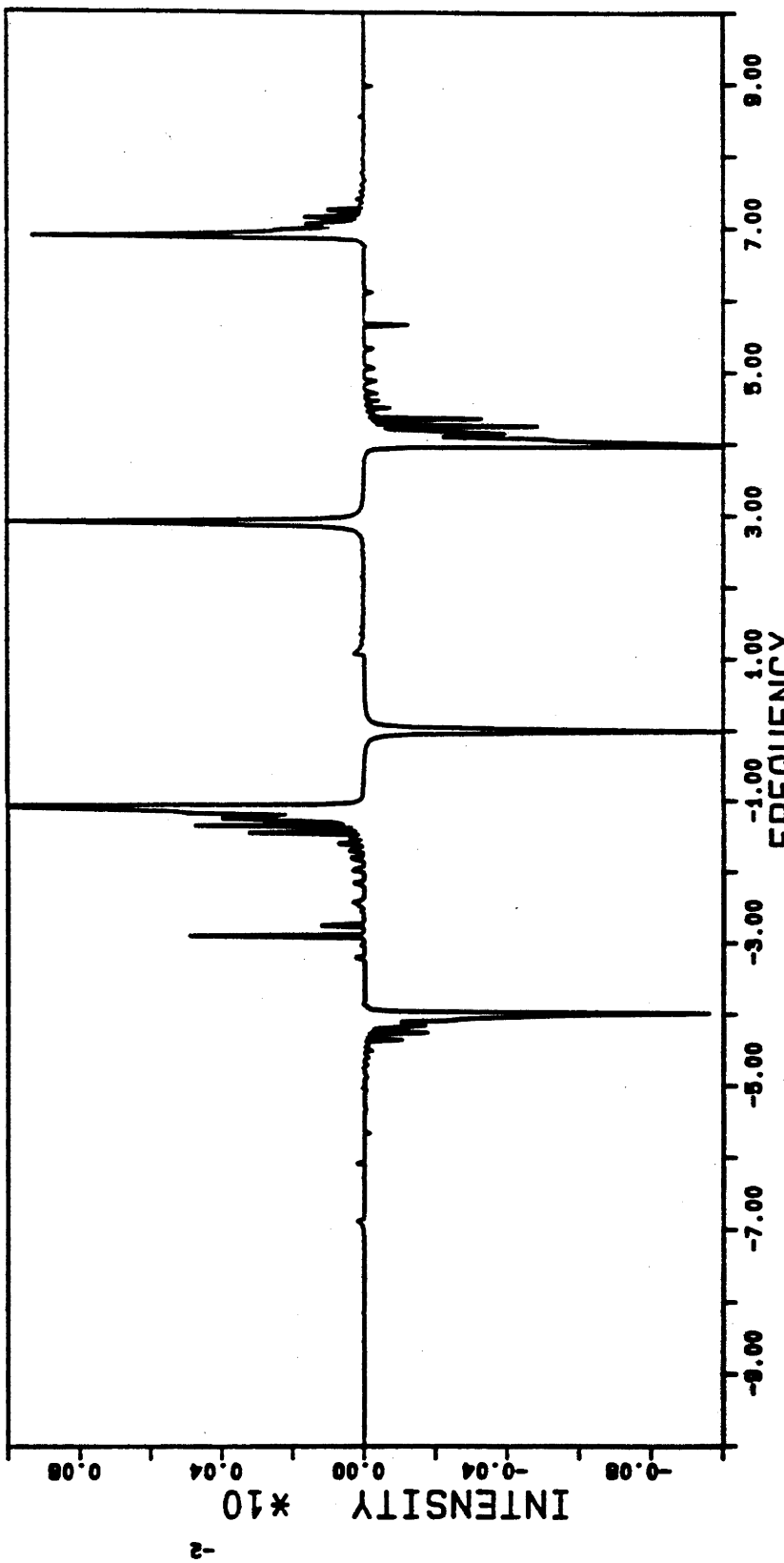

Figure 4.35 (e) Effect of variation of λ' on the calculated holeburning spectrum. The values of the parameters are λ = 30 GHz, feeding factor = 50, strain halfwidth (ΔE_G) = 600 GHz and λ'= 2 GHz

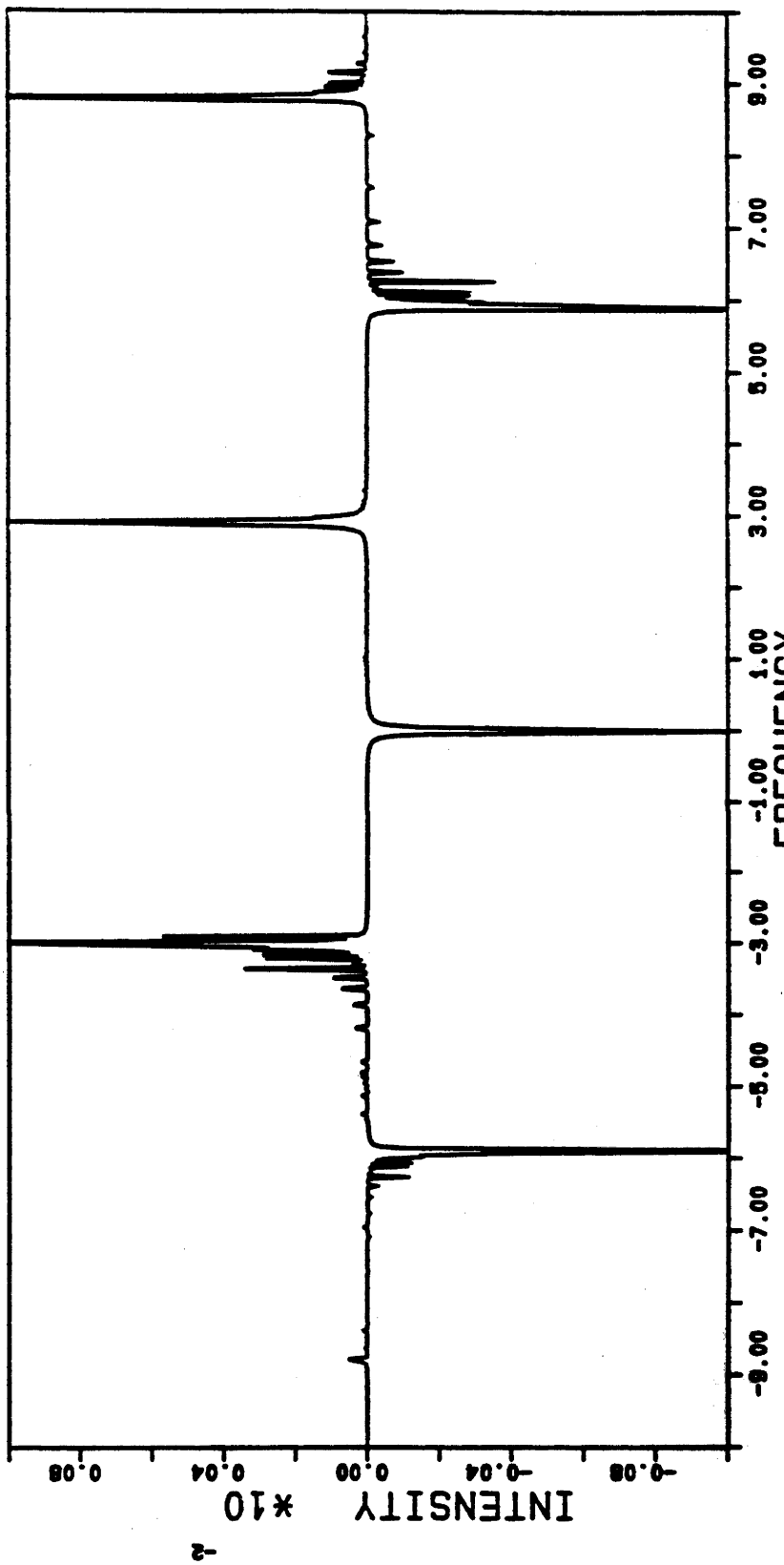

Figure 4.35 (f) Effect of variation of λ' on the calculated holeburning spectrum. The values of the parameters are λ = 30 GHz, feeding factor = 50, strain halfwidth (ΔE_G) = 600 GHz and λ'= 3 GHz

values λ, ΔE_G and the feeding factor are taken to be 30 GHz, 600 GHz and 50 respectively. It can be seen from figure 4.35 that at low values of λ' (figure 4.35 (a) through (d)) the intensities are not affected much and the only discernible affect of varying λ' is the shift in the positions of the low intensity features. However, at higher values of λ' the difference in transition intensities is not much (the Z level is mixed to a large extent with the X and Y levels) selective feeding loses its effect and features outside the 5 GHz range gain in intensity. This is contrary to experimental observations. Hence, from this data it can be concluded that the anisotropy in spin-orbit interaction is not large and λ' is small compared to λ.

4.15.12 EFFECT OF PHOTOCHEMICAL BLEACHING ON THE HOLEBURNING SPECTRUM

Upto this point, the effect of varying possible parameters on the holeburning spectrum has been considered. It can be seen that using the parameters, λ, ΔE_G, λ' and the feeding factor, the spectrum that can be generated is only in partial agreement with the experimentally observed spectrum. The extent of agreement and the limitations of the model on which the present calculation is based is considered further in the following section. All the calculations presented upto this point deal with effect of strain etc. on the holeburning spectrum with the tacit assumption that the centre is not altered on optical excitation. But, it is always possible that a centre can undergo photophysical or photochemical changes when it is in the opticallly excited state. To account for this possibility one more parameter is now introduced. The possibilty of photophysical holeburning is not considered as it requires more data (e.g. the exact nature of strain distribution etc.) and only photochemical holeburning is considered. As described in the previous chapter (CaO : F centre), photochemical holeburning involves the loss of an electron to the surrounding lattice. The effect of this electron loss on the holeburning spectrum depends on exact nature of the excited state at the time of electron loss. i.e. it depends on the state (or level) the electron was in at the time of loss. The following discussion will make this point clear. According to the present model, the zero-phonon transition is between $^3A_2$ ground state and ^3E excited state. No predictions are made about the existence and location of other energy levels of the N-V centre. In this section two possibilties are considered. One possibility is that there are no

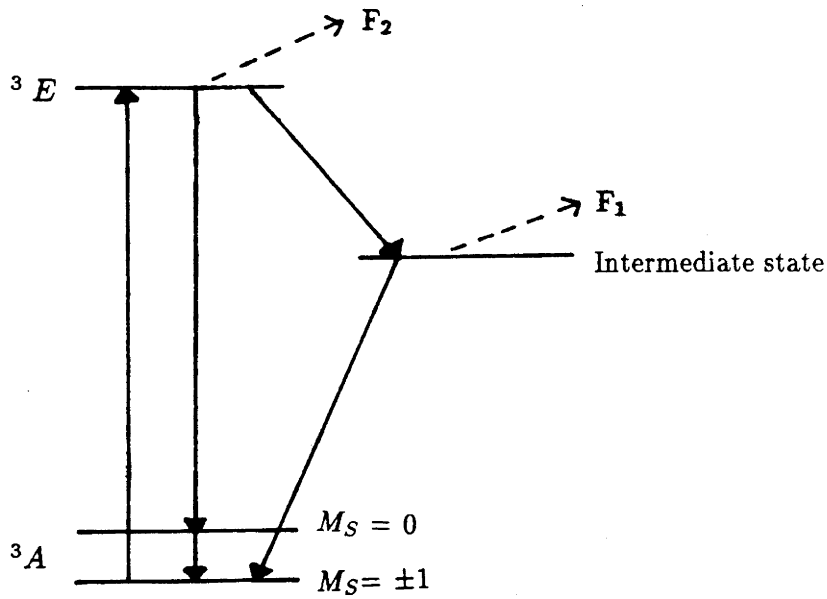

energy levels between the levels involved in the zero-phonon transition. The other possibility is that there is an intermediate level that presumably is *involved* in the selective feeding process. The effect of electron loss depends on whether the electron exited from the ^3E state or the intermediate state just hypothesised. If the electron was in the ^3E state its loss affects all antiholes of the holeburning spectrum equally. However, if the electron were to be in the intermediate state then *only* the intensities of the antiholes would be affected.

The situations discussed above were included in the calculation using two parameters F_1 and F_2. F_1 is the ratio of centres that are photochemically bleached from the intermediate state to the total number of centres that are optically excited. F_2 is the similar ratio when the electron loss is from the ^3E state. Before mentioning the details of calculation a remark about the magnitude of the effect of electron loss on the holeburning spectrum is in order. If fraction of centres (F_1) that are bleached is, for example, 0.25, then the magnitude of the antiholes is decreased by twice that fraction i.e. 0.5 . This is because loss of antihole intensity is replaced by equivalent gain in hole intensity at that frequency. Therefore, when $F_1 = 0.5$ the effect is just removal of antiholes from the two laser holeburning spectrum for the same value of parameters and $F_1 = 1$ represents the situation where all antiholes are replaced by equivalent holes. In the calculation, to account for this photoinduced bleaching, the antihole intensities of transitions ending $M_S = \pm 1$ level are multiplied by $(1 - 2F_1)$ and $(1 - 2F_2)$ is used as the multiplicative

multiplicative factor to the intensities of all antiholes. The results of this calculation are shown in figure 4.36 (a) through (d) where F_1 is varied from 0 to 1 in steps of 0.25 . Corresponding results obtained by varying F_2 in a similar fashion are shown in figure 4.37 (a) through (d).

Finally, an attempt is made to simulate the holeburning spectrum obtained by Harley *et al* (private communication) (figure 4.4 (c)). Since the the spectrum in figure 4.4(c) has equal intensities on both high and low energy sides the feeding factor for this trace is set equal to 1. Since no antiholes are observed in that spectrum F_1 is set equal to one. The spectra obtained then is shown in figure 4.38 .

4.15.13 DISCUSSION

From the holeburning spectra presented in this section, it is obvious that each of the parameters (ΔE_G, λ' and the feeding factor) used in the present model has an appreciable effect on the spectrum. In this section calculated holeburning spectra are compared with the experimental spectrum and the extent of success the model is discussed. Keeping in mind that the features seen in the experimental spectrum are rather sharp, the spectrum presented in figure 4.34 (e) is chosen for comparison (any other spectra presented later are equally good).

The model predicts correctly the hole at the burn laser frequency (0 GHz) and the sharp antiholes at $\pm$2.88 GHz. It predicts two other features at $\approx$1 GHz and $\approx$2 GHz. The feature at 1 GHz is predicted to be antihole which is in agreement with experiment but the feature at 2 GHz is predicted to be a hole while it is seen as an antihole in the experiment. The asymmetry seen in the experiment is well predicted by proper choice of the feeding factor (accounting for the preferential relaxation in the $M_S = \pm 1$ level. The model does not predict correctly the intensities of the central hole and the and the antihole at +2.88 GHz. From the numbers given in figure 4.42 (e), it can be seen that the central hole and the antihole are stronger by a factor $\approx$18 than shown in the figure. Further, the antihole feature predicted at $\approx$5 GHz is not seen in experiment.

It is obvious from the comparison that the predictions of the model are

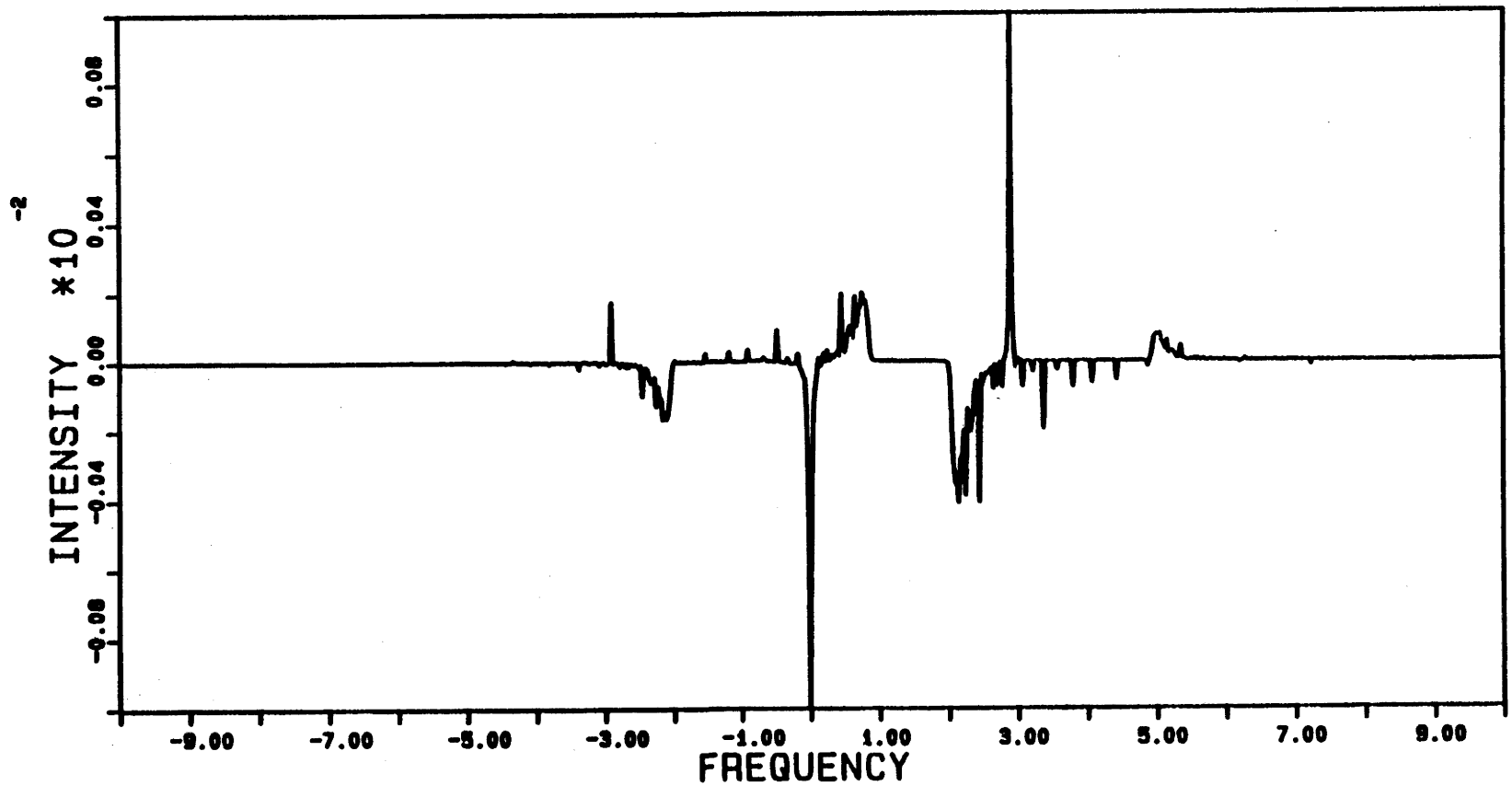

Figure 4.36 (a) Effect of variation of the bleaching factor F_1 (see text for definition of F_1) on the calculated holeburning spectrum. The values of the parameters are λ = 30 GHz,λ'= 1 GHz, feeding factor = 50 and strain halfwidth (ΔE_G) = 600 GHz. F_1 = 0.25 for this trace.

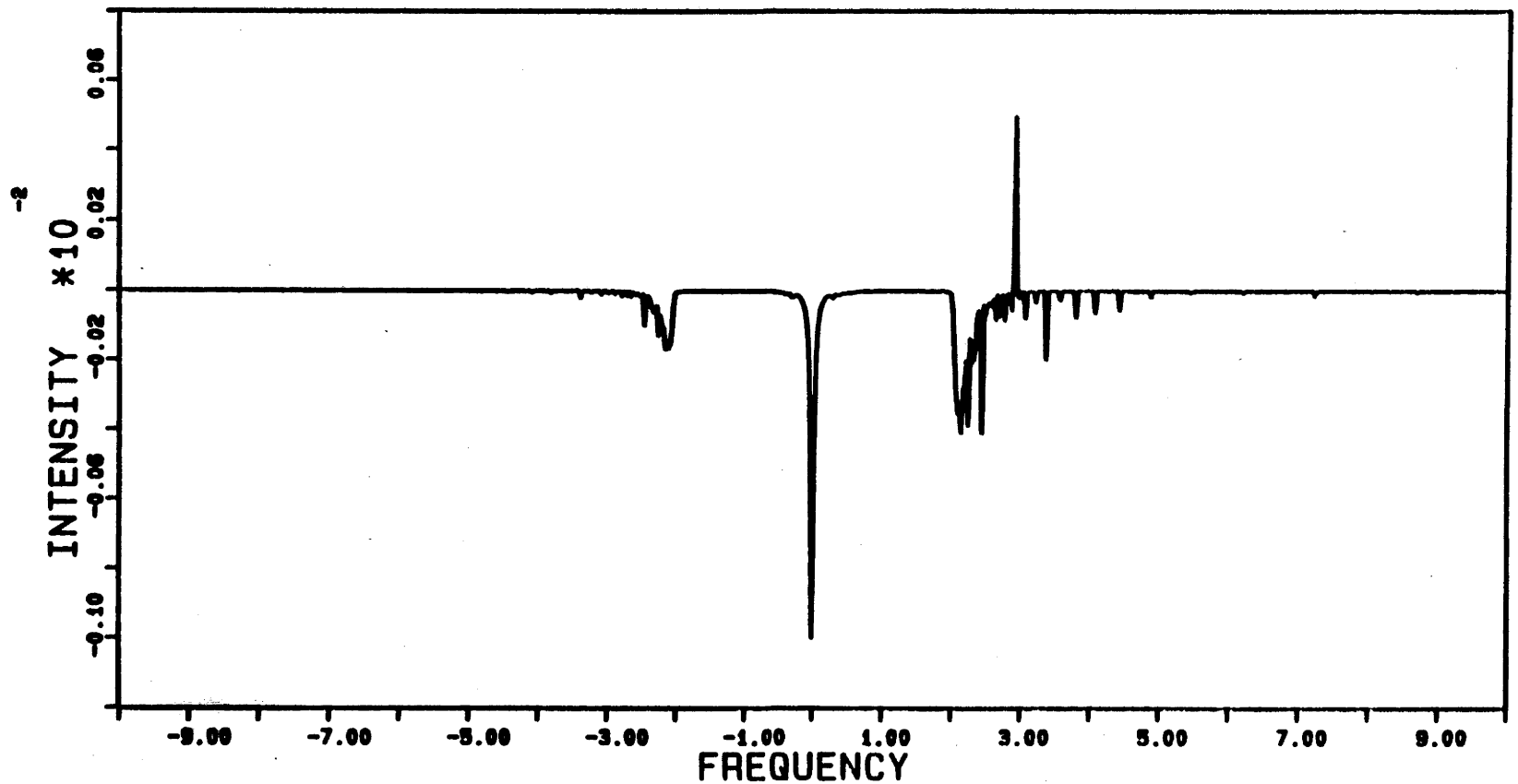

Figure 4.36 (b) Effect of variation of the bleaching factor F_1 on the calculated holeburning spectrum. The values of the parameters are λ = 30 GHz,λ'= 1 GHz, feeding factor = 50 and strain halfwidth (ΔE_G) = 600 GHz. F_1 = 0.50 for this trace.

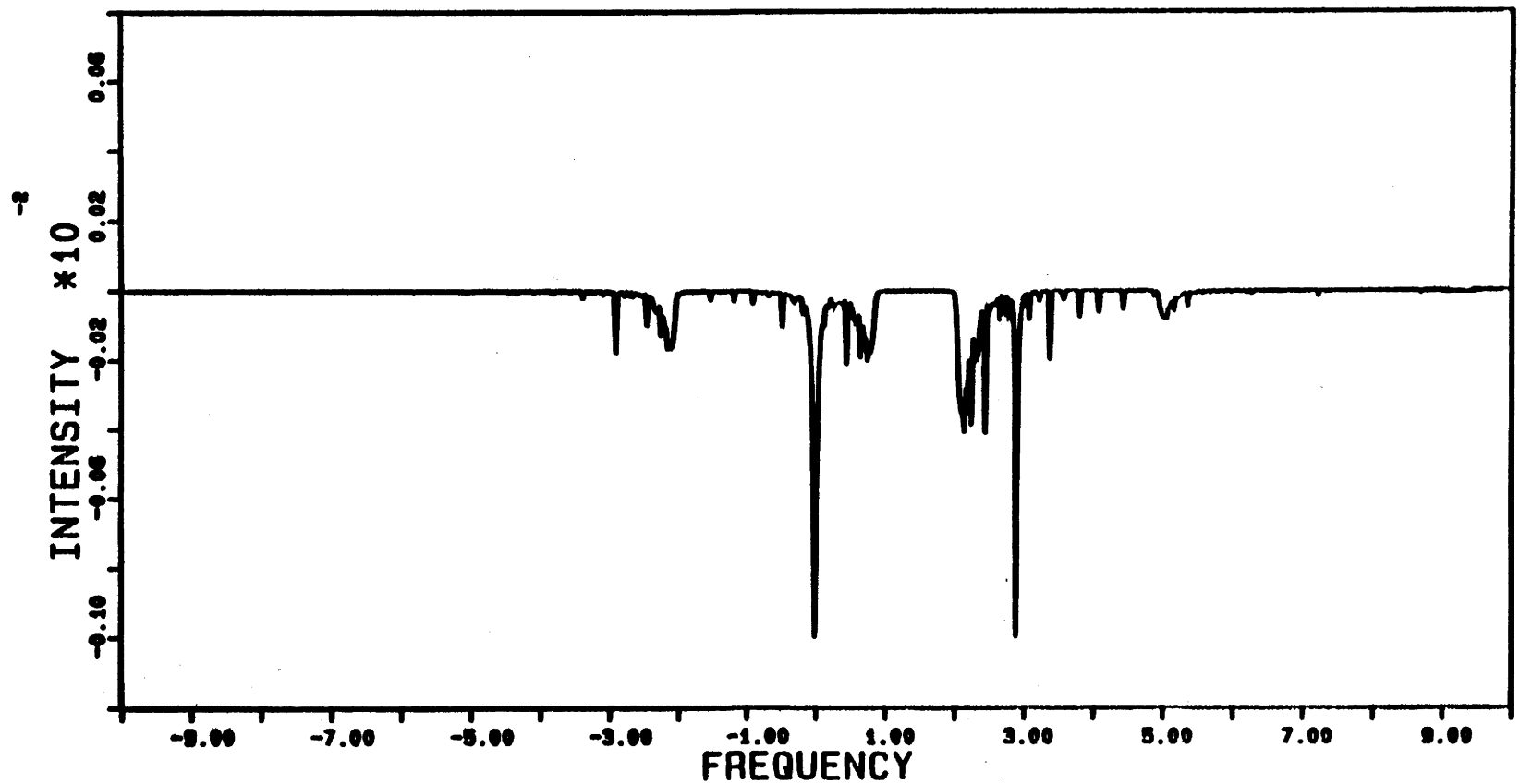

Figure 4.36 (c) Effect of variation of the bleaching factor F_1 on the calculated holeburning spectrum. The values of the parameters are λ = 30 GHz,λ'= 1 GHz, feeding factor = 50 and strain halfwidth (ΔE_G) = 600 GHz. F_1 = 0.75 for this trace.

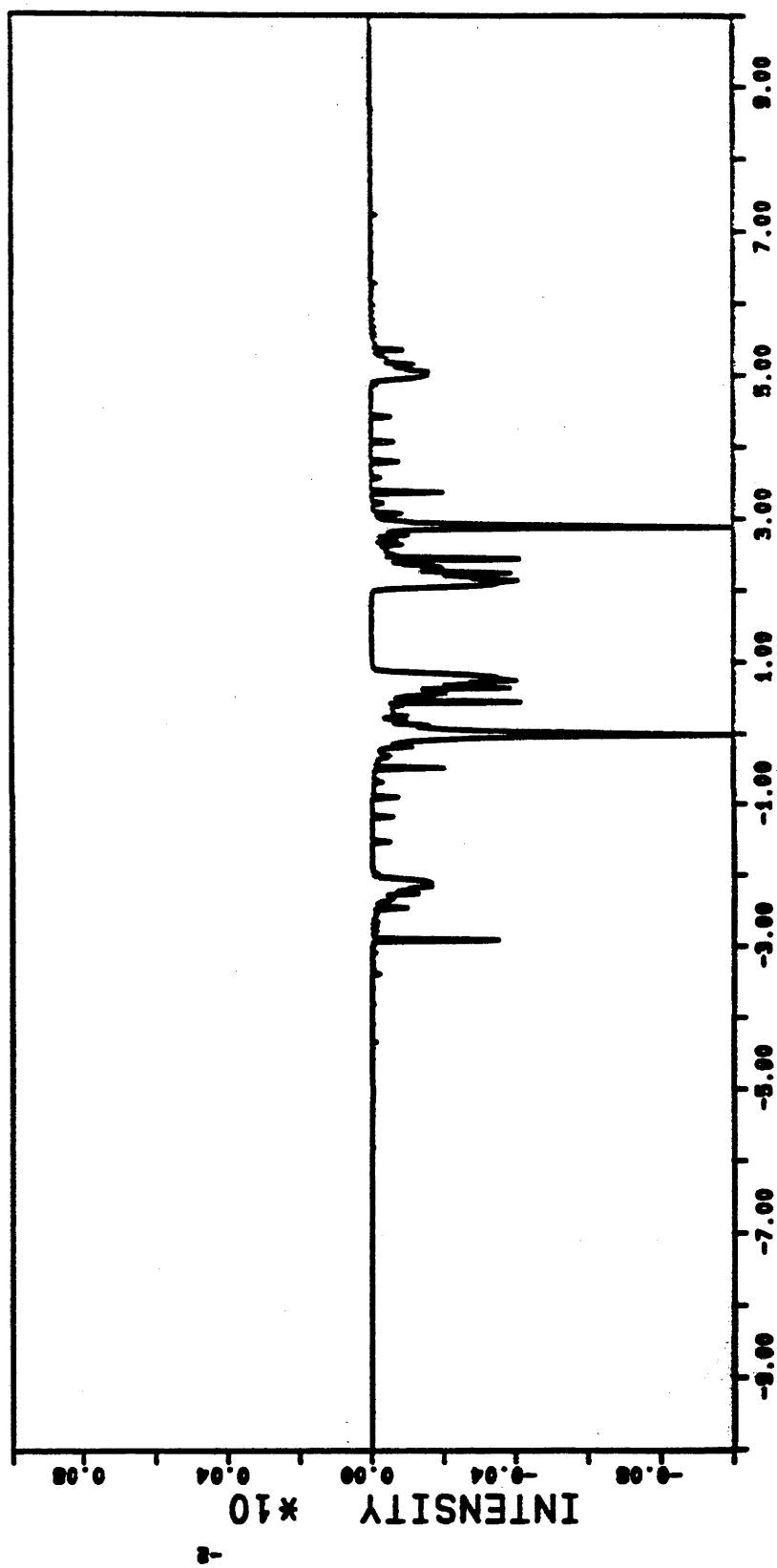

Figure 4.36 (d) Effect of variation of the bleaching factor F_1 on the calculated holeburning spectrum. The values of the parameters are $\lambda = 30$ GHz,$\lambda' = 1$ GHz, feeding factor = 50 and strain halfwidth $(\Delta E_G) = 600$ GHz. $F_1 = 1.0$ for this trace.

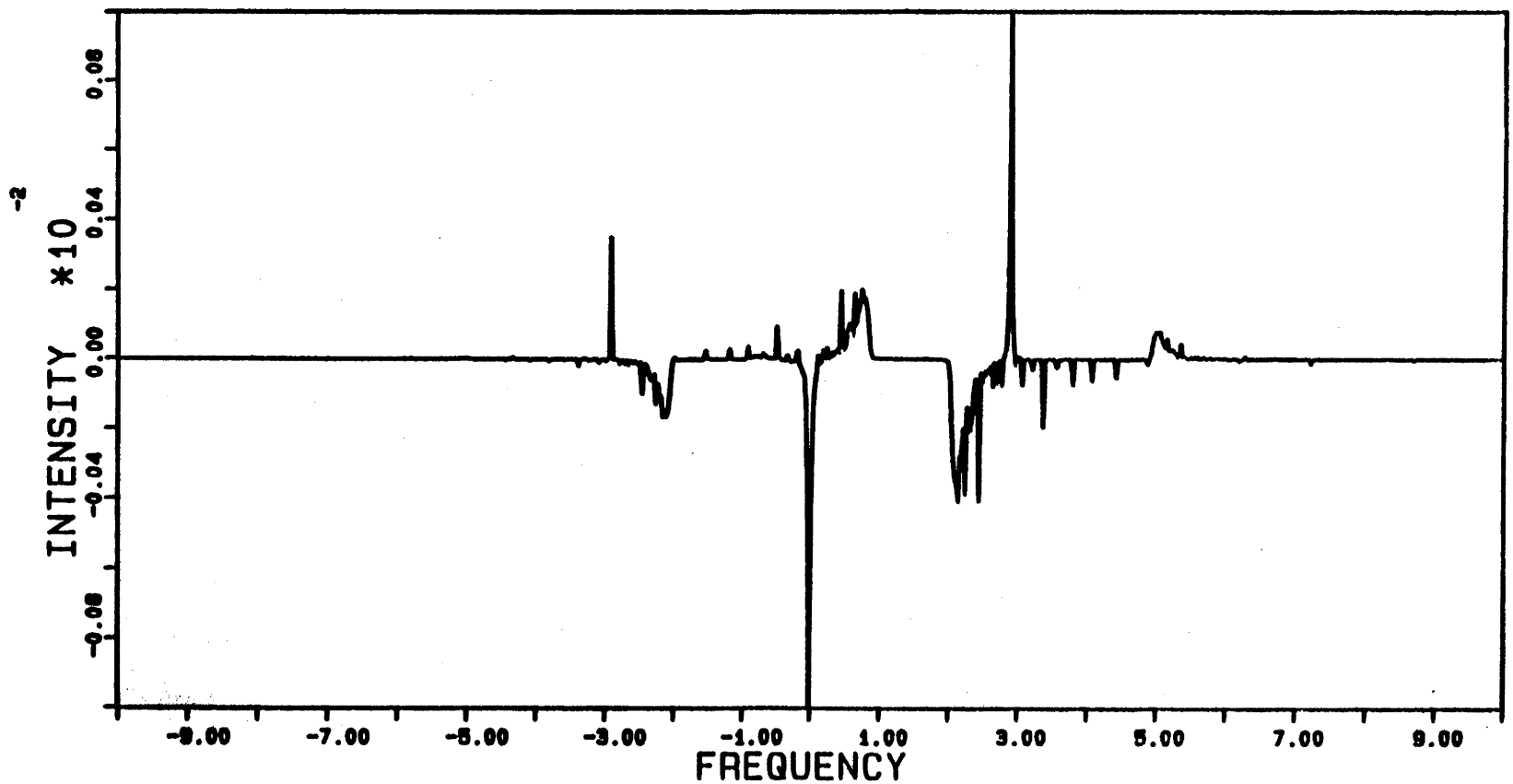

Figure 4.37 (a) Effect of variation of the bleaching factor F_2 (see text for definition of F_2) on the calculated holeburning spectrum. The values of the parameters are λ = 30 GHz,λ'= 1 GHz, feeding factor = 50 and strain halfwidth (ΔE_G) = 600 GHz. F_2 = 0.25 for this trace.

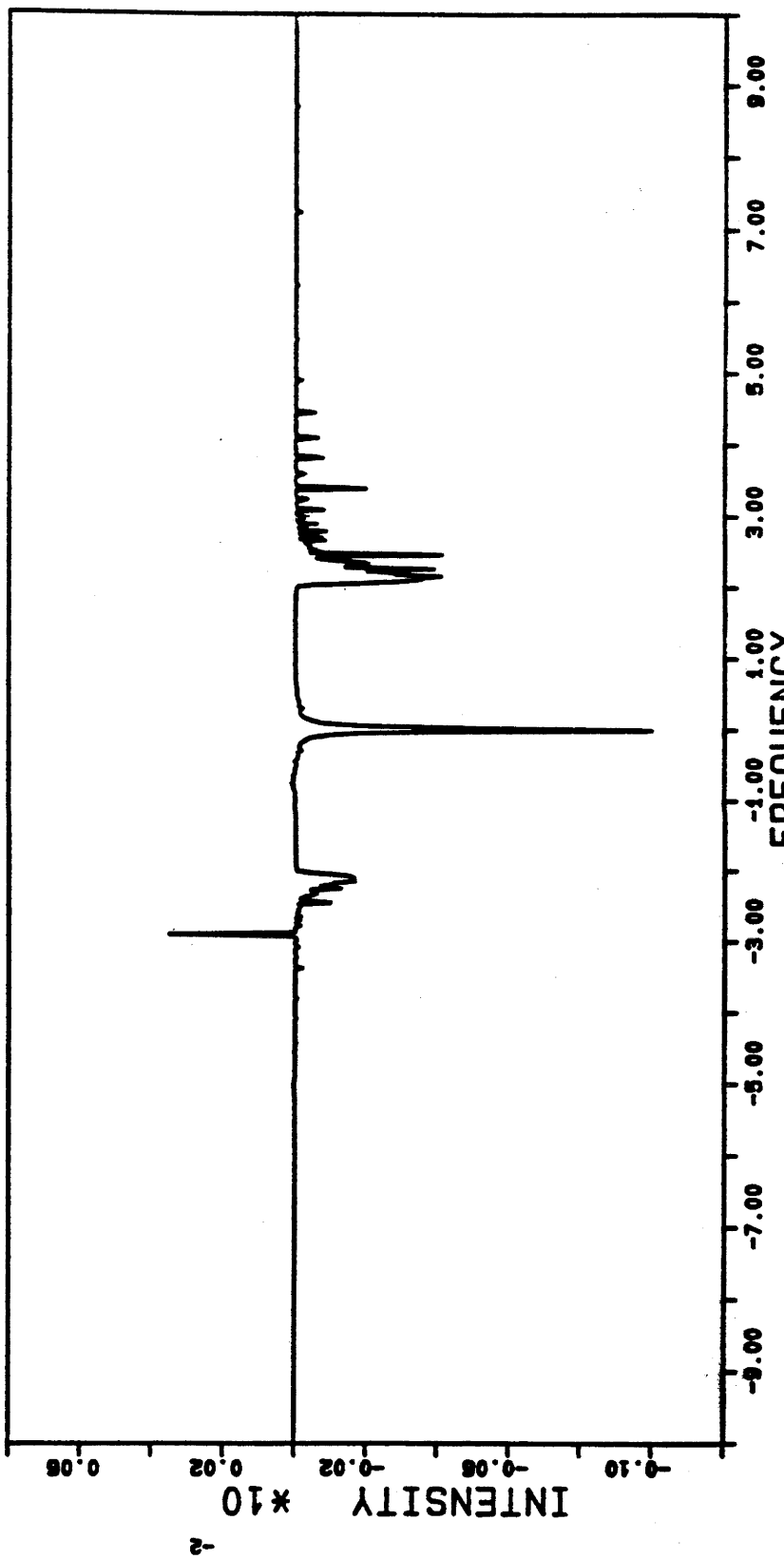

Figure 4.37 (b) Effect of variation of the bleaching factor F_2 on the calculated holeburning spectrum. The values of the parameters are $\lambda = 30$ GHz,$\lambda' = 1$ GHz, feeding factor = 50 and strain halfwidth (ΔE_G) = 600 GHz. $F_2 = 0.50$ for this trace.

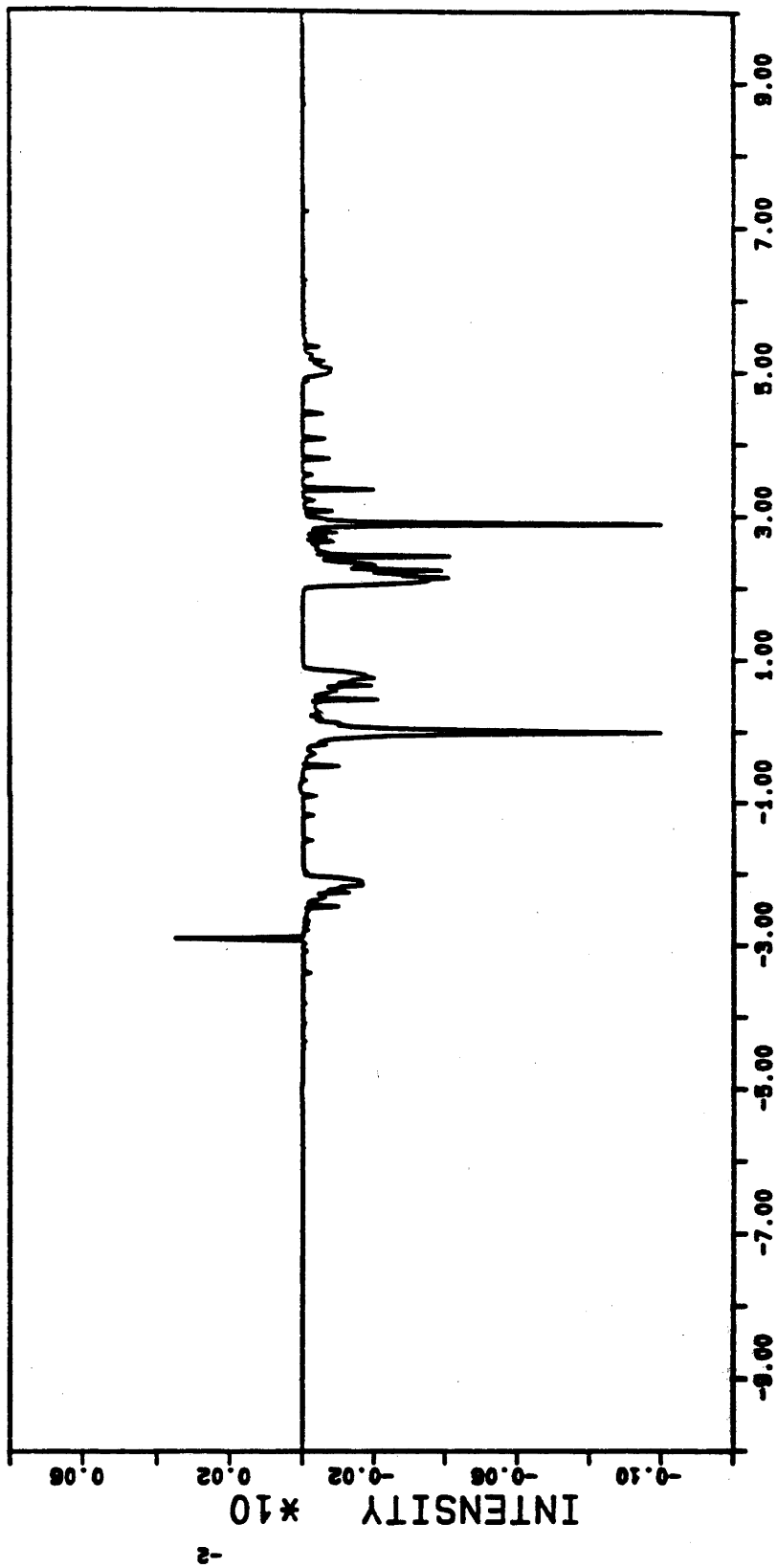

Figure 4.37 (c) Effect of variation of the bleaching factor F_2 on the calculated holeburning spectrum. The values of the parameters are λ = 30 GHz,λ'= 1 GHz, feeding factor = 50 and strain halfwidth (ΔE_G) = 600 GHz. F_2 = 0.75 for this trace.

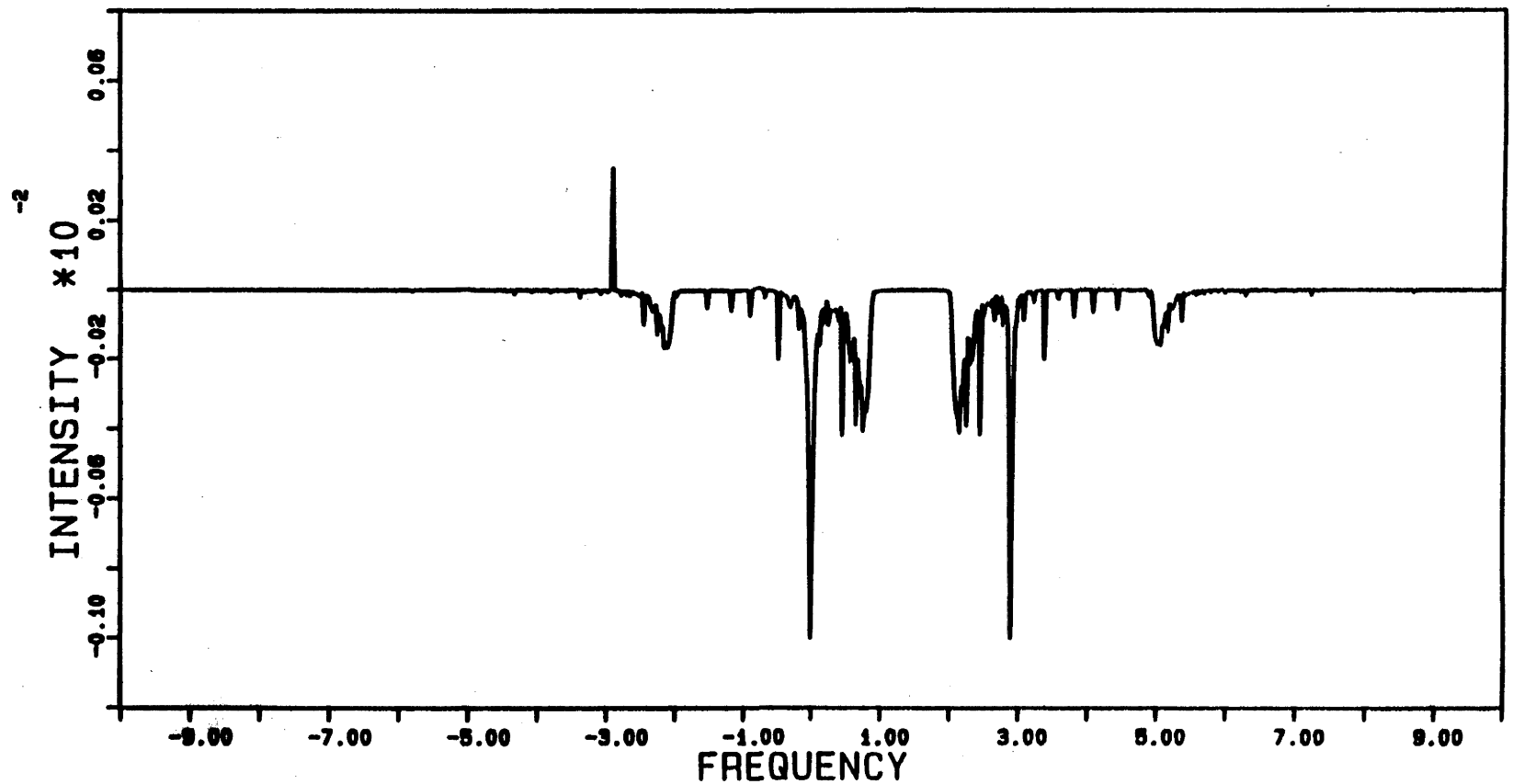

Figure 4.37 (d) Effect of variation of the bleaching factor F_2 on the calculated holeburning spectrum. The values of the parameters are λ = 30 GHz,λ'= 1 GHz, feeding factor = 50 and strain halfwidth (ΔE_G) = 600 GHz. F_2 = 1.0 for this trace.

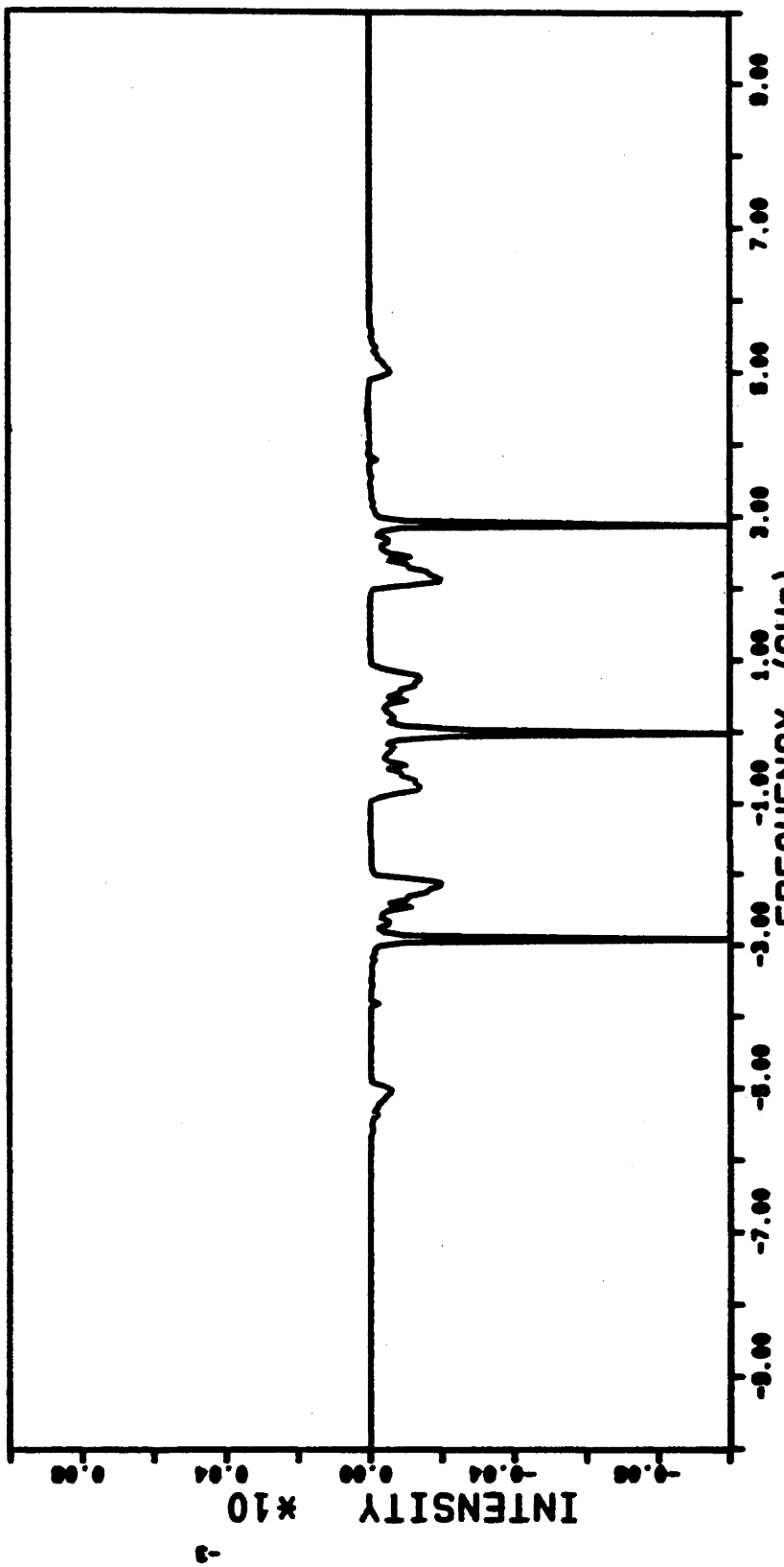

Figure 4.38 Holeburning spectrum obtained when there total bleaching and there is no selective feeding. Other parametres have the values λ = 30 GHz,λ'= 1 GHz and strain halfwidth (ΔE_G) = 600 GHz. F_2 = 1 for this trace.

only in partial agreement with experiment. In this situation, it is logical to check critically the assumptions made in the model. First assumption is the value of the strain halfwidth (ΔE_G) used in obtaining figure 4.34 (e). Its value is set to 600 GHz. This results in a broad strain distribution of centres peaking at $\approx$ 300 GHz and extending upto 900 GHz (figure 4.30). This value of strain is not unreasonable since diamonds are known to be highly strained. This value of strain is also in agreement with the observed halfwidth of the N-V centre zero-phonon line (section 4.1). Further, strain distributions with lesser values of halfwidths (ΔE_G) predict spectra with broad features (figure 4.34 (a) through (d)). The variation of the value of λ' affects the position as well as the intensity of the features seen in the spectrum. Since experimentally no features are observed outside the ± 3 GHz, it is concluded that the value of λ' is less than 1 GHz. With an upper limit of 1 GHz, the effect of variation of λ' is to shift the position of the hole and antihole referred to above. The value of the feeding factor (to account for preferential relaxation into $M_S = \pm 1$ level and equal to 50 in figure 4.34 (e)) is not very critical because its effect is just varying the relative intensities of the features on the high and low energy sides (figure 4.33 (a) through (f)). As shown in section 4.15.9 the present model considers the $M_S = \pm 1$ level to be lower than $M_S = 0$ level. The spectra with feeding factor greater than 1 show strong features on the high energy side of the central hole. This does not necessarily mean that model predicts preferential relaxation into the $M_S = \pm 1$ level. It is possible to obtain the same effect (strong spectral features on the high energy side) by interchanging the ordering of energy levels ($M_S = 0$ level lower than $M_S = \pm 1$ level) and assuming preferential relaxation into the $M_S = 0$ level. i.e. the present model only predicts preferential relaxation into the lowest energy level of the ^3A ground state. Since the assumptions made in the model are reasonable, its partial success can only be attributed to its simplicity. At present only one peak in the distribution of E strains is used to give the above holeburning spectrum. It is quite possible for such a distribution to have some structure particularly when it is noted that E strains can originate from different terms in the strain tensor (L_E and $L_{E'}$). Further peaks in the distribution would give rise to a modification of the holeburning spectrum including further peaks. However, before introducing a complex description of the holeburning, it would be necessary to investigate the spectrum over a wide range of samples with varying strain. This has not been undertaken here.

There is still a lack of understanding of why the central hole (at 0 GHz)

and the 2.88 GHz antihole is so much weaker than expected. This may be due to the very non linear situation involved and this has not been properly incorporated into the simple model. Further experiments on the linearity with power and perhaps holeburning in the presence of external stress may help to clarify whether the above model is correct.

4.16 CONCLUSIONS

Previous studies on the nitrogen vacancy centre have concluded that it has a C_{3v} symmetry. On the basis of uniaxial stress experiments, the zero-phonon line at 638 nm has been assigned to be 2.88 GHz due to $A \rightarrow E$ transition. Since, EPR at 2.88 GHz was observed only under optical illumination the states involved in the zero-phonon transition are assigned to be spin singlets. The 2.88 GHz resonance was explained to be due in $^3A_2$ metastable state.

Two laser holeburning experiments on diamond, the N-V centre yielded very interesting results. The antihole structure in this spectrum indicated clearly that the ground consists of more than one level. This was also indicated in the results of one laser holeburning. It has been proposed that the splittings in the levels involved in the transition could arise through nitrogen tunneling and this is independent of whether the optical transition is $^1A \rightarrow ^1E$ or $^3A \rightarrow ^3E$. The significant weakness however of the tunneling model giving rise to the structure in the holeburning spectrum is that it can not account for the observed zeeman splitting and the asymmetry in the spectrum.

The 2.88 GHz antihole in the two laser holeburning spectrum strongly suggested that $^3A_2$ state involving the 2.88 GHz microwave resonance is in fact the ground state. Further, MCD experiments showed a temperature dependence of the MCD signal which can be explained quite satisfactorily assuming a $^3A \rightarrow ^3E$ transition. Further support to $^3A \rightarrow ^3E$ assignment comes from the fact that the splitting patterns of the 2.88 GHz antihole is the same as the splitting of 2.88 GHz ODMR signal. This confirms that the separation of 2.88 GHz obtained in the holeburning spectrum is the same splitting as seen in ODMR and the zero field splitting of the ^3A state deduced from EPR data.

So, our experimental results can be explained satisfactorily assigning this transition to be $^3A \rightarrow ^3E$. The sole basis for the $^1A \rightarrow ^1E$ assignment is the lack of EPR before optical illumination. When it is realised that illumination causes selective feeding into one of the spin levels of ^3A and hence will improve the EPR sensitivity - perhaps enabling it to be detected in the presence of light but not otherwise. It has been reported (Holliday *et al* (1988) and Nisida *et al* (1988)) recently that EPR can, in some samples, be observed even *without* optical illumination. It is noted that all the experimental data can be seen to be consistent with the $^3A \rightarrow ^3E$ assignment made here. Furthermore, by simple consideration of strain and spin-orbit, it has been shown in the latter part of the chapter how a holeburning spectrum such as that observed can arise from.

Since the conclusion of experimental work reported in this chapter, three reports dealing with the N-V centre were published in literature and their results are discussed in the following. The report by Nisida *et al* (1988) contains some interesting results. On the basis of their study of the temperature dependence of the EPR signal they conclude that the ground state of the N-V centre is a spin singlet and that there is a metastable triplet state. The singlet-triplet separation is, from optical far infra red measurements, found to be 75.6 cm^{-1}. When excited optically the metastable triplet state is populated and an observable magnetic moment that can be measured using a SQUID magnetometer is produced. From the rate of decay of the magnetic moment when the optical excitation is switched off, they obtain a value of 27.4 secs for the lifetime of the triplet state. This value is supported by holeburning recovery experiments. The results of these experiments contradict our assignment of the ground state as a triplet and also the triplet lifetime differs from that reported by Loubser *et al* (1977). However, it is interesting to note that Nisida *et al* (1988) do observe (in high concentration samples) a EPR signal *without* optical excitation which supports our $^3A_2$ assignment of the ground state. van Oort *et al* (1988) obtained evidence for the triplet charecter of the N-V centre ground state using optically detected microwave spin coherence. The idea of the experiment is as follows. If the ground state is a spin triplet, its lifetime would be diminished on optical excitation, whereas if the triplet state is a metastable excited state its lifetime would be unaffected by optical excitation (from the ground state). Optically detected spin-locking experiments (Slichter (1978), Vreeker *et al* (1986)) were used to eliminate the effect of feeding processes on the triplet state dynamics. Optical pumping of the centre is at 450 nm and the flourescence intensity at

637 nm is used to monitor the spin-locked state. At a fixed optical pumping intensity the spin-locked state is found to decay with a time constant of 1.5 msecs. The decay is found to slow down linearly as the optical pumping intensity is decreased which suggests that the ground state of the N-V centre is indeed a spin triplet. Further, the decay constant of the spin-locked state (1.5 msecs) is comparable to lifetime of the 2.88 GHz antihole (500 μsecs $\pm$ 200 μsecs). Holliday *et al* (1988) reported the observation of spin-spin cross relaxation between the triplet state of the N-V centre and another colour centre (P1) in diamond as well as N-V centre of different orientations. The depth of the optical hole burnt at the peak of the zero phonon line using a narrow band laser (1 MHz) is used to probe the cross relaxation effects. It should be remembered (section 4.11) that transient one laser holeburning in this centre occurs due to non-equilibrium distribution of population between the spin levels. Spin levels of the various centres involved in the cross relaxation process are varied by using a magnetic field. Spin-spin cross relaxation between the optically excited N-V centre and its neighbouring centres reestablishes the thermal equilibrium. (This is so because the vast majority of the neighbouring centres are already in equilibrium with the lattice). Thus, cross relaxation manifests itself as a reduction in the transient hole depth. Though these results do not give any direct information spin multiplicity of the N-V centre it is worth noting that EPR resonance has been observed in the present case *without* optical excitation. Based on the data presented in this chapter and since the EPR has been observed without optical excitation, it is concluded that the zero phonon transition of the N-V centre is a $^3A \rightarrow ^3E$ and not a $^1A \rightarrow ^1E$ as previously proposed.

REFERENCES

1) Bloch P.D., Brocklesby W.S.,Harley R.T. and Henderson M.J.
J. de Physique, C7, 527 (1985)

2) Clark C.D. and Norris N.A.
J. Phys. C: Solid state physics, 4, 2223 (1971)

3) Collins A.T. ,Thomas M.F. and Jorge M.I.B.
J. Phys. C: Solid state physics, 16, 2177 (1983)

4) Cone R.L. , Harley R.T. and Leask M.J.M.
J. Phys. C: Solid state physics, 17, 3101 (1984)

5) Davies G. and Hamer M.F.
Proc. R. Soc. London A, 348, 285 (1976)

6) Davies G. and Lightowlers E.C.
J. Phys. C: Solid state physics, 3, 638 (1970)

7) Davies G. and Manson N.B.
in Industrial diamond review, pp50, February 1980.

8) Davis J.A. and Fitchen D.B.
Solid State Communications, 6, 505 (1968)

9) Harley R.T., Henderson M.J. and Macfarlane R.M.
J. Phys. C: Solid state physics, 17, l233 (1984)

10) Henry C.H.,Schnatterly S.C. and Slichter C.P.
Phys. Rev., A137, 583 (1965)

11) Holliday K., Manson N.B., Glasbeek M. and van Oort E.
(private communication, 1988)

12) Loubser J.H.N. and van Wyk J.A.
Diamond Research, 11, 4 (1977)

13) Manson N.B. Henderson M.J. and Harley R.T.
Report to de Beers Industrial diamonds corporation , (1985)

14) Mitchell E.W.J.
in *Science and technology of diamonds* (Ed. Burls J.)
Industrial diamonds information bureau, London. 1, 17 (1967)

15) Nisida Y., Mori K., Muro K., Mihara T., Demizu Y. Kato R.,
Asida M., Sato S. and Yazu S.
Post deadline poster at *Defects in insulating crystals*,
Parma (Italy) (1988)

16) van Oort E., Manson N.B. and Glasbeek M.
J. Phys. C: Solid state physics, 21, 4385 (1988)

17) du Preez L.
Ph.D Thesis, University of Witwatersrand (unpublished) (1965)

18) Robertson R., Fox J.J. and Martin A.E.
Proc. R. Soc. London A, 157, 579 (1936)

19) Shah J.A
Ph.D thesis, The Australian National University, (1976)

20) Slichter C.P.
Principles of magnetic resonance (Berlin:Springer) (1978)

21) Stephens P.J.
J. Chem. Phys., 52,3489 (1970)

22) Tanimoto D.H.,Ziniker W.M. and Kemp J.O.
Phys. Rev. Letters, 14, 645 (1965)

23) Vreeker R., Glasbeek M., Sleva E.T. and Zewail A. H.
Chem. Phys. Lett. 129, 117 (1986)

24) Watkins G.D.
Phys. Rev. , 155, 802 (1967)

25) Watkins G.D. and Corbett J.W.
Phys. Rev. 134, A1359 (1964)

Chapter 5

HOLEBURNING IN OTHER COLOUR CENTRES

Results of optical holeburning experiments in some other colour centres in various crystals are described in this chapter. All these experiments had to be left uncompleted because of various experimental problems. The experiments described in this chapter relate to the following centres, identified by their zero-phonon line position.

a) 571 nm line in CaO.
b) 644 nm line in NaF.
c) 642 nm line in MgO.

and the d) 677 nm line in CaF_2.

5.1 THE 571 nm LINE IN CaO

The 571 nm zero-phonon line in CaO is associated with an F aggregate centre. It can be produced rather easily. In our case it was observed in as received arc-grown crystals and neutron irradiated crystals and also in additively coloured crystals. It has orthorhombic symmetry (Henderson *et al*, 1968). No Zeeman effect or MCD has been observed (Gourley *et al*, 1972). It has been assigned to a pair of F centres aligned along a <110> direction (F_2 centre, Henderson, 1980). Since it was invariably present in all the samples that had the F centres in them, optical holeburning was attempted.

It was possible to holeburn in these centres (figure 5.1(a)). Hole width was dependent on laser power. Burning with low powers (~1 mw) gave optical holes with a width of ~400 MHz whereas with 50 mw the line widths were ~1 GHz. No magnetic field effects were observed and this is consistent with the absence of magnetic field effects on the inhomogeneously broadened zero-phonon line (Gourley *et al*, 1972). DC electric field causes some broadening of the holes but no discrete splitting is observed. The results are shown in figure 5.1 . The behaviour of this centre in an electric field is similar to that of the CaO:F centre. The main problem that hampered further studies on this centre was that the holes were very shallow and resulted in very poor signal to noise ratio when external perturbations were applied.

5.2 THE 644 nm LINE IN NaF

X-irradiated NaF exhibits several zero-phonon lines in the spectral region accessible to tunable dye lasers, the 644 nm line being one of them. This centre could be produced by X-irradiating nominally pure NaF crystals for about 20 hours. However, the formation of these centres was highly sample dependent. Presence of some unidentified impurity seems to strongly influence the centre formation. Holeburning in these centres produced broad holes (~2 GHz) that had a short lifetime (~2 secs).

The nature and symmetry of this centre are not known. Electric field splits the hole into well resolved components showing that the centre lacks inversion symmetry. When an electric field is applied along the <100> direction the hole splits into three well resolved components (figure 5.2(a)). Magnetic field shows no effect on this centre.

The experiment was done using the burn scan method described in chapter 4 and the waveform used to drive the laser is shown in figure 5.3 . By a suitable choice of the waveform shown in figure 5.3(a), it is possible to vary the burn-detect gap (τ_3). Note that the waveform is not symmetric about the time axis. It was observed that the width of the hole depends on the time gap between burning the hole and its detection. The results obtained using this method are tabulated in table 5.1 .

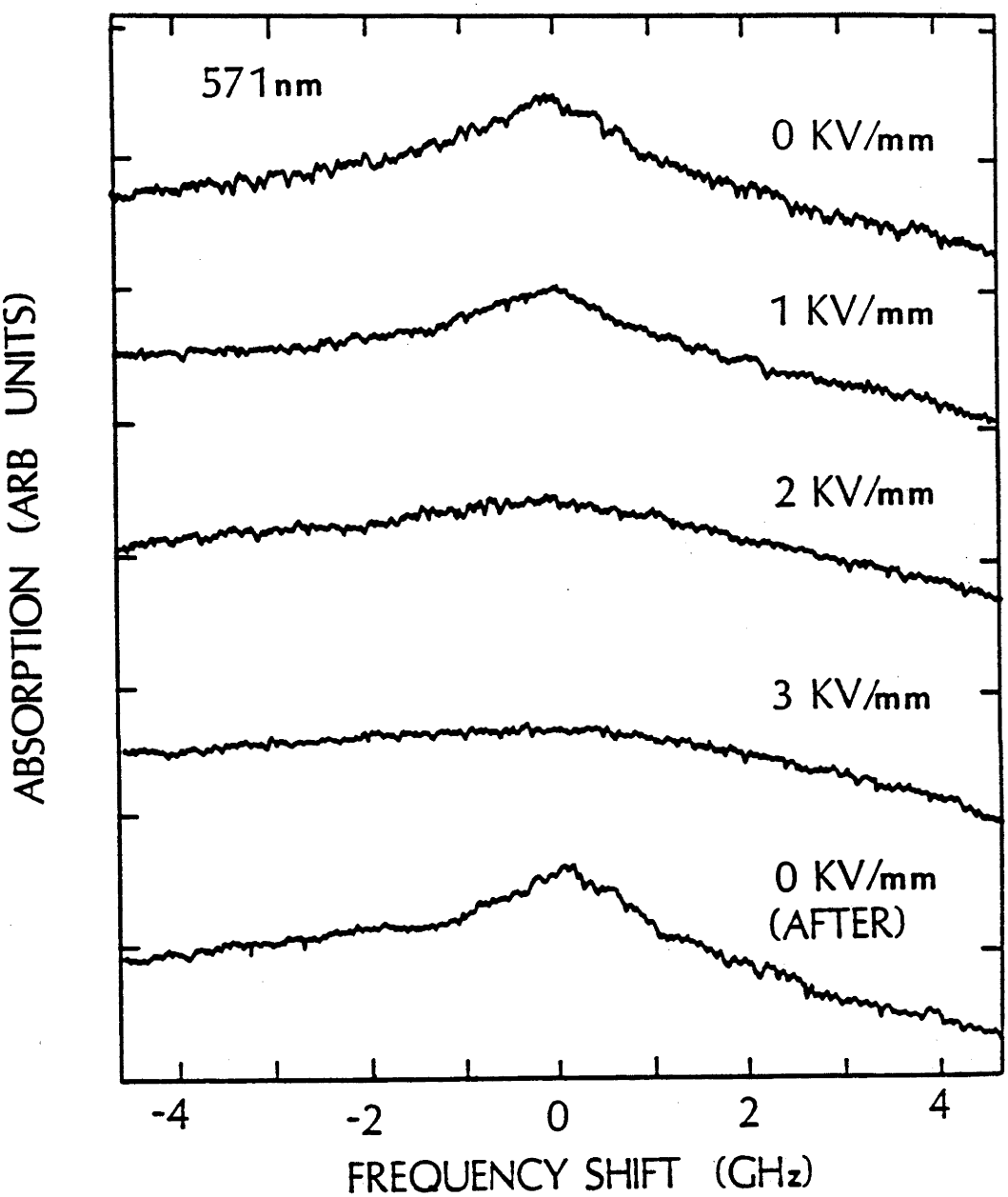

Figure 5.1 Optical hole in the 571 nm zero-phonon line in CaO (a) and stark splitting (electric field values as shown).

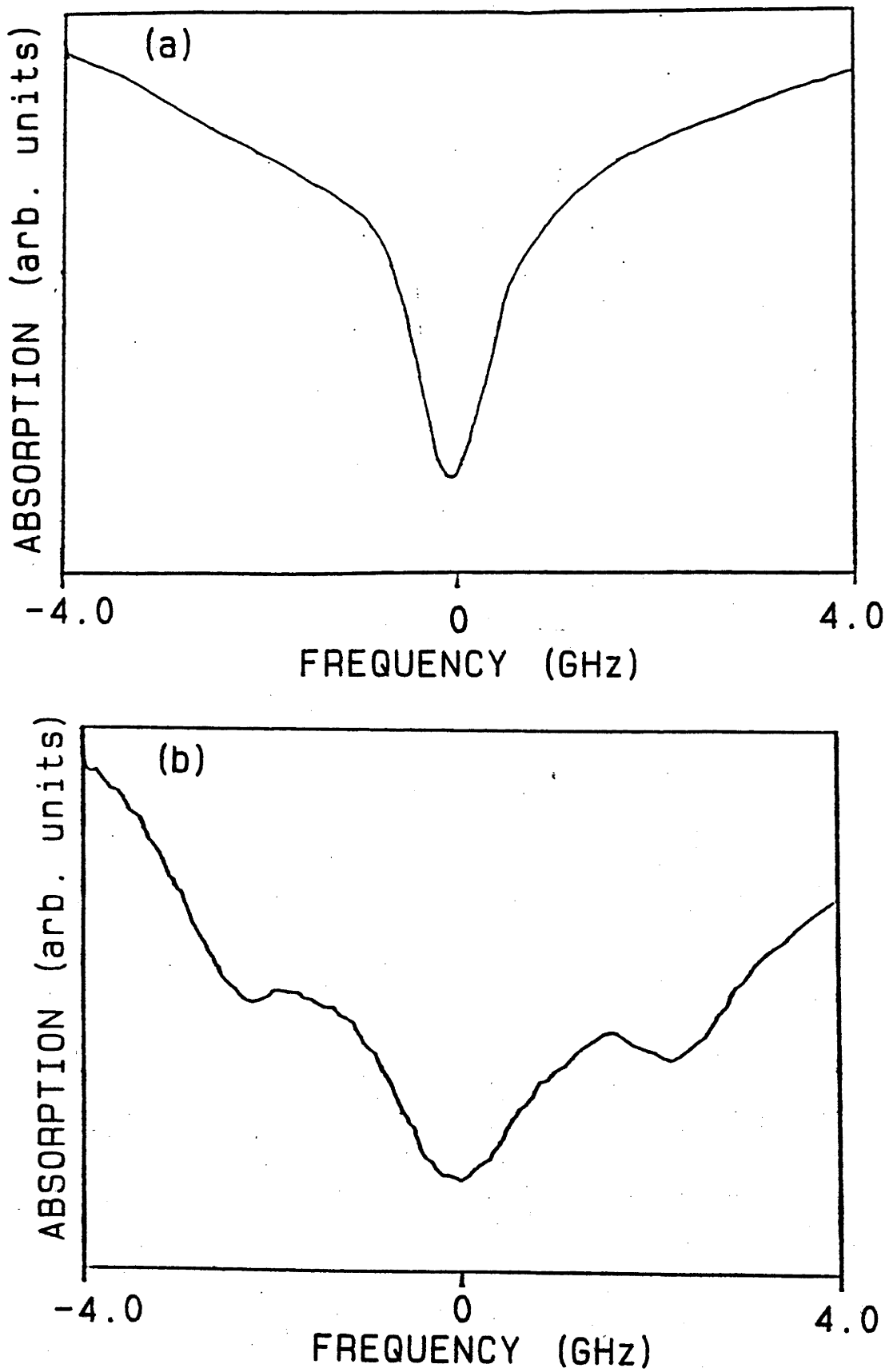

Figure 5.2 Optical hole in the 644 nm line in NaF (a) and effect of electric field (5kV/cm).

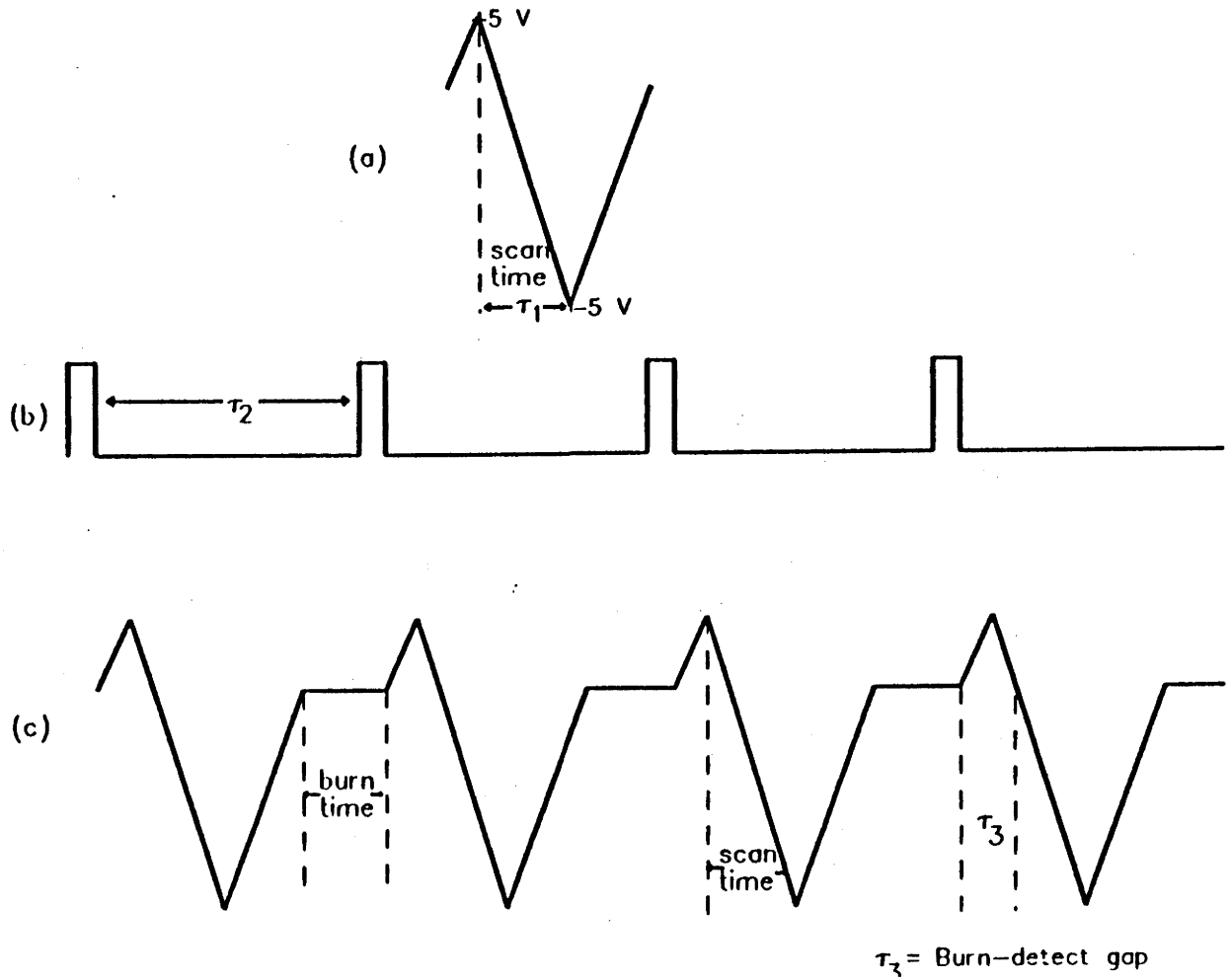

Figure 5.3 The waveform used to scan the ring laser frequency externally (c). The waveform in (a) is triggered by the pulse train (b) from another pulse generator to obtain the waveform in (c).

Burn time (msecs)	Burn scan gap (msecs)	Holewidth (FWHM)
2000	250	2 GHz
600	250	846
400	250	564
230	70	517
230	50	470
230	40	375
100	40	Hole not observed

The smallest holewidth that could be burned was 375 MHz. But it is unlikely that this represents the homogeneous width. This experiment was done when two high resolution lasers were not available in this laboratory. The shortest time gap possible in this experiment (that enabled us to get a full trace of the central hole) was 40 msecs.

Difficulty in producing the centres prevented further studies on these centres. Two laser holeburning experiments similar to the one used to determine the lifetime of the antihole structure in diamond should provide useful information about the characteristics of this hole.

5.3 THE 642 nm LINE IN MgO

This centre is present in neutron irradiated MgO crystals. On the basis of the uniaxial stress experiment results, Ludlow (1968) concluded that the zero-phonon line is due to an A→E transition (ground state A) transition of a centre with trigonal symmetry (C_{3v}). In heavily irradiated crystals the zero-phonon line width is large and in the present case it was 100 cm^{-1} (3000 GHz).

Optical holeburning in this centre gave a hole with 500 MHz width (figure 5.4). It was observed that the signal to noise ratio was much better when the holeburning was done using the burn scan method. This indicates that there is a fast decaying component in the hole with a lifetime of less than 1 sec. Application of electric and magnetic field did not split the hole and

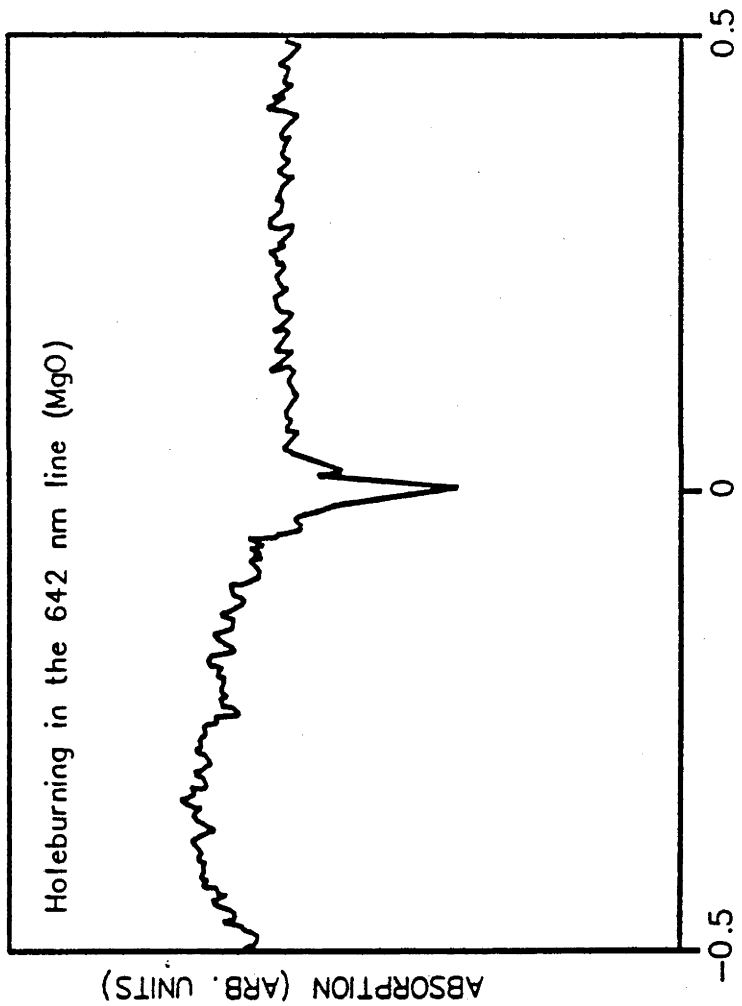

Figure 5.4 Optical hole in the 642 nm line in MgO.

experiments on this centre were not pursued further. However, again two laser hole burning experiments should be informative.

5.4 R CENTRE IN CaF_2

The 677 nm zero-phonon line in CaF_2 is associated with R centre. The R centre is formed when three F centres are in nearest neighbour positions along the <100> direction (Beaumont *et al*, 1972 a,b). When CaF_2 is additively coloured in calcium metal vapour, it forms F and F_2 (two F centres) centres. Quenching the crystals to room or liquid nitrogen temperatures after colouring improved the formation of these centres. The F centre absorption at 375 nm is known as the α band and the F_2 centre band at 524 nm is known as the β band. Exposure of these additively coloured crystals to light in the β band causes optical bleaching of the F_2 centres forming F_3 (R) centres. We have made several attempts at forming these F_3 centres but were never able to produce the β band. Instead, a band peaking at 545 nm was consistently observed. The absorption spectrum in our case was similar to that reported by Smakula (1950, 1953). Several parameters including colouring temperature, quenching temperature and rate of quenching etc. were varied but with no success. Crystals from different sources were tried as well. It is concluded that the formation of this centre is closely connected with some impurities in the crystal. No samples were therefore available for holeburning measurements.

REFERENCES

1) Beaumont J. , Harmer A. L. and Hayes W.
J. Phys. C: Solid state physics, 5, 257 (1972a)

2) Beaumont J. , Harmer A. L. and Hayes W.
J. Phys. C: Solid state physics, 5, 266 (1972b)

3) Gourley J. T. , Runciman W. A. and Vance E. R.
J. Phys. C: Solid state physics, 8, 2329 (1975)

4) Henderson B.
CRC Critical reviews of Solid state and Material sciences, 9, 1 (1980)

5) Henderson B. and King R. D.
phys. stat. sol. , 26, K147 (1968)

6) Ludlow I. K.
J. Phys. C (Proc. Phys. Soc), 1, 1194 (1968)

7) Smakula A.
Phys. Rev. , 77, 408 (1950)

8) Smakula A.
Phys. Rev. , 91, 1570 (1953)